ABSTRACT

Title of dissertation: COMETARY ESCAPE IN THE RESTRICTED CIRCULAR PLANAR: THREE BODY PROBLEM

Joseph R. Galante, Doctor of Philosophy, 2011

Dissertation directed by: Professor Vadim Kaloshin
Department of Mathematics

The classical principle of least action says that orbits of mechanical systems extremize action; an important subclass are those orbits that minimize action. This principle is utilized along with Aubry-Mather theory to construct regions of instability for a certain three body problem, given by a Hamiltonian system of two degrees of freedom. In principle, these methods can be applied to construct instability regions for a variety of Hamiltonian systems with 2 degrees of freedom.

The Hamiltonian model considered in this thesis describes the dynamics of a Sun-Jupiter-Comet system and under some simplifying assumptions, the existence of instabilities for the orbit of the comet is shown. In particular it is shown that a comet which starts close to an orbit in the shape of an ellipse of eccentricity $e = 0.66$ (fig. 1) can increase in eccentricity to beyond $e = 1$. Furthermore, there exist ejection orbits for the comet. Such orbits are initially well within the range of our solar system. This might give an indication of why most objects rotating around the Sun in our solar system have relatively low eccentricity.

Figure 1: Ellipse of eccentricity $e = 0.66$ (blue) surrounding the Sun-Jupiter system

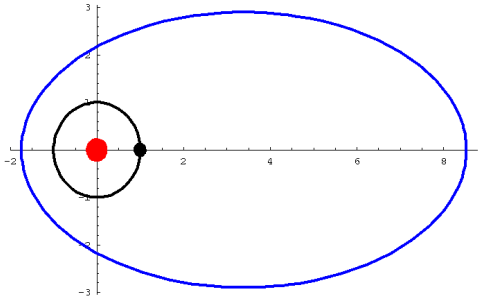

Several new theoretical tools are introduced in this thesis as well. The most notable is a checkable sufficient condition to verify that an exact area preserving map is an exact area preserving twist map in a certain coordinate system. This coordinate system is constructed by "spreading the cumulative twist" which arises from the long term dynamics of system. Many of the results of the thesis are 'computer assisted' and utilize recent advances in rigorous numerical integration. It is through the application of these advances in computing that it has become possible to state deep results for realistic solar systems. This has been the dream of many since humans first observed the stars so long ago.

COMETARY ESCAPE IN THE RESTRICTED CIRCULAR PLANAR THREE BODY PROBLEM

by

Joseph Robert Galante

Dissertation submitted to the Faculty of the Graduate School of the
University of Maryland, College Park in partial fulfillment
of the requirements for the degree of
Doctor of Philosophy
2011

Advisory Committee:
Professor Vadim Kaloshin, Chair/Advisor
Professor Giovanni Forni
Professor Brian Hunt
Professor Michael Jakobson
Professor Douglas Hamilton

Dedication

This thesis is dedicated to my parents, Barb and Joe Galante, for all their love and support during my many years of school.

Acknowledgments

I would like to thank the following individuals for providing guidance, advise, and support throughout my graduate career.

First and foremost, I would like to thank my academic advisor Vadim Kaloshin who introduced me to celestial mechanics and to problems of diffusion in Hamiltonian dynamics. Vadim's passion for mathematics often energized me and his amazing intuition guided me through the complexities of this thesis. I would also like to thank Misha Brin for encouraging me to go into dynamical systems, and for introducing me to Vadim.

Without the larger mathematical community, this thesis would not exist. Discussions with Rafael de la Llave helped me organize my results and highlight weak areas in exposition. I would like to thank John Mather for the example of a system in which a global twisting coordinate system does not exist. My academic advisor also discussed my thesis work with Alain Albouy, Alain Chenciner, Luigi Chierchia, Dmitry Dolgopyat, Jacques Fejoz, Rafael de la Llave, and Rick Moeckel, and relayed the results back to me. Discussions with Andrea Venturelli involving the applicability of Aubry-Mather theory to the RCP3BP helped refine the results and illustrate additional complexities.

I particularly grateful to Daniel Wilczak for assistance and advice on the CAPD library. I would also like to acknowledge discussions with Martin Berz, Kyoto Makino, and Alexander Wittig on rigorous numerics. Thanks to Kory Pennington, Paul Wright, Christian Sykes, and the Mathematics Department at the University

of Maryland - College Park for their generous donation of computer equipment and computer time which helped make the rigorous numerics feasible in a reasonable time.

I would like to thank my friends for fruitful mathematical discussions, as well as for just being awesome. In particular, I'd like to thank Moshe Adrian, David Aulicino, Marcel Guardia, Vincent Guingona, Kevin McGoff, Andy Sanders, James Tanis, and Jinxin Xue. Kevin gets a special thanks for tolerating me as an office mate for 6 years.

Finally, I would like to thank my family for their never ending support. My parents, Barb and Joe, have provided a endless supply of emotional (in some cases financial) support. My brother Alex provided me with lodging during my many trips throughout Pennsylvania to visit my academic advisor. My cousins Ashley and Damien generously furnished most of my apartment, and my Uncle Bob and Aunt Mar gave me invaluable career and life advise. Lastly, I'd like to thank my brother Nick for threatening to kick my ass if didn't graduate.

Table of Contents

List of Figures

List of Abbreviations

RCP3BP	Restricted Circular Planar Three Body Problem
2BP	Two Body Problem
2BP(SC)	Two Body Problem with primaries the Sun and the Comet
ADDV	Algebraically Deformed Delaunay Variables
DDDV	Dynamically Deformed Delaunay Variables
EAP	Exact Area Preserving
EAPT	Exact Area Preserving Twist
RI	Region of Instability
μ	Sun-Jupiter Mass Ratio
J_0	Jacobi Constant
$e^*(\mu, J_0)$	Critical eccentricity above which there are no invariant tori
ν	Constant related to size of splitting of separatrices.
e	Eccentricity
P_φ, G	Angular Momentum
r	Radius of the comet
$P_r = \dot{r}$	Radial velocity of the comet
φ	Angular position of the comet in rotating coordinates
ψ	is Angular position of the comet in non-rotating coordinates
u	Eccentric Anomoly
ℓ	Mean Anomoly
$\cdot_\nu$	An Algebraically Deformed Delaunay Variable
ω	Rotation Number
$\mathcal{H}(J_0)$	Hill Region
$\mathcal{H}^{out}(J_0)$	Outer Hill Region
$\mathcal{S}(J_0)$	Energy surface
$\mathcal{S}^{out}(J_0)$	Energy surface in the outer hill region
Σ_ω	Aubry Mather set with rotation number ω
P	is a Poincaré section used to define $\mathcal{F}$
$\mathcal{T}^2$	Rotational 2-torus
Ω	Domain of Definition of $\mathcal{F}$
$\mathcal{W}$	Domain where $\mathcal{F}_\nu$ can be made to twist
$\mathcal{D}$	Symplectic change of coordinates from Polar to Delaunay
$\mathcal{F}_{dyn}$	Poincare return map of RCP3BP in DDDV
$\mathcal{F}_\mu$	Poincare return map of RCP3BP in Delaunay variables
Tw^{Del}	Region where the map $\mathcal{F}_\mu$ is twisting in Delaunay
Tw^∞	Non-compact region above Tw^{Del}
d_S	Distance between Sun and Comet
$H_{2BP(SC)}$	Hamiltonian of the 2BP(SC) in rotating polar coordinates.
H_{Polar}	Hamiltonian of the RCP3BP in rotating polar coordinates.
ΔH	Perturbation Term
H_{Del}	Hamiltonian of the RCP3BP in Delaunay coordinates.
H_ν	Formal Hamiltonian used in enlarging domain of definition
M_h	Maupertius action functional
$\mathcal{I}$	Intervals are denoted with calligraphics
$(\cdot)^+$	Upper bound of absolute value of $\cdot$.

Chapter 1

Introduction

1.1 Statement of the Problem and the Main Results

This thesis analyzes the restricted circular planar three body problem (RCP3BP), a three body problem consisting of two massive primaries, called the Sun and Jupiter, and a massless comet. The Sun and Jupiter are assumed to perform uniform circular motion about their center of mass (see fig. 1.1). The system is normalized to mass one so the Sun has mass $1-\mu$ and Jupiter mass μ. The system is further normalized so that Jupiter rotates with period 2π, and the distance from the Sun to Jupiter is constant and also normalized to one. The goal is to understand the behavior of the massless comet whose position in polar coordinates is denoted (r, ψ). It is convenient to consider the system in a rotating frame of reference which rotates with unit speed in the same direction as Jupiter. In this system, the Sun and Jupiter are fixed points on the x-axis corresponding to $\psi = 0$. Let $(r, \varphi) = (r, \psi - t)$ denote the motion of the comet in the rotating frame of reference.

The RCP3BP has a conserved quantity known as the *Jacobi constant*.

$$J(r, \varphi, \dot{r}, \dot{\varphi}) = \frac{r^2}{2} + \frac{\mu}{d_J} + \frac{1-\mu}{d_S} - \frac{\dot{r}^2 + r^2\dot{\varphi}^2}{2} =: U(r, \varphi) - \frac{\dot{r}^2 + r^2\dot{\varphi}^2}{2}$$

Figure 1.1: The Sun-Jupiter-Comet system

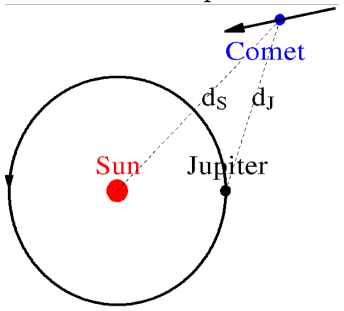

where d_J and d_S are distances to Jupiter and the Sun respectively.

$$\begin{aligned} d_J(r,\varphi) &:= \left(r^2 - 2(1-\mu)r\cos(\varphi) + (1-\mu)^2\right)^{\frac{1}{2}} \\ d_S(r,\varphi) &:= \left(r^2 + 2\mu r\cos(\varphi) + \mu^2\right)^{\frac{1}{2}} \end{aligned} \tag{1.1}$$

Denote by

$$\mathcal{H}(J_0) := \{(r,\varphi) :\ U \geq J_0\}$$

a set of points on the plane of motion (configuration space). Points in this set are called *the Hill regions* associated to the Jacobi constant J_0. These regions are the locations in the (r,φ) plane (shaded regions in fig. 1.2) where the comet is allowed to move.

Figure 1.2: Hill Regions (Blue) for $mu = 10^{-3}$ and $J_0 > 1.52$

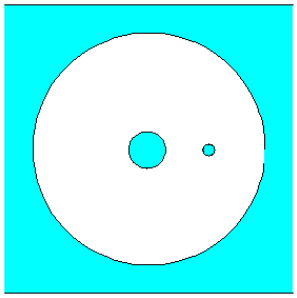

Fixing the Jacobi constant restricts dynamics to an invariant energy surface, denoted

$$\mathcal{S}(J_0) := \{(r,\varphi,\dot{r},\dot{\varphi}) : J(r,\varphi,\dot{r},\dot{\varphi}) = J_0\}$$

Most of these surfaces are smooth 3-dimensional manifolds. Denote by $RCP3BP(\mu, J_0)$ the RCP3BP with Sun-Jupiter mass ratio μ and dynamics restricted to the surface $\mathcal{S}(J_0)$.

It turns out that for $\mu \leq 10^{-3}$ and $J_0 \geq 1.52$ the set $\mathcal{H}(J_0)$ consists of three disjoint connected components: a region around the Sun called the *inner Hill region*, a region around Jupiter called the *lunar Hill region*, and noncompact region called the *outer Hill region*. The boundary of these regions can be found by considering the "zero velocity" curves which are on the boundary of the Hill regions [AKN]. In this thesis, only orbits contained in the outer Hill region, denoted by $\mathcal{H}^{out}(J_0)$, are considered. For convenience, denote $\mathcal{S}^{out}(J_0) = \mathcal{H}^{out}(J_0) \cap \mathcal{S}(J_0)$ and when dynamics in $\mathcal{S}^{out}(J_0)$ is considered, this shall refer exclusively to the case when the outer Hill region is disjoint from the other two.

Lemma 1.1.1. *For an orbit $(r, \psi)(t)$ in $\mathcal{H}^{out}(J_0)$, if $J_0 \in [1.52, 2]$, then $\frac{J_0^2}{2} - 33\mu \leq r(t)$ for all t.*

This lemma is proved in section A.2. As the position of Jupiter is at radius $1 - \mu$, this lemma implies for $\mu \leq 10^{-3}$ and $J_0 \geq 1.52$ that the comet remains bounded away from collisions with the Sun and Jupiter by a distance at least 8% of the Sun-Jupiter distance.

For small μ and away from collisions, the RCP3BP is nearly integrable and can be approximated with the Sun-Comet two body problem (2BP(SC)) corresponding to $\mu = 0$. Elliptic motions of a 2BP have two special points where the radial velocity $\dot{r}$ of the comet is zero. The *perihelion* is the closest point to the Sun[1],

[1]To be pedantic, the perihelion is technically defined to be a point in the orbit when $r \leq J_0^2$

denoted r^{perih}, and the *aphelion* is the farthest point from the Sun, denoted r^{apoh}. Define the *osculating (or instantaneous) eccentricity* $e(t)$ for the RCP3BP to be the eccentricity of the comet in the unperturbed 2BP(SC) system with initial conditions taken to be those of comet in the RCP3BP at time t.

Theorem 1.1.2. *Consider the RCP3BP*(μ, J_0) *with dynamics in* $\mathcal{S}^{out}$*. There exists a function* $e^* = e^*(\mu, J_0)$ *and there exist trajectories of a comet with initial eccentricity* $e^* = e^*(\mu, J_0)$ *that increase in eccentricity to beyond one in a manner so that the comet escapes the solar system to infinity. For example* $e^*(10^{-3}, 1.8) \leq 0.66$.

Suppose $\mathcal{T}^2 \subset \mathcal{S}(J_0)$ is an invariant set of the RCP3BP(μ, J_0) that is diffeomorphic to a 2-dimensional torus. Call $\mathcal{T}^2$ *rotational* if it cannot be continuously deformed inside $\mathcal{S}(J_0)$ to a closed curve or a single point. When $\mu = 0$ (i.e. when there is no perturbation), the problem reduces to the 2BP(SC) system and every such rotational 2-torus is defined by $\{e = e_0 \geq 0\}$. Bounded motions correspond to $e_0 \in [0, 1)$. In general for e bounded away from 1 and μ sufficiently small, many of these rotational 2-tori survive due to KAM [SM]. Celletti and Chierchia gave a computer assisted proof using $\mu \approx 10^{-3}$ and $J_0 \approx 1.76$ in the inner Hill region to show that near $e = 0.3$ there is a rotational 2-torus $\mathcal{T}^2$ separating $\mathcal{S}(J_0)$ into a compact "Below $\mathcal{T}^2$" component and a noncompact "Above $\mathcal{T}^2$" component [CC].

and $\dot{r} = 0$. It is **not** necessarily the closest point to the Sun. Rather it is when the comet is at the closest point to the center of mass of the system. The Sun is within μ of the center of mass. It turns out that in our Solar System, the radius of the Sun is approximately 0.00089 the Sun-Jupiter distance, so we allow this slight abuse in terminology for small μ [NASA].

Their proof may be adapted to the outer Hill region.[2] The method presented in this thesis is for the specific value of $J_0 = 1.8$, however it works for any $\mu \leq 10^{-3}$ and $J_0 \geq 1.52$.[3]

Figure 1.3: Various eccentricity orbits of the 2BP in the configuration space and on the cylinder $\mathbb{T}^2 \times I$

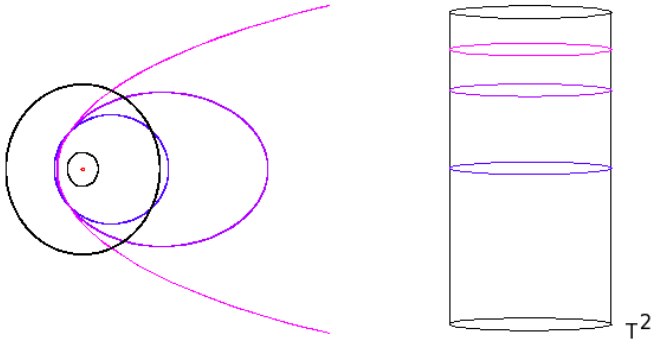

Define a *Region of Instability* (RI) for the RCP3BP(μ, J_0) as an open set in $\mathcal{S}(J_0)$ which has no rotational 2-dimensional tori inside.[4] If there is a rotational 2-torus, then it separates $\mathcal{S}(J_0)$ into an "above" and a "below" (see section 6.1 for precise definitions). This provides a topological obstruction to instability. As a matter of fact,

Theorem 1.1.3. *In the setting of Theorem 1.1.2, the RCP3BP(μ, J_0) has a region of instability which contains the region* $\{e \geq e^*(\mu, J_0)\}$.

[2]Personal Communication

[3]Values $\sqrt{2} \leq J_0 \leq 1.52$ require substantial additional work as the lunar Hill region and outer Hill region are no longer disjoint. For J_0 near or less than $\sqrt{2}$ collisions with Jupiter are hard to exclude.

[4]Birkhoff considered *compact invariant* regions of instability known as *Birkhoff Regions of Instability*. The motions considered for the RCP3BP are in a non-compact non-invariant RI and special care is taken to handle issues of non-compactness and non-invariance.

In 1922, Chazy gave a complete classification of the final motions of the spatial 3BP, i.e. a description of all possible states that a three body problem can approach as time goes to infinity. It turns out that there are seven types of final motions (see section 2.4 [AKN]). For the RCP3BP there are only four possible types of motion that the comet can exhibit.

- $H^{\pm}$ (*hyperbolic*): $r \to \infty$, $\dot{r} \to c > 0$ as $t \to \pm\infty$
- $P^{\pm}$ (*parabolic*): $r \to \infty$, $\dot{r} \to 0$ as $t \to \pm\infty$
- $B^{\pm}$ (*bounded*): $\limsup_{t\to\pm\infty} r = R_B < \infty$
- $OS^{\pm}$ (*bounded*): $\limsup_{t\to\pm\infty} r = \infty$, $\liminf_{t\to\pm\infty} r = R_{OS} < \infty$

The RCP3BP has a *full set of Chazy motions* if $H^- \cap H^+$, $H^{\pm} \cap P^{\mp}$, $H^{\pm} \cap B^{\mp}$, $H^{\pm} \cap OS^{\mp}$, $P^+ \cap P^-$, $P^{\pm} \cap B^{\mp}$, $P^{\pm} \cap OS^{\mp}$, $B^+ \cap B^-$, $B^{\pm} \cap OS^{\mp}$, $OS^+ \cap OS^-$ are all nonempty intersections, i.e. if any possible past and future of the comet's motion can be realized by a trajectory in the RCP3BP. A corollary to Theorem 1.1.3 states that this is possible for comets in the outer Hill region on an energy surface with $J_0 \geq 1.52$. Additionally it possible to spend arbitrarily long amounts of time in between approach of the final motions.

Corollary 1.1.4. *There is a full set of Chazy instabilities in the region* $e \geq e^*(\mu, J_0)$

The primary tools for this result are Aubry-Mather theory and rigorous numerical integration. It is not trivial to apply Aubry-Mather theory to the restricted circular planar three body problem since the typical usage requires the RI to be an invariant domain and invariance in not a given for the RCP3BP. It is important

to stress that trajectories are **not** constructed by means of numerical integration. After a mathematical framework is developed, a list of inequalities is derived. To have an explicit value of e^*, a computer is used to verify the range of validity of the inequalities, which are of two types: *analytic* and *dynamic*. Analytic inequalities **do not** make use to integration of the equations of motion. Dynamical inequalities **do involve integration**, but only over shorter periods of time. The software used can handle both types of inequalities in a mathematically rigorous way (see section E.1).

Relying on Mather's variational method ([Ma2],[Xia1], [BK]), in a RI it shall be shown that there is a full set of Chazy instabilities [AKN] (also see [Xia2]). Historically the existence of ejection orbits and Chazy instabilities for RCP3BP was established by Llibre and Simo [LS]. One can estimate their $e^*(0.001, 1.8) \approx 0.995$, however their motions belong to a horseshoe, while the ones presently considered have a fairly different nature: the orbits considered here are *local action minimizers and shadow closely a collection of Aubry-Mather sets.* The idea of constructing Chazy instabilities originated in the famous paper by Sitnikov [Si] (see also [Mo3] for conceptual and transparent exposition of Sitnikov's work). Alekseyev constructed oscillatory motions for the full spatial three body problem [Al].

1.2 Roadmap to the Results

Recall that motions of the comet in rotating polar coordinates (r, φ) can be viewed as the solutions to Hamilton's equations with a Hamiltonian of the form

$$H_{Polar} = H_{2BP(SC)} + \Delta H(r, \varphi) := \frac{P_r^2}{2} + \frac{P_\varphi^2}{2r^2} - P_\varphi - \frac{1}{r} + \Delta H(\mu; r, \varphi) \qquad (1.2)$$

where P_r and P_φ are the momenta variables conjugate to r and φ respectively (see e.g. [AKN]) and ΔH is the μ-small perturbation of the associated Sun-Comet two body problem (2BP(SC)). This system arises by initially considering the planar 3BP where the comet has mass m, and letting $m \to 0$. With the notations in (1.1), ΔH can be written

$$\Delta H(\mu; r, \varphi) := \frac{1}{r} - \frac{\mu}{d_J} - \frac{1-\mu}{d_S} = \frac{\mu(\mu-1)(1+3\cos(2\varphi))}{4r^3} + O(\frac{\mu}{r^4})$$

The proof starts with expressing equations of motion of RCP3BP in so called *Delaunay variables* (formally defined in section 3.1). These are action angle variables of the $2BP(SC)$ or, equivalently, of $RCP3BP$ with $\mu = 0$, and have two angular variables ℓ and g in $\mathbb{T}$, and two action variables $0 \leq G \leq L$. There is a canonical transformation

$$\mathcal{D} : (\ell, L, g, G) \to (r, \varphi, P_r, P_\varphi)$$

which converts Delaunay coordinates into symplectic polar coordinates. The image consists of all bounded motions of the $2BP(SC)$. The map $\mathcal{D}$ is more fully described in section 3.1.

It turns out that there is a good 2-dimensional Poincaré section $P \subset \mathcal{S}(J_0) = \{H = -J_0\}$ of the dynamics of $RCP3BP(\mu, J_0)$ in the outer Hill region. In other

words, a Poincaré map $\mathcal{F}_\mu : U \to P$ is well-defined on an open set $U \subset P$ homeomorphic to an annulus (see section 3.2, formula (3.5)). For $\mu = 0$ there are natural coordinates on $P \simeq \mathbb{T} \times \mathbb{R}_+ \ni (\ell, L)$ with $\ell \in \mathbb{T}$ and $L \geq 0$. It turns out that for $\mu = 0$ and $J_0 > 1.52$ quantities

$$L = L(e, J_0) \qquad \text{and} \qquad e = e(L, J_0) \tag{1.3}$$

are monotone implicit functions of each other. On the energy surface $\mathcal{S}(J_0)$ they satisfy an implicit relation roughly given by $J_0 = 1/(2L^2) + L\sqrt{1-e^2}$. Moreover, $L \to \infty$ as $e \to 1$ and vise versa on $\mathcal{S}^{out}(J_0)$. Below either the e or L-parametrization of the vertical (i.e. action) coordinate shall be used. When $\mu = 0$, the Poincaré map $\mathcal{F}_\mu$ has the form (compare with fig. 1.3)

$$\mathcal{F}_0 : (\ell, L) \to (\ell + 2\pi L^{-3}, L).$$

This map is clearly a twist map. (See [MF], [Ban], [Mo1] for discussion of twist maps). For small μ, the corresponding Poincaré map $\mathcal{F}_\mu$ is a small perturbation of $\mathcal{F}_0$ *only for* e *separated away from* 1.

In order to prove all the results stated above it is sufficient to perform a detailed analysis of $\mathcal{F}_\mu$. Analysis of $\mathcal{F}_\mu$ naturally divides into the following stages.

Stage 1. Determine a *twist region*, denoted $Tw^{Del} = \{e^-_{twist} \leq e \leq e^+_{twist}\}$ where $\mathcal{F}_\mu$ is a twist map.

This is done by derivation of sufficient condition to check an infinitesimal twist holds locally uniformly. This condition says that a function of certain first and second partial derivatives of H has to be strictly negative. See section 3.2 for details. The values e^-_{twist} and e^+_{twist} are computed by numerical extremization of this

function. It is important to notice that Tw^{Del} is **not invariant**, but is however compact. Even though $\mathcal{F}_\mu$ twists in Tw^{Del}, a priori there might be no invariant sets in Tw^{Del} at all.

Stage 2. Show that for each $n \geq N_0$ and each rotation number $\omega \in [\frac{1}{n+1}, \frac{1}{n}] \subset \mathbb{R}$ the corresponding Aubry-Mather set Σ_ω (formally defined in 6.1) of $\mathcal{F}_\mu$ has small vertical L-deviations on the cylinder, i.e. $\Sigma_\omega \subset \{(\ell, L) : L_n^- < L < L_n^+\}$. Using (1.3) we have $L_n^- = L_n^-(e_n^-, J_0),\ L_n^+ = L_n^+(e_n^+, J_0)$ for some $e_n^-,\ e_n^+$ and Σ_ω has osculating eccentricity localized in $[e_n^-, e_n^+]$. We call $[L_n^-, L_n^+]$ an *L-localization interval.*

This stage is accomplished using the *ordering condition* from Aubry-Mather theory. For a solution with rotation number $\omega \in [\frac{1}{n+1}, \frac{1}{n}]$, the ordering condition says that after n iterates of the Poincare map $\mathcal{F}_\mu$, the angular component makes at most one rotation around $\mathbb{T} \ni \ell$ and after $(n+1)$ iterates it makes a at least one. (See section 6.1 for formal definition.) Higher eccentricities have smaller rotation numbers which physically corresponds to the fact that high eccentricity comets have longer periods of revolution around the Sun. If the initial eccentricity is larger than e_n^+, then the trajectory rotates too slowly to have rotation number ω, and if the initial eccentricity is smaller than e_n^-, then the trajectory rotates too quickly to have rotation number ω.

A numerical scheme is developed to calculate $[e_n^-, e_n^+]$. Once localization intervals are known, rigorous numerical integration is used to construct a trajectories which crosses the localization interval. This implies that the Aubry-Mather set inside the localization interval is not an invariant curve. Doing this for a range of

localization intervals will open up a window of instability[5].

Stage 3. Rule out invariant curves to show the existence of a region of instability $\{e^* \leq e \leq e_{max}\} \subset Tw^{Del}$.

The idea is the following. Suppose Σ_ω is an invariant curve (an example of an Aubry-Mather set) for the EAPT $\mathcal{F}_\mu$ and denote by $\widetilde{\Sigma}_\omega$ a lift of Σ_ω to $\mathcal{S}(J_0)$. We prove that $\mathcal{D}^{-1}(\widetilde{\Sigma}_\omega)$ consists of action minimizers of the RCP3BP Lagrangian in polar coordinates. For ω relatively small, we show that action minimizers **cannot** visit a certain ℓ-strip on the cylinder $\mathbb{A} = \mathbb{T} \times \mathbb{R} \ni (\ell, L)$. This implies that there are no invariant curves for small ω or, equivalently, for highly eccentric motions. Section 2.1 outlines a heuristic method for destroying invariant curves in polar coordinates and in section 2.2 the results are made rigorous.

By combining steps 1, 2 and 3 with Mather's variational techniques (e.g. the Mather Connecting Theorem 6.1.3), a proof of Theorem 1.1.2 may be obtained in the case that $e \leq e_{max}$. It might not be surprising that the twist region Tw^{Del} is compact. Action-angle (Delaunay) variables are designed to describe the compact part of the dynamics and as motions approach unbounded (parabolic) motions, usage of these coordinates becomes less and less reliable. For example, they are not defined for Aubry-Mather sets $\widetilde{\Sigma}_\omega$ with very small rotation numbers ω. Thus, in order to prove existence of ejection/capture orbits, the existence of a semi-infinite RI (in the L direction) for the map $\mathcal{F}_\mu$ must be established. This leads to analysis of the non-compact part "above" Tw^{Del}, denoted Tw^{∞}.

Stage 4. Construction of symplectic deformation of Delaunay variables so that

[5]In fact this provides an alternative approach to the method used in Stage 3.

$\mathcal{F}_\mu$ is a twist map for nearly parabolic motions.

This is done through analysis of the dynamics of the RCP3BP in symplectic polar coordinates where the coordinate system is well-defined for all non-collision motions. It turns out that arguments of Stage 3 apply to Aubry-Mather sets in Tw^∞ (near the "top" boundary of Tw^{Del}) and exclude possibility of invariant curves of any small rotation number. This shows that a region of instability which contains $\{e \geq e^*\}$ is semi-infinite (in L).

The construction employed is of a fairly general nature and can be applied to other Hamiltonian systems. Note however that for an EAP map to be twisting in some symplectic coordinate system is far from granted. For example, pick an EAP with two elliptic islands which twist in different directions; such a map has no such symplectic coordinates. Stage 4 is broken up as follows.

Stage 4.1: Algebraic deformations of action-angle variables

Given a set of action-angle variables, there may be degeneracies which spoil the reduction of dynamics to an EAPT. For example Delaunay coordinates are only well defined for a compact region of the phase space and as $e \to 1$ motions tend to unbounded ones and Delaunay coordinates degenerate.

A method to produce a set of action-angle variables where a Poincaré return map is well defined shall be exhibited. The method amounts to an algebraic deformation of existing action-angle variables. For the RCP3BP, the deformed action-angle variables are similar to Delaunay without the singularities arising for $e \approx 1$ and they allow for a representation of nearly parabolic motions. While the algebraically deformed variables allow a return map to be defined, a priori it is not true that the

map is twisting. For RCP3BP, it turns out that twisting fails in the algebraically deformed Delaunay variables for exactly the same reason as for Delaunay variables.

Stage 4.2: A sufficient condition for twist

A sufficient condition for twisting is defined. The condition may be described as the property that long term, i.e. after several iterates, the map $\mathcal{F}_\mu$ is twisting. Call this *cumulative twist*. In polar coordinates for RCP3BP, the condition says transition times from the aphelion to the perihelion increase as the aphelion distance increases. The plan is to use the long term information about cumulative twist to create a coordinate system which has an EAPT map.

Stage 4.3: Construction of a dynamically defined direction field

A new direction field is built dynamically. The main idea is to 'spread the cumulative twist' along trajectories which comes from the sufficient condition in stage 4.2. This procedure works in a fairly general setting and is applicable to other Hamiltonian systems.

Stage 4.4: Construction of dynamically deformed coordinates

The vector field in stage 4.3 is used to construct a dynamic deformation of action-angle variables. The new coordinates are used to define a return map which is an EAPT. Once the property of twist is known, Aubry-Mather theory may be applied to the resulting twist map.

1.2.1 Additional Results

In addition to the main result on the existence of ejection orbits, a result on the speed of escape is outlined.

Theorem 1.2.1. *Consider $RCP3BP(\mu, J_0)$ with three disjoint Hill regions and consider dynamics on $\mathcal{S}^{out}(J_0)$. There exists functions $e^*(\mu, J_0)$ and $R(\mu, J_0, e_0)$ and there exist trajectories of a comet with initial eccentricity $e_0 > e^*(\mu, J_0)$ that increase in eccentricity beyond one after $R = R(\mu, J_0, e_0)$ passages by the Sun-Jupiter system. In other words, these orbits start with eccentricity e_0 and get ejected after $R(\mu, J_0, e_0)$ revolutions around the Sun. For example $e^*(10^{-3}, 1.8) \leq 0.66$ and $R(10^{-3}, 1.8, 0.9) \leq 30$, i.e. the time of escape is less than 85500 revolutions of Jupiter around the Sun.*

1.2.2 Papers

The work found in this thesis is the focus of several papers. The contributions of various papers are illustrated in figure 1.4.

Chapter 2 is contained in [GK1], as are parts of 3 and 6, as well as parts of appendices A-E. Chapters 3 and 4 are contained in [GK2], as are parts of 6, as well as parts of appendices A-E. Chapter 5 is contained in [GK3], as are parts of 3 and 6, as well as parts of appendices A-E. Chapter 7 is contained in [G1]. As this thesis is the synthesis of several papers, there are likely some redundant redundancies. I apologize for the inconvenience.

[GK1]-[GK3] complete Theorem 1.1.2 and Corollary 1.1.4. As of 3/14/2011,

Figure 1.4: Roadmap of Results

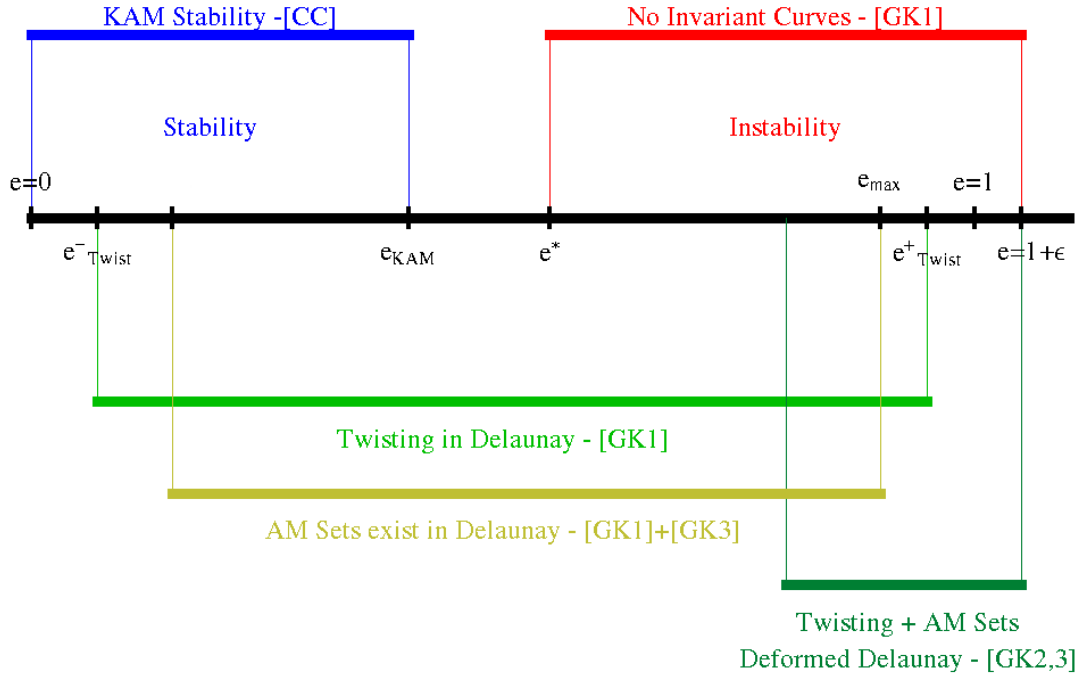

[GK1] has been accepted to publication in the Duke Journal of Mathematics and [GK2],[GK3] are awaiting submission. [G1] is reasonably independent of the other papers, only utilizing some basic estimates found in their appendices.

Historically [GK3] (which becomes chapter 5) was done first (roughly complete in late 2008), followed by [GK1] (fully complete in late 2010), then [GK2] (roughly complete early 2011). [GK3] was partially based on the unpublished notes [KN]. Some of these ideas are also found in the manuscript [KN2], however that note seems concerned with varying Jacobi constant $J_0 \geq 2$. A rough plan to produce instabilities may be found in the unpublished notes of [KNP], though these note includes neither the action comparison method, nor any mention of dynamically deformed variables. The author would like to thank his academic advisor Vadim Kaloshin, as well as Vadim's past collaborators who previously touched on the work

contained in this thesis and helped pave the way.

1.2.3 Organization of the Thesis

- Chapter 2 contains both the heuristics of the action comparison method and the rigorous formulation in terms of interval arithmetic. It completes Stage 3.
- Chapter 3 contains a description of Delaunay variables and analysis of twist in Delaunay variables. It contains the construction of a deformed coordinate system. It completes Stages 1 and contains an abstract formulation of the steps in Stage 4.
- Chapter 4 contains a proof that the abstract deformed coordinate system in Chapter 3 can be applied to the RCP3BP. It completes Stage 4.
- Chapter 5 contains a formulation of localization intervals for Delaunay variables. It completes Stage 2.
- Chapter 6 completes the proof of the main theorem on the existence of instabilities and contains a proof that all Chazy motions are realized.
- Chapter 7 contains additional work on estimating the speed of diffusion.
- Appendices A-E contain technical proofs and descriptions of the software.

The paper is organized in this fashion since results of Chapter 2 depend only on the dynamics in polar coordinates. In chapter 3, several new coordinate systems for the RCP3BP are introduced and it is assumed the reader is familiar with these

coordinate systems (especially Delaunay variables) in all subsequent chapters. It is also important to note that in many places some familiarity with interval arithmetic is assumed. The first part of appendix E contains a quick review of what is needed. Appendix F contains a quick review of some of the properties of the integrable 2BP(SC) which are used throughout this document.

Chapter 2

The Action Comparison Method

"Nature is thrifty in all its actions." - Maupertuis

2.1 Heuristics of the Action-Comparison Method

This section outlines a method for destroying invariant curves based on the method of comparing actions. The core of this method is illustrated by initially making several simplifying assumptions which are removed in later sections.

2.1.1 Action Minimization

The motions of the comet at position $q = (r, \varphi)$ and velocity v also satisfy the Euler-Lagrange equations with Lagrangian

$$L(r, \varphi, \dot{r}, \dot{\varphi}) = \frac{\langle v, v \rangle}{2} + \frac{1}{r} - \Delta H := \frac{\dot{r}^2}{2} + \frac{r^2(\dot{\varphi} + 1)^2}{2} + \frac{1}{r} - \Delta H(\mu; r, \varphi) \qquad (2.1)$$

and locally minimize action.

Notice L maps $\mathbb{R}^2 \times \mathbb{R}^2 \to \mathbb{R}$ and is a real analytic positive definite Lagrangian away from Jupiter and the Sun, e.g. in $\mathcal{H}^{out}(J_0)$. Let $(q_0, t_0), (q_1, t_1) \in \mathbb{R}^2 \times \mathbb{R}$. *Action* along an absolutely continuous curve $\gamma : [t_0, t_1] \to \mathbb{R}^2$ is defined to be

$$A(\gamma) = \int_{t_0}^{t_1} L\big(\gamma(t), \dot{\gamma}(t)\big) dt.$$

Definition: A curve $\gamma : [t_0, t_1] \to \mathbb{R}^2$ is *action-minimizing* if

$$A(\gamma) = \min_{\gamma:[t_0,t_1]\to\mathbb{R}^2:\gamma(t_0)=q_0,\gamma(t_1)=q_1} A(\gamma)$$

where minimum is taken over all absolutely continuous curves connecting q_0 to q_1. A curve $\gamma : \mathbb{R} \to \mathbb{R}^2$ is *globally action-minimizing* if it is action minimizing on every time interval $[t_0, t_1]$.

Lemma 2.1.1. *If $\mathcal{T}^2$ is a rotational 2-torus of RCP3BP, then every trajectory inside of $\mathcal{T}^2$ is globally action-minimizing.*

This result is proved in section 6.2. However let us consider the utility of the result now. The goal is to show that certain high eccentricity trajectories are **not** globally action minimizing. If this is so, then these trajectories are not contained in rotational 2-tori, and analysis of the location of these trajectories eliminates possible rotational 2-tori. (Recall that rotational 2-tori are obstructions to diffusion.) The main idea is that passing by Jupiter is cheaper at some times than at others. This difference in action may be exploited to producing instabilities. Heuristics for this are developed below and in a later section the method is made rigorous.

2.1.2 Solar Passages and Perihelion Angles

Consider a trajectory $\big(r(t), \varphi(t)\big) \in \mathcal{S}(J_0) \cap \mathcal{H}^{out}(J_0)$ such that

1. $r(t_1) = R$ for some time t_1
2. the trajectory passes through a perihelion $r^{perih} = r(t^{perih}) < J_0^2$ at some time $t^{perih} > t_1$. Recall $P_r = \dot{r} = 0$ at the perihelion. (Physically the perihelion is

the closest point to Sun.)

3. $r(t_2) = R$ for some time $t_2 > t^{perih}$

Call such a segment of trajectory $\big(r(t), \varphi(t)\big)_{t\in[t_1,t_2]}$ an *R–Solar passage* (see fig. 2.1). The *perihelion angle*, denoted φ^{perih}, is the angle the comet makes relative to the position of Jupiter when the comet is at the perihelion. Let $SP(J_0, R)$ be the set of all R–Solar passages.

Figure 2.1: An R–Solar passage

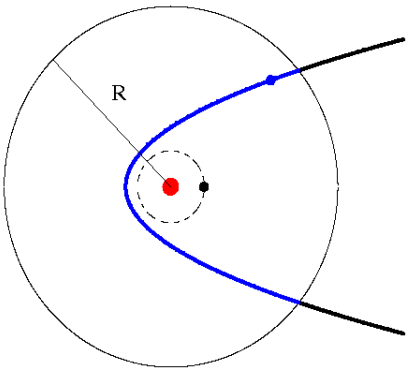

The following lemma guarantees existence of Solar passages.

Lemma 2.1.2. *Consider RCP3BP*(μ, J_0) *with* $\mu \leq 10^{-3}$ *and* $J_0 \geq 1.52$. *Suppose* $\gamma(t) = (r(t), \varphi(t)) \in \mathcal{S}^{out}(J_0)$ *is a trajectory such that for some sufficiently long interval of time it holds that* $e(t) \geq e_0$ *for some* $e_0 \in (0, 1)$. *Then there exists an* $R_{max}(e_0)$ *so that* $\gamma(t)$ *has R–Solar passages for all* $r^{perih} < R \leq R_{max}$. *Furthermore* $\frac{J_0^2}{2} - 33\mu \leq r^{perih} \leq J_0^2$.

A heuristic proof of this lemma is now presented for $J_0 = 1.8$. Recall that for the 2BP(SC), $\mu = 0$ and $\dot{e}(t) \equiv 0$. For $e \geq 0.45$ on $\mathcal{H}^{out}(1.8)$, trajectories are ellipses with aphelion distance to the origin $r^{apoh} \geq 5$. This indicates that there are

times $t_1 < t_2$ such that $r(t_1) = r(t_2) = R \leq r^{apoh}(e)$, and hence $\exists t^* \in [t_1, t_2]$ such that $\dot{r}(t) < 0$ (resp. > 0) for each $t \in (t_1, t^*)$ (resp. (t^*, t_2)). This implies that $r(t^*)$ is a minimum of $r(t)$ on the interval $[t_1, t_2]$. Simple analysis of ΔH shows that $|\Delta H| \leq \frac{2.7\mu}{r^3}$ for $r \geq 1.59$ (see e.g. appendix A.1). This implies that $\dot{e}(t) \simeq O(\mu/r^3)$ which is small since $\mu = 10^{-3}$, so the shape of the orbit is almost unchanged and hence the minimum, i.e. the perihelion, still exists under perturbation. Furthermore since $e_0 \approx e(t)$ holds for a sufficiently long time, there exists an $R_{max} \simeq r^{apoh}(e_0)$ so that there are R–Solar passages for all $r^{apoh} < R \leq R_{max}$. The lower bound on the radius follows from properties of $\mathcal{H}^{out}(1.8)$ and is approached with nearly parabolic motions while the upper bound follows from considering nearly circular motions of the comet.

This argument is made rigorous in section 2.2 when a large class of 5–Solar passages is exhaustively constructed with computer assistance and changes in $e(t)$ are rigorously estimated.

2.1.3 Bad Perihelion Angles

It turns out that certain R–Solar passages are not action minimizing and this depends heavily on the perihelion angle during the passage.

Theorem 2.1.3. *(Bad Angles Theorem) Consider RCP3BP(μ, J_0) and restrict dynamics to $\mathcal{S}^{out}(J_0)$. There is a function $e^*(\mu, J_0)$ such that for all initial eccentricities $e_0 > e^*(\mu, J_0)$, there exists an interval $[\varphi_-, \varphi_+]$ with $\varphi_\pm = \varphi_\pm\big(\mu, J_0, e_0\big)$ such that if $\big(r(t), \varphi(t)\big)_{t\in[t_1,t_2]}$ is an R–Solar passage and perihelion angle $\varphi^{perih} \in [\varphi_-, \varphi_+]$, then*

$\big(r(t), \varphi(t)\big)_{t\in[t_1,t_2]}$ *is* **not** *action-minimizing.*

A heuristic proof of the Bad Angles Theorem is presented later in this section and a rigorous proof is presented in section 2.2. The fact that there is an $e^*(\mu, J_0)$ such that there are no rotational 2-tori crossing the region $\{e \geq e^*(\mu, J_0)\}$ may be obtained by by combining Lemmas 2.1.2 and 2.1.1, and Theorem 2.1.3.

Proof of Theorem 1.1.3 : The proof is by contradiction. Suppose there is a rotational 2-torus $\mathcal{T}^2$ of RCP3BP(μ, J_0). Consider the intersection of $\mathcal{T}^2$ with perihelion/aphelion surface $\{\dot{r} = 0\}$. In polar coordinates $\dot{\varphi} < 0$ so trajectories intersect $\{\dot{r} = 0\}$ transversally and thus $\{\dot{r} = 0\} \cap \mathcal{T}^2$ is diffeomorphic to a compact one-dimensional manifold, i.e. the circle. This implies that for every perihelion angle $\varphi^{perih} = \varphi(t^{perih})$ there is a trajectory $\big(r(t), \varphi(t)\big)$ inside $\mathcal{T}^2$ with this perihelion angle. By Lemma 2.1.2, there is an R–Solar passage $\big(r(t), \varphi(t)\big)_{t\in[t_1,t_2]}$ with $t^{perih} \in [t_1, t_2]$ for this trajectory. By Theorem 2.1.3, this R–Solar passage is **not** action-minimizing, which contradicts Lemma 2.1.1. Thus, there are no rotational 2-tori for RCP3BP(μ, J_0) crossing $\{e \geq e^*(\mu, J_0)\}$. □

2.1.4 Action Decomposition

For the duration of this section, assume $\mu = 10^{-3}$ and $J_0 = 1.8$ for concreteness. Suppose $\gamma \in SP(1.8, R)$ is an R–Solar passage. Call a piece of trajectory of the RCP3BP where the radius is monotonically increasing or decreasing from R_1 to R_2 an (R_1, R_2) *segment*. γ can be decomposed into (fig. 2.2)

- γ^- – a $(R, 5)$ *segment*

- γ^{in} – a 5–Solar passage
- γ^{+} – a $(5, R)$ *segment*

Figure 2.2: Decomposition of γ into smaller arcs.

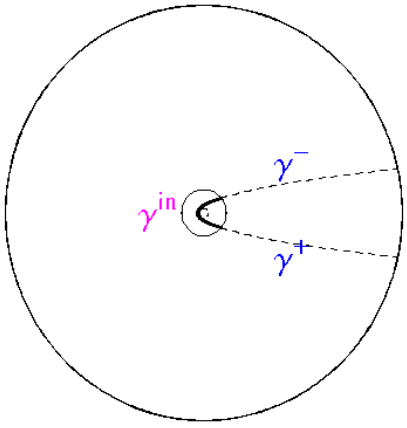

Remark: For $r \geq 5$ and $\mu = 10^{-3}$ one can show that $|\Delta H| \leq 10^{-5}$ (see e.g. section A.1). Call the region $\{r \geq 5\}$ the *outside region* since the comet is practically outside the range of influence of Jupiter. Call the region $\{r \leq 5\}$ the *kick region* as the comet's orbital parameters are perturbed (or kicked) more in this region.

Denote the action on each of the segments of γ by A^{-}_{out}, A_{in}, and A^{+}_{out} respectively. Hence

$$A(\gamma) = A^{-}_{out} + A_{in} + A^{+}_{out}.$$

2.1.5 Action Comparison in the Kick Region

It turns out that A_{in} has fairly sensitive dependence on the perihelion angle. The difference in actions can be explained physically by considering two scenarios. One possibility is that the comet is pulled along behind Jupiter, and gains velocity. This is a so called *gravity assist*, and when the comet leaves the perihelion, it is

flung further out than before. This case turns out to be action minimizing since the comet is getting a free ride from Jupiter. The other possibility is exactly the reverse. The comet is slowed down by Jupiter and is pulled more inward, as Jupiter attempts to capture it. Note that Jupiter can never actually capture the comet as a moon since the lunar Hill region around Jupiter is separated from the outer region by our choice of Jacobi constant.

Figure 2.3: Potential Capture (left) and Escape (right) (Motion of the system at times $t_1 < t_2 < t_3 < t_4$

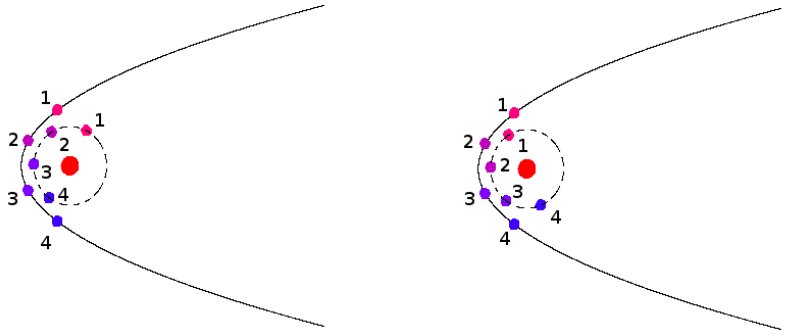

According to standard formulas [AKN], it turns out the eccentricity $e = \sqrt{1 - 2P_\varphi^2(J_0 - P_\varphi)}$. Thus one can also parameterize the 3-dimensional energy surface $\mathcal{S}(J_0)$ with coordinates (r, φ, P_φ). Denote by $SP(J_0, R, P_\varphi)$ the set of all R–Solar passages belonging to $\mathcal{S}(J_0)$ that have initial angular momentum P_φ. Define φ_{max}^{perih} and φ_{min}^{perih} as the angles such that

$$A_{in}(P_\varphi, \varphi_{max}^{perih}) := \max_{\gamma \in SP(J_0,R,P_\varphi)} A(\gamma^{in}), \qquad A_{in}(P_\varphi, \varphi_{min}^{perih}) := \min_{\gamma \in SP(J_0,R,P_\varphi)} A(\gamma^{in}) \tag{2.2}$$

Remark: It turns out that φ_{min}^{perih} and φ_{min}^{perih} depend slightly on P_φ. Ignore this for now to keep the argument simple.

Define the differences in action and angle to be:

$$\Delta A_{in}^{min} := \min_{P_\varphi} \Big(A_{in}(P_\varphi, \varphi_{max}^{perih}) - A_{in}(P_\varphi, \varphi_{min}^{perih}) \Big), \qquad \Delta\varphi := \varphi_{max}^{perih} - \varphi_{min}^{perih} \tag{2.3}$$

To get a feel for these quantities, consider $R = 26$–Solar passages corresponding to nearly parabolic motions ($P_\varphi \approx J_0$). A computer can then compute $\Delta A_{in}^{min} \approx 0.0163237$ and $\Delta\varphi \approx 1.076$. A detailed algorithm for rigorously computing these quantities is given in section 2.2. Plotted (fig. 2.4) is the perihelion angle φ^{perih} vs.

Figure 2.4: φ^{perih} vs. A_{in} for nearly parabolic motions

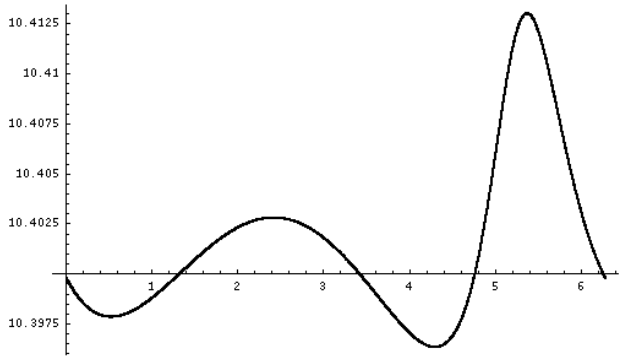

A_{in} the action for the particular set of 26–Solar passages corresponding to parabolic motion in the kick region.

2.1.6 Heuristic Outside Region Action Comparison

Suppose there is a rotational 2-torus $\mathcal{T}^2$. Then it has base $\mathbb{T}^2$ which can be parametrized by (t, φ). Specifying a perihelion fixes a time t^{perih} which leaves one free variable, φ^{perih}. Hence it is possible to make an R–Solar passage with any perihelion angle, including the bad angle φ_{max}^{perih} or some angle near it in the interval of bad angles. Suppose γ_{max} is a 26-Solar passage with perihelion angle

φ_{max}^{perih} (or near it) and initial angular momentum $P_\varphi \approx J_0$ (i.e. nearly parabolic motion). A procedure to construct γ_{test}, a new curve with smaller action than γ_{max}, i.e. $A(\gamma_{test}) < A(\gamma_{max})$ is now described. Doing this completes the proof of the Bad Angles Theorem since a neighborhood of φ_{max}^{perih} may be used for the interval of angles specified in the theorem. A contradiction to Lemma 2.1.1 can then be obtained to rule out the existence of the rotational 2-torus which contains γ_{max}.

For $r \geq 5$, ΔH and its derivatives with respect to r and φ are quite small (see Lemma 2.2.1), so it is not too bad to **approximate the RCP3BP by the 2BP(SC)** for the $(R, 5)$ and $(5, R)$ segments which are contained in the outside region. Doing so allows makes it possible explicitly compute the action without computer assistance. These approximations are made rigorous in section 2.2.

Heuristically, if the comet starts at $R = 26$ and has $\varphi^{perih} = \varphi_{max}^{perih}$, then by modifying the velocity of the $(26, 5)$ segment, the comet can slow down enough so that Jupiter moves from a position where the action is maximized to a position where action is minimized. The comet can then speed very slightly during the $(5, 26)$ segment to arrive at $R = 26$ at the same time as in the original case.

Note that it takes a finite amount of time ΔT for the angle of Jupiter relative to the comet to change by $\Delta\varphi$. In nonrotating coordinates Jupiter moves with unit speed, and for $r \geq 5$ the comet's angle remains nearly constant since $\dot{\psi} = \frac{P_\varphi}{r^2}$. (In rotating coordinates, Jupiter is fixed and the comet is moving with almost unit speed.) Hence $\Delta T \approx \Delta\varphi$. By Kepler's Second Law, for $r \geq 5$ the comet moves slower the further away it is from the Sun [AKN]. Denote the amount of time the comet spends in the $(26, 5)$ segment by T_{out}. To keep the argument simple, assume

by symmetry, this also the time spent in the $(5, 26)$ segment.

A very small change in velocity changes the amount of time to reach the perihelion considerably. Let

$$\lambda_{\pm} = \frac{T_{out}}{T_{out} \mp \Delta\varphi} \approx \frac{T_{out}}{T_{out} \mp \Delta T} \tag{2.4}$$

Recall γ_{max} is a 26–Solar passage such that the perihelion angle is φ_{max}^{perih} so that γ_{max}^{in} **maximizes** action over all 5–Solar passages. Consider a new curve γ_{test} where

- the velocity of the $(26, 5)$ segment is $\dot{\gamma}_{test}^{-} = \lambda_{-} \cdot \dot{\gamma}_{max}^{-}$
- γ_{test}^{in} is a 5–Solar passage which minimizes action over all 5–Solar passages, i.e. the perihelion angle of γ_{test} is φ_{min}^{perih}.
- the velocity of the $(5, 26)$ segment is $\dot{\gamma}_{test}^{+} = \lambda_{+} \cdot \dot{\gamma}_{max}^{+}$

Claim: Suppose $\gamma \in SP(1.8, 26)$ has initial angular momentum $P_{\varphi} \approx J_0$ (i.e. it is nearly parabolic) and has perihelion angle $\varphi^{perih} \in [\varphi_{max}^{perih} - \Delta, \varphi_{max}^{perih} + \Delta]$ for Δ small, e.g. $\Delta = 0.000025$. Let γ_{test} be constructed as above. Then $A(\gamma) - A(\gamma_{test}) > 0$ and γ is not a global action minimizer.

Now calculate the difference in actions between γ_{max} and γ_{test}, starting with the action of the rescaled $(26, 5)$ segment γ_{test}^{-}. The Hamiltonian of the 2BP(SC) approximation for parabolic motion gives $\frac{\langle v,v \rangle}{2} = \frac{P_r^2}{2} + \frac{P_{\varphi}^2}{2r^2} = \frac{1}{r}$, where $v = \dot{\gamma}_{max}$ is

the velocity of γ_{max}.

$$\begin{aligned} A(\gamma^-_{test}) &= \int_{t(5)\cdot\lambda_-}^{t(26)\cdot\lambda_-} (\frac{\lambda_-^2 \langle v, v\rangle}{2} + \frac{1}{r})(\frac{t}{\lambda_-})dt \\ &= \int_{t(5)}^{t(26)} \lambda_- \cdot \big(\lambda_-^2(\frac{1}{r(u)}) + \frac{1}{r(u)}\big)du \\ &= \int_5^{26} \frac{\lambda_-^3 + \lambda_-}{r\dot{r}}dr \\ &= \int_5^{26} \frac{\lambda_-^3 + \lambda_-}{\sqrt{2r - 1.8^2}}dr \end{aligned}$$

Remarks: The second line comes from a linear change of variables and the last line comes from solving $H_{2BP}(r, \varphi, \dot{r}, 1.8) = -1.8$ for $\dot{r}$, as this corresponds to parabolic motion on $\mathcal{S}(1.8)$ The limits of integration change since the comet must start and end at the same place with respect to (r, φ) in the scaled and unscaled cases. By symmetry from the 2BP(SC) approximation, the $(5, R)$ segment γ^+_{test} is the same computation only using λ_+. The unscaled trajectories γ^+_{max} and γ^-_{max} use the same computation, only using $\lambda = 1$.

Consider the following formulas relating time and radius for 2BP parabolic motions.

Lemma 2.1.4. *For parabolic motions in the 2BP,*

$$\begin{aligned} r(t) &= \frac{1}{2}\left(3t + \sqrt{J_0^6 + 9t^2}\right)^{2/3} + \frac{J_0^4}{2\left(3t + \sqrt{J_0^6 + 9t^2}\right)^{2/3}} - \frac{J_0^2}{2} \\ t(r) &= \frac{1}{3}\sqrt{2r^3 + 3J_0^2r^2 - J_0^6} \end{aligned}$$

Proof: These can be derived from formulas in [AKN] section 2.1. □

Using the formulas in Lemma 2.1.4 yields $T_{out} \approx 60.918$ and

$$\lambda_- \approx 0.9844 \qquad \lambda_+ \approx 1.0161$$

$$A(\gamma^-_{max}) \approx 8.7657 \qquad A(\gamma^+_{max}) \approx 8.7657$$

$$A(\gamma^-_{test}) \approx 8.4956 \qquad A(\gamma^+_{test}) \approx 9.0507.$$

Now compute the difference in action between the curves γ_{max} and γ_{test}:

$$\begin{aligned} A(\gamma_{max}) - A(\gamma_{test}) &\geq \Delta A^{min}_{in} + \big(A(\gamma^-_{max}) - A(\gamma^-_{test})\big) + \big(A(\gamma^+_{max}) - A(\gamma^+_{test})\big) \\ &\approx 0.000978235 > 0 \end{aligned}$$

Further analysis indicates that picking any other radius larger than $R = 26$ also produces a strictly positive result. The reason is that spending more time in the outside region increases T_{out}, which pushes the λ's closer to 1, which makes the differences in action on the $(5, 26)$ and $(26, 5)$ segments smaller, and hence increases the difference in actions between γ_{max} and γ_{test}. Hence there are no rotational 2-tori corresponding to $R \geq 26$, i.e. $e \geq 0.88$.

The next section is dedicated to making the action comparison method mathematically rigorous.

2.2 Rigorous Action Comparison

In this section mathematically rigorous estimates are developed to use in place of the heuristics in section 2.1. It turns out that by modifying R–Solar passages to incorporate elliptic motions, the value of $e^*(0.001, 1.8)$ can be lowered down to $e^* \leq 0.66$ at the cost of increasing complexity of the estimates. This section relies on

the technical appendices and computer assisted methods for some of the estimates.

2.2.1 The Intervalization of the RCP3BP

The following formula nicely changes between time and radius.

$$\int_{t_0}^{t_1} dt = \int_{r_0}^{r_1} \frac{dr}{\dot{r}}$$

Away from parabolic motions[1], this integral can be rearranged into the form:

$$t_1 - t_0 = \int_{r_0}^{r_1} \frac{r dr}{\sqrt{2C(r^+ - r)(r - r^-)}} \tag{2.5}$$

$$r_+ := \frac{1 + \sqrt{1 - 2CP_\varphi^2}}{2C} \qquad\qquad r_- := \frac{P_\varphi^2}{1 + \sqrt{1 - 2CP_\varphi^2}}$$

$$C := J_0 - P_\varphi + \Delta H$$

In the case when $\mu = 0$, the integral can be evaluated explicitly since $\Delta H = 0$ and $P_\varphi \equiv P_\varphi(0)$. In the RCP3BP with $\mu > 0$, there are no longer these luxuries as r_+ and r_- are no longer constant; rather they depend on time. However away from parabolic motions in the outside region these quantities do not change much since the perturbative effects of Jupiter are too faint to make much of a difference. Our goal is to "intervalize" the problem, i.e. to use a computer to generate rigorous bounds on the above terms and use interval arithmetic (appendix E.1.1) to manipulate the bounds.

The first step to carrying out this procedure is to get precise estimates on the perturbation terms. Some simple analysis shows

[1]Nearly parabolic motions are addressed in appendix D.2

Lemma 2.2.1. *For* $r \geq 1.6$ *and* $\mu = 10^{-3}$, $|\Delta H| \leq \frac{2.7\mu}{r^3}$, $|\frac{\partial \Delta H}{\partial r}| \leq \frac{12.4\mu}{r^4}$, *and* $|\frac{\partial \Delta H}{\partial \varphi}| \leq \frac{28.6\mu}{r^3}$.

While these bounds are adequate for exposition, they are not quite accurate enough for our purposes. In appendix A.1 a function $(|\Delta H|)^+(r)$ is defined so that for all $\varphi \in \mathbb{T}$ and $r > 1 + \mu$ it holds that $(|\Delta H|)^+(r) \geq |\Delta H(r, \varphi)|$. Functions $(|\frac{\partial \Delta H}{\partial r}|)^+(r)$ and $(|\frac{\partial \Delta H}{\partial \varphi}|)^+(r)$ are defined similarly.

Very accurate estimates on how P_φ changes dynamically with time (or radius) are also required. Appendix B.1 contains the construction of a function $\rho(r)$ such that $P_\varphi(t) \in P_\varphi(0) + [-\rho(r(t)), \rho(r(t))]$ for t the time between an aphelion and the following perihelion. Using $\rho(r)$ and some data from rigorous integration (sect. 2.2.7), one can prove the following lemma.

Lemma 2.2.2 (Bounds on change in angular momentum)**.** *Assume* $\mu = 10^{-3}$, $J_0 = 1.8$, *and* $P_\varphi(t) \in [1.66, 1.81]$ *(i.e.* $e(t) \in [0.48, 1.04]$*) for a sufficiently long time interval. Then*

1. *When approaching a perihelion from the previous aphelion (or from infinity), angular momentum does not change by more than* 0.0216μ *over the entire outside region.*

2. *When approaching a perihelion from the previous aphelion (or from infinity), angular momentum does not change by more than* 4.449μ.

3. *Angular momentum won't change by more than* 1.444μ *after an R–Solar passage.*

Moreover by time reversal the same bounds hold when leaving the Sun, and are valid until the next aphelion.

It is not hard to prove (see appendix B.1):

Lemma 2.2.3. *For $\mu = 10^{-3}$ and $J_0 = 1.8$, then $\rho(r) \leq \frac{18.2\mu}{r^3}$ for $r \geq 1.6$. Moreover $\rho(r) \leq \frac{2.7\mu}{r^3}$ for $r \geq 5$.*

This should not come as a great surprise since $P_\varphi(t) - P_\varphi(0) = \int_0^t -\frac{\partial \Delta H}{\partial \varphi} dt$, so angular momentum changes solely due to the perturbation term which is of order $O(\frac{\mu}{r^3})$.

2.2.2 Elongated Solar Passages

In section 2.1.6, it was assumed that the $(5, R)$ and $(R, 5)$ segments of an R–Solar passage were pieces of the 2BP(SC) corresponding to parabolic motion. This is unnatural for low eccentricity orbits where the comet does not make large R–Solar passages. It more accurate to use pieces of elliptic orbits. From formula (2.4), observe that it is in our favor for the comet to spend as much time as possible in the outside region since $\lambda_\pm \to 1$ as $T_{out} \to \infty$. By Kepler's Second Law, the comet moves the slowest, and hence spends the most time near an aphelion [AKN]. When constructing the test curve γ_{test}, this is exploited and instead of using $(5, R)$ and $(R, 5)$ segments, pieces of elliptic trajectory which have aphelions are used. Specifically start the comet at $r = 5$, advance to an aphelion $r = R$, and move back to $r = 5$. Call this a $(5, R, 5)$ *segment*. Now consider curves γ that decompose into (see fig. 2.5)

- γ^- – a $(5, R_1, 5)$-segment, defined for $t_1 \leq t_5$
- γ^{in} – a 5–Solar passage, defined for $t_5 \leq t_5'$
- γ^+ – a $(5, R_2, 5)$-segment, defined for $t_5' \leq t_2$

Call these curves *elongated Solar passages*. Such curves exist by an argument similar to Lemma 2.1.2, under the additional assumption that $e(t) \leq 1 - \epsilon$ for some $\epsilon > 0$ for a sufficiently long time interval. This additional condition simply says that in order to have a elongated Solar passage, the comet's eccentricity must stay strictly below $e = 1$ for a long time enough time to allow for the existence of the two aphelions.

Figure 2.5: An example of a elongated Solar passage

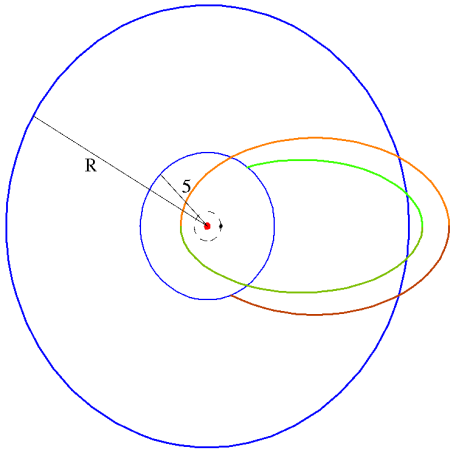

2.2.3 Asymmetry in the Outside Region

The approximations on the RCP3BP made with parabolic 2BP(SC) motions in 2.1.6 made use of the fact that the 2BP(SC) approximation of γ^- and γ^+ before and after a 5–Solar passage were the same. This is not true in general (see fig.

2.5). When the comet passes through the kick region, Jupiter changes the angular momentum of the comet. This changes the orbit of the comet in the outside region. In fact, this is the mechanism which allows capture and escape to occur. The change in angular momentum after a 5–Solar passage means the aphelions before and after the 5–Solar passage are different, i.e. in general $R_1 \neq R_2$ in a elongated Solar passage. This means that γ^- and γ^+ spend different amounts of time in the outside region, and hence λ_- and λ_+ are not directly related.

Previously, the computation for the action comparison in the case of parabolic motions in the outside region could be worked out by hand in a short amount of time. The case of elliptic motions involves more complex integrals and it becomes necessary to use a computer to estimate them. These estimates in the outside region, as well as the rigorous numerical integration used in the kick region, work by so called interval arithmetic (see appendix E.1). Since the numerical integrator only works for efficiently shorter intervals of time (e.g. 5–Solar passages), then work must be done to set up estimates in a way to minimize computer run-time. At the same time, the estimates must efficiently capture the behavior in the outside region which is done by less accurate by hand computations. Machinery shall be developed to overcome both technical difficulties at once.

Consider a elongated Solar passage γ, and suppose the angular momentum satisfies $P_\varphi(t) \in \mathcal{I}_-$ for all $t \in [t_1, t_5]$, i.e. where γ^- is defined. Let $P_\varphi(t_5)$ denote the angular momentum at the start of the 5–Solar passage γ^{in}, and suppose $P_\varphi(t_5) \in \mathcal{I}$. The size of the interval $\mathcal{I}$ is ultimately chosen to make the rigorous numerics work efficiently on a computer. Suppose the angular momentum satisfies $P_\varphi(t) \in \mathcal{I}_+$ for

all $t \in [t_5', t_2]$, i.e. where γ^+ is defined.

Given $\mathcal{I}$, its possible to derive enclosures for $\mathcal{I}_\pm$ using Lemma 2.2.2. For example, in order to reach the interval $\mathcal{I}$ at time t_5, initial conditions must be contained in $\mathcal{I} + [-2\rho(5), 2\rho(5)] = \mathcal{I}_-$ since this accounts for a change in angular momentum in the outside region. The bound of $2\rho(5)$ is because the comet passes between $r = 5$ and the aphelion twice, once leaving the Sun, and once approaching.

Let $(\Delta P_\varphi)_{kick}(\mathcal{I})$ denote the enclosure of possible changes in angular momentum after passing through the kick region when entering with angular momentum $P_\varphi \in \mathcal{I}$. (This quantity is rigorously estimated in a later subsection.) This means that when leaving the kick region, $P_\varphi \in \mathcal{I} + (\Delta P_\varphi)_{kick}(\mathcal{I})$. Then when the comet is leaving the Sun and is in the outside region, $P_\varphi \in \mathcal{I} + (\Delta P_\varphi)_{kick}(\mathcal{I}) + 2[-\rho(5), \rho(5)] = \mathcal{I}_+$. For (non-elongated) R-Solar passages, the factor of 2 can be removed.

2.2.4 Bounds on Time and Radius

All of equations (2.5) shall be estimated in detail. Suppose $\mathcal{I} = P_\varphi^* + [-w, w]$ and $|(\Delta P_\varphi)_{kick}(\mathcal{I})| \leq M$. Call $[-w, w]$ the *window* around P_φ^*. It is an artifact of the rigorous numerics. Use $()^\pm$ to denote upper and lower bounds (see appendices E.1 and A). Lower case letters denote values before the 5–Solar passage and upper case letters denote values after the 5–Solar passage respectively. Let

$$c^\pm := J_0 - P_\varphi^* \pm \left(2\rho(5) + w + (|\Delta H|)^+(5)\right)$$
$$C^\pm := J_0 - P_\varphi^* \pm \left(2\rho(5) + w + M + (|\Delta H|)^+(5)\right)$$

Clearly the above quantities bound $C = J_0 - P_\varphi + \Delta H$ before and after

a 5–Solar passage. (The formal definitions of $(|\Delta H|)^+(r)$ and $\rho(r)$ are found in appendices A.1 and B.1 respectively.)

The 2BP(SC) is an integrable system and specifying Jacobi constant J_0 and P_φ specifies the shape of the ellipse of orbit. Let $\text{2BP}\big(r_0, \varphi_0; J_0, P_\varphi(0)\big)$ denote the 2BP(SC) with initial conditions (r_0, φ_0), $H_{2BP(SC)} = -J_0$, and $P_\varphi = P_\varphi(0)$. Since $\mu = 10^{-3}$, then the RCP3BP(μ, J_0) with the same initial conditions behaves like $\text{2BP}\big(r_0, \varphi_0; J_0, P_\varphi(0)\big)$ if r_0 is sufficiently large. For $J_0 = 1.8$ and a given $(r_0, \varphi_0, P_\varphi^*)$, consider the four special Sun-Comet two body problems with initial conditions $P_\varphi(0) \equiv P_\varphi^* \pm (2\rho(5) + w)$, $P_\varphi(0) \equiv P_\varphi^* \pm (2\rho(5) + w + M)$. Call the 2BPs with these angular momenta the *extreme 2BPs* with respect to P_φ^*. These shall be used to approximate the RCP3BP far from the Sun.

Consider an elongated Solar passage γ of the RCP3BP with angular momentum $P_\varphi(t_5) \in \mathcal{I} = P_\varphi^* + [-w, w]$ at the start of a 5–Solar passage. Then for $t \in [t_1, t_5]$, γ has $P_\varphi(t) \in P_\varphi^* \pm (2\rho(5) + w)$. This is to say that the angular momentum ns the RCP3BP is bounded in between that of the extreme 2BP's with $P_\varphi(0) \equiv P_\varphi^* \pm (2\rho(5) + w)$ in the outside region. A similar statement can be made about times $t \in [t_5', t_2]$.

Examination of formulas (2.5) indicates that by bounding P_φ, a bound on the time spent in the outside region may also be obtained. Moreover, once bounds on time are obtained, these can be used to obtain bounds on the action in the outside region. Hence in order to carry out the action comparison rigorously using the elongated Solar passages for RCP3BP, it is suffices to carry it out using extreme 2BP approximations in the outside region. The values of action for RCP3BP are

contained within the range of values obtained by performing the action comparison using extreme 2BPs.

For small w it follows from Lemma 2.2.2 that the range of angular momenta is not more than 3μ between the extreme 2BPs, so in the outside region away and away from nearly parabolic motions (e.g. $e < 0.96$), there are not any qualitative differences which arise from using the extreme 2BP approximations. For nearly parabolic motions $e > 0.96$, a similar analysis holds if extreme 2BP approximations are used for R–Solar passages. In practice, the window sizes w are selected large enough to be amenable to the rigorous numerics, but not so large as to introduce qualitatively different phenomenon.

In light of the integrals in appendix D, note that for the 2BP(SC), the time from the aphelion to $r = 5$ is given by

$$T_{out} = \frac{I_1(r_-, r_+, 5, r_+)}{\sqrt{2(J_0 - P_\varphi)}}$$

where r_- and r_+ are given in formula 2.5. For the RCP3BP, these quantities can be estimated as

$$\begin{aligned}
r_-^{\pm} :=& \frac{(P_\varphi^* \pm 2\rho(5) \pm w)^2}{1 + \sqrt{1 - 2(c^{\pm})(P_\varphi^* \pm 2\rho(5) \pm w)^2}} \\
r_+^{\pm} :=& \frac{1 + \sqrt{1 - 2(c^{\mp})(P_\varphi^* \mp 2\rho(5) \mp w)^2}}{2(c^{\mp})} \\
R_-^{\pm} :=& \frac{(P_\varphi^* \pm 2\rho(5) \pm w \pm M)^2}{1 + \sqrt{1 - 2(C^{\pm})(P_\varphi^* \pm 2\rho(5) \pm w)^2}} \\
R_+^{\pm} :=& \frac{1 + \sqrt{1 - 2(C^{\mp})(P_\varphi^* \mp 2\rho(5) \mp w \mp M)^2}}{2(C^{\mp})}
\end{aligned}$$

Remarks on Notation: All of these quantities are functions of P_φ^*, w, M, and J_0. The above notation is adopted for brevity. Note that lower bounds are denoted $()^-$, upper bounds are denoted $()^+$, and the subscripts $()_\pm$ indicate different extreme 2BPs. Furthermore the when reading the expressions, adopt the convention that $x^\pm = a \pm b \pm c$ means $x^\pm = a \pm (b + c)$, i.e. specifying a sign choice on the left hand sign specifies all choices on the right hand side. This notation avoids overuse of parenthesis. Conceptually, one should think of such expressions as intervals. For example to understand $(P_\varphi^* \pm 2\rho(5) \pm w \pm M)$, it is easier to think of it as some bound on $P_\varphi(t)$ over some range of time.

For RCP3BP, let $t_{out} = t_5 - t_1$ be the time γ^- spends in the outside region, i.e. the time spent from initial conditions until the start of 5–Solar passage. Let $T_{out} = t_2 - t_5'$ be the time γ^+ spends in the outside region, i.e. the time spent from the end of 5–Solar passage until the final conditions. These times will be estimated shortly.

Estimate on quantities in the action comparison can be obtained from the estimates on P_φ, ΔH, r^{perih}, and r^{apoh}. Define

$$b_{out}^\pm(k) := \frac{I_k(r_-^\pm, r_+^\mp, 5, r_+^\mp)}{\sqrt{2(c^\mp)}} \qquad B_{out}^\pm(k) := \frac{I_k(R_-^\pm, R_+^\mp, 5, R_+^\mp)}{\sqrt{2(C^\mp)}}$$

where the I_k are integrals defined in appendix D. The signs of $()_\pm^\pm$ are chosen so that they are all consistent with using a single extreme 2BP for each of the 4 possible bounds $b_{out}^\pm$, $B_{out}^\pm$. It follows that $t_{out} \in 2[b_{out}^-(1), b_{out}^+(1)]$ and $T_{out} \in 2[B_{out}^-(1), B_{out}^+(1)]$. The factor of 2 comes from the fact the distance from $r = 5$ to an aphelion is traversed twice in an elongated Solar passage. The other values of k

are used later. In the case of an R-Solar passage, the factor of 2 can be removed.

2.2.5 λ estimates

If $(r(t), \varphi(t), \dot{r}(t), \dot{\varphi}(t))$ is a solution to the Euler-Lagrange equations, then the rescaled trajectory

$$\left(r(\frac{t}{\lambda}), \varphi(\frac{t}{\lambda}), \lambda\dot{r}(\frac{t}{\lambda}), \lambda\dot{\varphi}(\frac{t}{\lambda})\right) = \big(r_\lambda(t), \varphi_\lambda(t), \dot{r}_\lambda(t), \dot{\varphi}_\lambda(t)\big)$$

is also a solution to the Euler-Lagrange equations. The equations of motion give

$$\dot{\varphi} = -1 + \frac{P_\varphi}{r^2} \qquad\qquad \dot{\varphi_\lambda} = (-1 + \frac{P_\varphi}{r^2})\lambda$$

Hence

$$\varphi(t) = \varphi(0) - t + \int_0^t \frac{P_\varphi(s)}{r(s)^2} ds \qquad \varphi_\lambda(t) = \varphi(0) - \lambda t + \lambda \int_0^t \frac{P_\varphi(s)}{r(s)^2} ds$$

Now compute the differences in angle over time and solve for λ to get

$$\lambda(t) = 1 - \frac{\varphi_\lambda(t) - \varphi(t)}{t - \int_0^t \frac{P_\varphi(s)}{r^2(s)} ds} \tag{2.6}$$

This formula is used for λ as opposed to formula (2.4) since it explicitly uses the motion of the comet in the rotating frame whereas formula (2.4) made the approximation that the comet rotates with speed 2π (or equivalently does not rotate at all in the fixed frame). This is not necessarily a big difference in the outside region, but nonetheless must be justified. Formula (2.6) says how much of a rescaling λ is needed if the difference $\Delta\varphi = \big(\varphi_\lambda(t) - \varphi(t)\big)$ of angles is specified from the rescaled and original trajectories at time t. Note that when using formula (2.6), it is more convenient to calculate the difference in angles at the start of the 5–Solar passage

γ^{in} since then estimates of λ require only data about the outside region. Define the angles $\varphi^{t_5}_{max}(P_\varphi)$ and $\varphi^{t_5}_{min}(P_\varphi)$ such that

$$A_{in}(P_\varphi, \varphi^{t_5}_{max}(P_\varphi)) := \max_\gamma A(\gamma^{in}) \qquad A_{in}(P_\varphi, \varphi^{t_5}_{min}(P_\varphi)) := \min_\gamma A(\gamma^{in})$$

where the minimum and maximum are taken over all elongated Solar passages on the energy surface $\mathcal{S}(J_0)$ with angular momentum $P_\varphi(t_5) = P_\varphi$ at the start of 5–Solar passage (compare to (2.2)). Define the difference in action and angle with respect to an interval of initial conditions to be (compare to (2.3)):

$$\Delta A^{min}_{in}(\mathcal{I}) := \min_{P_\varphi \in \mathcal{I}} \left(A_{in}(P_\varphi, \varphi^{t_5}_{max}(P_\varphi)) - A_{in}(P_\varphi, \varphi^{t_5}_{min}(P_\varphi)) \right)$$

$$\Delta\varphi^{t_5}(\mathcal{I}) := \varphi^{t_5}_{max}(\mathcal{I}) - \varphi^{t_5}_{min}(\mathcal{I})$$

As defined, $\Delta\varphi^{t_5}(\mathcal{I})$ is an interval and methods to enclose it are developed shortly. Using $\Delta\varphi^{t_5}$ is acceptable since this new difference in angles with the newly defined minimal and maximal angles will flow into solutions with perihelion angles which minimize or maximize action. Hence the Bad Angles Theorem still applies. The test curve γ_{test} is constructed as in section 2.1.6 by means of slowing down on γ^-_{test}, making a cheaper 5-Solar passage on γ^{in}_{test}, and speeding up on γ^+_{test}.

Now estimate $\lambda_\pm$ using each of the extreme 2BPs listed in section 2.2.4. First estimate

$$\int_0^t \frac{P_\varphi(s)}{r^2(s)} ds = \int_{r(0)}^{r(t)} \frac{dr}{\dot{r} r^2} = \int_{r_0}^{r_1} \frac{P_\varphi dr}{\sqrt{2(J_0 - P_\varphi + \Delta H) r (r^{apoh} - r)(r - r^{perih})}}$$

which for motions away from $e = 1$ looks like the integral I_{-1} from appendix D

multiplied by P_φ. Let

$$d := [(P_\varphi^* - 2\rho(5) - w) \cdot b_{out}^-(-1), (P_\varphi^* + 2\rho(5) + w) \cdot b_{out}^+(-1)]$$

$$D := [(P_\varphi^* - 2\rho(5) - w - M) \cdot B_{out}^-(-1), (P_\varphi^* + 2\rho(5) + w + M) \cdot B_{out}^+(-1)]$$

Let $\lambda_\pm(\mathcal{I})$ denote the interval of scalings $\lambda_\pm$ needed for construct the test curves γ_{test} corresponding to γ_{max}, an elongated Solar passage with perihelion angle φ_{max}^{perih} and $P_\varphi(t_5) \in \mathcal{I}$. Then let

$$\lambda_-^\pm(\mathcal{I}) := 1 - \frac{(\Delta\varphi(t_5))(\mathcal{I})}{2\big([b_{out}^-(1), b_{out}^+(1)] - d\big)} \quad \lambda_+^\pm(\mathcal{I}) := 1 + \frac{(\Delta\varphi(t_5))(\mathcal{I})}{2\big([B_{out}^-(1), B_{out}^+(1)] - D\big)}$$

The signs in $\lambda_\pm^\pm$ come about by examining the action comparison in the kick region and noting the angle corresponding to maximal action comes after the angle corresponding to the minimal action, i.e. it is less than π to the right of φ_{min}^{perih}, and more than π to the left on the circle (see fig 2.4). A slower moving the comet has $\lambda_- < 1$ which has action in the kick region between the maximum action and the minimum action Thinking of this another way, since $\dot{\varphi} < 0$, slowing down means spending more time in the outside region, which means φ decreases. The factor of 2 in the denominator can be removed when considering R-Solar passages.

2.2.6 Action Decomposition

Using $H = -J_0$, it follows that for elliptic motions $\frac{\langle v,v\rangle}{2} = \frac{P_r^2}{2} + \frac{P_\varphi^2}{2r^2} = \frac{1}{r} - \Delta H - J_0 + P_\varphi$ where $v = \dot{\gamma}_{max}$. The rescaled action for the elliptic case is

$$\begin{aligned} A(\lambda, t_0, t_1) &= \int_{t_0\lambda}^{t_1\lambda} (\frac{\lambda^2 \langle v, v\rangle}{2} + \frac{1}{r} - \Delta H)(\frac{t}{\lambda})dt \\ &= \lambda \int_{t_0}^{t_1} (\lambda^2(\frac{1}{r} - \Delta H - J_0 + P_\varphi) + \frac{1}{r} - \Delta H)(u)du \\ &= \int_{t_0}^{t_1} \frac{\lambda^3 + \lambda}{r} dt + \int_{t_0}^{t_1} \lambda^3(-J_0 + P_\varphi)dt + \int_{t_0}^{t_1} (\lambda^3 + \lambda)(-\Delta H)dt. \end{aligned}$$

Define

$$\begin{aligned} A_P(\lambda, t_0, t_1) &:= \int_{t_0}^{t_1} \frac{\lambda^3 + \lambda}{r} dt \\ A_K(\lambda, t_0, t_1) &:= \int_{t_0}^{t_1} \lambda^3(-J_0 + P_\varphi)dt \\ A_{\Delta H}(\lambda, t_0, t_1) &:= \int_{t_0}^{t_1} (\lambda^3 + \lambda)(-\Delta H)dt \end{aligned}$$

so that $A = A_P + A_K + A_{\Delta H}$. To do the action comparison one must to estimate

$$\begin{aligned} &A(1, t_{out}) - A(\lambda_-, t_{out}) + A(1, T_{out}) - A(\lambda_+, T_{out}) \\ &= A_P(1, t_{out}) - A_P(\lambda_-, t_{out}) + A_P(1, T_{out}) - A_P(\lambda_+, T_{out}) \\ &\quad + A_K(1, t_{out}) - A_K(\lambda_-, t_{out}) + A_K(1, T_{out}) - A_K(\lambda_+, T_{out}) \\ &\quad + A_{\Delta H}(1, t_{out}) - A_{\Delta H}(\lambda_-, t_{out}) + A_{\Delta H}(1, T_{out}) - A_{\Delta H}(\lambda_+, T_{out}) \end{aligned}$$

To estimate each of these terms, the strategy is to get lower and upper bounds by using the extreme 2BP's.

2.2.6.1 $A_{\Delta H}$ estimates

$$
\begin{aligned}
&A_{\Delta H}(1, t_{out}) - A_{\Delta H}(\lambda_-, t_{out}) + A_{\Delta H}(1, T_{out}) - A_{\Delta H}(\lambda_+, T_{out}) \\
&\quad = \int_{t_{out}} (2 - \lambda_-^3 - \lambda_-)(-\Delta H)dt + \int_{T_{out}} (2 - \lambda_+^3 - \lambda_+)(-\Delta H)dt \\
&\quad \in 2[b_{out}^-(1), b_{out}^+(1)](2 - [\lambda_-^-, \lambda_-^+]^3 - [\lambda_-^-, \lambda_-^+]) \cdot (|\Delta H|)^+(5)[-1, 1] \\
&\quad + 2[B_{out}^-(1), B_{out}^+(1)](2 - [\lambda_+^-, \lambda_+^+]^3 - [\lambda_+^-, \lambda_+^+]) \cdot (|\Delta H|)^+(5)[-1, 1]
\end{aligned}
$$

This term is small, usually of the order $10\mu^2$, and no additional refinements need to be made to this estimate.

2.2.6.2 A_K estimates

Estimate

$$
\begin{aligned}
&A_K(1, t_{out}) - A_K(\lambda_-, t_{out}) + A_K(1, T_{out}) - A_K(\lambda_+, T_{out}) \\
&\qquad = \int_{t_{out}} \left(1 - \lambda_-^3\right)(-J_0 + P_\varphi)dt + \int_{T_{out}} \left(1 - \lambda_+^3\right)(-J_0 + P_\varphi)dt
\end{aligned}
$$

using the extreme 2BPs. To keep notation simple, let $\min(\mathcal{I}_-) = m_-$, $\max(\mathcal{I}_-) = m_+$, $\min(\mathcal{I}_-) = M_-$, and $\max(\mathcal{I}_+) = M_+$.

$$
\begin{aligned}
&\int_{t_{out}} \left(1 - \lambda_-^3\right)(-J_0 + P_\varphi)dt + \int_{T_{out}} \left(1 - \lambda_+^3\right)(-J_0 + P_\varphi)dt \\
&\quad \subset 2[\left(b_{out}^-(1)\right) \cdot \left(1 - (\lambda_-^-)^3\right) \cdot \left(- J_0 + m_-\right), \left(b_{out}^+(1)\right) \cdot \left(1 - (\lambda_-^+)^3\right) \cdot \left(- J_0 + m_+\right)] \\
&\qquad + 2[\left(B_{out}^-(1)\right) \cdot \left(1 - (\lambda_+^+)^3\right) \cdot \left(- J_0 + M_-\right), \left(B_{out}^+(1)\right) \cdot \left(1 - (\lambda_+^-)^3\right) \cdot \left(- J_0 + M_+\right)]
\end{aligned}
$$

Note the logic of the interval bounds. For example $b^-_{out}(1)$ is paired with λ^-_- and m_- since smaller angular momentum means a smaller aphelion, meaning less time is spent in the outside region, i.e. a smaller t_{out}, and less time in the outside region means a worse λ value, i.e. farther from one, i.e. a smaller $\lambda_- < 1$. The logic for the other pairings is similar.

2.2.6.3 A_P estimates

Now estimate

$$\begin{aligned} &A_P(1, t_{out}) - A_P(\lambda_-, t_{out}) + A_P(1, T_{out}) - A_P(\lambda_+, T_{out}) \\ &\qquad = \int_{t_{out}} \frac{2 - (\lambda_-^3 + \lambda_-)}{r} dt + \int_{T_{out}} \frac{2 - (\lambda_+^3 + \lambda_+)}{r} dt \end{aligned}$$

using the extreme 2BPs. Note that these integrals look like I_0 from appendix D after appropriate change of variables. To keep notation simple, let $\min(\mathcal{I}_-) = m_-$, $\max(\mathcal{I}_-) = m_+$, $\min(\mathcal{I}_-) = M_-$, and $\max(\mathcal{I}_+) = M_+$.

$$\begin{aligned} &\int_{t_{out}} \frac{2 - (\lambda_-^3 + \lambda_-)}{r} dt + \int_{T_{out}} \frac{2 - (\lambda_+^3 + \lambda_+)}{r} dt \\ &\quad \subset 2[\big(b^-_{out}(0)\big) \cdot \big(2 - (\lambda^-_-)^3 - \lambda^-_-\big), \big(b^+_{out}(0)\big) \cdot \big(2 - (\lambda^+_-)^3 - \lambda^+_-\big)] \\ &\qquad + 2[\big(B^+_{out}(0)\big) \cdot \big(2 - (\lambda^-_+)^3 - \lambda^-_+\big), \big(B^-_{out}(0)\big) \cdot \big(2 - (\lambda^+_+)^3 - \lambda^+_+\big)] \end{aligned}$$

Remark: The bounds for A_P, A_K, and $A_{\Delta H}$ are readily computable on a computer. It is fairly easy to develop formulas to handle the action comparison for nearly parabolic motions using standard R-Solar passages. After some initial setup, the formulas from this section remain almost unchanged. See appendix D.2 for details.

2.2.7 Rigorous Computation of Action in the Kick Region

In this subsection precise estimates on how action varies in the kick region are developed for $\mu = 10^{-3}$ and $J_0 = 1.8$. The CAPD package is programmed to rigorously integrate trajectories over 5–Solar passages and record $\Delta A_{in}^{min}(\mathcal{I})$, $\Delta\varphi^{t_5}(\mathcal{I})$, $(\Delta P_\varphi)_{kick}(\mathcal{I})$, and the time to cross the kick region.

Theorem 2.2.4. *For RCP3BP*$(0.001, 1.8)$ *and* $P_\varphi \in [1.6875, 1.81]$*, i.e. for* $e \in [0.6, 1.03]$*,*

$$\Delta A_{in}^{min}([1.6875, 1.81]) \geq 15.9748\mu$$

$$\Delta\varphi^{t_5}([1.6875, 1.81]) \leq 1.2495$$

$$|(\Delta P_\varphi)_{kick}([1.6875, 1.81])| \leq 1.40093\mu$$

Furthermore, for $P_\varphi \in [1.71, 1.81]$*, the maximum time to cross the kick region is less than* 19.5256 *time units, i.e. approximately* 3 *revolutions of Jupiter.*

Proof: The CAPD package can be programmed to rigorously integrate trajectories over a 5–Solar passage. This makes use of interval arithmetic to enclosure numerical solutions of ODEs over short periods of time in rigorously verified ϵ-tubes. It works by moving small boxes of initial conditions under the flow. By covering a domain with many small boxes, CAPD can move the entire domain. See appendices E.1 and E.2 for more details on CAPD and interval arithmetic.

Note that action can also be simultaneously solved for when computing the solution to an ODE by noting that since action is the integral of the Lagrangian (2.1) i.e. $A(t) = \int_0^t L(s)ds$, then $\dot{A} = L(t)$, and $L(t)$ depends only on the polar

variables at time t, which are known after one step of the integrator.

For each 5-Solar passage, use initial conditions $A(0) = 0$, $r = 5$, $P_\varphi \in [1.6875, 1.81]$, $\varphi \in \mathbb{T}$. Subdivide $[1.6875, 1.81]$ into 4901 boxes of size 0.000025, and subdivide $[-\pi, \pi]$ into 12567 boxes of size 0.000025. Use the implicit definition of $P_r = \sqrt{2\big(1.8 - \frac{P_\varphi^2}{2r^2} + \frac{2}{r} - \Delta H(r, \varphi)\big)}$ on the energy surface $\mathcal{S}(1.8)$.

Use CAPD with a 5^{th} order Taylor Method and adaptive time-step sizes of $h \leq 0.1$ to rigorously integrate trajectories until they cross $\{r = 5\}$ again. Record the action before and after the box of trajectories crosses $\{r = 5\}$. Then make an interval out of the lower and upper bounds on action while crossing. Since the box is small, with the use of adaptive step size, the width of the action interval is small, and it accurately measures action for the box of initial conditions being integrated over the 5–Solar Passage. Do this for each trajectory with a fixed box of P_φ's, i.e. for $P_\varphi(t_5) \in P_\varphi^* + [-w, w] = \mathcal{I}$ with $w = 0.0000125$ and $P_\varphi^* = 1.6875 + 0.000025k$, $k = 0, .., 4901$. In this fashion the interval $P_\varphi \in [1.6875, 1.81]$ is covered. The action difference for each k is bounded using the largest lower bound of all the action intervals, and smallest upper bound. Actual differences could be larger. Also recorded is the angle of the initial conditions which produces each extremal box, the maximum change in angular momentum for each window of initial condition $\mathcal{I}$, and the exit times.

This gives the data in the statement of the theorem. In fact, this method produces an extensive list of boxes and bounds, i.e. *this method checks a large set of inequalities used in the action comparison.* For each P_φ, there is a picture like figure 2.4. The differences in action are plotted in figure 2.6. □

Figure 2.6: Lower bounds on $\Delta A_{in}^{min}(P_\varphi)$ vs. P_φ

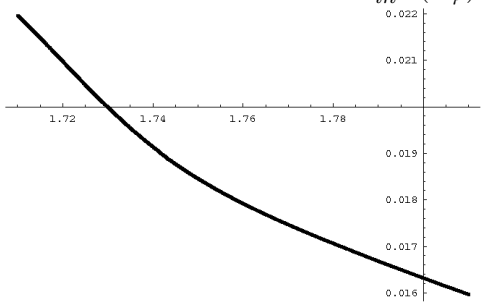

Figure 2.7: Upper bounds on the maximum time to cross the kick region

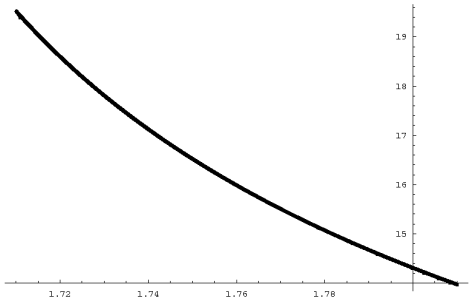

Remark: This setup is expensive and took 15 computers 2 weeks to complete the comparison. Fortunately the integration of each box of initial conditions is independent of the others and the problem naturally lends itself to parallel computation. The programs and data for this procedure are available upon request (see appendix E.2). Note that choice of parameters can effect bounds obtained and running time. For the choice of parameters used in the theorem, the integration time needed to cross the kick region is small, less than 19.5256 time units. For the $\mu = 0.001$ and $J_0 \geq 1.52$, the CAPD integrator works well for the RCP3BP over short time intervals, say for less than 50 time units. However more for lengthy integrations, additional work is needed to validate the behavior of a solution. In appendix E.1.3 a method for long time integration is presented.

Using the above estimates for the outside region, as well as the rigorous in-

tegration data for the kick region, a program was written to compare action. The result is the estimate in the main theorem that $e^*(0.001, 1.8) \leq 0.66$. The software is general enough to handle other values of μ and J_0. See appendix E.2.

Chapter 3

Action-Angle Variables for the RCP3BP

3.1 An Algebraic Deformation of Action-Angle Variables

In this section, an algebraic deformation of action-angle variables is introduced. The deformed coordinates shall ultimately make it possible to obtain action-angle representations of trajectories with nearly parabolic motions, something Delaunay variables has difficulty with. First let us introduce the class of systems considered and offer a formulation of action-angle variables for this class. Consider an integrable C^r Hamiltonian ($r \geq 3$)

$$H_0(q_1, q_2, p_1, p_2) = \frac{p_1^2}{2} + V_{\text{eff}}(q_1, p_2)$$

with 2 degrees of freedom, where V_{eff} is a C^r ($r \geq 3$) function with a unique minimum in the variable q_1 for a fixed p_2, and suppose the minimum is strictly negative. (If it is not strictly negative, it suffices to add a constant to V_{eff} to ensure this property). The function V_{eff} is typically known as the effective potential.

Suppose $q_1^* = q_1^*(p_2)$ is the unique point minimum point of V_{eff}, i.e. where $\frac{\partial V_{\text{eff}}}{\partial q_1}(q_1^*(p_2), p_2) = 0$. Let $E_{min} = V_{\text{eff}}(q_1^*(p_2), p_2)$ be the minimum value for V_{eff}. Fixing an energy surface $H_0 = E$ implicitly defines one of the variables, say p_2. Let $S_E = \{(q_1, p_1) : H_0(q_1, q_2, p_1, p_2) = E\}$ be the level sets of the Hamiltonian (see fig. 3.1). For $E = E_{min}$ the curve S_E is degenerate and consists of a single

point. For sufficiently small $E \geq E_{min}$, the set S_E is compact and there exists points $q_1^-(E) \leq q_1^*(p_2(E)) \leq q_1^+(E)$ where S_E intersects the axis $p_1 = 0$. Such points exist since H_0 is convex in p_1. Denote the area under the curve S_E by

$$A(E) = \int_{q_1^-(E)}^{q_1^+(E)} \sqrt{2(E - V_{\text{eff}}(q, p_2))} dq$$

Let $L(E) = \frac{A(E)}{2\pi}$. This formula can be inverted to solve for E. Define the inversion

Figure 3.1: Level sets for the 2BP(SC) system in (r, P_r) variables

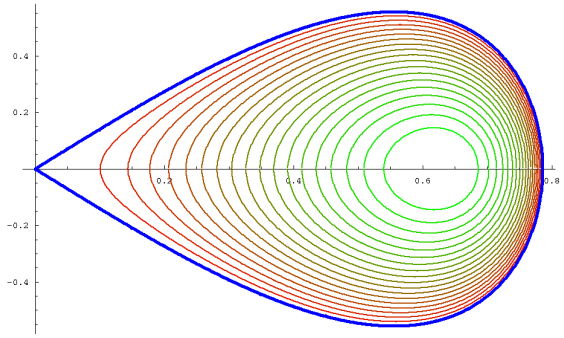

h so that $h(L; p_2) = E$. By Arnold-Liouville, this to produces a generating function

$$S(q_1, q_2, L, G) = q_2 G + \int_{q_1^-(L,G)}^{q_1} \sqrt{2(h(L, G) - V_{\text{eff}}(q, G))} dq$$

and the generating function defines a symplectic change of coordinates from (q_1, q_2, p_1, p_2) to action-angle coordinates (L, ℓ, G, g). Call the change of coordinates Ψ. Notice that Ψ is only well defined when the area $A(E)$ is finite. If the effective potential is such that $A(E) = \infty$ for some $E = E_\infty$, then action-angle variables are not well defined; namely $L \to \infty$ in some spots near $E = E_\infty$. Suppose there exists such an $E_\infty < \infty$. Then action-angle variables are only defined in the region $\Omega_0 = \bigcup_{E \in [E_{min}, E_\infty]} S_E$.

Now if $H = H_0 + \Delta H$, where ΔH is a small perturbation of the integrable Hamiltonian H_0, then the generating function still converts to action-angle variables

in the region Ω_0. However, this region is **not invariant** under the Hamiltonian flow and it is possible for solutions to enter into a region where action-angle coordinates are not well defined. Later in this section, a method is developed to deform the action-angle variables so that they are well defined for a region larger than Ω_0.

3.1.1 Delaunay Variables

As a model for this type of system, consider the action-angle variables for the 2BP which are classically known as Delaunay variables. These variables were originally used to describe bounded motions(i.e. $e \in [0, 1)$) of the 2BP and hence when applied to RCP3BP, Delaunay variables have singularities for motions near $e = 1$, the so called *nearly parabolic motions*. However this is precisely the region where the diffusion is expected. Note that in the rotating frame of coordinates, the Hamiltonian has an additional term from the gyroscopic force. This causes the degeneracies at $e = 1$ to appear when $H_{2BP(SC)} + P_\varphi = 0$, i.e when $P_\varphi = -H_{2BP(SC)} = J_0$ when dynamics is considered on the energy surface $\mathcal{S}(J_0)$. A derivation of Delaunay variables can be found in [GPS], [SS] (also see [AKN] and [CC] for some nice exposition). In short, they arise by considering the generating function

$$S(r, \varphi, L, G) = \varphi G + \int_{r^{perih}(L,G)}^{r} \left(\sqrt{\frac{-1}{L^2} - \frac{G^2}{r^2} + \frac{2}{r}}\right) dr$$

This gives the canonical transformation $\mathcal{D}(\ell, g, L, G) = (r, \varphi, P_r, P_\varphi)$ from Delaunay variables to symplectic polar variables where $r^{perih} = L^2(1 - \sqrt{1 - \frac{G^2}{L^2}})$ is the perihelion of the 2BP(SC) expressed in terms of L, G. The image of $\mathcal{D}$ is only defined

for bounded motions of the 2BP(SC) with $(\ell, g) \in \mathbb{T}^2$ and $0 \leq G \leq L$.

For the 2BP, L^2 is the semi-major axis of the ellipse of the orbit, so by Kepler's Third Law, the period $T = 2\pi L^3$. Upon examination of the generating function observe $G = P_\varphi$ is *angular momentum*, or alternatively LG is the semi-minor axis of the ellipse of the orbit. The variable $\ell \in \mathbb{T}$ is the *mean anomaly* which is $\ell = \pi \mod 2\pi$ at the aphelion, $\ell = 0 \mod 2\pi$ at the perihelion, and in general $(\ell - \ell_0) = \frac{2\pi}{T}t$. The quantity $(g + t)$ can be interpreted as the perihelion angle (in non-rotating coordinates g itself plays this role). The radius r can be expressed in Delaunay coordinates by $r = L^2(1 - e\cos(u))$ where the eccentricity $e = \sqrt{1 - \frac{G^2}{L^2}}$, and u, called *the mean anomaly*, is given implicitly by the

$$u - e\sin(u) = \ell. \tag{3.1}$$

A more detailed description of Delaunay variables can be found in [AKN] or [CC]. Applying the canonical transformation $\mathcal{D}$ to the Hamiltonian for the 2BP(SC) in rotating polar coordinates gives

$$H_{2BP(SC)} \circ \mathcal{D}^{-1} = -\frac{1}{2L^2} - G$$

Note that S satisfies $\det(\frac{\partial^2 S}{\partial(r,\phi)\partial(L,G)}) = \frac{L^3}{P_r} \neq 0$. Hence in general there exists a canonical transformation from polar to Delaunay. It is provided by the above generating function and is well defined inside of the homoclinic loop (see Figure 3.2). Hence where it is well defined, one gets Delaunay variables for RCP3BP using the generating function S. This yields

$$H_{Del} = H_{Polar} \circ \mathcal{D}^{-1} = -\frac{1}{2L^2} - G + \Delta H(L, G, \ell, g), \tag{3.2}$$

where the perturbation term is converted to Delaunay. As the "where it makes sense" indicates, Delaunay variables are not defined for the RCP3BP for nearly parabolic motions. More specifically Delaunay variables are not defined very close to separatrices corresponding to nearly parabolic motions in RCP3BP. It is possible that the perturbation can push a highly elliptic orbit into a hyperbolic orbit with $e > 1$ (in fact this is desired in Theorem 1.1.2). In Delaunay variables, this corresponds to $L \to \infty$ and occurs near places where the separatrices leave the homoclinic loop of the 2BP(SC) in which Delaunay variables are defined (see Figure 3.2).

Figure 3.2: Deviation of RCP3BP Separatrices (colored) from 2BP(SC) Homoclinic loop (blue) in $(\frac{1}{\sqrt{r}}, P_r)$ variables

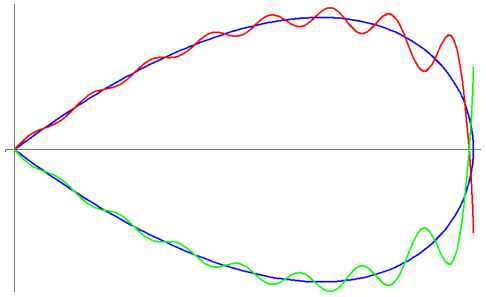

3.1.2 An Algebraic Deformation

To overcome the technical issue that action-angle variables are not well defined near separatrices, an approach to enlarge the domain where action-angle variables are well defined is sought. Geometrically the approach corresponds to encapsulating the separatrices in a larger domain (see Figure 3.3). Mathematically, the trick reduces to applying the Arnold-Liouville theorem with a different integrable Hamiltonian on a nearby energy surface to produce a different domain where action-

angle-variables are well defined. The energy should be chosen so that the size of the new domain is large enough to capture behaviors of trajectories which are close to the separatrices. To illustrate the trick for the RCP3BP, consider action-angle variables for the Hamiltonian

$$H_\nu(r, P_r, P_\varphi) := \frac{P_r^2}{2} + \frac{(P_\varphi - \nu)^2}{2r^2} - \frac{1}{r} \tag{3.3}$$

Action-angle variables are defined inside of bounded level sets corresponding to $H_\nu < 0$. In fact for appropriate choice of ν, these sets contains a large enough part of nearly parabolic motions for RCP3BP(μ, J_0).

The parabolic separatrices for the RCP3BP, denoted by $\mathcal{P}_\mu^+$ (resp. $\mathcal{P}_\mu^-$), are defined to be the set of points (r, φ, P_r) such that $(r, \varphi, P_r)(0) = (r_0, \varphi_0, 0)$, $P_r(t) > 0$ for all $t > 0$ (resp. $P_r(t) < 0$ for all $t < 0$), and $\lim_{t\to\infty} P_r(t) = 0$ (resp. $\lim_{t\to-\infty} P_r(t) = 0$). In the case of 2BP(SC), then separatrices on the energy surface $\mathcal{S}^{out}(J_0)$ are given for all $\varphi_0 \in \mathbb{T}$ by

$$(r, P_r)^\pm = \left(r, \pm\sqrt{\frac{2}{r} - \frac{J_0^2}{r^2}}\right) \tag{3.4}$$

A theorem of McGehee [McG] guarantees these objects exist and are one dimensional C^∞ smooth manifolds for all μ. In the case of μ small, more can be said.

Theorem 3.1.1. *There exists $\nu = \nu(\mu, J_0)$ such that the forward and backward separatrices $(r, P_r)^\pm(\varphi_0)$ of RCP3BP(μ, J_0) are contained inside the homoclinic loop given by $H_\nu(r, P_r, J_0) = 0$ for all $\varphi_0 \in \mathbb{T}^1$. In particular, when $J_0 = 1.8$ and $\mu = 0.001$, then $\nu \leq 2.8\mu$.*

Proof of this theorem is contains in appendix C.3. Theorem 3.1.1 encloses the nearly parabolic solutions of the RCP3BP on the energy surface $\mathcal{S}^{out}(J_0)$ inside of the

Figure 3.3: Containment of RCP3BP separatrices inside the larger homoclinic loop of H_ν in $(\frac{1}{\sqrt{r}}, P_r)$ variables

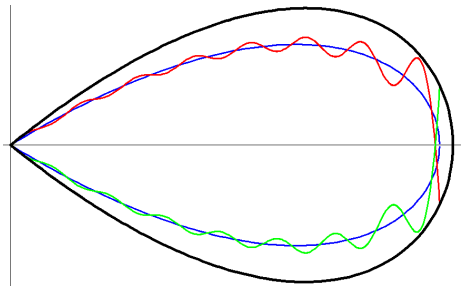

homoclinic loop defined by $H_\nu(r, P_r, J_0) = 0$. Make a canonical change of variables to action-angle coordinates inside of this loop via the Arnold-Liouville theorem. Call the map inducing the change of coordinates $\mathcal{D}_\nu : (L_\nu, G_\nu, \ell_\nu, g_\nu) = (r, \varphi, P_r, P_\varphi)$ and call the coordinates $\mathcal{D}_\nu(L_\nu, G_\nu, \ell_\nu, g_\nu)$ given by $\mathcal{D}_\nu$ *algebraically deformed Delaunay variables (ADDV)*. Note that $\mathcal{D}_\nu = \mathcal{D} \circ (P_\varphi \mapsto P_\varphi - \nu)$ so $\mathcal{D}_\nu$ is clearly a canonical change of coordinates. Specifically $dr \wedge dP_r + d\varphi \wedge dP_\varphi = dL_\nu \wedge d\ell_\nu + dG_\nu \wedge dg_\nu$.

Remark: It is important to note that no dynamics is being used from the formal Hamiltonian H_ν. It is only used to define the domain of definition $\mathcal{D}_\nu$.

The new homoclinic loop defined by $H_\nu(r, P_r, J_0) = 0$ inside of which ADDV are well defined contains the homoclinic loop $H_{2BP(SC)}(r, P_r, J_0) = -J_0$ (see formula 1.2 for definition of $H_{2BP(SC)}$) in which the original Delaunay variables were defined (see fig. 3.3). Because the new loop is larger, some solutions whose positions in polar coordinates that could not be expressed in Delaunay now have representations in ADDV. Note that ADDV also becomes undefined, however, it does so away from the separatrices of H_{Polar} on the energy surface $\mathcal{S}^{out}(J_0)$.

3.1.2.1 The relation between Delaunay and ADDV

One might wonder how Algebraically Deformed Delaunay Variables (ADDVs) are related to the usual Delaunay variables. By definition, the ADDVs $(L_\nu, G_\nu, \ell_\nu, g_\nu)$ are the action-angle variables for the Hamiltonian H_ν which are 'close' to those of the 2BP Hamiltonian. Indeed when $\nu = 0$ they are the Delaunay variables. By construction one can see that immediately that $G_\nu = G - \nu$. From examination of the Hamiltonians, it can also be shown that $\frac{1}{L_\nu^2} = \frac{1}{L^2} + 2\nu$. Geometrically, for a fixed energy, the lobes in ADDV have more area than the lobes in Delaunay and the variables L,L_ν measure the area of such lobes. This has the effect that L_ν is finite in regions where L has become infinity. The relations to convert from symplectic polar to ADDV can be derived by noting $\mathcal{D}^{-1} \circ \mathcal{D}_\nu = (P_\varphi \mapsto P_\varphi - \nu)$. For example, $r = L_\nu^2(1 - e_\nu \cos(u_\nu))$, where $u_\nu - e_\nu \sin(u_\nu) = \ell_\nu$ and $e_\nu = \sqrt{1 - \frac{G_\nu^2}{L_\nu^2}}$. It is not hard to show that $e_\nu \leq e$ and the deformation can be thought of as 'eccentricity decreasing' in some sense.

3.2 Twisting in Delaunay and Deformed Delaunay

Consider the Poincaré section $P = \{g = 0 \mod 2\pi\} \subset \mathcal{S}(J_0)$. Lemma A.3.2 shows that $-1.025 \leq \dot{g} \leq -0.9975$ for $J_0 = 1.8$ and $\mu \leq 10^{-3}$, and hence P is well defined. Consider the Poincaré return map $\mathcal{F} : \mathcal{S}^{out}(J_0) \cap P \mapsto \mathcal{S}^{out}(J_0) \cap P$ defined by

$$\mathcal{F} = \mathcal{F}_{\mu,J_0} : (\ell_0, L_0) \mapsto (\ell_1, L_1) = \big(\ell(t_\Gamma, \ell_0, L_0), L(t_P, \ell_0, L_0)\big) \tag{3.5}$$

where $t_P > 0$ is the first return time to P. In this section, the return map $\mathcal{F}$ is shown to be an exact area preserving twist (EAPT) map in Delaunay coordinates for a region

$L \in [L^-_{twist}(\mu, J_0), L^+_{twist}(\mu, J_0)]$. (See [Ban], [MF], [Mo1], [G], and [S] for exposition on EAPT maps.) Numerically a computer can find $[1.611, 15.94] \subset [L^-_{twist}, L^+_{twist}]$ for $\mu = 10^{-3}$ and $J_0 = 1.8$. This translates into $[0.07, 0.994] \subset [e^-_{twist}, e^+_{twist}]$ and gives the twist region Tw^{Del}. It turns out that similar methods can be used to find the twist region in ADDV; this is discussed at the end of the section.

3.2.1 Twisting Conditions

Our goal is to develop an explicit condition which can be numerically checked to verify twist. The energy reduction formulas found in the appendix C.2 make it possible to write an autonomous Hamiltonian system as a time dependent Hamiltonian. Following the construction for 2 degrees of freedom, fix μ and J_0 so that $H = -J_0$ (i.e. restrict dynamics to $\mathcal{S}(J_0)$) and write $G = G(L, \ell, g, J_0)$ implicitly in terms of the others variables. The construction in appendix C.2 produces a time dependent Hamiltonian $\tilde{H}_{J_0}(L, \ell, \tilde{t})$ where $\tilde{t} = g$ is now the time variable. The construction is well defined since $\dot{g} = -1 + \frac{\partial \Delta H}{\partial G} = -1 + O(\frac{\mu}{L^6}) < 0$ for μ small. Furthermore, from the construction, one can compute

$$\frac{\partial}{\partial L}\tilde{H}_{J_0}(L, \ell, \tilde{t}) = \frac{\left(\frac{\partial H(L,\ell,g,G(L,\ell,g,J_0))}{\partial L}\right)}{\left(\frac{\partial H(L,\ell,g,G(L,\ell,g,J_0))}{\partial G}\right)}$$

Now look at the second derivative with respect to L.

$$\frac{\partial}{\partial L}\left(\frac{\partial \tilde{H}_{J_0}(L,\ell,\tilde{t})}{\partial L}\right) = \frac{\partial}{\partial L}\left(\frac{\left(\frac{\partial H(L,\ell,g,G(L,\ell,g,J_0))}{\partial L}\right)}{\left(\frac{\partial H(L,\ell,g,G(L,\ell,g,J_0))}{\partial G}\right)}\right)$$
$$= \frac{\left(\frac{\partial H}{\partial G}\right)\left(\frac{\partial^2 H}{\partial L^2} + \frac{\partial^2 H}{\partial L \partial G}\frac{\partial G}{\partial L}\right) - \left(\frac{\partial H}{\partial L}\right)\left(\frac{\partial^2 H}{\partial L \partial G} + \frac{\partial^2 H}{\partial G^2}\frac{\partial G}{\partial L}\right)}{\left(\frac{\partial H}{\partial G}\right)^2}$$

There is a $\frac{\partial G}{\partial L}$ to be dealt with. From the Hamiltonian (3.2), G is implicitly defined by

$$G = J_0 - \frac{1}{2L^2} + \Delta H(L,\ell,g,G(J_0,L,\ell,g))$$

Differentiate this expression to obtain

$$\left(\frac{\partial G}{\partial L}\right) = L^{-3} + \left(\frac{\partial \Delta H}{\partial L}\right) + \left(\frac{\partial \Delta H}{\partial G}\right)\left(\frac{\partial G}{\partial L}\right)$$

and solve to find

$$\frac{\partial G}{\partial L} = \frac{L^{-3} + \left(\frac{\partial \Delta H}{\partial L}\right)}{1 - \left(\frac{\partial \Delta H}{\partial G}\right)}$$

One can now compute the partial derivatives of H (see e.g. section A.3) and plug everything into the above expression for $\frac{\partial}{\partial L}\left(\frac{\partial \tilde{H}_{J_0}(L,\ell,\tilde{t})}{\partial L}\right)$. With the aid of a computer it is possible to estimate this term, which is denoted the *twist term*. Let us examine why this derivative is so important now.

3.2.2 Proof of the EAPT property for $\mathcal{F}_\mu$

Since $\mathcal{F}_\mu$ arises as the Poincaré return map of an autonomous 2-degree of freedom Hamiltonian, it is exact and area preserving. The twist condition for $\mathcal{F}_\mu$ is equivalent to $\frac{\partial \ell_1}{\partial L_0} = \frac{\partial \ell(t_P,\ell_0,L_0)}{\partial L_0} < 0$ [Ban],[MF].

Claim: $\frac{\partial}{\partial L}\left(\frac{\partial \tilde{H}_{J_0}(L,\ell,\tilde{t})}{\partial L}\right)$ is of constant sign in a domain Ω if and only if $\mathcal{F}_\mu$ is an exact area preserving twist map in Ω.

Proof: Consider the equations of first variation:

$$\frac{d}{d\tilde{t}}\begin{pmatrix} \frac{\partial \ell}{\partial \ell_0} & \frac{\partial \ell}{\partial L_0} \\ \frac{\partial L}{\partial \ell_0} & \frac{\partial L}{\partial L_0} \end{pmatrix} = \begin{pmatrix} \frac{\partial^2 \tilde{H}_{J_0}}{\partial \ell \partial L} & \frac{\partial^2 \tilde{H}_{J_0}}{\partial L^2} \\ -\frac{\partial^2 \tilde{H}_{J_0}}{\partial \ell^2} & -\frac{\partial^2 \tilde{H}_{J_0}}{\partial \ell \partial L} \end{pmatrix} \begin{pmatrix} \frac{\partial \ell}{\partial \ell_0} & \frac{\partial \ell}{\partial L_0} \\ \frac{\partial L}{\partial \ell_0} & \frac{\partial L}{\partial L_0} \end{pmatrix}.$$

In particular, at time $\tilde{t} = 0$ it holds that

$$\frac{d}{d\tilde{t}}\left(\frac{\partial \ell}{\partial L_0}\right)|_{\tilde{t}=0} = \frac{\partial^2 \tilde{H}_{J_0}}{\partial L^2}|_{\tilde{t}=0}$$

Hence the sign of $\frac{\partial^2 \tilde{H}_{J_0}}{\partial L^2}|_{\tilde{t}=0}$ determines whether $\frac{\partial \ell}{\partial L_0}$ is decreasing or increasing near $\tilde{t} = 0$. But $\frac{\partial \ell}{\partial L_0}|_{\tilde{t}=0} = 0$ so the sign of $\frac{\partial^2 \tilde{H}_{J_0}}{\partial L^2}$ determines the sign of $\frac{\partial \ell}{\partial L_0}\big|_{\tilde{t}=0}$ in a neighborhood of $\tilde{t} = 0$, i.e. it determines twist for the flow over a small increment of time. So if $\operatorname{sign}\left(\frac{\partial^2 \tilde{H}_{J_0}}{\partial L^2}\right)$ is constant for all $\tilde{t} \in [0, 2\pi], \ell_0 \in \mathbb{T}$, and L_0 in some interval, then the map $\mathcal{F}_\mu$ is twisting in that region. □

In the case $\mu = 0$, then the twist term satisfies $\frac{\partial \ell_1}{\partial L_0} = -\frac{3}{L_0^4} \cdot 2\pi < 0$. Then for $\mu > 0$ it is natural to require $\frac{\partial \ell_1}{\partial L_0} = -\frac{3}{L_0^4} \cdot 2\pi + O(\mu) < 0$ for twist in RCP3BP.[1] It is possible for large L_0 that the $O(\mu)$ perturbation terms overwhelm the $-\frac{3}{L_0^4}$ and change the sign of twist term. This is why twisting can fail.

Lemma 3.2.1. *In Delaunay variables for RCP3BP*$(0.001, 1.8)$*, the map* $\mathcal{F}_\mu$ *is twisting for* $e^-_{twist}(0.001, 1.8) \leq 0.07 \leq e \leq 0.994 \leq e^+_{twist}(0.001, 1.8)$.

Proof: A computer can be programmed to compute the partial derivative symbolically, then evaluate the twist term and verify it remains of constant sign for $L \in [1.611, 15.94]$. Converting this into a statement about eccentricity gives the

[1] Calculation of the twist term indicates this sign should be positive, however one must account for the fact that under the time rescaling in the energy reduction $\tilde{t} = g \approx -t$.

claimed bounds. The computer may also be used to obtain specific examples outside the twist interval where the map fails to twist correctly. □

Remark: The above argument shows that the time-ϵ map for some small ϵ of the flow is twist map. By demonstrating that this holds at every instant of time t (i.e. for every value of $g \in \mathbb{T}$) in the region $[e^-_{twist}, e^+_{twist}]$ one concludes that $\mathcal{F}_\mu$ is an EAPT. In section 3.3, a method is developed to prove that in certain coordinates, there is a map $\mathcal{F}$ which is an EAPT for $\epsilon = 2\pi$. Furthermore the map is twisting in a certain domain which includes points with $e > 1$.

3.2.3 Twisting in ADDV

Denote by $\mathcal{F}^\nu = \mathcal{F}^\nu_\mu(J_0)$ an EAP map arising from RCP3BP(μ, J_0) in ADDV coordinates on the section $\{g_\nu = 0 \mod 2\pi\}$. It is possible to derive an expression to check for twisting in ADDV. This is done in exactly the same manner as above. A similar lemma holds.

Lemma 3.2.2. *In ADDV for RCP3BP*$(0.001, 1.8)$ *let* $\nu = 2.8\mu$. *Then the map* $\mathcal{F}^\nu_\mu$ *is twisting for* $0 \leq e \leq 0.984$ *and is not twisting for some values corresponding to* $e > 0.984$.

While it is true that $\mathcal{F}^\nu$ is *defined* for nearly parabolic motions, without the property of twist, it is useless for the purposes of applying Aubry-Mather theory. This is remedied in the next section.

3.3 The Method of Spreading Cumulative Twist

This section studies a time-periodic Hamiltonian $H(\ell, L, t)$ and its convexity with respect to L. Presence of such convexity implies that the natural time 2π-map Poincaré map $F : (\ell, L) \to (\ell', L')$ is twisting. Twisting enable one to apply Aubry-Mather theory.

Sufficient conditions shall be stated on H for existence of a time-periodic canonical change of coordinates Ψ such that $H \circ \Psi(\ell, L, t)$ is convex in L. For the RCP3BP, these conditions essentially reduce to $\frac{\partial T}{\partial r^{apoh}} > 0$, i.e. increasing the aphelion radius increases the period of revolution. For the duration of this section, work shall be conducted in a general setting as there are likely further applications of the result of this section to other time periodic Hamiltonian systems. Comments considering applicability to RCP3BP are scattered throughout and the actual application to the RCP3BP is carried out in section 4.2.

One can also work out the construction below for exact area-preserving maps, i.e. for the discrete time. Notice that existence of twisting coordinate system is *not granted*. For example, pick an EAP map with two elliptic islands which twist in different directions; such a map has no such symplectic coordinates.

Consider a C^r Hamiltonian $H(\ell, L, s)$ periodic in ℓ and s with period 2π and well defined in a region $\mathcal{U} \subset \mathbb{A} \times \mathbb{T} = \mathbb{T} \times \mathbb{R} \times \mathbb{T}$ with $r \geq 3$. Let $\Phi_t(\ell, L, s)$ be the flow of H. In particular, the time–component of $\pi_3 \circ \Phi_s$ satisfies $\pi_3 \circ \Phi_t(\ell, L, s) = s + t$. This implies that the equations of variation of $H(\ell, L, s)$ preserve 2-dimensional

subspaces tangent to the cylinder component. Namely,

$$d\Phi_t : T_{(\ell,L,s)}\mathbb{A} \to T_{\Phi_t(\ell,L,s)}\mathbb{A}.$$

Thus, the tangent space to the cylinder $\mathbb{A}$ at (ℓ, L, s) is mapped into the tangent space to $\mathbb{A}$ at $\Phi_t(\ell, L, s)$. Denote the restriction of $d\Phi_t$ to $T_{(\ell,L,s)}\mathbb{A}$ by $d\Phi_t^*$. It can also be defined using the following commutative diagram. Let $\pi : T_{(\ell,L,t)}(\mathbb{A} \times \mathbb{T}) \to T_{(\ell,L,t)}\mathbb{A}$ be the natural projection. Then

$$\begin{array}{ccc} T_{(\cdot,\cdot,s)}(\mathbb{A} \times \mathbb{T}) & \xrightarrow{d\Phi_t} & T_{(\cdot,\cdot,t+s)}(\mathbb{A} \times \mathbb{T}) \\ \downarrow \ \pi & & \downarrow \ \pi \\ T_{(\cdot,\cdot,s)}\mathbb{A} & \xrightarrow{d\Phi_t^*} & T_{(\cdot,\cdot,t+s)}\mathbb{A}. \end{array}$$

Here we study *evolution of the tangent space to the cylinder* $T_{(\cdot,\cdot,\cdot)}\mathbb{A}$ *naturally embedded into the ambient tangent space* $T_{(\cdot,\cdot,s)}(\mathbb{A} \times \mathbb{T})$.

A time-periodic Hamiltonian $H(\ell, L, t)$ can arise from an autonomous two degree of freedom Hamiltonian $\overline{H}$. When one restricts $\overline{H}$ to an energy surface and reduces order (see e.g [A] sect. 45), it leads to a time-periodic Hamiltonian. For example this can be done to the Hamiltonians from section 3.1.

Fix a section Σ, e.g. $\{\ell = 0 \mod 2\pi\}$, and define the return times of $(0, L, t) \in \Sigma$ to be

$$T_+(L,t) = \min\{t^* > t \text{ such that } \ell_{t^*} = 0\}$$

$$T_-(L,t) = \max\{t^* < t \text{ such that } \ell_{t^*} = 0\}$$

Definition 3.3.1. *Let* $\mathcal{W}$ *be the set of* $(\ell, L, t) \in \mathbb{T} \times \mathbb{R}_+ \times \mathbb{T}$ *such that*

1. *the return time to the section* Σ *is finite:* $T_\pm(L,t) < \infty$ *for any* $(0, L, t) \in \Sigma$.

2. *every point inside* $(\ell, L, t) \in \mathcal{W}$ *arises by flowing from a point in the section* Σ*:* $\exists t_\pm$ *such that* $\ell_{t_\pm} = 0 \mod 2\pi$ *for* $t_- \leq t \leq t_+$

3. *the angle of twisting is uniformly bounded away by* $\frac{\pi}{2}$ *for all time between* $T_-(L,t)$ *and* $T_+(L,t)$*. More exactly, there exists* $\kappa > 0$ *such that for any* $(0, L, s) \in \mathcal{W}$*,*

$$d\Phi_t^*(0,L,s)(0,1)\cdot(0,1) \geq \kappa \left\| d\Phi_t^*(0,L,s)(0,1) \right\| \qquad \text{for any } 0 \leq t \leq T_+(L,s)$$

$$d\Phi_{-t}^*(0,L,s)(0,1)\cdot(0,1) \geq \kappa \left\| d\Phi_{-t}^*(0,L,s)(0,1) \right\| \qquad \text{for any } 0 \leq t \leq T_-(L,s).$$

4. *moving in the action* L *direction on the section* $\Sigma \cap \mathcal{W}$ *decreases the return time* T*:* $\frac{\partial T_\pm}{\partial L}(L_{t_\pm}, t_\pm)|_{L=L_{t_\pm}} < 0$.

Notice that the region $\mathcal{W}$ can be *non–invariant* and non–compact[2]. The first 2 conditions are nothing more than an abstract definition of a non–invariant region to be investigated. For the RCP3BP it corresponds to "inside parabolic" initial conditions (see Appendix 4.2). The third condition prohibits the dynamics from twisting a vertical vector by more than $\frac{\pi}{2}$. The fourth condition is the "sufficient condition" needed to ensure twist. It says that there is *cumulative twist*.

Theorem 3.3.2. *Suppose* $\mathcal{W}$*, defined above, is non-empty for the flow of a* C^r *(*$r \geq 3$*) Hamiltonian* $H(\ell, L, s)$ *periodic in* ℓ *and* s *with period* 2π *and well defined on* $\mathcal{W}$*. Then there is a* C^{r-1} *smooth periodic family* $\{\Psi_s\}_{s\in\mathbb{T}}$ *of canonical coordinate changes* $\Psi : (\ell, L; s) \to (\ell_s^{dyn}, L_s^{dyn}; s)$ *such that* $\forall s \in \mathbb{T}$ *the composition* $H \circ \Psi^{-1}(\ell_s^{dyn}, L_s^{dyn}; s)$ *is convex with respect to* L_s^{dyn} *in* $\Psi(\mathcal{W})$*; specifically* $\partial^2_{L_s^{dyn} L_s^{dyn}}(H \circ \Psi^{-1})|_{\Psi(\mathcal{W})} > 0$.

[2]In the case $\mathcal{W}$ is known to be compact, the first two conditions can be replaced with that condition that angular ℓ component moves with positive velocity: $\dot{\ell} = \partial_L H > 0$.

On one side having a possibly non–invariant region $\mathcal{W}$ gives more flexibility for applications of Aubry–Mather theory, on the other side this causes more concerns in proving existence of Aubry-Mather sets. Usually Aubry-Mather theory is done inside of an invariant region. The issue of non-invariance is handled for the RCP3BP in section 6.2.

Up to non-invariance conditions (1–2) and no overtwisting (3), Theorem 3.3.2 says that

If there is a cumulative twist, then after a canonical coordinate change there is a twist.

Consider a C^{r-2} ($r \geq 3$) smooth direction field in $T\mathbb{A} \times \mathbb{T}$, i.e. a family of directions $v_{(\ell,L,s)} \in T_{(\ell,L,s)}\mathbb{A}$ with $(\ell, L, s) \in \mathcal{W}$ which is C^{r-2} smooth in (ℓ, L, s). Since $d\Phi_t^*$ preserves the tangent spaces to the cylinder $T_{\mathcal{W}}\mathbb{A}$, both $d\Phi_t^*(\ell, L, s)v_{(\ell,L,s)}$ and $v_{\Phi_t(\ell,L,s)}$ belong to the 2-dimensional space with induced orientation. Therefore, the sign of the wedge product is well defined. Define the function

$$\delta(\ell, L, s) := \lim_{t\to 0} \frac{d\Phi_t^*(\ell, L, s)v_{(\ell,L,s)} \wedge v_{\Phi_t(\ell,L,s)}}{t}.$$

Definition 3.3.3. *A vector field is called twisted (or a twisting direction field) if the sign of $\delta(\ell, L, s)$ is constant and nonzero $\forall(\ell, L, s) \in \mathcal{W}$.*

Geometrically twist means a vector makes an angle with its image under the flow of the equations of variation. $\delta(\ell, L, s)$ measures the rate of twisting at the point (ℓ, L, s). Notice that for convex Hamiltonians, the vertical direction field $v_{(\ell,L,s)} \equiv (0, 1)$ is twisted. For example, for the 2BP(SC) we have $\delta(\ell, L, s) = -\frac{3}{L^4}$. The failure of twist for the RCP3BP geometrically indicates that there are spots

where the vertical vector is pointing in the incorrect direction. See figure 3.4.

The proof of Theorem 3.3.2 consists of two steps. The first step is to **construct** Γ, a twisting direction field. This is done by via "spreading twist" to produce a direction field along a single orbit. This construction extends smoothly to the whole set $\mathcal{W}$. The second step is to use the direction field Γ to construct a smooth canonical coordinate change. This is accomplished by straightening the direction field Γ.

Figure 3.4: A twisted direction field (left) and the failure of twist (right) at the point x and its forward images

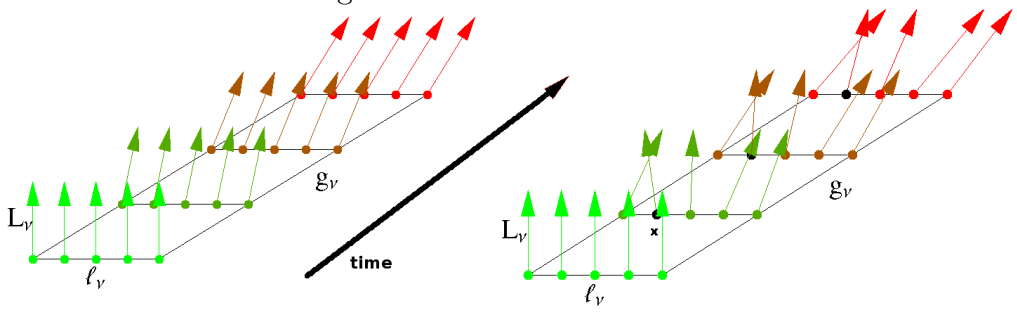

Lemma 3.3.4. *There exists a C^{r-2} smooth twisting direction field Γ on $T_{\mathcal{W}}\mathbb{A}$.*

Proof: First, let us show how to spread twist along a single trajectory and construct a twisting direction field.

Consider a trajectory with initial conditions $(0, L_0, t_0) \in \Sigma \cap \mathcal{W}$. Let $p_t := \Phi_t(0, L_0, t_0)$ be a parametrization of points along the trajectory. Such a parameterization exists by conditions (1) and (2). By condition (1), $T = T_+(L_0, t_0) < +\infty$. Define the tangent vectors $v_0^* := (0, 1) \in T_{(0,L_0,t_0)}\mathbb{A}$ and $v_T^* := (0, 1) \in T_{(\ell_T, L_T, t_0+T)}\mathbb{A}$.

Construction shall now begin on a C^{r-2} smooth family $\{v_t\}_{0 \le t \le T}$ where v_t's are non-vanishing tangent vectors at p_t's. Suppose $w : [0, 1] \to [0, 1]$ is a C^{r-2} smooth monotone strictly increasing function with $w(0) = 0, w(1) = 1, w^{(k)}(0) = w^{(k)}(1) = 0$

for any $1 \leq k \leq r-2$. Suppose $\lambda : [0,1] \to \mathbb{R}_+$ is a C^∞ function such that $\lambda|_{[0,1/3]} \equiv 1/T_+(L_0,t_0)$ and $\lambda|_{[2/3,1]} \equiv 1/T_-(L_0,t_0)$. Define for $0 \leq \alpha \leq 1$

$$v_{\alpha T} := \lambda(\alpha)\Big(\big(1-w(\alpha)\big)\ d\Phi^*_{\alpha T}\big(v_0^*\big) + w(\alpha)\ d\Phi^*_{-(1-\alpha)T}\big(v_T^*\big)\Big). \tag{3.6}$$

Notice the vector field $\{v_t\}_{0\leq t\leq T}$ has non-vanishing vertical component due to no over twisting condition (3).

To see smoothness of the direction field along an orbit away from Σ, note that $d\Phi^*$ and $T = T(L_0,t_0)$ are C^{r-2}–smooth by smooth dependence in initial conditions. Since w, λ are at least C^{r-2} smooth, then dependence on α is C^{r-2}-smooth and hence $\{v_t\}_{t\in[0,T]}$ is a C^{r-2}-smooth family along the trajectory away from Σ. At the section Σ, note that v_0 and v_T are parallel to $(0,1)$ so the *direction* field is continuous.

To prove C^{r-2} smoothness on Σ recall that $\lambda'(\alpha) \equiv 0$ for $\alpha \in [0,1/3] \cup [2/3,1]$ and for these α's consider

$$\begin{aligned}\frac{\partial}{\partial\alpha}\big(v_{\alpha T}\big) = \lambda(\alpha)\Big(& d\Phi^*_{\alpha T}\big(v_0\big)\cdot(-w'(\alpha)) + \big(1-\alpha\big)\frac{\partial}{\partial\alpha}\left(d\Phi^*_{\alpha T}\big(v_0\big)\right)\cdot T \\ &+ d\Phi^*_{-(1-\alpha)T}\big(v_T\big)\cdot w'(\alpha) + w(\alpha)\frac{\partial}{\partial\alpha}\left(d\Phi^*_{-(1-\alpha)T}\big(v_T\big)\right)\cdot T\Big).\end{aligned}$$

C^1 smoothness on Σ follows provided $\frac{\partial}{\partial t}v_t|_\Sigma$ match for $t>0$ and $t<0$ at every point in $\Sigma\cap\mathcal{W}$. The above procedure views every point on $\Sigma\cap\mathcal{W}$ as either $(0,L_0,t_0)$ or as the image $\Phi_{T'}(0,L_0',t_0')$ of a different point $(0,L_0',t_0') \in \Sigma\cap\mathcal{W}$, where $T' = T_+(0,L_0',t_0')$. Thus, C^1 smoothness of $\{v_t\}_{t\in[0,T]}$ follows since the above formula implies

$$\left(\frac{\partial}{\partial\alpha}\big(v_{\alpha T}\big)\right)|_{\alpha=0} = \frac{\partial}{\partial t}\left(d\Phi^*_t\big(v_0\big)\right)|_{t=0} \quad\text{and}\quad \left(\frac{\partial}{\partial\alpha}\big(v_{\alpha T}\big)\right)|_{\alpha=1} = \frac{\partial}{\partial t}\left(d\Phi^*_t\big(v_T\big)\right)|_{t=0}.$$

Similarly one can prove smoothness of higher order.

It turns out that on the section Σ the vector field $\{v_t\}_{t\in[0,T]}$ is not twisting. To rectify this problem, introduce the following modification. Fix $\epsilon \ll T$, and suppose $u : \mathbb{R} \to \mathbb{R}$ is a C^{r-2} smooth function such that $u(\pm\epsilon) = u(0) = 0$, $u'(0) > 0$, $u^{(k)}(\pm\epsilon) = 0$ for any $1 \leq k \leq r-2$, u is nonzero everywhere else inside of $(-\epsilon, \epsilon)$, and u is identically zero outside of $(-\epsilon, \epsilon)$. Consider the following perturbation of $\{v_t\}_{t\in[0,T]}$. Let

$$v_t' = \big(1 - u(t)\big)v_t + u(t)v_t^{\perp}$$

where $v_t^{\perp}$ denotes a unit vector orthogonal to v_t so that $v_t \wedge v_t^{\perp} > 0$. Clearly the new direction field $\{v_t'\}$ is a smooth perturbation of $\{v_t\}$ since u is smooth and $v_t^{\perp}$ is smooth since v_t is smooth.

To prove twist, compute $d\Phi_t^*(\ell, L, s)v'_{(\ell,L,s)} \wedge v'_{\Phi_t(\ell,L,s)} =$

$$\begin{aligned}
&d\Phi_t^*(\ell, L, s)\Big(\big(1 - u(s)\big)v_{(\ell,L,s)} + u(s)v^{\perp}_{(\ell,L,s)}\Big) \wedge \Big(\big(1 - u(t+s)\big)v_{\Phi_t(\ell,L,s)} + u(t+s)v^{\perp}_{\Phi_t(\ell,L,s)}\Big) \\
&\quad = \big(1 - u(s)\big)\big(1 - u(s+t)\big)d\Phi_t^*(\ell, L, s)v_{(\ell,L,s)} \wedge v_{\Phi_t(\ell,L,s)} \\
&\qquad + u(s)\big(1 - u(t+s)\big)d\Phi_t^*(\ell, L, s)v^{\perp}_{(\ell,L,s)} \wedge v_{\Phi_t(\ell,L,s)} \\
&\qquad + \big(1 - u(s)\big)u(t+s)d\Phi_t^*(\ell, L, s)v_{(\ell,L,s)} \wedge v^{\perp}_{\Phi_t(\ell,L,s)} \\
&\qquad + u(s)u(t+s)d\Phi_t^*(\ell, L, s)v^{\perp}_{(\ell,L,s)} \wedge v^{\perp}_{\Phi_t(\ell,L,s)},
\end{aligned}$$

then divide the above quantities by t and take the limit as $t \to 0$ to compute the function δ for $\{v_t'\}$. Denote this quantity by $\delta_{v'}$ and the twist term for $\{v_t\}_{t\in[0,T]}$ as δ_v. Notice that $d\Phi_t^*(\ell, L, s)v^{\perp}_{(\ell,L,s)} \wedge v^{\perp}_{\Phi_t(\ell,L,s)}$ and $d\Phi_t^*(\ell, L, s)v_{(\ell,L,s)} \wedge v_{\Phi_t(\ell,L,s)}$ are the

same. This produces

$$\begin{aligned}\delta_{v'}(\ell, L, s) &= \big(1 - u(s)\big)^2 \delta_v(\ell, L, s) + u(s)^2 \delta_v(\ell, L, s) \\ &\quad + \left(\lim_{t \to 0} \frac{u(s)\big(1 - u(t+s)\big) - \big(1 - u(s)\big)u(t+s)}{t} \right) v^{\perp}_{(\ell,L,s)} \wedge v_{(\ell,L,s)} \\ &= \Big(\big(1 - u(s)\big)^2 + u(s)^2 \Big) \delta_v(\ell, L, s) + u'(s).\end{aligned}$$

Notice that condition (4) implies that $d\Phi_T^* v_0 \wedge v_T > 0$. Moreover, for any $0 < \alpha < 1$ we have $d\Phi^*_{\alpha T} v_0 \wedge d\Phi^*_{-(1-\alpha)T} v_T > 0$ uniformly in α, because $d\Phi^*_{-(1-\alpha)T}$ is an orientation preserving, non-degenerate diffeomorphism. Replace v by $\lambda(\alpha)\, d\Phi^*_{\alpha T} v_0$, $v^{\perp}$ by $\lambda(\alpha)\, d\Phi^*_{-(1-\alpha)T} v_T$, t by αT, and u by w in the calculation above. Then

$$\delta_v(\Phi_{\alpha T}(0, L, s)) = w'(\alpha)\, \lambda^2(\alpha)\, d\Phi^*_{\alpha T} v_0 \wedge d\Phi^*_{-(1-\alpha)T} v_T.$$

Note that on the section Σ it holds that $u'(0) > 0$ by choice of u, so $\{v_t'\}$ is twisting on Σ. Furthermore, since the vector field $\{v_t\}$ is twisting away from Σ, i.e. $\delta_v(\ell, L, s) > 0$ off of Σ, then it is possible to choose u on the compact interval $[-\epsilon, \epsilon]$ so that $\delta_{v'}(\ell, L, s)$ is strictly positive.

Hence $\{v_t'\}_{t \in [0,T]}$ is a twisting vector field along the trajectory p_t. Note that v_t, and as a result v_t', are not continuous across Σ. While the length of v_t experiences jump, the *direction does not.* Indeed, size λ is identically constant on each side of Σ separately. The magnitude of λ is selected to match time derivatives on both sides so the vector field defines a smooth *direction field* across Σ. Note the construction of the vector field for a single trajectory p_t extends smoothly to all of $\mathcal{W}$; use this to induce the direction field that is Γ. $\square$

3.3.1 Dynamically Deformed Variables

In this section, a new canonical coordinate system is created which respects the property of twist. The new variables are denoted (L_{dyn}, ℓ_{dyn}); call them *dynamically deformed variables*. One way to think of dynamically deformed variables is to think that at each point in the flow, the coordinate system is dynamically changed to one in which the twist property holds infinitesimally. The new action direction arises from a straightening of the direction field Γ. Stated as a lemma:

Lemma 3.3.5. *Suppose Γ is the smooth direction field as constructed in Lemma 3.3.4. Then there exists a C^{r-2}-smooth time-periodic family of symplectic maps $\Psi_s : (\ell, L, s) \to (\ell_{dyn}, L_{dyn}, s)$ which straightens the direction field Γ.*

Proof: Note that the direction field Γ is defined only on $\mathcal{W}$. Moreover, the angle with the horizontal component is strictly positive (see formula (3.6) and comments below it). Γ can be extended smoothly to whole cylinder in the following manner. Let $\mathcal{U}_\epsilon$ be an ϵ neighborhood, $\epsilon > 0$ of the set $\mathcal{W}$. On $\mathcal{U}_\epsilon \cap \partial\mathcal{W}$, leave the direction field Γ as defined on $\partial\mathcal{W}$. On $\mathbb{A} - \mathcal{U}_\epsilon^{int}$, define the direction field Γ to be the vertical direction field which is identically $(0, 1)$ everywhere. On $\mathcal{U}_\epsilon - \mathcal{W}$ define the vector field Γ to be a smooth interpolation between vectors on the boundaries, i.e. smoothly interpolate between $\Gamma|_{\partial\mathcal{W}}$ and $(0, 1)$.

Suppose $\mathcal{C}_0 = \{(L^*, \ell) | \ell \in \mathbb{T}\}$ is a horizontal circle which intersects the section Σ at height L^*. Consider the images of $\mathcal{C}_0$ after integration along Γ for time t, where unit velocity is used along Γ. Denote the images $\mathcal{C}_t$. Clearly the $\mathcal{C}_t$ are diffeomorphic to circles. Additionally, since $\Gamma|_{\mathcal{W}} = (0, 1)$, then for all L_0 there

exists t_0 such that $\mathcal{C}_{t_0} \cap \mathcal{W} = L_0$. Hence one can introduce the parameterization $y(L_0) = \mathcal{C}_{t_0}$. Furthermore condition (3) and formula (3.6) imply that $\{y(L_0)\}_{L_0 \geq L^*}$ is a foliation of the annulus $[L^*, \infty] \times \mathbb{T}$ and that curves $y(L_0)$ always intersect the direction field Γ transversally. Define

$$L_{dyn}(L_0) := \text{the area between } y(L_0) \text{ and } \mathcal{C}_0.$$

Since there is already a symplectic form $d\ell \wedge dL$ on the cylinder, formally the dual angular variable ℓ_{dyn} can be defined so that

$$d\ell \wedge dL = d\ell_{dyn} \wedge dL_{dyn}.$$

This is well defined since vectors in Γ always make a nonzero angle with the curves $y(L_0)$.

Figure 3.5: Γ(left) and its straightening (right) under canonical change of coordinates

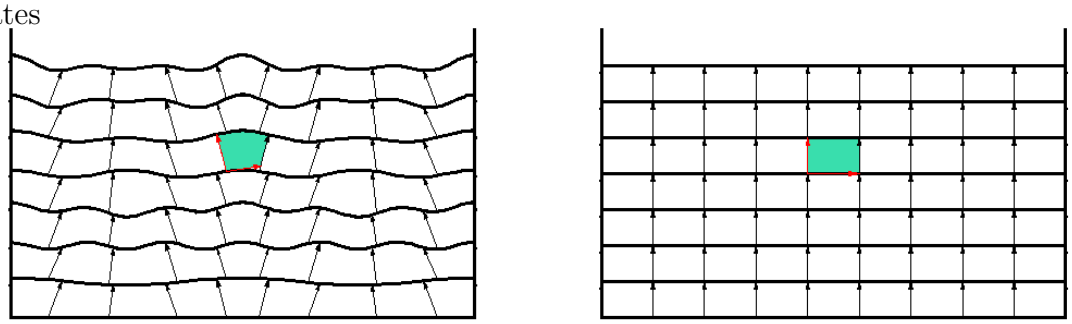

To see this geometrically, consider curves $y(L_0)$ and $y(L_0+\epsilon)$ with ϵ sufficiently small. At the point $(\ell, L, s) \in y(L_0)$, the direction field Γ defines a unique direction $v = v_{(\ell,L,s)}$ pointing from the circle $y(L_0)$ to the circle $y(L_0 + \epsilon)$. Suppose w is a vector of length ϵ tangent to $y(L_0)$ at the point (ℓ, L, s). Then since Γ makes a nonzero angle with $y(L_0)$ it holds that $v \wedge w = O(\epsilon^2)$ is a nonzero area element.

At the point (ℓ, L, s), straighten the direction field Γ so that the vector v is pointing vertically, i.e. think of v as the a new action direction, denoted L_{dyn}, and think of the ℓ_{dyn} direction as being specified by straightening the vector w to point horizontally. The length of the vector in the ℓ_{dyn} direction can be scaled to preserve the area $v \wedge w$ up to order $O(\epsilon^2)$. As $\epsilon \to 0$, this produces a smooth area form which induces a smooth canonical change of coordinates $\Psi_s : (\ell, L, s) \to (\ell_{dyn}, L_{dyn}, s)$. $\square$

By construction, the dynamically defined coordinate system (ℓ_{dyn}, L_{dyn}, s) has the property of twist along trajectories of H. Hence convexity of H in dynamically deformed variables follows.

Chapter 4

A Sufficient Condition for Twist in the RCP3BP

4.1 Twisting in Polar Coordinates

In section 3.2 it is argued that in terms of the motions of the comet, twisting says high eccentricity comets revolve around the sun more slowly than their low eccentricity counterparts. In this section, this idea is rephrased in a rigorous fashion to give a meaning to twisting in polar coordinates. This done by noting that on a fixed energy surface when the comet is at the aphelion, increasing eccentricity corresponds to increasing the semi–major axis of the ellipse of motion. By Kepler's Laws, increasing the semi-major axis corresponds to increasing the period of revolution. Let us make this rigorous now.

Definition: For a given set of initial conditions $(r, \varphi, P_r, P_\varphi)(0) = (r_0, \varphi_0, 0, P_{\varphi_0})$, with $r_0 > J_0^2$ such that the comet is at the aphelion, consider the motion of the comet starting at the aphelion and moving towards the perihelion. Define $T(r_0, \varphi_0, P_{\varphi_0})$ be the smallest positive time such that $P_r\big(T(r_0, \varphi_0, P_{\varphi_0})\big) = 0$, i.e. the time to the next perihelion. Call T the *one-half period* of the comet. A formulation of twist in polar coordinates is given in the following theorem.

Theorem 4.1.1. *There exists an $R > J_0^2$ such that for all $r \geq R$, the quantity $\frac{\partial T}{\partial r_0}|_{r_0=r} > 0$. In particular, this holds for $\mu = 10^{-3}$, Jacobi constant $J_0 = 1.8$, and $R = 15$ (corresponding to $e > 0.8$).*

Figure 4.1: The Effect of Increasing r_0

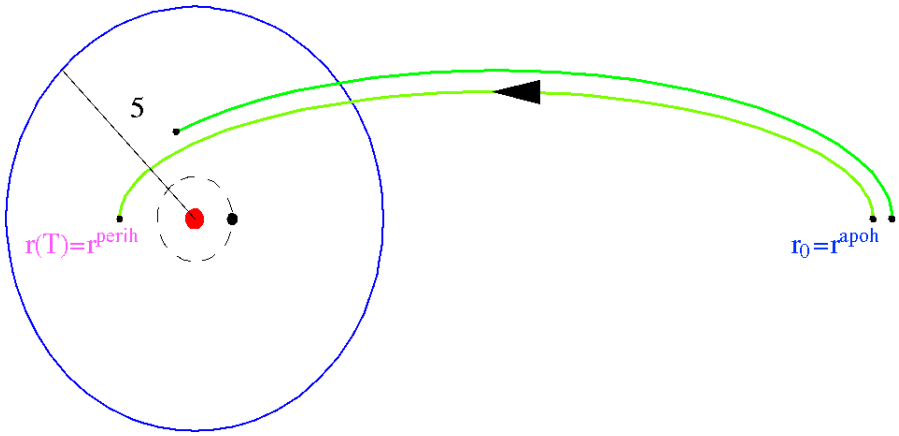

Let us offer a heuristic proof of this result now. In the two body problem, Kepler's Third Law states that the one-half period $T = \pi a^{\frac{3}{2}}$ where the semi-major axis $a = \frac{r^{apoh} - r^{perih}}{2} \approx \frac{r^{apoh}}{2}$ for large eccentricities. Taking initial conditions to be $r_0 = r^{apoh} > J_0^2$, then $a \approx \frac{1}{2} r_0$. Computing $\frac{\partial T}{\partial r_0} = \frac{3}{4}\pi a^{1/2} > 0$ says that increasing the semi-major axis, i.e. increasing r^{apoh}, increases the half period of the comet. To prove this result for the RCP3BP, one must justify these approximations, as well as carefully account for the effects of the perturbation term.

Proof of Theorem 4.1.1 : Formally compute $\frac{\partial T}{\partial r_0}$.

$$\frac{\partial}{\partial r_0}\Big(P_r\big(T(r_0, \varphi_0, P_{\varphi_0}), (r_0, \varphi_0, P_{\varphi_0})\big)\Big) = \dot{P}_r(T) \cdot \frac{\partial T}{\partial r_0} + \frac{\partial P_r}{\partial r_0}(T) = 0$$

Solving for $\frac{\partial T}{\partial r_0}$ yields

$$\frac{\partial T}{\partial r_0} = -\frac{\frac{\partial P_r}{\partial r_0}(T)}{\dot{P}_r(T)}. \tag{4.1}$$

One must show for nearly parabolic comets that $\dot{P}_r(T) > 0$ so that equation (4.1) is well defined.

Lemma 4.1.2. *There exists an $e_0 = e_0(\mu, J_0)$ such that if $e(t) \geq e_0$ for $t \in [0, T]$ then $\dot{P}_r(T) > 0$ (where T is the half period). In particular $e_0(0.001, 1.8) \leq 0.13$.*

Proof of Lemma: Examining the equations of motion, note that

$$\dot{P}_r = \frac{P_\varphi^2}{r^3} - \frac{1}{r^2} - \frac{\partial \Delta H}{\partial r}$$

and $\frac{\partial \Delta H}{\partial r} = O(\frac{\mu}{r^4})$. Furthermore $|\frac{\partial \Delta H}{\partial r}| \leq (|\frac{\partial \Delta H}{\partial r}|)^+$ (see A.1).

Now $\dot{P}_r$ is increasing as a function of P_φ so it suffices to have a lower bound on P_φ to bound $\dot{P}_r$. Recall that $e = \sqrt{1 - 2P_\varphi^2(J_0 - P_\varphi)}$ (this follows from formulas in [AKN]) so that on a fixed energy surface e is a monotone increasing function of P_φ. Hence requiring $e(t) \geq e_0$ for $t \in [0, T]$ is equivalent to requiring $P_\varphi(t) \geq P_\varphi^*(e_0)$ for some $P_\varphi^*(e_0)$ implicitly defined.

Then it suffices to consider the lower bound $\dot{P}_r \geq \frac{(P_\varphi^*(e_0))^2}{r^3} - \frac{1}{r^2} - (|\frac{\partial \Delta H}{\partial r}|)^+ =: f(e_0, r, \mu)$. For μ small, $f(e_0, r, \mu)$ is a decreasing function of r in the outer Hill region, hence it suffices to show $f(e_0, r^*, \mu) > 0$ for some $r^* \geq r^{perih}$ (only behavior near $t = T$, i.e. near the perihelion, is of concern). From [AKN], for the 2BP(SC), $r^{perih} = \frac{1-e_0}{2(J_0 - P_\varphi^*(e_0))}$ and this quantity is decreasing as a function of e_0. Thus it suffices to use $r^* = \frac{1-e_0}{2(J_0 - P_\varphi^*(e_0))}$ since $e(t) \geq e_0$ so $r^* \geq r^{perih}$.

When $\mu = 0$, for any $e_0 > 0$ one can verify if $r < P_\varphi^2$, then $\dot{P}_r > 0$; in particular $\dot{P}_r(T) > 0$ at time T when the comet is at the perihelion. By the intermediate value theorem, for any (μ, J_0) with μ sufficiently small there is some $e_0(\mu, J_0)$ for which $\dot{P}_r(T) > 0$.

For $(\mu, J_0) = (0.001, 1.8)$, then $e \in [0.13, 1]$ implies $P_\varphi \in [1.61, 1.8]$ and $r^{perih} \leq 2.31103$. Using the explicit formula for $(|\frac{\partial \Delta H}{\partial r}|)^+$ from appendix A.1 then yields $\dot{P}_r(T) > 0.0225404$. □

To complete the proof of Theorem 4.1.1 it remains to show that $\frac{\partial P_r}{\partial r_0}(T) < 0$.

Lemma 4.1.3. *Consider RCP3BP*$(10^{-3}, 1.8)$ *and suppose the initial conditions for the flow are at the aphelion. If* $\left(\frac{\partial r}{\partial r_0}, \frac{\partial \varphi}{\partial r_0}, \frac{\partial P_r}{\partial r_0}\right)(0) = (1, 0, 0)$ *and the remaining initial condition satisfies (B.2). Then* $\frac{\partial P_r}{\partial r_0}(T) < 0$ *where* T *is the first positive time there is a perihelion.*

Remark: Condition (B.2) gives a way to constrain the initial conditions to the tangent space of $\mathcal{S}(J_0)$. In general initial conditions to the equations of variations for this system are in $\mathbb{R}^4$, however since dynamics are restricted to $\mathcal{S}(J_0)$, then tangent space dynamics must also be restricted.

Proof of Lemma: Note that

$$\frac{\partial P_r}{\partial r_0} = \left(\frac{\partial P_r}{\partial P_\varphi}\right)\left(\frac{\partial P_\varphi}{\partial P_{\varphi_0}}\right)\left(\frac{\partial P_{\varphi_0}}{\partial r_0}\right)$$

We know from the claim in Theorem B.2.1 that $\left(\frac{\partial P_\varphi}{\partial P_{\varphi_0}}\right)(T) > 0$. (This is expected since for the 2BP(SC), $\left(\frac{\partial P_\varphi}{\partial P_{\varphi_0}}\right)(T) \equiv 1$.

Constraining dynamics to the energy surface $\mathcal{S}(J_0)$ implicitly defines $P_r = P_r(J_0, r, \varphi, P_\varphi)$. The relation is given by

$$P_r(J_0, r, \varphi, P_\varphi) = \pm\sqrt{-2J_0 + 2P_\varphi - \frac{P_\varphi^2}{r^2} + \frac{2}{r} - 2\Delta H(r, \varphi)} \tag{4.2}$$

Differentiate this formula (for $P_r \leq 0$) to obtain

$$\frac{\partial P_r}{\partial P_\varphi} = \frac{1 - \frac{P_\varphi}{r^2}}{P_r} < 0$$

since the denominator is positive for $r \geq 1.5$ and $P_\varphi \leq 1.81$ and $P_r \leq 0$ for $t \in [0, T]$.

On the energy surface $\mathcal{S}(J_0)$ we can solve to find

$$P_\varphi = r^2 - \sqrt{2r - 2J_0 r^2 - P_r^2 r^2 + r^4 - 2r^2 \Delta H(r, \varphi)}$$

When $t = 0$, then $P_r = 0$, $r = r_+$ (the aphelion radius) and the expression simplifies. Compute the derivative of the simplified expression to find:

$$\frac{\partial P_{\varphi_0}}{\partial r_0} = \frac{-1 + 2r_+(J_0 - P_\varphi + \Delta H) + r_+^2 \frac{\partial \Delta H}{\partial r}}{r_+^2 - P_\varphi}. \tag{4.3}$$

For r large, the denominator is positive. This certainly holds at the aphelion. Note that formally, the aphelion satisfies

$$r_+ = \frac{1 + \sqrt{1 - P_\varphi^2(J_0 - P_\varphi + \Delta H)}}{2(J_0 - P_\varphi + \Delta H)}$$

Hence at the aphelion, the numerator of (4.3) simplifies to become $\sqrt{1 - P_\varphi^2(J_0 - P_\varphi + \Delta H)} + r_+^2 \frac{\partial \Delta H}{\partial r}$. It not hard to show that for $J_0 = 1.8$, $r \geq 1.5$, and $P_\varphi \geq 1.7$, the first term in this expression is at least 0.64 and second term is larger than -0.007. Hence the numerator, and (4.3) are positive. It follows that $\frac{\partial P_r}{\partial r_0}(T) < 0$ □

4.2 Application of Theorem 3.3.2 to the RCP3BP

This section shows that Theorem 3.3.2 can be applied to the RCP3BP$(10^{-3}, 1.8)$. Let $H(\ell_\nu, L_\nu, t)$ be the energy-reduced Hamiltonian of the RCP3BP in algebraically deformed Delaunay variables. (See [A] sect. 45 for a refresher on how to do energy reductions in our settings.) In the context of the RCP3BP, the existence of a coordinate system with concavity, i.e $\partial^2_{L_s^{dyn} L_s^{dyn}}(H \circ \Psi^{-1})|_{\Psi(\mathcal{W})} < 0$ is highly desired since then Aubry-Mather theory may be applied. In the case of the 2BP(SC), the convexity requirement boils down to the statement that $\partial_{LL} H = -\frac{3}{L^4}$.

Start the application of Theorem 3.3.2 by fixing a section $\Sigma = \{\ell_\nu = \pi \mod 2\pi\}$, i.e. the aphelion surface. The main result of section 4.1 says $\frac{\partial T}{\partial r_0} > 0$

where T is the half period of comet and r_0 is an aphelion radius. This condition can be reformulated to say $\frac{\partial T}{\partial L_\nu(0)} > 0$ by noting that

$$\frac{\partial T}{\partial L_\nu(0)} = \frac{\partial T}{\partial r_0}\,\frac{\partial r_0}{\partial L_\nu(0)} \qquad \text{where} \qquad \frac{\partial r_0}{\partial L_\nu(0)} = \frac{2r_0}{L_\nu(0)} + \frac{G_\nu(0)^2}{L_\nu(0)e_\nu(0)} > 0.$$

The second identity follows from formulas for converting polar to Delaunay at the aphelion. Hence condition (4) of Definition 3.3.1 is satisfied[1].

4.2.1 Domain of Definition for RCP3BP

Let us construct a domain of relevant solutions for the RCP3BP where condition (2) of definition 3.3.1 is satisfied. When using algebraically deformed Delaunay variables (see chapter 3), the domain of definition was enlarged, increasing the number of solutions which have representations in action-angle variables. However not all of the points inside the homoclinic loop generated from H_ν are of interest. For example some of the points outside of the separatrices make one passage by the Sun-Jupiter system then escape the Solar System. By the way ADDV are defined, it is possible for solutions near the separatrix to flow out of the homoclinic loop where the coordinate system is not well defined. This is because the area inside of the homoclinic loop for H_ν is not an invariant set for the flow induced the Hamiltonian for the RCP3BP.

Definition 4.2.1. *An initial condition is inside parabolic if the following three conditions all hold (fig. 4.2):*

- *If $\dot{r} > 0$, then $\exists t > 0$ such that $\dot{r} = 0$, i.e. there is an aphelion in the future.*

[1]Note that due to negative convexity, the sign of the derivative is reversed

- *If $\dot{r} < 0$, then $\exists t < 0$ such that $\dot{r} = 0$, i.e. there is a perihelion in the past.*
- *For some finite times $t_- < 0 < t_+$ it holds that $|\psi(t_+) - \psi(t_-)| = 4\pi$.*

Figure 4.2: A trajectory with inside parabolic initial conditions

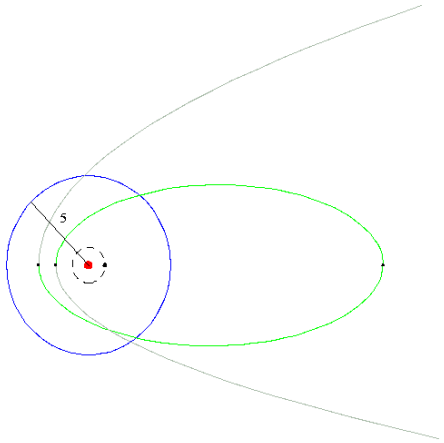

Denote the class of inside parabolic initial conditions for Jacobi constant J_0 by $IP(J_0)$. Notice that hyperbolic or parabolic orbits satisfy $|\psi(t_+) - \psi(t_-)| < 2\pi$. If an orbit of RCP3BP goes to directed infinity in the past and in the future makes one loop around the sun before going to directed infinity, then $|\psi(t_+) - \psi(t_-)|$ can be close to 2π.

Inside parabolic curves are considered since their representations in algebraically deformed Delaunay variables have the action variable L_ν finite for at least one revolution around the sun. Unfortunately, not all of $IP(J_0)$ is contained inside the new homoclinic loop since it is still possible for a separatrix to leave the new homoclinic loop. These points are ignored as they have too high eccentricity to matter. The initial conditions that matter to the proof of Theorem 1.1.2 are those inside parabolic motions which are inside of the homoclinic loop for H_ν (see fig. 4.3). Let

$$\Omega(J_0, \mu) = IP(J_0) \cap \{P_\varphi \leq J_0, \varphi \in \mathbb{S}^1, r_\nu^{perih} \leq r, |P_r| \leq \sqrt{\frac{2}{r} - \frac{(P_\varphi - \nu)^2}{r^2}}\ \}$$

where r_ν^{perih} is the smallest perihelion radius allowed in the deformed homoclinic loop. This is implicitly defined by $0 = H_\nu(r_\nu^{perih}, 0, J_0)$. (See equation (3.3) for definition of H_ν and Theorem 3.1.1 for how to find ν in terms of μ.)

Figure 4.3: Domain of Definition in $(\frac{1}{\sqrt{r}}, \dot{r}$ variables

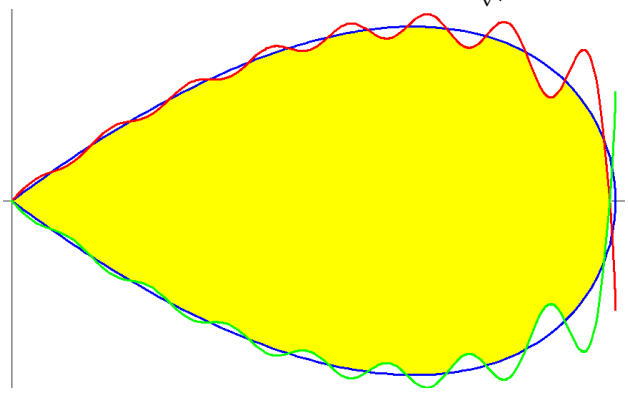

Take $\mathcal{W} := \Omega(J_0, \mu) \cap \{e \geq 0.46\}$ so the aphelion's radii are at least $r^{apoh} = 5$ (this is needed because chapter 2 results must ultimately be applied). Condition (2) of Definition 3.3.1 follows by construction since points in $\mathcal{W}$ are in the class of inside parabolic motions (see section 4.2.1). Conditions (1) and (3) of Definition 3.3.1 must still be verified for trajectories in $\mathcal{W}$.

4.2.2 Verification of condition (1)

To show condition (1) of Definition 3.3.1, note that for every inside parabolic orbit starting at a perihelion, there is an aphelion for some $0 < t^*$. Let $(\ell_\nu^*, L_\nu^*, t^*)$ be such an aphelion point. Let $P_\varphi(t)$ be angular momentum along the orbit. Lemma 2.2.2 says that

$$|P_\varphi(t) - P_\varphi(0)| \leq 4.5\mu \text{ for } 0 \leq t \leq t^*$$

and by the relations in section 3.1.2.1 this implies that $L_\nu(T) - L_\nu(0)$ is finite (since $2\nu > 4.5\mu$), where T is the return time to the section $\Sigma = \{\ell_\nu = \pi \mod 2\pi\}$. Moreover the bound is uniform in any compact region $\{L_\nu \leq \text{const}\}$. This implies that return time T is finite and condition (1) holds.

4.2.3 Bounds on angle of twist in the RCP3BP

In this section, condition (3) of Definition 3.3.1 is verified. Suppose $H = H(L_\nu, \ell_\nu, s)$ is the reduced RCP3BP Hamiltonian where $s = g_\nu$ is the rescaled time and G_ν is an implicit function of J_0 and the other algebraically deformed Delaunay variables. Recall that the angle of twist $\eta(t) = \eta(t; L_\nu(0), 0, s)$ from the vertical is given by the formula

$$\tan(\eta(t)) = \frac{\left(\frac{\partial \ell_\nu(t)}{\partial L_\nu(0)}\right)}{\left(\frac{\partial L_\nu(t)}{\partial L_\nu(0)}\right)} \tag{4.4}$$

where the initial conditions are taken to be $(0, L_\nu(0), s) \in \Sigma = \{\ell_\nu = \pi \mod 2\pi\}$. (See [MF] for abstract statement about angle of twist.)

Lemma 4.2.2. *Consider RCP3BP*$(10^{-3}, 1.8)$. *For all* $(0, L_\nu(0), s) \in \Sigma = \{\ell_\nu = \pi \mod 2\pi\}$ *for* $0 \leq t \leq T(L_\nu(0), s)$ *the angle of twist* $\eta(t) \in [-\kappa, \kappa]$ *for some* $\kappa < \frac{\pi}{2}$ *where* T *is the return time to* Σ.

For the 2BP(SC), it not hard to show why the angle of twist from the vertical is uniformly bounded away from $\frac{\pi}{2}$. Note that the angle η of twist from the vertical in Delaunay variables can be explicitly computed for the 2BP(SC). It is given by

$$\tan(\eta) = \frac{\left(\frac{\partial \ell}{\partial L_0}\right)(t)}{\left(\frac{\partial L}{\partial L_0}\right)(t)} = -\frac{3t}{L_0^4}$$

Hence $\eta = \arctan(-\frac{3t}{L_0^4})$ and this function is decreasing as a function of t for $t \geq 0$. Recall the period of the 2BP(SC) is $T = 2\pi L^3$. For $t \in [0, T]$ it follows that the minimum is angle is $\arctan(-\frac{6\pi}{L_0})$. For $L_0 \geq 1.86$ (i.e. when $r^{apoh} > 5$ on $\mathcal{S}(1.8)$) it follows that $0 \geq \eta(t) \geq -1.47244 > -\frac{\pi}{2}$. The case for $t \leq 0$ is symmetric in the 2BP(SC).

Proof of Lemma 4.2.2: Examination of formula (4.4) reveals that the angle of twist rotates by more than an angle of $\frac{\pi}{2}$ from the vertical if at some point in the flow $|\tan \eta| = \infty$. This happens if and only if the numerator becomes infinite or the denominator becomes zero. Hence it suffices to have a uniform lower bound on $\frac{\partial L_\nu}{\partial L_\nu(0)}$ and a uniform upper bound on $\frac{\partial \ell_\nu}{\partial L_\nu(0)}$ over one full period for all trajectories considered.

Note that condition (3) requires bounds in both forward and backward time for an individual trajectory. By condition (2) every point on the section Σ has a pre–image and an image of Σ and bounding the angle of twist uniformly for all trajectories forward in time is enough to also bound the angle of twist uniformly for trajectories in reverse time. Hence it suffices to generate uniform bounds over all trajectories which are approaching the sun from an aphelion in forward time.

The method of proof is to convert from algebraically deformed Delaunay variables into polar, then use bounds on equations in polar coordinates. Bounds are computed with the assistance of a computer in the kick region, and with some by-hand calculations in the outside region.

It is easier to make calculations using $G = P_\varphi$ since this variable can be computed using polar coordinates. For a fixed energy surface $\mathcal{S}(J_0)$, the variable

$L_\nu = L_\nu(J_0, \ell_\nu, G_\nu, s) \approx \frac{1}{\sqrt{2(J_0 - G_\nu)}}$ can be implicitly defined. It follows that the formula for angle of twist can be rewritten as

$$\frac{\left(\frac{\partial \ell_\nu}{\partial L_\nu(0)}\right)}{\left(\frac{\partial L_\nu}{\partial L_\nu(0)}\right)} = \frac{\left(\frac{\partial \ell_\nu}{\partial G_\nu(0)}\right)\left(\frac{\partial G_\nu(0)}{\partial L_\nu(0)}\right)}{\left(\frac{\partial L_\nu}{\partial G_\nu}\right)\left(\frac{\partial G_\nu}{\partial G_\nu(0)}\right)\left(\frac{\partial G_\nu(0)}{\partial L_\nu(0)}\right)} = \frac{\left(\frac{\partial \ell_\nu}{\partial G_\nu(0)}\right)}{\left(\frac{\partial G_\nu}{\partial G_\nu(0)}\right)\left(\frac{\partial L_\nu}{\partial G_\nu}\right)} = \frac{\left(\frac{\partial \ell_\nu}{\partial G(0)}\right)\left(\frac{\partial G(0)}{\partial G_\nu(0)}\right)}{\left(\frac{\partial L_\nu}{\partial G_\nu}\right)\left(\frac{\partial G_\nu}{\partial G}\right)\left(\frac{\partial G}{\partial G(0)}\right)\left(\frac{\partial G(0)}{\partial G_\nu(0)}\right)}$$

$$= \frac{\frac{\partial \ell_\nu}{\partial G(0)}}{\left(\frac{\partial G}{\partial G(0)}\right)\left(\frac{\partial G_\nu}{\partial G}\right)\left(\frac{\partial L_\nu}{\partial G_\nu}\right)} = \frac{\left(\frac{\partial \ell_\nu}{\partial G_\nu(0)}\right)\left(\frac{\partial G_\nu(0)}{\partial G(0)}\right)\left(\frac{\partial G_\nu}{\partial L_\nu}\right)}{\left(\frac{\partial G}{\partial G(0)}\right)\left(\frac{\partial G_\nu}{\partial G}\right)} \tag{4.5}$$

Since $G_\nu = G - \nu$, then $\frac{\partial G_\nu}{\partial G} = \frac{\partial G_\nu(0)}{\partial G(0)} = 1$. By Lemma A.3.4, $\left|\left(\frac{\partial G_\nu}{\partial L_\nu}\right)\right| \leq 0.350529$. By Theorem B.2.1, $\left(\frac{\partial G(t)}{\partial G(0)}\right) \in [0.12, 1.79]$. (These lemmas arose through detailed analysis of perturbation terms and so are relegated to the technical appendices. For the 2BP(SC), $\left(\frac{\partial G}{\partial L}\right) = L^{-3}$ and $\left(\frac{\partial G}{\partial G_0}\right) = 1$.) It follows that the denominator does not goto zero.

It remains to analyze the numerator. First note that since inside parabolic motions have well defined algebraically deformed Delaunay variables, then along a trajectory the equations of variation are also well defined. Working over the class of inside parabolic motions guarantees finite return times to an aphelion (see e.g. the previous section where condition (1) was shown). Since the segment of trajectory is finite, then there is a uniform bound on $\left(\frac{\partial \ell_\nu}{\partial G(0)}\right)$ over the entire revolution. It follows that the angle of twist cannot become $\frac{\pi}{2}$ by the numerator going to infinity.

It remains to show that the supremum of the angle of twist over the set $\mathcal{W}$ is uniformly bounded away from $\frac{\pi}{2}$. The rest of the chapter is devoted to this task. It suffices to prove:

Claim: $\left|\left(\frac{\partial \ell_\nu}{\partial G_\nu(0)}\right)\left(\frac{\partial G_\nu}{\partial L_\nu}\right)\right| \leq C < \infty$ for all points with initial conditions in $\mathcal{W} \cap \Sigma$.

The proof of this claim involves heavy analysis of perturbation terms and is

found in appendix C.4.

Since there is uniform upper bound on the numerator of (4.5) and a uniform lower bound on the denominator over all inside parabolic motions, then it follows that there is a uniform bound away from $\frac{\pi}{2}$. $\square$

Chapter 5

Localization of Aubry-Mather Sets

5.1 Indicators of non-integrability

In this section, heuristic techniques to measure how much the RCP3BP differs from the integrable 2BP(SC) system are developed. The dynamics far away from the sun is nearly integrable since the influence of Jupiter is negligible. It is only close to the sun that the perturbation term grows enough to qualitatively effect the dynamics.

When $\mu = 10^{-3}$ for $r \geq 5$, one can show that $|\Delta H| \leq 10^{-5}$ (see e.g. section A). For any mass ratio μ, define $r_{kick} = r_{kick}(\mu)$ to be the minimal radius so that $\forall r > r_{kick}$ it holds that $|\Delta H| \leq \frac{\mu}{100}$. Hence $r_{kick}(10^{-3}) = 5$. Recall that the region $\{r > r_{kick}\}$ is denoted as the *outside region* and the region $\{r \leq r_{kick}\}$ is denoted as the *kick region*.

Consider eccentricities which are known to be in the twist region Tw^{Del}. (See e.g. section 3.2.) Let T be the *fundamental period* of the comet, i.e. the time it takes the comet to make one complete revolution around the Sun-Jupiter system. By Kepler's Third Law, a solution with initial condition L_0 has $T \approx 2\pi L_0^3$.

Definition: For some $\Delta L > 0$ we say $L(t)$ satisfies the $(L_0, \Delta L)$ - *Containment Assumption* on $[0, T]$ if $\forall t \in [0, T]$, $L(t) \in [L_0 - \Delta L, L_0 + \Delta L]$. Call the interval $\mathcal{I}(L_0, \Delta L) = [L_0 - \Delta L, L_0 + \Delta L]$ the *containment interval*.

Define the following quantities to measure non-integrability of the system.

$$\delta L(L_0, \ell_0) = |L\big(t_P(L_0, \ell_0)\big) - L_0| \qquad \delta \ell(L_0, \ell_0) = \ell\big(t_P(L_0, \ell_0)\big) - \ell_0$$

where $t_P \approx -2\pi$ is first return time to the section $P = \{g = 0 \mod 2\pi\}$.

5.1.1 Heuristic Estimates for ΔL, δL and an a priori bound for ΔL

One can do some non-rigorous numerics to get rough estimates by fixing L_0 and looking at solutions over the fundamental period $T \approx 2\pi L_0^3$. The estimates below are worked out using $\mu = 10^{-3}$ and $J_0 = 1.8$ to get a feel for the quantities involved. Non-rigorous numerics for $16^{1/3} \leq L_0 \leq 30^{1/3}$ (i.e. $0.72 \leq e \leq 0.83$) indicate that

$$\delta L \approx 0.015 \qquad \Delta L \approx 0.03$$

The numerics also indicate that the bulk of the change in L occurs in the kick region. (Jupiter has *kicked* the comet.) In the outside region, $\delta L \approx 0.001$. This makes sense since $\Delta H = O(\frac{\mu}{r^3})$ so their should be less influence of Jupiter far away from the Sun-Jupiter system.

Using the 2BP(SC) as an approximation for motion of the comet, it takes approximately $18.7527 \approx 6\pi \approx 3$ iterates of $\mathcal{F}$ to cross the kick region. Hence, the **most** L can increase during one fundamental period is about $3 \cdot 0.015 + (n-3) \cdot 0.001$, where $n \approx L_0^{-3}$ is the total number of iterates needed to complete one revolution around the sun. For the range of values considered, this gives an upper bound on $\Delta L \approx 0.07$. Later an iterative scheme is developed to approximate ΔL and obtain consecutively better upper bounds for containment intervals.

One might wonder if an a priori bound for ΔL always exists. Note that

$$L = L(J_0, G, \ell, g) = \frac{1}{\sqrt{2(J_0 - G + \Delta H)}}$$

is an implicit function of the other Delaunay variables on the energy surface $\mathcal{S}(J_0)$. Then to obtain a bound for L over one fundamental period, it suffices to have bounds for G and ΔH. Bounds for ΔH are obtained in appendix A. Additionally in Lemma 2.2.2 estimates change in angular momentum $P_\varphi = G$ over a period. This lemma can be used obtain finite bounds for containment intervals of solutions with eccentricities $e \leq 0.96$. Above this value, it may be possible for the perturbation term to perturb an comet elliptic comet into a parabolic or hyperbolic orbit with $e \geq 1$ over the course of one fundamental period. This would correspond to $L \to \infty$ at some point in the orbit. Degeneracies for nearly parabolic motions in the Delaunay coordinate system limit the effectiveness of our methods.

The alternate coordinate systems discussed in chapter 3 do not suffer degeneracies for nearly parabolic motions. In both of algebraically deformed and dynamically deformed Delaunay variables, it is possible to obtain finite bounds on containment intervals since as $e \to 1$, the corresponding action variables remain bounded. Hence in what follows, there are no additional theoretical difficulties in carrying out the below constructions in Algebraically Defined Delaunay Variables or Dynamically Deformed Delaunay Variables, however the actual numerics may become more complicated. In order to get a feeling for the numerics, we focus on Delaunay variables and remain in a region away from nearly parabolic motions.

For low eccentricities, the bound on angular momentum in Lemma 2.2.2 gives

us reasonable bounds ΔL, e.g. $\Delta L = 1$ works for solutions with $e \leq 0.9$. However these rough bounds are typically far from optimal. Let us pursue an algorithm to produce much more accurate bounds.

5.1.2 Separation of Dynamics in Delaunay Variables

In this subsection a scheme to separate the dynamics into nearly integrable and non–integrable dynamics in Delaunay variables is developed. Ultimately the kick and outside regions shall be expressed in Delaunay.

Observe that $r = L^2(1 - ecos(u)) \approx \frac{J_0^2+u^2L^2}{2}$. Fixing r and J_0 allows one to estimate the product uL. Let

$$K(r, J_0) := \sqrt{2r - J_0^2}.$$

Then on $\mathcal{S}^{out}(J_0)$ when $r \leq r_{kick}$, $|uL| \lesssim K(r_{kick}, J_0)$. Note that $K(5, 1.8) = 2.6$.

Figure 5.1: The kick interval in the (u, L) plane

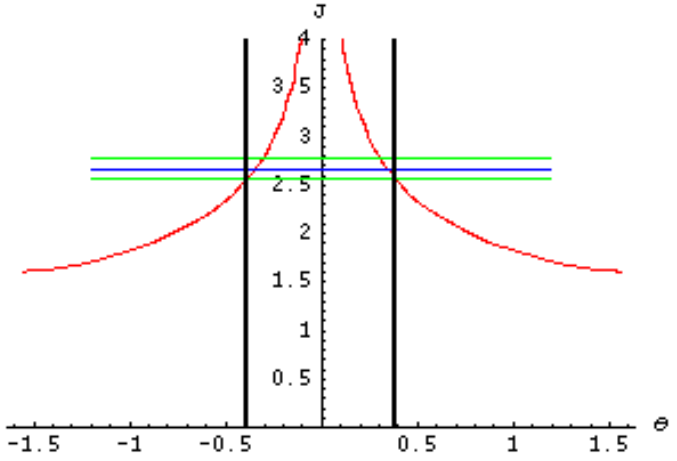

Fix J_0 and r_{kick} and consider the graph of the equation $u \cdot L = K(r_{kick}, J_0)$ on the uL plane. The graph consists of two hyperbolas. Suppose $\mathcal{I}(L_0, \Delta L)$ is a

containment interval for L_0. Call $[-\frac{K(r_{kick},J_0)}{L_0-\Delta L}, \frac{K(r_{kick},J_0)}{L_0-\Delta L}] \subset \mathbb{T} \ni u$ the *kick interval*. Geometrically the kick interval is the largest interval in u between the hyperbolas contained inside the containment interval on the uL plane (see fig. 5.1), and physically it corresponds to the place in the orbit where the comet has radius $r \lesssim r_{kick}$.

Let N be the number of iterates to cross the kick interval. Observe in figure 5.1 that the kick interval gets smaller for large L_0 values. Hence we expect an upper bound on N for L_0 sufficiently large. In fact this is the case.

Lemma 5.1.1. *For $\mu = 10^{-3}$, $J_0 = 1.8$, and $17^{\frac{1}{3}} \leq L \leq 8$ (i.e. for $0.7415 \leq e \leq 0.9747$), it takes at most 3 iterates to cross the kick interval.*

Proof: First precise bounds on the radius are established when solution is in the kick interval. Then rigorous numerical integration is used to estimate the time to cross the kick interval in polar coordinates. This data is then combined to estimate the number of iterates needed to cross the kick interval.

In appendix A, it is estimated that $\Delta H \in [-0.00063, 0.00063]$ for $r \geq 1.61$ and $\mu = 0.001$. The lower bound of 1.61 on radius is also found in that appendix. Since solutions are on $\mathcal{S}(J_0)$, then $G = J_0 - \frac{1}{2L^2} + \Delta H(r, \varphi)$. Since $e = \sqrt{1 - \frac{G^2}{L^2}}$ by definition, then bounds on ΔH and on L can be translated to bounds on e. In particular $17^{\frac{1}{3}} \leq L \leq 8$ implies $0.7415 \leq e \leq 0.9747$.

Let $u_\pm = \pm\frac{K(r_{kick},J_0)}{L}$. Recall $r_{kick}(10^{-3}) = 5$. Let $r_\pm = L^2(1 - e\cos(u_\pm))$. Then using the bounds on eccentricity, if $17^{\frac{1}{3}} \leq L \leq 8$, then $4 \leq r_\pm \leq 4.9$. Hence to determine the time to cross the kick interval it suffices to examine all trajectories on $\mathcal{S}(1.8)$ with $0.7415 \leq e \leq 0.9747$ which start at the $r = 5$ and measure the time

it takes these trajectories to cross $r = 5$ again.

Heuristic estimates of the time to cross the kick region can be found by approximating the RCP3BP with the 2BP(SC). See for example formula (2.5). These rough heuristics yield a maximum crossing time of 19.4861. The proof of Theorem 2.2.4 gives a method to bound the time for trajectories to go from $r = 5$ to $r = 5$. The method arises from rigorous numerical integration of the equations of motion. The computer finds the crossing time to be at most 18.2934 for the class of trajectories considered in the statement of the lemma.

To compute the number of iterates needed, estimates on return times to the section $\{g = 0 \mod 2\pi\}$ are needed. In Lemma A.3.2 it is established that $1.025 \geq |\dot{g}| \geq 0.9975$. Hence it takes at most $\frac{18.2934}{2\pi 0.9975} \leq 3$ iterates of $\mathcal{F}$ to cross the kick interval for the class of trajectories considered in the statement of the lemma. $\square$

Let us use the kick interval to separate the dynamics into nearly integrable and non-integrable pieces. Let $(\ell', L') = \mathcal{F}_\mu(\ell, L)$. Let u, u' be the eccentric anomalies which arise by solving Kepler's equation (3.1). Define the *Delaunay kick region* and *Delaunay outside region in the* (ℓ, L)*–plane* as follows:

$$\begin{aligned} R_{kick}(L_0, \Delta L) =& \{(\ell, L) : \ L \in \mathcal{I}(L_0, \Delta L), |uL| \leq K(r_{kick}, J_0) \text{ or } |u'L'| \leq K(r_{kick}, J_0)\} \\ R_{out}(L_0, \Delta L) =& \mathcal{I}(L_0, \Delta L) \times \mathbb{T} - R_{kick}(L_0, \Delta L), \end{aligned} \tag{5.1}$$

where $\mathcal{I}(L_0, \Delta L) = [L_0 - \Delta L, L_0 + \Delta L]$ is some confidence interval. Note that it takes 3 iterates of $\mathcal{F}_\mu$ to cross R_{kick} by Lemma 5.1.1.

5.1.3 Refinement of the Delaunay Kick and Outside Regions

In this subsection, a procedure to iteratively refine a containment interval's width $\Delta L = \Delta L^i$ is given. These refinements can be used to more accurately determine the Delaunay kick and outside regions. The algorithm requires $\Delta L = \Delta L^0$ as some known bound, obtained for example from estimates in section 5.1.1. Given a ΔL^i, it is possible to measure the errors from integrability in the Delaunay kick and outside regions by defining

$$\begin{aligned}
\delta L^{\text{kick}}_{(L_0,\Delta L^i)} &= \sup_{(L,\ell)\in R^i_{kick}(L_0,\Delta L^i)} \delta L(L,\ell), \quad \delta L^{\text{out}}_{(L_0,\Delta L^i)} = \sup_{(L,\ell)\in R^i_{out}(L_0,\Delta L^i)} \delta L(L,\ell),\\
\delta \ell^{\text{kick,min}}_{(L_0,\Delta L^i)} &= \inf_{(L,\ell)\in R^i_{kick}(L_0,\Delta L^i)} \delta \ell(L,\ell), \quad \delta \ell^{\text{out,min}}_{(L_0,\Delta L^i)} = \inf_{(L,\ell)\in R^i_{out}(L_0,\Delta L^i)} \delta \ell(L,\ell),\\
\delta \ell^{\text{kick,max}}_{(L_0,\Delta L^i)} &= \sup_{(L,\ell)\in R^i_{kick}(L_0,\Delta L^i)} \delta \ell(L,\ell), \quad \delta \ell^{\text{out,max}}_{(L_0,\Delta L^i)} = \sup_{(L,\ell)\in R^i_{out}(L_0,\Delta L^i)} \delta \ell(L,\ell).
\end{aligned} \tag{5.2}$$

Let $n = \lceil L_0^3 \rceil$. Then the fundamental period $T \approx 2\pi n$. Use the above estimates to inductively define

$$\Delta L^{i+1} = N\delta L^{\text{kick}}_{(L_0,\Delta L^i)} + (n-N)\cdot \delta L^{\text{out}}_{(L_0,\Delta L^i)} \tag{5.3}$$

where N is the number of iterates to cross the kick region. To start the algorithm, the following condition is required to hold:

$$\Delta L^1 \leq \Delta L^0.$$

This bound is satisfied if the estimates in section 5.1.1 based off of Lemma 2.2.2 are used. Indeed these give worse case bounds. The heuristic estimates found in section 5.1.1 can also be used to obtain a reasonable value of ΔL^0. For example when $\mu = 10^{-3}$ and $J_0 = 1.8$, the bound $\Delta L^0 = 0.1 > 0.07$ may be used to start the

algorithm for $16^{1/3} \leq L \leq 30^{1/3}$. For these parameters, Lemma 5.1.1 tells us $N = 3$ as well. If ΔL^1 is not smaller than ΔL^0, the initial guess of ΔL^0 was poor, and a larger initial value must be selected.

Let us examine the potential convergence of the sequence $\{\Delta L^i\}_{i\geq 0}$ by examining how changing ΔL^i effects ΔL^{i+1}. Note that decreasing ΔL^i reduces the size of the kick region R_{kick} since fewer solutions are included when taking the supremums in the definitions of the δL^{kick} and δL^{out} values. Fewer solutions are included because the thickness of the regions in the L direction has decreased (see equation (5.1) and figure 5.1), even though the boundary between the kick and outside region remains the same. Similarly picking a larger ΔL^i increases the size of the kick region R_{kick}. From this observation, it follows from the inductive definition that $\{\Delta L^i\}$ is decreasing sequence.

There is a certain degree of flexibility here. Indeed, if there is some error in the bounds (say from a computer approximation) with $\Delta L^i_{approx} \approx \Delta L^i$ and $\Delta L^i_{approx} \leq \Delta L^{i-1}$, then the sequence still convergences. Care must be taken when using a computer since mathematically values at the tail end of the sequence $\{\Delta L^i\}$ converge, but on a computer rounding errors from floating point arithmetic may spoil convergence when $|\Delta L^i - \Delta L^{i+1}|$ becomes smaller than machine-ϵ. In practice it suffices to iterate until $|\Delta L^i - \Delta L^{i+1}|$ is within some specified tolerance larger than machine precision.

Figure 5.2: The idea behind localization intervals on the (L, ℓ) cylinder

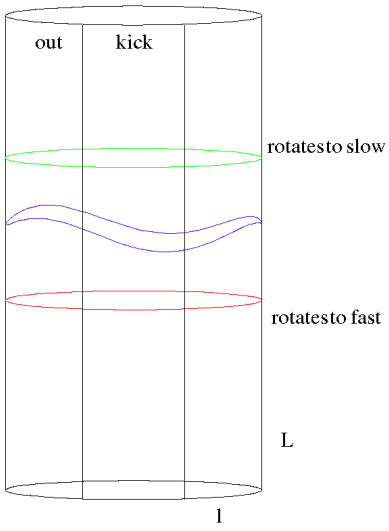

5.2 Localization Intervals

The goal of this section is to construct intervals in the L direction which contain all solutions of a given rotation number. An explicit numerical algorithm is developed to efficiently compute these intervals. The estimates on non-integrability from the previous section along with the ordering condition from Aubry-Mather theory are used to produce the explicit bounds required for algorithm.

Definition: For a specified rotation symbol[1] $\omega \in [\frac{1}{n+1}+, \frac{1}{n}-]$, call the interval $\mathcal{L}_n \subset \mathbb{R} \ni L$ a *localization interval* for ω if the Aubry-Mather set $\Sigma_\omega \in \mathcal{L}_n \times \mathbb{T}$.

The next theorem gives the existence of finite localization intervals in the twist region Tw^{Del} where the map $\mathcal{F}_\mu$ is twisting in Delaunay variables. The key to the proof establishing that for a specified a rotation number ω, it is possible to start so

[1]It turns out there are three *rotation symbols* ordered as $\frac{p}{q}- < \frac{p}{q} < \frac{p}{q}+$ associated to the rational number $\frac{p}{q}$. An irrational rotation symbol is the same as the irrational rotation number. See section 6.2 for more details.

high up on the cylinder that solutions rotates too slowly have the rotation number ω. See figure 5.2. The method of proof leads to a numerical algorithm to compute localization intervals. We remark that the proof also holds for the deformed action-angle coordinate systems used in 3 and gives finite localization intervals in the region Tw^{∞}.

Theorem 5.2.1 (Localization Intervals)**.** *Fix mass ratio μ, Jacobi constant J_0, and rotation symbol $\omega \in [\frac{1}{n+1}+, \frac{1}{n}-]$. Suppose $A_n < \omega^{-\frac{1}{3}}$ and ΔL are nonnegative real numbers such that the $(A_n, \Delta L)$ containment assumption is satisfied for all solutions with initial conditions $L_0 = A_n$. Suppose $B_n > \omega^{-\frac{1}{3}}$ and $\Delta L'$ are nonnegative real numbers such that the $(B_n, \Delta L')$ containment assumption is satisfied for all solutions with initial conditions $L_0 = B_n$. Further suppose that*

$$N\delta\ell^{kick,min}_{(A_n,\Delta L)} + (n-N)\delta\ell^{out,min}_{(A_n,\Delta L)} \geq 2\pi \tag{5.4}$$

$$N\delta\ell^{kick,max}_{(B_n,\Delta L')} + (n+1-N)\delta\ell^{out,max}_{(B_n,\Delta L')} \leq 2\pi \tag{5.5}$$

holds, where N is the number of iterates needed to cross the Delaunay kick region. Then $[A_n, B_n]$ is an ω-localization interval. Moreover $A_n, B_n < \infty$.

Proof: Suppose a solution with initial condition $L_0 = A_n$ satisfies the $(A_n, \Delta L)$ containment assumption. By the assumptions on $A_n < \omega^{-\frac{1}{3}} \leq (n+1)^{\frac{1}{3}}$ and ΔL, then $L_0, ...L_n \in [A_n - \Delta L, A_n + \Delta L]$. We seek to violate the following condition:

$$\ell_n - \ell_0 < 2\pi \tag{5.6}$$

which says that after one fundamental period $T \approx 2\pi A_n^3$, the variable ℓ should have changed by at most 2π. This is what it means to have $\omega \leq \frac{1}{n}-$. The above

inequality is an instance of an ordering condition found in Aubry-Mather theory. See section 6.2 for a more general statement about ordering conditions. Note that since $\omega < \frac{1}{n}-$ that periodic orbits of period n are not considered, which is why there is a strict inequality in (5.6).

Violation of the ordering condition (5.6) means solutions rotate too fast to have rotation symbol less than $\frac{1}{n}-$. Let us examine when this occurs. Recall that

$$\dot{L} = -\partial_\ell \Delta H,$$

$$\dot{\ell} = L^{-3} + \partial_L \Delta H.$$

A worst case scenario is 'overspeeding' where the L_i's increase with maximum possible speed, which causes the ℓ-velocity to decrease, and the trajectory to slow down in the ℓ-direction. Now define the sequence L_i^+ by

$$\begin{cases} L_0^+ = A_n & \\ L_i^+ = A_n + i\delta L^{\text{kick}}_{(A_n,\Delta L^i)} & i = 1, 2, \ldots, N \\ L_i^+ = A_n + N\delta L^{\text{kick}}_{(A_n,\Delta L^i)} + (i-N)\delta L^{\text{out,max}}_{(A_n,\Delta L^i)} & i = N, \ldots, n \end{cases}$$

Since the comet visits the kick interval at most N times during one fundamental period, and the most L can increase in one iterate is $\delta L^{\text{kick}}_{(A_n,\Delta L)}$ in the Delaunay kick region and $\delta L^{\text{out}}_{(A_n,\Delta L)}$ in the Delaunay outside region, then the L_i^+'s are the fastest increasing sequence which satisfies then $(A_n, \Delta L)$-containment assumption. Let us

estimate the amount of rotation in ℓ this sequence exhibits by calculating

$$\begin{aligned}\ell_n - \ell_0 &= \sum_{i=0}^{n-1} \ell_{i+1} - \ell_i \\ &\geq \sum_{kick} (\ell_{i+1} - \ell_i) + \sum_{outside} (\ell_{i+1} - \ell_i) \\ &\geq N\delta\ell^{kick,min}_{(A_n,\Delta L)} + (n-N)\delta\ell^{out,min}_{(A_n,\Delta L)}\end{aligned}$$

where the last line follows from the fact that it takes at most N iterates to cross the kick region. By choice of A_n, specifically property (5.4), the sequence $\{L_i^+\}$ violates the ordering condition (5.6). The value of A_n is low enough on the cylinder that trajectories must make more than one full turn after n iterates. Hence an Aubry-Mather set with $\omega < \frac{1}{n}-$ must have L at least A_n.

To prove the upper bound of the localization interval, a similar argument can be made. Suppose a solution with initial condition $L_0 = B_n$ satisfies the $(B_n, \Delta L')$ containment assumption. By the assumptions on $B_n > \omega^{-\frac{1}{3}} \geq n^3$ and $\Delta L'$, then $L_0, ...L_{n+1} \in [B_n - \Delta L', B_n + \Delta L']$. We seek to violate the following condition

$$\ell_{n+1} - \ell_0 > 2\pi. \tag{5.7}$$

which says that after one fundamental period $T \approx 2\pi B_n^3$, the variable ℓ should have changed by at least 2π. This is what is means to have $\omega \geq \frac{1}{n+1}+$. Again note that (5.7) is a strict equality since the case of a periodic orbit of period $n+1$ is ruled out by choice of rotation symbols.

A worst case scenario in this case is 'underspeeding' where the L_i's decrease with maximum possible speed, which causes the ℓ-velocity to increase, and the trajectory to speed down in the ℓ-direction.

Consider the sequence

$$\begin{cases} L_0^- = B_n & \\ L_i^- = B_n - i\delta L^{\text{kick}}_{(B_n,\Delta L')} & i = 1, 2, \ldots, N \\ L_i^- = B_n - N\delta L^{\text{kick}}_{(B_n,\Delta L')} - (i-N)\delta L^{\text{out}}_{(B_n,\Delta L')} & i = N, \ldots, n+1. \end{cases}$$

By construction, this is the fastest decreasing sequence of L's which satisfy the $(B_n, \Delta L')$ containment assumption. Let us estimate the amount of rotation in ℓ this sequence exhibits by calculating

$$\begin{aligned} \ell_{n+1} - \ell_0 &= \sum_{i=0}^{n} \ell_{i+1} - \ell_i \\ &\leq \sum_{kicks} (\ell_{i+1} - \ell_i) + \sum_{outer} (\ell_{i+1} - \ell_i) \\ &\leq N\delta \ell^{kick,max}_{(B_n,\Delta L')} + (n+1-N)\delta \ell^{out,max}_{(B_n,\Delta L')} \end{aligned}$$

where the last line follows from the fact that it takes at most N iterates to cross the kick region. By choice of B_n, specifically property (5.5), the sequence $\{L_i^-\}$ violates the ordering condition (5.7). The value of B_n is high enough on the cylinder that trajectories must make less than one full turn after $n+1$ iterates. Hence an Aubry-Mather set with $\omega > \frac{1}{n+1}+$ must have L at most B_n. □

Remark: The interval $[A_n, B_n]$ in the Localization Intervals Theorem is not necessarily optimal, i.e. it is possible that there is a localization interval $[\tilde{A}_n, \tilde{B}_n] \subset [A_n, B_n]$. Ideally one selects the largest A_n and the smallest B_n which satisfies the hypothesis of the Theorem. Even then, the theorem gives only a sufficient condition, not necessary condition for the interval to be a localization interval, i.e. it is still possible there is a smaller localization interval.

5.2.1 A Numerical Algorithm to Compute Localization Intervals

The Localization Interval Theorem is designed for ease of computation. Consider the following algorithm.

1. Suppose $L \in [L_x, L_y]$. Divide up the (ℓ, L) space $\mathbb{T} \times [L_x, L_y]$ into a large number of small rectangular boxes. Fix N, M large positive integers. Let $a_i = i\frac{2\pi}{N}$, $b_j = j\frac{L_y - L_x}{M}$. Consider boxes of the form $R_{i,j} = [a_i, a_{i+1}] \times [b_j, b_{j+1}]$. Use COSY-JERI, a rigorous integrator (described in the appendix E.1) to rigorously transport a box of initial conditions $R_{i,j}$ for one iterate of $\mathcal{F}$. COSY-JERI can be used to compute the quantities δL and $\delta\ell$ for each box. In fact, it produces upper and lower bounds for each of these quantities which are rigorous and which account for rounding error from the computer. Store all this information.[2]

2. Input a rotation number ω and machine precision ϵ. Let $I = 0$ and $J = 0$.

3. Input ΔL^0, an estimate on the size of containment intervals for $L \in [L_x, L_y]$. This estimate can be generated using the heuristics found in section 5.1.1.

4. Find largest k and smallest k' so that interval $\Delta L^I \subset [b_k, b_{k'}]$.

5. Compute extremized terms in formulas (5.2) using the associated containment interval $\mathcal{I}(b_J, \Delta L^I)$. This is quick and requires only the stored data from step

[2]Step 1 is done independently of the other steps. All the rigorous numerical integration is contained in step 1. Any other algorithm to produce the desired bounds may be used. Mathematica can produce accurate (but non-rigorous) estimates of the quantities in this step.

1. Adopt the convention that if the curve $uL = K(r_{kick}, J_0)$ passes through a box, then record the values associated to the box as being in both the outside and kick regions.

6. Use the iterative formula (5.3) to find ΔL^{I+1}. If $\Delta L^I > \Delta L^{I+1}$, then a bad initial guess was made in step 3 for ΔL^0, or the numbers N, M are too small. Go back to step 1, and use a larger N and M or go back to step 3 and use a larger ΔL^0. Otherwise, $\Delta L^{I+1} \leq \Delta L^I$. If $|\Delta L^{I+1} - \Delta L^I| > 2\epsilon$, then let $I := I + 1$ and goto step 4. Otherwise goto step 7.

7. Use the data from step 1 to check the hypothesis in the Localization Intervals Theorem. If b_J satisfies one of the conditions (5.4), output **true**. Otherwise output **false**. Record this information. Let $I := 0$ and $J := J + 1$. If $J = M$, then end. Otherwise goto back to step 3.

For a fixed ω, the algorithm assigns a 'true' or 'false' to each integer $j \in [0, M-1]$. True if the ordering conditions are violated holds for some b_J, and false if the hypothesis of the theorem do not hold. The intervals b_J where the ordering conditions holds contain the localization intervals by construction since the complement is where ordering fails. This gives an approximation for the localization intervals. Specifically, the localization interval $[A_n, B_n] \subset [b_J, b'_J]$ where b_J is the smallest b value for which the algorithm returns true and b'_J is the largest b value for which the algorithm returns true. Note that the size of the boxes in L direction (controlled by M) limits our accuracy for the size of the localization intervals. Using larger M increases accuracy, but at the cost of increasing computation time.

5.2.2 Numerical Results for Localization Intervals

The numerical algorithm in section 5.2.1 may be applied to the case $\mu = 10^{-3}$ and $J_0 = 1.8$. Divide up $L \in [L_x, L_y] = [2.35, 3.4375]$ into $M = 261$ intervals of size $\frac{1}{240}$. Divide up $\ell \in [0, 2\pi]$ into $N = 1024$ intervals of size $\frac{2\pi}{1024}$. Note the L values are inside of the twist region Tw^{Del} (see section 3.2). Apply the numerical algorithm from section 5.2.1 to approximate the localization intervals. These computations are very lengthy and can take many hours of computer time (19,440,062s = 225 days) to complete. See details on the method of integration in chapter E. Our calculations find the following localization intervals.

$$n = 14 : \ L \in [2.408333333333333, 2.466666666666667]$$

$$n = 15 : \ L \in [2.462500000000000, 2.520833333333333]$$

$$n = 16 : \ L \in [2.516666666666667, 2.575000000000000]$$

$$n = 17 : \ L \in [2.570833333333333, 2.620833333333334]$$

$$n = 18 : \ L \in [2.616666666666667, 2.670833333333333]$$

$$n = 19 : \ L \in [2.666666666666667, 2.716666666666667]$$

$$n = 20 : \ L \in [2.712500000000000, 2.762500000000000]$$

$$n = 21 : \ L \in [2.758333333333333, 2.804166666666667]$$

$$n = 22 : \ L \in [2.800000000000000, 2.845833333333333]$$

$$n = 23 : \ L \in [2.841666666666667, 2.887500000000000]$$

$$n = 24 : \ L \in [2.883333333333333, 2.925000000000000]$$

$$n = 25 : \ L \in [2.920833333333333, 2.962500000000000]$$

$$n = 26 : \ L \in [2.958333333333333, 3.004166666666667]$$

$$n = 27 : \ L \in [2.995833333333334, 3.037500000000000]$$

$$n = 28 : \ L \in [3.033333333333334, 3.075000000000000]$$

$$n = 29 : \ L \in [3.070833333333333, 3.108333333333333]$$

$$n = 30 : \ L \in [3.104166666666667, 3.141666666666667]$$

5.3 Crossings

Corollary 5.3.1 (Crossings)**.** *Suppose* $\omega \in [\frac{1}{n+1}+, \frac{1}{n}-]$*, and* $[b_J, b_{J'}]$ *is the approximate localization interval computed with the numerical algorithm in section 5.2.1, and whose existence is guaranteed by the Localization Intervals Theorem. Suppose there is a trajectory* $\{(L_i, \ell_i)\}$ *of* $\mathcal{F}$ *such that* $L_0 < b_J$ *and there is an* $N \in \mathbb{Z}$ *such that* $L_N > b_{J'}$*. Then the Aubry-Mather set* Σ_ω *is* **not** *an invariant curve.*

Proof: If for some $\omega \in [\frac{1}{n+1}, \frac{1}{n}]$ the corresponding Aubry-Mather set Σ_ω is an invariant curve, then by the Localization Interval Theorem, it is contained inside of $[b_k, b_{k'}] \times \mathbb{T}$. This implies there is no trajectory which starts below the curve Σ_ω and passes above it. Below and above are well defined notions because Σ_ω is a Lipschitz graph over $\mathbb{T}$ (see [MF]). This is a contradiction for $\omega \in [\frac{1}{n+1}+, \frac{1}{n}-]$. □

To find crossings, it suffices to convert the L localization intervals into G localization intervals by $G = 1.8 - \frac{1}{2L^2} + \Delta H$. Bounds on ΔH are known, $|\Delta H| \leq$

0.00063 (see appendix A), and with them its possible obtain appropriate enclosures. Once in terms of $G = P_\varphi$, it suffices to use polar coordinates to find a trajectory which crosses the G localization interval. This is done since integration in polar is much quicker due to the fact that the equations of motion are much simpler than those in Delaunay. Below is the data for the crossing solutions. 'IC' the initial condition in polar with coordinates $(r, \varphi, P_r, P_\varphi)$. T is the time to cross the localization interval. The range of L values the trajectory assumes is given.

- $n = 18, T = 1500$

  IC: $(11.882750717370106, 3.866366342271249, -0.024625597427182747, 1.7267051815071077)$

  L Range: $[2.604, 2.683]$

- $n = 19, T = 1500$

  IC: $(5.01, 6.283185307179586, -0.3715957930145508, 1.72898)$

  L Range: $[2.648, 2.747]$

- $n = 20, T = 1500$

  IC: $(5, 3.436116964863836, -0.3773091819709596, 1.73111)$

  L Range: $[2.690, 2.783]$

- $n = 21, T = 2000$

  IC: $(4.263811806062144, 5.233883200329416, -0.4224129822178366, 1.7377381471786353)$

  L Range: $[2.719, 2.835]$

- $n = 22, T = 1541$

  IC: $(9.359317378038725, 3.957177159072638, 0.2197328531636448, 1.7344673150647805)$

  L Range: $[2.757, 2.881]$

- $n = 23, T = 1584$

  IC: $(14.039965526307196, 3.5135666542693986, 0.0023316149314888592, 1.736425237043458)$

  L Range: $[2.795, 2.947]$

- $n = 24, T = 2472$

  IC: $(11.812906753494273, 1.257110055261819, 0.1499017007611752, 1.7373980380662546)$

  L Range: $[2.819, 2.973]$

- $n = 25, T = 2005$

  IC: $(9.221213881804852, 2.0075139824889248, 0.24400191401211596, 1.739107823003018)$

  L Range: $[2.859, 3.024]$

- $n = 26, T = 1793$

  IC: $(6.9285220034089114, 5.047263708867263, -0.32897852787229304, 1.7413678940444803)$

  L Range: $[2.903, 3.058]$

- $n = 27$ AND $n = 28, T = 2118$

  IC: $(6.427536659398464, 3.383038880595336, -0.3511117427396554, 1.7428168698946467)$

  L Range: $[2.944, 3.100]$

Remark: All digits of accuracy are needed due to extreme sensitivity on initial conditions.

Each of these initial conditions is integrated using the COSY-JERI integrator as described in appendix E. Typical run time might be about a week to verify a solution. However a nonrigorous numerical integrator can easily compute such a solution quickly. In fact this is how these solutions were found; Mathematica was programmed to integrate a large number of solutions and check for crossings. Note

as well that in some cases the crossing trajectories are well above and below the known localization interval bounds. This is because when working with rigorous numerics the integrator must account for noise in the form of rounding errors and as a consequence, an extra buffer is needed to ensure the crossing is verified.

Figure 5.3: $n = 28$ crossing - P_φ vs. time

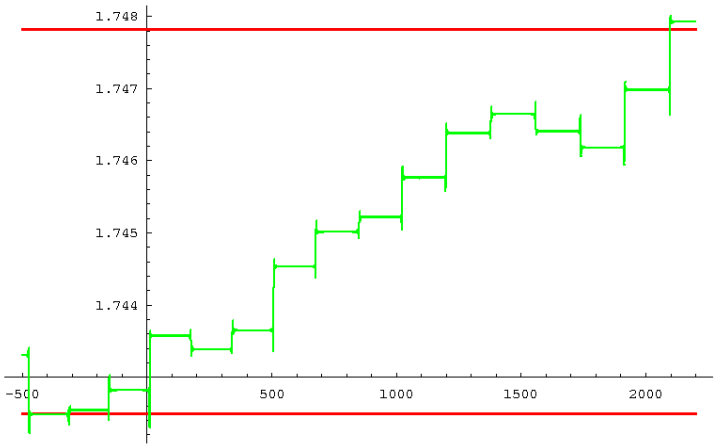

Remark: Note in figure 5.3 that one can clearly see the 'kicks' when the comet comes close to the sun. They are large jumps which separate flat regions to form a type of bizarre staircase. Also note how the function is flat most of the time. The flatness is a visual indication that the problem is nearly integrable far from the sun since the perturbation term is small away from the sun and hence angular momentum remains nearly constant.

In light of the numerical data above,

Theorem 5.3.2. *For RCP3BP*$(0.001, 1.8)$ *there are no invariant curves with rotation number between* $\frac{1}{28}$ *and* $\frac{1}{18}$. *Hence there are no invariant curves between* $0.748 \leq e \leq 0.826$.

Proof: If there was an invariant curve of rotation number $\omega \in [\frac{1}{28}, \frac{1}{18}]$,

then it would be contained in some localization interval. But there are trajectories which cross localization intervals for all Aubry-Mather sets of the specified rotation number. Contradiction. Hence there are no invariant curves. □

Chapter 6

Applicability of Aubry-Mather Theory to the RCP3BP

6.1 A quick review of Aubry-Mather theory

Call a compact invariant region C is bounded by two rotationally invariant curves C_- and C_+ such that there are no rotationally invariant curves in between C_- and C_+ a *Birkhoff Region of Instability* (BRI). In such BRIs, Birkhoff showed the existence of orbits coming arbitrarily close to C_- and C_+ (see [MF]). A much stronger result given by Mather in [Ma2] which allows one to specify neighborhoods of certain invariant sets which the orbit must pass through. Before stating this result, a quick overview of basic facts of Aubry-Mather theory shall be given. This review is primarily drawn from [Ban], [MF], [G], [Mo1], [S], and [BK].

Suppose $F : \mathbb{T} \times \mathbb{R} \to \mathbb{T} \times \mathbb{R}$ is a C^r $(r \geq 1)$ map. Let $\tilde{F} : \mathbb{R} \times \mathbb{R} \to \mathbb{R}$ be the lift of F to the universal cover. Let π denote the canonical projection of $\mathbb{R}$ onto $\mathbb{T}$. Call an F *exact area preserving twist map (EAPT)* if and only if

- F is area preserving: $|\det(dF)| = 1$.
- F is *exact*: if for any non-contractible curve γ the oriented area between γ and its image $F(\gamma)$ is zero.
- F is *twist*: if for $\tilde{F} = (\tilde{F}_\theta, \tilde{F}_I)$ the sign $(\partial_I \tilde{F}_\theta)$ is constant and nonzero. This implies that the image of a vertical line in the cylinder is tilted in one direction

relative to the vertical direction.

Consider the bi-infinite sequence $\{\tilde{F}^i(\tilde{\theta}_0, \tilde{I}_0) = (\tilde{\theta}_i, \tilde{I}_i)\}$ of images. It turns out that every EAPT can be described by a *generating function* $h : \mathbb{R} \times \mathbb{R} \to \mathbb{R}$. This can be described via the generating function by

$$\tilde{I}_k = -\partial_1 h(\tilde{\theta}_k, \tilde{\theta}_{k+1}) \qquad \tilde{I}_{k+1} = \partial_2 h(\tilde{\theta}_k, \tilde{\theta}_{k+1})$$

The definition of h is extended to segments by

$$h(\tilde{\theta}_0, \tilde{\theta}_1, ...\tilde{\theta}_n) = \sum_{i=0}^{n-1} h(\tilde{\theta}_i, \tilde{\theta}_{i+1})$$

Definition: A segment $(\tilde{\theta}_0, \tilde{\theta}_1, ...\tilde{\theta}_n)$ is *minimizing* if for any other segment $(\tilde{\theta}'_0, \tilde{\theta}'_1, ...\tilde{\theta}'_n)$ with $\tilde{\theta}_0 = \tilde{\theta}'_0$ and $\tilde{\theta}_n = \tilde{\theta}'_n$, then

$$h(\theta_0, \theta_1, ...\theta_n) < h(\theta'_0, \theta'_1, ...\theta'_n)$$

A sequence $\{\tilde{\theta}_i\}$ is *minimal* if every finite segment in the sequence is minimal. Minimal sequences are action minimizing. More specifically, the generating function $h(\theta_0, \theta_1)$ gives the minimal action to move between θ_0 and θ_1 in one iterate of $\tilde{F}$. Notice that

$$\partial_2 h(\theta_{k-1}, \theta_k) + \partial_1 h(\theta_k, \theta_{k+1}) = 0 \text{ for all } k \in \mathbb{Z}$$

is a discrete version of the Euler-Lagrange equations. Let $\widetilde{St}(h)$ denote the set of all orbits which satisfy the discrete (EL) equations. Call such orbits *stationary orbits*. Stationary orbits are extremizers. Let $\widetilde{\Sigma}(h) \subset \widetilde{St}(h)$ denote the set of all action minimizing orbits and note that $\widetilde{\Sigma}(h) \subset \widetilde{St}(h)$ and this implies $\pi(\widetilde{\Sigma}(h)) = \Sigma(h) \subset St(h) = \pi(\widetilde{St}(h))$.

For a stationary configuration $\Theta = \{\tilde{\theta}_k\}$ call the piecewise linear graph connecting $(k, \tilde{\theta}_k)$ with $(k+1, \tilde{\theta}_{k+1})$ for each $k \in \mathbb{Z}$ *the Aubry graph.* Suppose for a stationary configuration $\Theta = \{\tilde{\theta}_k\}$ the limit

$$\omega = \omega(\Theta) = \lim_{k\to\infty} \frac{\tilde{\theta}_k}{k}$$

exists. Call ω the *rotation number of* Θ. Geometrically ω is the average slope of the Aubry graph of Θ.

Theorem 6.1.1 (Aubry,Mather)**.** *Every minimal configuration has a rotation number. Conversely, for every $\omega \in \mathbb{R}$ there is a minimal configuration with rotation number ω.*

Let $\Sigma_\omega = \{\Theta \in \Sigma(h) | \omega(\Theta) = \omega\}$ be the set of all minimal configurations of rotation number ω. This set is called an *Aubry-Mather set of rotation number* ω.

Some additional information about Aubry-Mather sets with rational rotation numbers is required to understand parts of this thesis. Pick a rational rotation number $\omega = \frac{p}{q}$. Let $\Sigma^{per}_{p/q}$ be the set of action minimizing periodic points of period q and rotation number p/q. Two periodic points θ^- and θ^+ are adjacent elements of $\Sigma^{per}_{p/q}$ if $\tilde{\theta}^-$ and $\tilde{\theta}^+$ have no other elements of $\widetilde{\Sigma}^{per}_{p/q}$ between them ([Ban]). For adjacent periodic points θ^- and θ^+ in $\Sigma^{per}_{p/q}$ let

$$\Sigma^+_{p/q}(\theta^-, \theta^+) = \{\theta \in \Sigma_{p/q} : \ \theta \text{ is } \alpha \text{ (resp. } \omega\text{)–asymptotic to } \theta^- \text{ (resp. } \theta^+\text{)}\}$$

$$\Sigma^-_{p/q}(\theta^-, \theta^+) = \{\theta \in \Sigma_{p/q} : \ \theta \text{ is } \alpha \text{ (resp. } \omega\text{)–asymptotic to } \theta^+ \text{ (resp. } \theta^-\text{)}\}$$

$$\Sigma^\pm_{p/q} = \bigcup_{\theta^- \text{ adjacent to } \theta^+ \text{ in } \Sigma^{per}_{p/q}} \Sigma^\pm_{p/q}(\theta^-, \theta^+)$$

Theorem 6.1.2 (Structure theorem: Rational case $\omega = p/q \in \mathbb{Q}$)**.** *The Aubry-Mather set $\Sigma_{p/q}$ is a disjoint union of $\Sigma^{per}_{p/q}$, $\Sigma^{+}_{p/q}$, and $\Sigma^{-}_{p/q}$. Moreover, $\Sigma^{per}_{p/q}$ is always non-empty and if $\Sigma^{per}_{p/q}$ is not a curve, then $\Sigma^{-}_{p/q}$ and $\Sigma^{+}_{p/q}$ are non-empty too.*

In order to distinguish such invariant sets, follow Mather (see e.g. [MF] §13) and introduce rotation symbols ω^*. If Θ has an irrational rotation number ω, then its rotation symbol is $\omega^* = \omega$. In the rational case we have three options:

1. If $\Theta \in \Sigma^{-}_{p/q}$, then its rotation symbol is $p/q-$.
2. If $\Theta \in \Sigma^{per}_{p/q}$, then its rotation symbol is p/q.
3. If $\Theta \in \Sigma^{+}_{p/q}$, then its rotation symbol is $p/q+$.

There is an ordering on the set of rotation symbols given by $\omega^* < \bar{\omega}^*$ iff either underlying numbers satisfy $\omega < \bar{\omega}$ or $\omega = \bar{\omega} = p/q$ and $p/q- < p/q < p/q+$.

It turns out that minimizers satisfy the following ordering condition:

Ordering condition: *If $\Theta = \{\tilde{\theta}_k\}$ is a minimal configuration for rotation symbol $\omega^* \leq p/q$, then $\tilde{\theta}_{k+q} \leq \tilde{\theta}_k + p$ for all $k \in \mathbb{Z}$.*

Using a sophisticated variational problem with constraints Mather [Ma2] proved the following theorem about existence of connecting orbits:

Theorem 6.1.3 (Mather Connecting Theorem)**.** *Suppose $\omega_1 < \alpha_1, \alpha_2 < \omega_2$ and suppose there are no rotationally invariant curves with rotation number $\omega \in (\omega_1, \omega_2)$ in a BRI. Then there is a trajectory in the phase space whose α-limit set lies in the Aubry-Mather set Σ_{α_1} and whose ω-limit sets lies in Σ_{α_2}. Moreover, for a sequence of rotation numbers $\{\alpha_i\}_{i\in\mathbb{Z}}$, $\alpha_i \in (\omega_1, \omega_2)$ and a sequence of positive numbers $\{\epsilon_i\}$,*

there exists an orbit in the phase space $\{p_j\}$ *and an increasing bi-infinite sequence of integers* $j(i)$ *such that the* $dist(\Sigma_{\alpha_i}, p_{j(i)}) < \epsilon_i$ *for all* $i \in \mathbb{Z}$. *[Ma2]*

Presently there are simplifications of this proof in [Be], [BK],and [Xia1]. Unfortunately the region we consider for our analysis of the RCP3BP is **not** invariant as trajectories can leak out of Tw^{Del} to higher eccentricities. However it turns out that the hypothesis of a BRI in Mather Connecting Theorem can be relaxed slightly without affecting the conclusion. We shall do so using the EAPT $\mathcal{F}_{dyn}$ and the domain $Tw^{Del} \cup \mathcal{W}$. The key is to specify the location of local and global minimizers, which is done using the methods in chapter 5.

6.2 The Applicability of Aubry-Mather Theory to the RCP3BP

In chapter 3, is was shown that the map $\mathcal{F}$ is an EAPT on a certain domain, and hence it is possible to apply the results of Aubry-Mather theory in this domain. Recall that the map $\mathcal{F}_\mu$ is defined as follows. Starting with the RCP3BP in Delaunay coordinates, the dynamics is restricted to the 3 dimensional energy surface $\mathcal{S}(J_0)$. The restricted dynamics has a naturally defined Poincaré map $\mathcal{F}_\mu : \{g = 0 \mod 2\pi\} \to \{g = 0 \mod 2\pi\}$. Recall that the action comparison is formulated in polar coordinates, and the comparison performed with the Lagrangian dual to the polar Hamiltonian which has two degrees of freedom. Not only have coordinate systems changed, but the dimension has been reduced.

Unfortunately and somewhat surprisingly, the Hamiltonian of RCP3BP in polar is convex, while in Delaunay coordinates it has a concave component (in L)

and a degeneracy (in G). Thus, to connect polar and Delaunay dynamics requires additional care. In this section, the connection between the polar Lagrangian and the map $\mathcal{F}_\mu$ is justified. The following lemma is needed to bridge the gap between the two different types of dynamics.

Lemma 6.2.1. *Suppose $\mathcal{F}_\mu$ has a rotational curve[1] $\mathcal{T}^1 \subset Tw^{Del}$. Then there is an action minimizing rotational 2-torus $\mathcal{T}^2$ for the flow of the Hamiltonian H_{Polar}.*

See [Be2] for a much more general and powerful statement regarding the persistence of action minimizing sets under canonical coordinate change.

The plan for this section is following. A proof of Lemma 6.2.1 established by connecting the dynamics of three dynamical systems, namely the systems with H_{Polar}, H_{Del}, and $\mathcal{F}_\mu$. Once in place, the lemma allows one to apply the action comparison method in polar coordinates to rule out the existence of rotational curves for the map $\mathcal{F}_\mu$. (Recall that rotational curves are obstructions to diffusion.) Next work shall commence to apply the Mather Connecting Theorem to the map $\mathcal{F}_\mu$ in the region of instability. Special care must be taken since the instability region is not invariant. The Mather Connecting Theorem provides existence of connecting orbits for the map $\mathcal{F}_\mu$ and instabilities for the map $\mathcal{F}_\mu$ are mirrored by motions of the comet in polar coordinates.

[1]Rotational curves are invariant curves which are not homotopically equivalent to single points.

6.2.1 Proof of Lemma 6.2.1

$$\boxed{\text{1: Rotating Polar Coordinates: } H = H_{Polar}(r, \varphi, P_r, P_\varphi)}$$

$$\Uparrow$$

$$\boxed{\text{2: Delaunay Coordinates: } H = H_{Del}(\ell, L, g, G)}$$

$$\Updownarrow$$

$$\boxed{\text{3: Reduced Energy Coordinates: } \mathcal{F} = \mathcal{F}_\mu(\ell, L)}$$

First let us formulate the three systems described in the diagram above. Equation (1.2) formulates the RCP3BP in rotating polar coordinates with a Hamiltonian H_{Polar}. Given H_{Polar}, the Delaunay Map $\mathcal{D}$ from section 3.1 can be applied to convert from polar to Delaunay variables away from parabolic motions. The Hamiltonian becomes H_{Del} given by Equation (3.2). It is not necessarily clear that H_{Del} convex or that action minimizers will exist. Consider the energy reduction procedure described in appendix C.2 applied to the Hamiltonian H_{Del}. Call the energy reduced Hamiltonian $\tilde{H}_{J_0}$. By construction, orbits of $\tilde{H}_{J_0}$ and orbits of H_{Del} are equivalent on the energy surface $\mathcal{S}(J_0)$ when G is written implicitly in terms of energy and the other Delaunay variables. $\tilde{H}_{J_0}$ is the time-periodic Hamiltonian with 1.5 degrees of freedom used in section 3.2, and by the results of that section the Poincaré map $\mathcal{F}_\mu$ formulated from $\tilde{H}_{J_0}$ is an EAPT on a certain domain.

Lemma 6.2.2. *There are no rotational curves for the map $\mathcal{F}_\mu$ if and only if there are no rotational 2-tori for the flow of the Hamiltonian H_{Del}.*

Proof: This claim follows from the general results on Poincaré Maps. □

From the claim it suffices to show that a rotational 2-tori for the flow of the Hamiltonian H_{Del} maps under $\mathcal{D}$ to an action minimizing rotational 2-tori for the flow of the Hamiltonian H_{Polar}. Action minimizing in this context means action minimizing with respect to the Lagrangian L which is Legendre transform of the polar Hamiltonian H_{Polar}.

To go between 1 and 2, some additional machinery is required. A priori when making a canonical change of coordinates, the image $\mathcal{D}(\mathcal{T}^2)$ of a rotational 2-torus $\mathcal{T}^2$ in Delaunay is not necessarily a graph over the base anymore. All that can be said is that $\mathcal{D}(\mathcal{T}^2)$ is an invariant object under the flow since the change of variables $\mathcal{D}$ is a smooth diffeomorphism away from parabolic motions. Hence it must be shown that $\mathcal{D}(\mathcal{T}^2)$ is rotational and that it is action minimizing.

Lemma 6.2.3. *Suppose $\mathcal{T}^2$ is a rotational 2-torus for the flow of the Hamiltonian H_{Del}. Then $\mathcal{D}(\mathcal{T}^2)$ is a rotational 2-torus for the flow of the Hamiltonian H_{Polar}.*

Proof: Suppose $\mathcal{T}^2$ is a rotational 2-torus for the flow of the Hamiltonian H_{Del} and $\mathcal{D}(\mathcal{T}^2)$ is its image. It must be shown that the P_r and P_φ components of $\mathcal{D}(\mathcal{T}^2)$ are graphs over the base (r, φ). Since dynamics is restricted to the energy surface $H = -J_0$ in both coordinate systems, then it holds that

$$P_\varphi = P_\varphi(r, \varphi, P_r; J_0) = r^2 - \sqrt{r^4 + 2r - r^2(P_r^2 + 2J_0 + 2\Delta H(r, \varphi))}$$

Hence if P_r is a graph over the base (r, φ), i.e. $P_r = P_r(r, \varphi)$, then it follows that P_φ is also a graph over the base.

A careful analysis of the map $\mathcal{D}$ indicates

$$r = L^2(1 - e\cos(u)) \qquad Pr = \frac{Le\sin(u)}{r}$$
$$\varphi = g + 2\arctan(\sqrt{\frac{1+e}{1-e}}\tan(\frac{u}{2})) \qquad P_\varphi = G$$
$$\ell = u - e\sin(u) \qquad e = \sqrt{1 - \frac{G^2}{L^2}}$$

For constant L and G (e.g. in the 2BP(SC)), then (r, P_r) is a function of the variable u only. It turns out that P_r is a double graph over r in an "onion" (see fig. 6.1). This is because fixing r fixes u, which in turn fixes P_r up to sign. Rotation inside the "onion" corresponds to rotation in the ℓ direction, the "layer" of the onion corresponds to the L direction. The G and P_φ directions are the same, and rotation in the g direction corresponds to rotation in the φ direction. In this case, being rotational in Delaunay translates to being rotational in polar, with the caveat that the P_r may be a double graph.

Figure 6.1: Integrable Torus Blue in $(\phi, P_\varphi, \frac{1}{\sqrt{r}}, P_r)$ coordinates

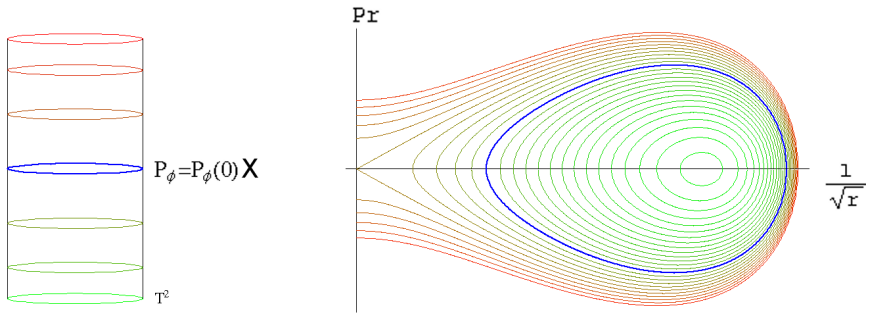

The case when L, G are non-constant is not that much worse. We seek to show the double graph property for P_r, i.e. we seek to show that $\mathcal{D}(\mathcal{T}^2) \cap \{P_r \geq 0\}$

and $\mathcal{D}(\mathcal{T}^2) \cap \{P_r \leq 0\}$ are graphs. Suppose not. Then there two points on $\mathcal{D}(\mathcal{T}^2)$ which have the same (r, φ) coordinates, but have two different P_r coordinates, $P_r^1 > P_r^2 > 0$. But when $\dot{r} = P_r > 0$, then r is a monotone strictly increasing function. Furthermore $\dot{\varphi} < 0$, so φ is a monotone strictly decreasing. Since $\mathcal{D}(\mathcal{T}^2)$ is invariant under the flow, there cannot be two distinct points (r, φ, P_r^1) and (r, φ, P_r^2) with $P_r^1 \neq P_r^2$ since this would contradict the monotonicity of r or φ. Hence the image of $\mathcal{D}(\mathcal{T}^2)$ is rotational. □

The reason the rotational (graph) property is desired is the following lemma.

Lemma 6.2.4. *(McDuff/Salamon [MS]) Suppose $H : \Omega \times \mathbb{R}^n \to \mathbb{R}$ where $\Omega \subset \mathbb{R}^n$ is a Hamiltonian which satisfies the Legendre condition $\frac{\partial^2 H}{\partial p^2} > 0$. Moreover, assume for every $q \in \Omega$ the map $\mathbb{R}^n \to \mathbb{R}^n$ given by $p \mapsto \partial_p H(q, p)$ has a global inverse so the inverse Legendre transformation gives rise to a Lagrangian $L : \Omega \times \mathbb{R}^n \to \mathbb{R}$. Let $S : \Omega \to \mathbb{R}$ be a solution of the Hamilton-Jacobi equation $H(q, \partial_q S) = E$. Suppose $\gamma : [t_0, t_1] \to \Omega$ is invariant under the flow of H with $\dot{\gamma} = \partial_p H\big(q, \partial_q S(p)\big)$, and suppose $\xi : [t_0, t_1] \to \Omega$ is any absolutely continuous function such that $\xi(t_0) = \gamma(t_0)$ and $\xi(t_1) = \gamma(t_1)$. Then γ is action minimizing. Specifically,*

$$\int_{t_0}^{t_1} L(\gamma, \dot{\gamma}) dt \leq \int_{t_0}^{t_1} L(\xi, \dot{\xi}) dt$$

To complete the proof of Lemma 6.2.1, appeal to Lemma 2.1.1 which states that rotational 2-tori in polar are action minimizers. This turns out to be a corollary of Lemma 6.2.4.

Proof of Lemma 2.1.1: The polar Hamiltonian for RCP3BP satisfies the requirements of Lemma 6.2.4; namely it is convex. See Lemma C.1.1. However one

must be a bit careful in its application. Lemma 6.2.4 requires that if an invariant curve γ is contained inside of an invariant torus $\mathcal{T}^2$, then $\mathcal{T}^2$ is a graph over the base. In polar, $P_r = P_r(r, \varphi)$ and $P_\varphi = P_\varphi(r, \varphi)$ are graphs over (r, φ) on the invariant torus. In Lemma 6.2.3 a small ambiguity arose from the fact that $\pm P_r(r, \varphi)$ could both be on an invariant torus (for example an invariant curve could pass through an aphelion or perihelion which causes the sign of P_r to change). It is true that $\mathcal{T}^2 \cap \{P_r \geq 0\}$ and $\mathcal{T}^2 \cap \{P_r \leq 0\}$ are graphs over (r, φ). To apply Lemma 6.2.4 for an invariant curve γ, note that it suffices to decompose γ into pieces where $P_r \geq 0$ and $P_r \leq 0$, and apply Lemma 6.2.4 to the respective pieces. □

This completes the proof of Lemma 6.2.1. □

Remark: The conclusion of Lemma 6.2.1 also holds using the dynamically deformed coordinate system for the map $\mathcal{F}_{dyn}$ in the domain $\mathcal{W}$ where the map is known to be twisting. Now instead of passing from polar to Delaunay, consider passing from polar to algebraically deformed Delaunay variables (ADDV), then from ADDV to dynamically deformed Delaunay variables (DDDV) (see 3). The formulas for passing from Polar to ADDV in Lemma 6.2.3 remain identical except for the addition of a subscript ν on all Delaunay variables. Hence arguments involving the graph property go through unchanged. To see that the image in ADDV of an rotational graph which originated in DDDV is rotational note that the curve straightening which produces DDDV from ADDV always rotates vectors by strictly than less $\frac{\pi}{2}$ so the direction of the flow (i.e. the ℓ direction) remains the same and is never interchanged with the action (i.e. L direction).

6.2.2 Connecting Orbits

In this subsection the hypothesis of the Mather Connecting Theorem (Theorem 6.1.3) are relaxed slightly which allows for analysis of dynamics of the RCP3BP as described by the map $\mathcal{F}_\mu$, or alternatively $\mathcal{F}_{dyn}$ for nearly parabolic motions. For maps, the twist regions are free of invariant curves by results of chapter 2 and Lemma 6.2.1, however neither domain is invariant. The key to relaxing the invariance hypothesis of the Mather Connecting Theorem is to specify the location the minimizing, i.e. Aubry Mather sets. This is the aim of the next several lemmas.

Lemma 6.2.5. *For any $c > 0$ there is a c-neighborhood $N(\omega, c)$ of the Aubry Mather set Σ_ω for $\omega > 0$ which has well defined action-angle (ADDV) coordinates.*

Remark: Recall that by construction algebraically deformed Delaunay variables (ADDV) are defined for nearly parabolic motions. The results of section 4.2 may be used to produce dynamically deformed Delaunay variables on a set $\mathcal{W}$ which contains a large subset of nearly parabolic motions. Using these dynamically deformed variables, the dynamics may be reduced to that of an EAPT map $\mathcal{F}_{dyn}$ defined in a semi-infinite domain. Hence it suffices to show that action-angle variables are well defined in ADDV.

Proof of Lemma 6.2.5: After passing through a perihelion, a solution either has an aphelion in its future, or it does not. If it does not have an aphelion in the future, the comet must exit parabolically or hyperbolically. Solutions which exit the Solar System hyperbolically do not have well defined rotation numbers since they must eventually leave the neighborhood of the separatrices where algebraically

deformed Delaunay variables (ADDV) are defined. Parabolic solutions have rotation number $\omega = 0$ since they correspond to separatrices which are converging to the fixed point at infinity in $(\frac{1}{\sqrt{r}}, P_r)$ variables (see fig. 3.2).

The separatrices are contained in the domain of definition of ADDV by construction (see fig 4.3). Furthermore, all other trajectories in the domain of definition contain an aphelion in their futures and trajectories remain inside the domain of definition until that aphelion is reached. Hence these solutions have well defined algebraically deformed variables.

Solutions with aphelions stay some bounded distance way from the separatrices and the boundary of the domain of definition. When expressed in ADDV, then these points in the domain of definition have a finite L_ν value (recall $L_\nu \to \infty$ at the boundary of the domain of definition). See figures 4.3 and 3.3. But then Aubry-Mather sets which contain these types of solutions must have rotation numbers $\omega > 0$. Since L_ν is bounded, then we can take as large of a neighborhood in the L_ν direction as desired around the Aubry-Mather set Σ_ω for $\omega > 0$. □

Lemma 6.2.6. *Let* $\omega_{max} = \sup\{\omega : \Sigma_\omega \subset Tw^{Del} \cup Tw^{\infty}\}$ *be the maximal rotation number for Aubry-Mather sets which are contained in the twist region* $Tw^{Del} \cup Tw^{\infty}$. *There is a continuous function* $c(\omega) > 0$ *such that for all* $\omega \in (0, \omega_{max})$, *there is a* $c(\omega)$*–neighborhood* $N(\omega, c)$ *of* Σ_ω *contained in* $Tw^{Del} \cup Tw^{\infty}$.

Proof: This follows from results in chapter 5 on localization of Aubry-Mather sets.

Consider the collection of neighborhoods for $\omega, \omega' \in (0, \omega_{max})$:

$$N(\omega, \omega', c) := \bigcup_{\rho \in (\omega, \omega')} N(\rho, c).$$

Lemma 6.2.7. *There exists $c > 0$ such that an orbit of $\mathcal{F}_{dyn}$ connecting Σ_ω and $\Sigma_{\omega'}$ belongs $N(\omega, \omega', c)$.*

The lemma follows from careful study of Mather's original proofs. [Xia1] contains a simpler approach to these results. Simply follow Xia's exposition and note that almost connecting orbits stay in a $2c$ neighborhood of Σ_ω and $\Sigma_{\omega'}$. Such a c is guaranteed to exist by Lemma 6.2.5 and the Mather Connecting Theorem may be applied in the non-invariant region $N(\omega, \omega', c)$. The main theorem on the

Figure 6.2: Neighborhoods of Aubry-Mather Sets in the (ℓ, L) cylinder

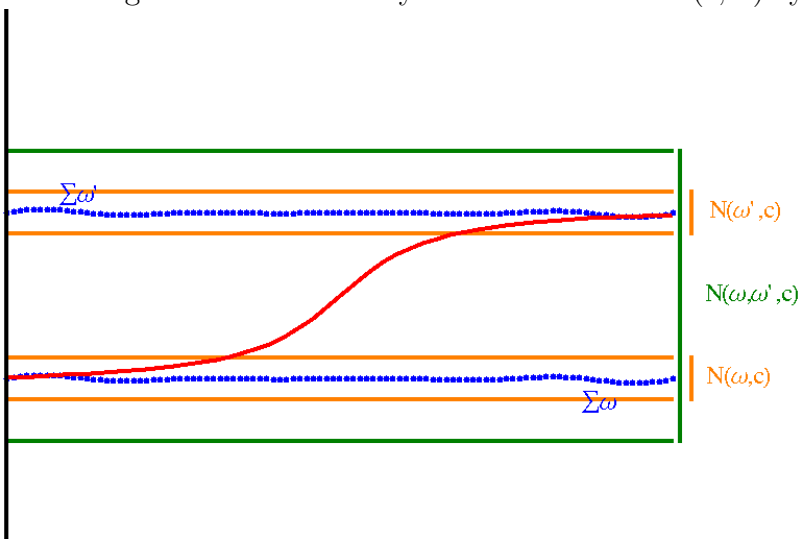

existence of instabilities for the RCP3BP may now be proved.

Proof of Theorem 1.1.2: To get a diffusing orbit in polar coordinates, the Mather Connecting Theorem is used to provide the existence of an orbit of $\mathcal{F}_{dyn}$ with specified properties.

Smaller rotation numbers correspond to slower rotation around the base $\mathbb{T}$ in the ℓ direction, but this is to say that smaller rotation numbers correspond to higher eccentricities. To start 'at the bottom' of the region of instability, choose rotation numbers $\{\omega_i\}_{i<0}$ corresponding to eccentricities near $e = e^*(\mu, J_0) \ll 1$ and pick the $\{\epsilon_i\}_{i<0}$ to come arbitrarily close to the desired rotation numbers. In negative time the trajectory given by the Mather Connecting Theorem shall limit to a bounded Aubry-Mather set of positive rotation number.

To diffuse upwards, select a finite sequence of ω_i's sufficiently close and by Lemma 6.2.7, connecting orbits remain in a neighborhood $N(\omega, \omega', c)$ of the Aubry-Mather sets for some c.

We claim there exists a ω^* such that solutions in a neighborhood of Σ_{ω^*} escape to infinity after a final passage by the Sun-Jupiter system. Provided such an ω^* exists, select the ω_i's in Mather's Connecting theorem to approach this ω^* in order to escape. Note that Lemma 6.2.7 holds for almost connecting orbits between $\omega = \omega^*$ and $\omega = 0$. Simply pick neighborhoods for $\omega, \omega' \to 0$ with $c \to 0$. Hence the trajectory can always remain in the neighborhood of minimizers. It remains to show that ω^* exists.

Consider solutions that have $e(t) < 1$ for $t \leq 0$, but eventually leave the homoclinic loop where action-angle variables are well defined (see fig. 3.3.) Escape is possible if $e(t) \geq 1$ for all sufficiently large t. In order to produce such solutions, note that if a comet is exiting the solar system, then at some point, it must make a last passage by the Sun-Jupiter system. During this passage, Jupiter perturbs the eccentricity by some quantity Δe. If the comet has initial eccentricity e^{exit}

sufficiently close to one before a close passage, and after this passage $e = e^{exit} + \Delta e > 1$ is large enough, then the comet exits the solar system hyperbolically.

To verify this magnitude of jump is possible, the jump in eccentricity is phrased in terms of a jump in angular momentum. Then the results in section B.1 apply. It turns out that to exit after a passage by the Sun on $\mathcal{S}^{out}(1.8)$ then $P_\varphi > 1.8 + 0.04\mu$ when $r = 5$. When passing by the Sun-Jupiter system, the jump in angular momentum can be as large as μ (this follows from the rigorous numerics in Theorem 2.2.4). It follows that Δe can be as large as 0.07μ for nearly parabolic motions. Hence for $e^{exit} = 1 - 0.07\mu$ escape is possible after a single passage by the Sun-Jupiter system.

Since $e^{exit} < 1$, then a solutions with e^{exit} have a finite L_ν value, denoted L_ν^{exit}, since $L_\nu = L_\nu(J_0, e)$. Since $L_\nu^{exit} < \infty$ there is an Aubry-Mather set Σ_{ω^*} with rotation number $\omega^* > 0$ and a neighborhood $N(\omega^*, c) \subset [L_\nu^{exit}, \infty]$. □

Remark: While elements of the proof explicitly used constants derived from $J_0 = 1.8$ and $\mu = 10^{-3}$, the software used is robust enough to handle other constants. See chapter E.

One could visualize the Aubry-Mather sets as the remainders of tori after a perturbation has been filled them with infinitely many small holes. To envision a diffusing orbit, first imagine unrolling the cylinder on the real plane. A diffusing orbit will be one which "climbs a set of stairs", i.e. increases in the holes of the Aubry-Mather set, and then follows the remnants of a torus of higher rotation number for a while. The largest increase ("taking a step") occurs primarily at times when the comet is at the perihelion. See figure 6.3.

Figure 6.3: A Diffusing Orbit (ℓ vs. e)

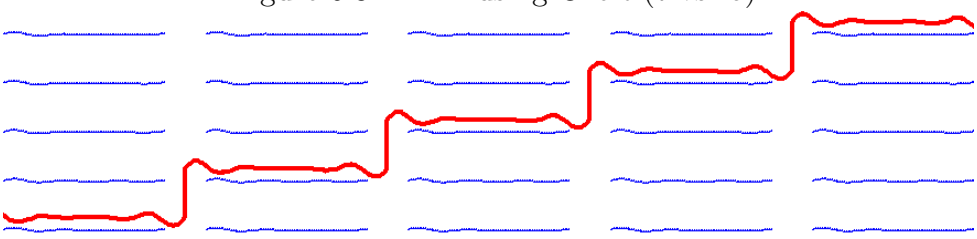

6.2.3 Proof of Chazy Motions

Proof of Corollary 1.1.4: Realization of Chazy Motions is an easily consequence of the application of Mather's variational methods. It suffices to describe how to get the desired behavior in one direction, since achieving different behaviors in forward and backward time is obtained by concatenation of two one-sided sequences of rotation numbers.

In order to achieve bounded motions, pick diffusing orbits to limit to an Aubry-Mather set Σ_ω with $\omega > \omega^* > 0$ where ω^* is defined in the proof of Theorem 1.1.2. More specifically pick sequences $\omega_i \to \omega$ and $\epsilon_i \to 0$ in Mather's Connecting Theorem. For example, ω could correspond to the rotation number for some rotationally invariant curve of low eccentricity, say a KAM curve.

In order to get unbounded hyperbolic motions, use the method described in the proof of Theorem 1.1.2. Namely, approach the rotation number ω^* before a perihelion, and after a perihelion, a neighborhood of these solutions is carried to infinity hyperbolically.

Since $\mathcal{U} = N(\omega^*, c(\omega^*)) \cap \{P_r = 0\}$ contains solutions with $|\dot{r}| \to c > 0$ as $t \to \infty$, then in some larger neighborhood $\hat{\mathcal{U}}$ there are points which escapes with $|\dot{r}| \to 0$, i.e. parabolically, by smooth dependence on initial conditions. In the

unperturbed case $\mathcal{F}_0$ has a fixed point at infinity and the homoclinic loop at infinity corresponding to parabolic motion. In the perturbed case $\mu > 0$, the separatrices no longer overlap, and some of points on the separatrices have eccentricities less than one. While the separatrices themselves have rotation number $\omega = 0$, they lay in the neighborhood of Σ_{ω^*} at the perihelion. To limit to parabolic motions, it is possible to pick a finite sequence of $\omega_i \to \omega^*$ and ϵ_i sufficiently small solutions to constrain solutions into a neighborhood where escape is possible. Then select as the tail of the sequence rotation numbers $\omega_i \to 0$ and $\epsilon_i \to 0$. The diffusing trajectory then must have a parabolic tail.

To get oscillatory orbits, pick a sequence of rotation numbers ω_i with a subsequence $\omega_{i_k} \to 0$ and every other term in the sequence bounded away from rotation number $\omega = 0$. Pick the ϵ_i so that the neighborhood of ω_{i_k} is so small that the neighborhood never intersects the separatrices when leaving the sun. Since the time between an aphelion and perihelion is finite, this is possible. Physically this constrains the comet to always have an aphelion and turn around to make another pass by the Sun-Jupiter system. □

Chapter 7

Estimating the Speed of Diffusion

7.1 Introduction

The strategy for bounding diffusion time is to produce an orbit which escapes the Solar System after a minimal number of revolutions around the Sun. Physically, this orbit corresponds to a comet getting a nearly maximal gravity assist from Jupiter after each passage by the Sun-Jupiter system. Mathematically, 'cheap' channels are constructed near action minimizing Aubry-Mather sets which the comet follows for long periods of time far from the Sun. The results of chapter 2 say that Aubry-Mather sets in a certain domain are not invariant curves. In this domain, when the comet is close to the Sun, it is possible to jump through the holes in the Aubry-Mather sets increase eccentricity (see e.g. figure 6.3). The magnitude of the jumps dictates the speed of diffusion. In an abstract sense, it is known that the size of the jump is $O(\mu)$. To make obtain concrete numbers, a computer is used to estimate the magnitude of the jumps. This makes it possible to obtain the specific numbers used in Theorem 1.2.1.

Plan of the Proof of Theorem 1.2.1:

1. **Lagrangian Formulation**. The RCP3BP is formulated in terms of Lagrangian formalism using rotating polar variables. This was originally introduced in section 2.1. Instead of the usual action, the Maupertuis formulation

of action is used. This constrains minimizers to be on the fixed energy surface $\mathcal{S}^{out}(J_0)$. Section 7.2 discusses this further.

2. **Variational Problem with Constraints**. Constrained minimizers are introduced in section 7.3. An abstract variational problem with constraints is defined, whose solution (known as constrained minimizer) is a diffusing orbit. In section 7.4, a variational problem for the RCP3BP is formulated where constraints are on the angular variable φ. Explicit construction of constraints is the focus of next several steps.

3. **Action Comparison**. The action comparison method in 2 is modified to construct the constraints that the comets must pass through during a passage by the Sun-Jupiter system to be action minimizing. The modification is necessary to show the presence of interior minima. The heuristics of the action comparison are introduced in section 7.5.

4. **Jumps in Eccentricity**. Analytic work far away from the Sun and computer assisted work near the Sun are used to analyze how much eccentricity changes when the comet makes a passage by the Sun-Jupiter system. This is introduced in section 7.6.

5. **Construction of Diffusing Orbits**. The constraints are explicitly constructed so that pseudo-trajectories which passes through the constrains increase in eccentricity in a nearly maximal way. In a neighborhood of the pseudo-trajectory there is a diffusing trajectory. Explicitly counting the num-

ber of passages by the Sun-Jupiter system completes the proof. This is introduced in section 7.7.

6. **Alternative Approach** In section 7.8 an alternative method of constructing diffusing orbits which does not utilize variational techniques is introduced. This method is primarily numerical in nature and may be useful for applications.

Remark 1: the numerical results of this chapter still need verification via interval arithmetic. Good heuristics have been developed, however the actual numerical values are subject to change. Essentially the analog of section 2.2 needs to be completed using the modified action comparison developed in section 7.5. Work has begun on this, however it is not at a sufficiently developed level that it warrants inclusion the present work.

Remark 2: The proof of Theorem 1.1.2 in no way depends on the results of this chapter. In fact Theorem 1.2.1 provides alternative verification of 1.1.2 in the domain where the variational problem has the solution and there is a diffusing orbit.

7.2 Lagrangian Formulation

This section formulates the problem in terms of Lagrangian formalism. Recall that when minimizing the action functional (see e.g section 2.1.1), the start and end positions in the configuration space are fixed as is the time to move between the start and end points. A priori energy of the minimizer cannot be specified. But to construct diffusing orbits on an energy surface, this is precisely what is required.

This is remedied by using the Maupertuis formulation of minimizers which makes it possible to a priori specify the energy of minimizers.

Notice the RCP3BP Lagrangian given by (2.1) can be decomposed as $L = L_2 + L_1 + L_0$ where L_i are homogeneous of degree i with respect to velocity.

$$L_0 = \frac{r^2}{2} + \frac{1}{r} - \Delta H(r, \varphi) \qquad L_1 = \dot{\varphi} r^2 \qquad L_2 = \frac{\dot{r}^2}{2} + \frac{\dot{\varphi}^2 r^2}{2}$$

Let $q_0, q_1 \in \mathbb{R}^2 \ni (r, \varphi)$ and consider absolutely continuous curves $\gamma : [t_0, t_1] \to \mathbb{R}^2$ with $\gamma(t_i) = q_i$. Define the Maupertuis functional to be

$$M_h(\gamma) := \int_{t_0}^{t_1} (2\sqrt{(L_0 + h)L_2} + L_1)\big(\gamma(t), \dot{\gamma}(t)\big) dt$$

Remark: Since the integrand is homogeneous, it does not matter what $(t_1 - t_0)$ is and hence $M_h(\gamma)$ is independent of parameterization of γ.

It was noted by Rick Moeckel that minimizers of M_h **do exist** for the RCP3BP (see [Moe] sect. 2). Moeckel's Theorem applies to the case of the RCP3BP in rotating polar coordinates in a compact subset of the outer Hill region away from the boundary. This theorem applies to the present construction since only finite length curves contained between two passages of the Sun are constructed. These curves have a finite maximal radius from the Sun, so it suffices to use Moeckel's Theorem in a compact region which is contains the class curves which shall be constructed.

It turns out that minimizers to M_h are on the energy surface $H = h$. An absolutely continuous curve γ is *on the energy surface* $H = h$ if $H(\gamma, \dot{\gamma}) = h$ wherever the derivative is defined. Denote such curves by γ_h. Define the Maupertuis action

between q_0 and q_1 to be

$$M_h(q_0, q_1) := \inf_{\gamma_h} M_h(\gamma_h)$$

Direct calculation shows that $H = L_2 - L_0 = h$, hence on the energy surface $H = h$,

$$2\sqrt{L_2(L_0 + h)} + L_1 = 2(L_0 + h) + L_1 = L + h. \tag{7.1}$$

As a consequence of the above identity, Kozlov provides the following theorem about minimizers (see [AKN] section 4):

Theorem 7.2.1 (Kovlov)**.** *Suppose $\gamma_h : [t_0, t_1] \to \mathbb{R}^2$ is a smooth curve on the energy surface $H = h$ that does not intersect the boundary of the Hill regions. Then γ_h is a solution to the Euler-Lagrange equations if and only if γ_h is a critical point of M_h.*

As a consequence of Theorem 7.2.1, Lemma 2.1.1, and formula 7.1, trajectories inside of the rotational tori are minimizers for the Maupertuis action. Hence when constructing diffusing orbits, one may remain in a neighborhood of a rotational torus to reduce the Maupertuis action. Far away from the Sun, this is easy as rotational tori are flat; they look like the rotational tori from the integrable 2BP(SC).

7.3 Constrained Minimizers

This section explores the idea of constraining minimizers for the Maupertuis action. This idea appears to have originated in a paper by Bangert where he considers Aubry Mather Theory on geodesic flows of $\mathbb{T}^2$ in order to obtain minimizers with specified dynamical properties [Ban]. By imposing constraints on the choice of

curves to minimize over, the property of global action minimization is lost. However it is still possible to construct curves which are local minimizers, and hence satisfy the Euler-Lagrange equations (i.e. are solutions to our Hamiltonian) by Theorem 7.2.1. It is these trajectories which can exhibit diffusion if the constraints are carefully chosen.

Let

$$M_h(q_0, q_1, ..., q_n) := \sum_{i=0}^{n-1} M_h(q_i, q_{i+1})$$

(note the analog to the generating function h found in section 6.1). For $\mathcal{I} = \{I_i\}_{1 \leq i \leq n-1}$ a collection compact intervals with nonempty interiors, let

$$M_h(q_0, q_n; \mathcal{I}) := \min_{a_i \in I_i} M_h(q_0, ..., q_n) \tag{7.2}$$

Definition 7.3.1. *A trajectory γ with endpoints q_0, q_n passing through the points $q_i \in I_i$ for all i that minimizes $M_h(q_0, .., q_n)$ is known as a constrained minimizer. The intervals I_i are known as constraints.*

Curves which pass through the constraints are not necessarily trajectories. This is because passage through a constraint may require a curve to pass through bad region that increases the Maupertuis action. Since $M_h(q_0, q_1, ..., q_n)$ smoothly depends on the a_i's, then if a curve γ passes through an expensive point q_i for some $1 \leq i \leq n-1$, then a nearby curve $\tilde{\gamma}$ which passes through $\tilde{q}_i$ can reduce the value of $M_h(q_0, ..., q_n)$. Since each I_i is compact, $M_h(q_0, ..., q_n)$ has a minimum value, and the curve that achieves the minimum satisfies the Euler-Lagrange equations by Theorem 7.2.1 and hence is realized as a trajectory to the Hamiltonian system. This idea is formally stated in the following lemma (motivated by the notations in [Xia1]):

Lemma 7.3.2. *For $\mathcal{I} = \{I_i\}_{1 \leq i \leq n}$ a collection compact intervals with nonempty interiors, if $\forall i$,*

$$M_h(...q_{i-1}, b, q_{i+1}) > \min_{q_i \in I_i} M_h(...q_{i-1}, q_i, q_{i+1}) \text{ for } b \in \partial I_i$$

then the constrained minimizer passes through the interior of I_i.

Proof: It is always possible to find $a^* \in I_i$ with $M_h(...q_{i-1}, a^*, q_{i+1}) = \min_{q_i \in I_i} M_h(...q_{i-1}, q_i, q_{i+1})$ since I_i is a compact interval with nonempty interior and $M_h(...q_{i-1}, q_i, q_{i+1})$ smoothly depends on q_i since only finite length pieces of trajectory are considered. (Simply consider all possible finite length curves connecting q_{i-1} to q_{i+1} passing through I_i on $H = h$.) Since $M_h(...q_{i-1}, b, q_{i+1}) > M_h(...q_{i-1}, a^*, q_{i+1})$ then this implies the constrained minimizer is on the interior of I_i (see fig. 7.1). □

Figure 7.1: More expensive curves touch the boundary and cheaper ones pass on the interior (picture in configuration space)

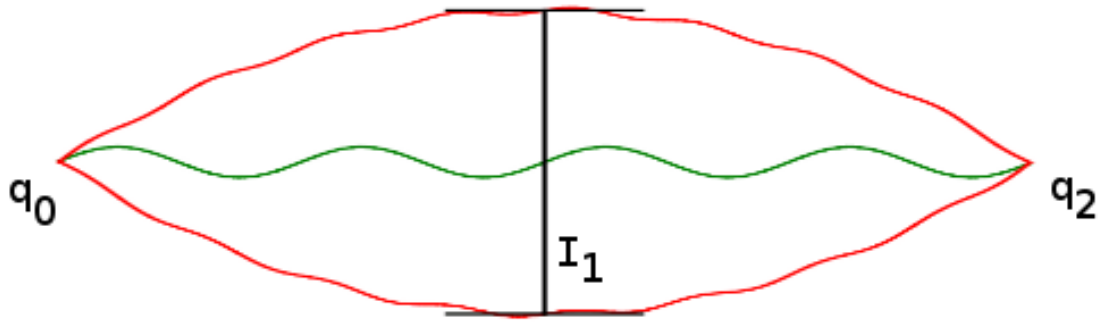

It is not obvious that Lemma 7.3.2 can be applied in practice as there may not necessarily be a curve on the energy surface which passes through all the constraints. For example the constraints could be arranged so that a trajectory passing between

them would have to travel far too fast to remain on the energy surface $H = h$. To apply the Lemma in practice, the constraints $\mathcal{I}$ must be carefully constructed in way so that trajectories passing through the boundaries of the constraints maximize Maupertuis action. This is idea is presented in section 7.5. Furthermore, the constraints should be arranged in a way that constrained minimizers correspond to trajectories which are increasing in eccentricity. This is carried out in section 7.7.

It is worth mentioning John Mather uses constrained minimizers in his proof of the 'Mather Connecting Theorem' [Ma2]. Mather's original proof is rather difficult to read and in [Xia1], Xia and introduces a more natural notion of constrained minimizer. Specifically the proof makes use of so called *joint barrier functions* whose minimizers connect Aubry Mather sets of two different, but nearby rotation numbers. Mather's proof produces a connecting orbit only for rotation numbers of Aubry-Mather sets which are 'sufficiently close', but due to the general nature of the problem he considers, no quantitative bounds are given. The full strength of Mather's result is not needed for Theorem 1.2.1. However specific about the RCP3BP is required to gain enough information to make 'sufficiently close' precise. This allows a result to be proved which is in a spirit of Mather's original work.

7.4 A Variational Problem with Constraints

A variational problem is defined in this section whose solution to is a constrained minimizer which diffuses in a controlled way. Recall that the Hamiltonian for the RCP3BP has two degrees of freedom (see 1.2). The configuration space of is

$(r, \varphi) \in \mathbb{R}^2$. It is important to emphasize for that the RCP3BP in a rotating frame, the variable φ measures the *relative position* of comet with respect to Jupiter.

Fix

- an energy surface $\mathcal{S}^{out}(J_0)$, i.e. fix $H = -J_0$,
- a section $\Pi = \{r = R\}$ where $R > \frac{3J_0^2}{2}$, which is diffeomorphic to $\mathbb{T} \ni \varphi$
- a positive integer N,
- a collection of compact intervals $\mathcal{I} = \{I_i\}_{0 \leq i \leq N-1}$ with nonempty interiors

With these quantities fixed, the variational problem (7.2) reduces to finding constrained minimizers γ_{-J_0} on the energy surface $\mathcal{S}(J_0)$ that achieve the minimum

$$M_{-J_0}(\varphi_0, \varphi_N; \mathcal{I}) := \min_{\varphi_i \in I_i} M_{-J_0}\big((R, \varphi_0), (R, \varphi_1)...(R, \varphi_N)\big) \tag{7.3}$$

Since the Hamiltonian is 2 degrees of freedom, specifying J_0 fixes one variable (say P_r) and specifying passage through the section Π twice fixes another two variables (say (r, φ)). This leaves the fourth variable (say P_φ) free. Indeed changing P_φ effects how long orbits spend in the outside region (i.e. as $P_\varphi \to J_0$ then time way from Sun goes to ∞), and this effects what happens when the comet returns to the Sun. Changing P_φ slightly for orbits with eccentricities close to one gives Jupiter sufficient time to rotate so that on the next passage by the Sun, the comet is passing the section Π at a different angle with respect to Jupiter. This effects the possible constraints that the comet could pass through. Then placing constraints on φ which the comet must pass through controls behavior in the region far from the Sun.

The next several sections are dedicated to construction of the constraints $\mathcal{I}$ so when Lemma 7.3.2 is applied, the constrained minimizers are trajectories which increase in eccentricity. The goal is to construct a diffusing orbit which starts close to a rotational torus and then proceeds to quickly exit the Solar system.

7.5 An Action Comparison

The idea of this method is similar to that of chapter 2 where differences in action from passing by the Sun-Jupiter system are exploited. In this section, things are arranged so that the comet to passes by in a cheap valley in a neighborhood of the trajectory with minimal Maupertuis action. The angles which mark the tops of mountains that carve out the valley must be explicitly specified. The goal is to prove that when a comet passes through 3 consecutive sections Π, then during the second passage through Π, it must pass through the interior of a constraint to minimize the Maupertuis functional. Lemma 7.3.2 then applies. This procedure is now formalized.

7.5.1 Solar Passages and Action Decompositions

Recall the concept of R–Solar passage from section 2.1.2. An analogous object may be defined where the comet starts and ends at radius R, but in between passes through an aphelion $r(t^*) = r^{apoh} > J_0^2$. Recall that mathematically $\dot{r} = 0$ at the aphelion, and physically it is the farthest point to Sun.) Call such a segment an *outer R–Solar passage.*

Suppose γ is an elongated Solar passage. Then γ decomposes into (see fig. 2.5)

- γ^- – an outer R–Solar passage, defined for $t_0 \leq t_1$
- γ^{in} – a R–Solar passage, defined for $t_1 \leq t_2$
- γ^+ – an outer R–Solar passage, defined for $t_2 \leq t_3$

Denote the decompose the Maupertuis action on each of the segments by M^-_{out}, M_{in}, and M^+_{out} respectively. Then

$$M_h(\gamma) = M^-_{out}(\gamma) + M_{in}(\gamma) + M^+_{out}(\gamma).$$

7.5.2 Bad Angles

Define a *section angle*, denoted φ^Π, to be the angle the comet makes relative to the position of Jupiter when the comet is at the section $\Pi = \{r = R\}$. For a fixed angular momenta P_φ it turns out that M_{in} sensitively depends on section angle and in fact has 4 extreme points - two maxima and two minima (see figure 7.2). This fact is not proved rigorously; instead criteria to locate the extrema are formalized and a computer is used to find their approximate locations. The formalism involves interval arithmetic and is postponed to another document.

Let $M_{in}(P_\varphi, \varphi) = M_{in}(\gamma)$ where γ is a R–Solar passage on $\mathcal{S}(J_0)$ with initial conditions (R, φ, P_φ).

Claim: $M_{in}(P_\varphi, \varphi)$ is a smooth curve over $\varphi \in \mathbb{T}$.

Proof: The Lagrangian and hence $M_{in}(\gamma)$ smoothly depend on initial conditions. $\square$

Fix $R > \frac{3J_0^2}{2}$ and P_φ. Define $\varphi^\Pi_{max} = \varphi^\Pi_{max}(J_0, R, P_\varphi)$ and $\varphi^\Pi_{min} = \varphi^\Pi_{min}(J_0, R, P_\varphi)$ as the angles such that

$$M_{in}(P_\varphi, \varphi^\Pi_{max}) := \max_{\gamma \in SP(J_0,R,P_\varphi)} M(\gamma^{in}), \quad M_{in}(P_\varphi, \varphi^\Pi_{min}) := \min_{\gamma \in SP(J_0,R,P_\varphi)} M(\gamma^{in})$$

These angles exist by compactness of $\mathbb{T}$ since fixing (R, J_0, P_φ) leaves only $\varphi \in \mathbb{T}$ free. A priori, it is not obvious these angles are unique. A computer may be used to approximate these angles and later establish this fact. It is more difficult to prove the existence of local minima and maxima which are different from global minima and maxima since compactness and continuity cannot be to prove them into existence. For now, assume the two other extrema are known and they are ordered so that

$$\varphi^\Pi_{min} \leq \varphi^\Pi_{loc,min} \leq \varphi^\Pi_{loc,max} \leq \varphi^\Pi_{max}$$

Call the angles $\varphi^\Pi_{loc,max}, \varphi^\Pi_{max}$ *bad angles* since they locally maximize the Maupertuis action.

7.5.3 Action Comparison

Let φ^Π_{bad} be a bad angle, either $\varphi^\Pi_{loc,max}(P_\varphi)$ or $\varphi^\Pi_{max}(P_\varphi)$. Define

$$\Delta M^{bad}_{in}(P_\varphi) := M_{in}(P_\varphi, \varphi^\Pi_{bad}(P_\varphi)) - M_{in}(P_\varphi, \varphi^\Pi_{min}(P_\varphi))$$

$$\Delta\varphi^\Pi(P_\varphi) := \varphi^\Pi_{bad}(P_\varphi) - \varphi^\Pi_{min}(P_\varphi).$$

Figure 7.2: φ^{Π} vs. M_{in} for $J_0 = 1.8$, $R = 5$, $P_\varphi = 1.8$

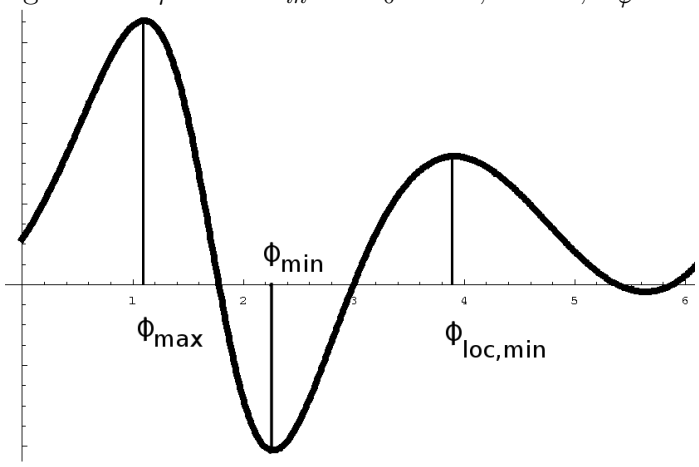

Information about the location of the bad angles is used to define the constraints. Initially a family of constraints $\{I(P_\varphi)\}$ is considered, then use additional numerics are used to pick a subset with the property that trajectories which pass through them have eccentricity increasing nearly maximally.

Definition 7.5.1. *A constraint $I = I(P_\varphi)$ is an interval of angles $I(P_\varphi) = [\varphi^{\Pi}_{max}(P_\varphi), \varphi^{\Pi}_{loc,max}(P_\varphi)]$ with $\varphi^{\Pi}_{min}(P_\varphi) \in I(P_\varphi)$.*

The idea of the comparison in the outside region is the same as that of section 2.1.6. Suppose γ_{max} is an elongated Solar passage with section angle φ^{Π}_{bad}. A procedure to construct γ_{test}, a new curve with smaller Maupertuis action, i.e. $M(\gamma_{test}) < M(\gamma_{max})$, is described.

Heuristically, if the comet is in a sufficiently elliptic orbit and passes near a bad (i.e. expensive) angle, then by modifying the velocity of the first outer R–Solar passage γ^-, the comet can slow down enough so that Jupiter moves from a position where the Maupertuis action is maximized to a position where the Maupertuis action is minimized in γ^{in}. The comet can then speed very slightly during the second outer

R–Solar passage γ^+ to arrive at the back at the endpoint.

Note that it takes a finite amount of time ΔT for the angle of Jupiter relative to the comet to change by $\Delta\varphi^{\Pi}$. In non-rotating coordinates Jupiter moves with unit speed, and for $r \geq R \geq 5$ the comet's angle remains nearly constant since $\dot{\psi} = \frac{P_\varphi}{r^2}$. (In rotating coordinates, Jupiter is fixed and the comet is moving with almost unit speed.) Hence $\Delta T \approx \Delta\varphi^{\Pi}$. By Kepler's Second Law, for $r \geq R$ the comet moves slower the further away it is from the Sun [AKN]. Denote the amount of time the comet spends in the first outer R–Solar passage, γ^-_{max}, by $T_{out} \approx \frac{\pi}{2\sqrt{2}(J_0 - P_\varphi)^{\frac{3}{2}}}$. To keep the argument simple, assume by symmetry, this also the time spent in the γ^+_{max} segment.

A very small change in velocity changes the amount of time to reach the section Π considerably. Let

$$\lambda_\pm := \frac{T_{out}}{T_{out} \mp \Delta\varphi^{\Pi}_{bad}} \approx \frac{T_{out}}{T_{out} \mp \Delta T}$$

$$(P_\varphi)_{\lambda_\pm} := J_0 - (J_0 - P_\varphi)\lambda_\pm^{\frac{2}{3}}$$

Recall γ_{max} is an elongated Solar passage such that the section angle is φ^{Π}_{bad} and γ^{in}_{max} **maximizes** action over all R–Solar passages. Consider a new curve γ_{test} which consists of

- an outer R–Solar passage on the energy surface $H = -J_0$ with angular momentum $(P_\varphi)_{\lambda_-}$. This trajectory moves slightly slower than γ^-_{max}.
- γ^{in}_{test} is a R–Solar passage which minimizes Maupertuis action over all R–Solar passages, i.e. the section angle of γ_{test} is φ^{Π}_{min}.

- an outer R–Solar passage on the energy surface $H = -J_0$ with angular momentum $(P_\varphi)_{\lambda_+}$. This trajectory moves slightly faster than γ^+_{max}.

Remark: This is slightly different class of test curves than constructed in section 2.1.6. The reason for the difference is that in chapter 2, the classical action comparison requires the start and end times to remain unchanged. In this chapter, the Maupertuis action is used and this requires that the curve γ remains on the energy surface $\mathcal{S}^{out}(J_0)$.

Claim: Suppose γ_{max} is an elongated Solar passage which has initial angular momentum $P_\varphi \geq 1.74$ on the energy surface $\mathcal{S}^{out}(1.8)$ and has section angle $\varphi^\Pi \in [\varphi^\Pi_{bad} - \Delta, \varphi^\Pi_{bad} + \Delta]$ for Δ small, e.g. $\Delta = 0.000025$. Let γ_{test} be constructed as above. Then $M(\gamma_{max}) - M(\gamma_{test}) > 0$ and γ_{max} is not a global action minimizer for the Maupertuis action.

Proof: Computer Assisted. CAPD is used to rigorously integrate a class of 5–Solar passages and compute the Maupertuis action for each passage. The test trajectories can be constructed as described and Mathematica can be used to perform the action comparison in the outside region. □

Remark: The last part of the proof which uses Mathematica is currently non-rigorous. The results in the outside region must be 'intervalized' as in section 2.2.

Note that the Maupertuis action difference in polar coordinates can be decom-

posed as

$$\begin{aligned}\Delta M(\gamma) &= M^-_{out}(\gamma) + M_{in}(\gamma) + M^+_{out}(\gamma) - \inf_{\tilde{\gamma}} \left(M^-_{out}(\tilde{\gamma}) + M_{in}(\tilde{\gamma}) + M^+_{out}(\tilde{\gamma})\right) \\ &\geq \left(M^-_{out}(\gamma) - \inf_{\tilde{\gamma}} M^-_{out}(\tilde{\gamma})\right) + \left(M_{in}(\gamma) - \inf_{\tilde{\gamma}} M_{in}(\tilde{\gamma})\right) + \left(M^+_{out}(\gamma) - \inf_{\tilde{\gamma}} M^+_{out}(\tilde{\gamma})\right) \\ &\geq \left(M^-_{out}(\gamma) - M^-_{out}(\gamma_{test})\right) + \left(M_{in}(\gamma) - M_{in}(\gamma_{test})\right) + \left(M^+_{out}(\gamma) - M^+_{out}(\gamma_{test})\right)\end{aligned}$$

where γ_{test} is constructed as above. The comparison method makes a lower bound on the Maupertuis action difference. By proving the lower bound is strictly positive, the possibility that γ is on a rotational torus (see theorem 7.2.1) or more abstractly on some Aubry-Mather set is ruled out. The action comparison method can be interpreted to say that if γ is an elongated Solar passage with section angle $\varphi^{\Pi} \in \partial I$, then $\Delta M(\gamma_{r^{perih},\varphi^{\Pi}}, I) > 0$. It follows from Lemma 7.3.2 that constrained minimizers must then pass on the interior of the constraint, i.e. they won't ever pass through bad angles.

7.6 Jumps in Eccentricity

In the last section, a continuum of constraints was generated. In this section, a specific subset is selected. The desired subset is one which increases the eccentricity of trajectories that pass through it nearly maximally. To find this subset, good estimates on the magnitude of jumps in eccentricity are required.

While it is conceptually easy to think of a jump in terms of eccentricity, as a matter of practice it is more convenient to measure a jump in terms of angular momentum. On the energy surface $\mathcal{S}^{out}(J_0)$, eccentricity is monotonically increasing

as a function of P_φ. Hence it suffices to estimate the jump in angular momentum. This data may be obtained from Lemma 2.2.2.

7.6.1 Behavior close to the Sun

This subsection studies how angular momentum can change after an R-Solar passage. Some computer assistance is required since the perturbation terms are difficult to estimate by hand in the kick region.

If $\{0 = \varphi^0, \varphi^1, ..., \varphi^n = 2\pi\}$ is a partition of $\mathbb{T}$ with $\varphi^{i+1} - \varphi^i = \frac{2\pi}{2^M}$ for some M large (e.g. $M > 6$), then it is possible to compute the change in angular momentum over an R-Solar passage with $\varphi \in [\varphi^i, \varphi^{i+1}]$ for a given initial angular momentum P_φ. Let

$$\Delta P_\varphi(i, P_\varphi) := \min_{\varphi \in [\varphi^i, \varphi^{i+1}]} \big(P_\varphi(T, \varphi) - P_\varphi(0)\big)$$

where $P_\varphi(0)$ is the angular momentum at the start of the R–Solar Passage and $P_\varphi(T, \varphi)$ is the angular momentum at the end of the R–Solar passage on $\mathcal{S}(J_0)$ starting with an initial angle φ. Hence a mapping $(i, P_\varphi) \mapsto \Delta P_\varphi(i, P_\varphi)$ is obtained which measures the difference in angular momentum before and after an R–Solar passage.

Remark: The 'min' is taken in the definition of the difference to ensure that the actual difference is strictly larger when using rigorous numerics. It is important to take M large since as M increases the numbers then become more accurate.

If $I(P_\varphi) \neq \mathbb{T}$ is a constraint, then for a sufficiently fine partition there exist

integers $j \leq k$ such that

$$\bigcup_{i=j}^{k} [\varphi^i, \varphi^{i+1}] \subset I(P_\varphi) \subset \bigcup_{i=j-1}^{k+1} [\varphi^i, \varphi^{i+1}]$$

Let

$$\Delta P_\varphi^+(I(P_\varphi)) := \max_{j \leq i \leq k} \Delta P_\varphi(i, P_\varphi)$$

The angular momentum can increase by at least ΔP_φ^+ when passing through the interior of the constraint (the choice of j, k ensures passage on the interior). Let i^* be such that $\Delta P_\varphi(I(P_\varphi)) = \Delta P_\varphi^+(i^*, P_\varphi)$. Call the interval $[\varphi_{i^*}, \varphi_{i^*+1}] \subset int(I(P_\varphi))$ the interval *the interval of maximal increase.*

Lemma 7.6.1. *For $\mu = 10^{-3}$, $J_0 = 1.8$, $e \geq 0.9$ (i.e. $P_\varphi \geq 1.77$), and $R = 5$ then $\Delta P_\varphi^+(I(P_\varphi)) \geq 1.1\mu$.*

Proof: A computer is programmed to calculate the above quantities. □

Remark: Phrased in terms of rotation numbers, this produces a quantitative bound on the size of gaps in rotation number a solution can jump between in the Mather Connecting Theorem. Specifically, it is possible to jump between neighborhoods of Aubry Mather sets with differences in rotation number between 0.10μ and 0.82μ after making a 5-Solar Passage. Since this quantity is bounded from below by a positive constant, then *it is possible to make a finite number of Solar passages then escape the Solar System.*

7.6.2 Behavior Far from the Sun

Lemma 2.2.2 gives explicit bounds on the change in angular momentum far from the Sun. This can be parlayed into information about when it is possible to exit the Solar system. Specifically in order to escape the Solar-System in RCP3BP$(0.001, 1.8)$ *after* a 5–Solar Passage, it is sufficient for a comet to have $P_\varphi^{exit} := 1.8 + 0.0215298\mu$ (also see proof of Theorem 1.1.2 in section 6.2.2). Leaving with this angular momentum ensures the small perturbations in the outside region do not push the comet back into an elliptic orbit.

7.7 Construction of a Diffusing Orbit

Recall that

$$\dot{\varphi} = -1 + \frac{P_\varphi}{r^2}$$

so

$$\varphi(T) - \varphi(0) = -T + \int_0^T \frac{P_\varphi}{r^2} dt \approx -T.$$

where T is the return time to the section Π, i.e. the period of revolution for the comet. To connect this quantity to angular momentum, we note that

$$T \approx \frac{\pi}{\sqrt{2}(J_0 - P_\varphi)^{\frac{3}{2}}}.$$

Then for P_φ close to J_0, the period is large and only a very small change in angular momentum is needed to make a change in the period of more than 2π. Put another way, it is easier to diffuse when the comet is already of high eccentricity. See section 7.8 for another way to exploit this phenomenon.

Suppose a comet on $\mathcal{S}^{out}(1.8)$ has initial angular momentum $P_\varphi^0 = 1.77$. The above results on change in angular momentum can be used to iteratively compute

$$P_\varphi^j = P_\varphi^{j-1} + \Delta P_\varphi^+(I(P_\varphi^j))$$

starting the iteration with P_φ^0. Let N be the smallest positive integer when $P_\varphi^N \geq P_\varphi^{exit}$. The sequence of angular momenta P_φ^j has a corresponding sequence of constraints $\{I(P_\varphi^j)\}$ through which the comet must pass in order to achieve maximal increase in angular momentum.

Lemma 7.7.1. *For $\mathcal{S}^{out}(1.8)$, $\mu = 0.001$, and $P_\varphi^0 = 1.77$ then $k = 29$.*

Proof: Computer assisted[1]. □

Remark: Work is being conducted to improve this bound to the $k \approx 80$ and decrease $P_\varphi^0 \approx 1.7$. This would explicitly establish an escaping orbit which starts around $e = 0.66$.

With the construction of the constraints complete, proof of Theorem 1.1.2 follows from Lemma 7.3.2, and the fact is takes $N = 29 + 1$ constraints (passage through a constraint occurs once per revolution around the sun). By construction of the constraints, a comet which passages through the interior makes a nearly maximal increase increase after a revolution, hence the constrained minimizer is a diffusing orbit which escapes in nearly minimal time. □

[1]Rigorous numerics still pending

7.8 Using gravity assists to construct diffusing orbits

This section outlines a procedure to produce diffusing orbits which does **not** depend on variational methods. It is a straightforward numerical algorithm.

Start by noting that since the Hamiltonian $H = H(r, \varphi, P_r, P_\varphi)$ is two degrees of freedom, then fixing an energy surface $\mathcal{S}^{out}(J_0)$ implicitly defines one of the variables. Take this variable to be $P_r = P_r(J_0, R, \varphi, P_\varphi)$, which is given by formula 4.2. Define $T_{in}(\varphi, P_\varphi)$ to be the time it takes a trajectory to make an R-Solar passage. Define $T_{out}(\varphi, P_\varphi)$ to be the time it takes a trajectory to make an outer R-Solar passage.

Suppose $\Phi_t(r, \varphi, P_r, P_\varphi)$ is the flow for the RCP3BP. On a fixed energy surface, introduce the following shorthand notation. Let

$$\Phi_{in}(\varphi, P_\varphi) = (\varphi, P_\varphi)|_{\Phi_{T_{in}}(R,\varphi,P_r(J_0,R,\varphi,P_\varphi),P_\varphi)}$$

$$\Phi_{out}(\varphi, P_\varphi) = (\varphi, P_\varphi)|_{\Phi_{T_{out}}(R,\varphi,P_r(J_0,R,\varphi,P_\varphi),P_\varphi)}$$

Hence Φ_{in} and Φ_{out} are maps of $\mathbb{T}\times\mathbb{R}$ to itself. The map Φ_{in} is easily analyzable by a computer; just integration over short segments of trajectory. The map Φ_{out} behaves almost exactly like a return map for the 2BP(SC).

Lemma 7.8.1. *$\Phi_{out}(\varphi, P_\varphi) \in \mathbb{T} \times [P_\varphi - 2\rho(R), P_\varphi + 2\rho(R)]$ where $\rho(R)$ is defined in section B.1. (For $\mu = 0.001$,$J_0 = 1.8$ and $R = 5$, then $\rho(5) = 0.0215298\mu$.)*

Proof: The is a rephrasing of Lemma 2.2.2. □

Lemma 7.8.2. $|P_\varphi|_{\Phi_{in}(\varphi(0),P_\varphi(0))} - P_\varphi(0)| \lesssim \mu$.

Proof: This is a subset of what is proved in Theorem 2.2.4. The data that is produced in the proof of the theorem can give an explicit upper bound. □

Lemma 7.8.3. *Suppose* $[P_\varphi^-, P_\varphi^+]$ *is an interval of angular momenta with thickness* $P_\varphi^+ - P_\varphi^- \geq C(\mu, J_0, P_\varphi^-)\mu$. *There exists a function* $C = C(\mu, J_0, P_\varphi) \approx J_0 - P_\varphi$ *with* $C(\mu, J_0, P_\varphi) \to 0$ *as* $P_\varphi \to J_0$ *so that* $[0, 2\pi] \subset \varphi|_{\Phi_{out}(\varphi, [P_\varphi^-, P_\varphi^+])}$.

Proof: $T_{out} \approx \frac{\pi}{\sqrt{2}(J_0 - P_\varphi)^{\frac{3}{2}}}$ and as $P_\varphi \to J_0$, then small changes in angular momentum make large changes in period. Since $\varphi \approx -t$, then for a sufficiently large interval of angular momenta, the image spans the unit circle. A computer can explicitly find the function C to measure the size of the interval of initial conditions needed. □

The first lemma says angular momentum doesn't change much far from the Sun. The second lemma says near the Sun, angular momentum can jump by size μ. The third lemma is the key. It says that Jupiter acts as a scatterer and spreads out a small interval of initial conditions. Armed with these lemmas one can construct diffusing orbits.

The algorithm involves iterative evaluation of Φ_{in} and Φ_{out} on graphs of angular momentum over the circle. If $G = \{(\varphi, P_\varphi(\varphi)) | \varphi \in \mathbb{R}\}$, then define $\pi(G) = \{(\varphi_0, \inf_{\varphi = \varphi_0 \mod 2\pi} P_\varphi(\varphi)) | \varphi_0 \in \mathbb{T}\}$ to be the lower projection of G back onto the base, i.e. if one point on $\mathbb{T}$ has two points above it, take the lower one.

Consider the following algorithm to construct diffusing orbits.

1. Select P_φ^0 and set $G_0 = \{(\varphi, P_\varphi^0) | \varphi \in \mathbb{T}\}$ where P_φ^0 is sufficiently large. Let $i = 0$.

2. Compute $G_{i+1} = \Phi_{in}(G_i)$. Compute the angle φ_{max} such that

$$P_\varphi|_{\Phi_{in}(\varphi_{max}, P_\varphi(\varphi_{max}))} > P_\varphi|_{\Phi_{in}(\varphi, P_\varphi(\varphi))}$$

for angles $\varphi \neq \varphi_{max}$. I.e. the angle φ_{max} makes the largest jump in angular momentum.

3. Select an interval I_i such that $\varphi_{max} \in I_i$ and for $G_{I_i} = \{(\varphi, P_\varphi(\varphi)) \in G_i | \varphi \in I_i\}$ it holds that $[0, 2\pi] \subset \varphi|_{\Phi_{out} \circ \Phi_{in}(G_{I_i})}$. By the second lemma, there is a large jump in angular momentum, and by the third lemma, for sufficiently large initial angular momenta, the gap in angular momenta is large enough to get that the image spans the whole circle $\mathbb{T}$.

4. Compute $G_{i+1} = \pi(\Phi_{out} \circ \Phi_{in}(G_{I_i}))$. If $T_{out} = +\infty$, terminate the algorithm as this corresponds to cometary escape. Otherwise let $i := i + 1$ and go back to step 2.

Iteration of the algorithm terminates when an angular momentum satisfying the exit condition is located. The algorithm allows one to zero in on an escaping trajectory. Each interval $I_i \in \mathbb{T}$ contains initial conditions for a trajectory which makes one maximal jump. For $i > 0$, these intervals have pullbacks under the flow back to the initial conditions. Let $\tilde{I}_i$ be the pullback of the i^{th} interval under $(\Phi_{out} \circ \Phi_{in})^i$, i.e. a pullback to the initial conditions. By the third lemma, this is nonempty and contained inside of I_0. Let

$$\Lambda = I_0 \cap \tilde{I}_1 \cap ... \cap \cap \tilde{I}_k$$

where the I_k the interval generated when the algorithm terminates. Then all initial conditions in Λ are escaping orbits.

Physically this numerical procedure simply selects initial conditions so that the comet gets nearly maximal gravity assists after each passage by the Sun.

Application: For those readers who are concerned with industrial applications of this work, consider the following. Replace 'comet' with 'space craft'. This algorithm gives a quick way to construct diffusing orbits, which is to say it gives an efficient way to produce trajectories of space craft which use no fuel but nonetheless travel great distances. Of course the actual Solar System contains more planets than just Jupiter (a likely motivation for space exploration in the first place) so it is left to the reader to work out the details in a multi-planet scenario.

Appendix A

Estimates on Perturbation Terms

A.1 Estimates on ΔH and Polar Derivatives

Tight estimates on the perturbation term ΔH and its derivatives are needed in order to get good numerics. The Taylor series expansion of ΔH in $\frac{1}{r}$ yields

$$\Delta H(r, \varphi; \mu) = \sum_{i=1}^{\infty} (-1)^i \frac{\mu(1-\mu)\big(\mu^i - (\mu-1)^i\big)}{r^{i+2}} P_{i+1}(\cos(\varphi))$$

where P_i is the i^{th} Legendre Polynomial, and is given by the recursive formula

$$(i+1)P_{i+1}(x) = (2i+1)xP_i(x) - iP_{i-1}(x).$$

(See formula 1.1.) Expansions of Newtonian potentials were one of the reasons Legendre considered these polynomials. In fact

$$\frac{1}{\sqrt{1-2xt+t^2}} = \sum_{n=0}^{\infty} P_n(x)t^n$$

For $x \in (1,1)$, $|P_i(x)| < 1$ and $|P_i(\pm 1)| = 1$. From this, one concludes that the series expansion for ΔH converges provided μ is small and $r > 1+\mu$, e.g. when the comet is in the outside region. One can also show that $|P_i'(x)| \leq \frac{i(i+1)}{2}$ for $x \in [-1,1]$. See e.g. [R] for formulas and derivation of Legendre Polynomials.

Bounding the Legendre Polynomials produce bounds on the perturbation terms

which are independent of φ. Do this to define

$$\max_{\varphi} |\Delta H(r,\varphi;\mu)| \le (|\Delta H|)^{+}(r) \qquad \max_{\varphi} |\partial_{\varphi}\Delta H(r,\varphi;\mu)| \le (|\frac{\partial \Delta H}{\partial \varphi}|)^{+}(r)$$

$$\max_{\varphi} |\partial_{r}\Delta H(r,\varphi;\mu)| \le (|\frac{\partial \Delta H}{\partial r}|)^{+}(r) \qquad \max_{\varphi} |\partial^2_{r\varphi}\Delta H(r,\varphi;\mu)| \le (|\frac{\partial^2 \Delta H}{\partial r \partial \varphi}|)^{+}$$

$$\max_{\varphi} |\partial^2_{\varphi\varphi}\Delta H(r,\varphi;\mu)| \le (|\frac{\partial^2 \Delta H}{\partial \varphi^2}|)^{+} \qquad \max_{\varphi} |\partial^2_{rr}\Delta H(r,\varphi;\mu)| \le (|\frac{\partial^2 \Delta H}{\partial r^2}|)^{+}$$

$$(|\Delta H|)^{+}(r) := \frac{\mu(1-\mu)}{r(r-1+\mu)(r+\mu)} = O(\frac{\mu}{r^3})$$

$$(|\frac{\partial \Delta H}{\partial \varphi}|)^{+}(r) := \frac{\mu(1-\mu)r\big(1+3r(r-1)+\mu(6r-3)+3\mu^2\big)}{(r-1+\mu)^3(r+\mu)^3} = O(\frac{\mu}{r^3})$$

$$(|\frac{\partial \Delta H}{\partial r}|)^{+}(r) := -\frac{1}{r^2} + \frac{\mu}{(r-1+\mu)^2} + \frac{1-\mu}{(r+\mu)^2} = O(\frac{\mu}{r^4})$$

$$(|\frac{\partial^2 \Delta H}{\partial r \partial \varphi}|)^{+} := \mu(1-\mu)\left(\frac{3(1-\mu)}{(r-1+\mu)^4} + \frac{2}{(r-1+\mu)^3} + \frac{3\mu}{(\mu+r)^4} - \frac{2}{(\mu+r)^3}\right) = O(\frac{\mu}{r^4})$$

$$(|\frac{\partial^2 \Delta H}{\partial \varphi^2}|)^{+} := 3\mu(1-\mu)\left(\frac{(1-\mu)^3}{(r-1+\mu)^5} + \frac{\mu^3}{(\mu+r)^5}\right) = O(\frac{\mu}{r^5})$$

$$(|\frac{\partial^2 \Delta H}{\partial r^2}|)^{+} := -\frac{2}{r^3} + \frac{2\mu}{(r-1+\mu)^3} + \frac{2(1-\mu)}{(\mu+r)^3} = O(\frac{\mu}{r^5})$$

Remark: All of these estimates are independent of the Jacobi constant. For $r \ge 1.5$ and $\mu = 0.001$, even more explicit estimates can be made.

$$\max_{\varphi} |\Delta H(r,\varphi;\mu)| \le \frac{3\mu}{r^3} \qquad \max_{\varphi} |\partial_{\varphi}\Delta H(r,\varphi;\mu)| \le \frac{39\mu}{r^3}$$

$$\max_{\varphi} |\partial_{r}\Delta H(r,\varphi;\mu)| \le \frac{15\mu}{r^4} \qquad \max_{\varphi} |\partial^2_{r\varphi}\Delta H(r,\varphi;\mu)| \le \frac{319\mu}{r^4}$$

$$\max_{\varphi} |\partial^2_{\varphi\varphi}\Delta H(r,\varphi;\mu)| \le \frac{719\mu}{r^5} \qquad \max_{\varphi} |\partial^2_{rr}\Delta H(r,\varphi;\mu)| \le \frac{108\mu}{r^5}$$

A.2 Bounds on the Perihelion

Consider the case $\mu = 10^{-3}$ and $J_0 = 1.8$. It is useful to have some initial bounds on angular momentum and minimal radius. The 2BP(SC) for elliptic and parabolic motions are known to have minimum perihelion radius $r^{perih} \ge \frac{J_0^2}{2}$.

One can easily prove for a fixed angle φ, that the radius of the perihelion is decreasing as a function of P_φ. It suffices to examine perihelions at the φ-critical points of ΔH. The critical points are at $\varphi = 0, \pi$ and $\cos(\varphi) = \frac{1-2\mu}{2r}$. Since ΔH is algebraic in r at those critical points, a CAS can solve and find the minimum perihelion radius for elliptic and parabolic motions. This is how Lemma 1.1.1 is proved. Doing so for $J_0 = 1.8$, $\mu = 10^{-3}$, and $P_\varphi \leq 1.81$ yields the $r^{perih} \geq 1.61839 \geq \frac{1.8^2}{2} - 2\mu$. Doing this for all eccentricities and Jacobi constants with $J_0 \in [1.52, 2]$ yields $r^{perih} \geq \frac{1.8^2}{2} - 33\mu$.

The class of solutions that need to be analyze for the proof of Theorem 1.1.2 has $P_\varphi \leq 1.81$, i.e. $e \leq 1.0324$. Computing the minimum perihelion radius for this class yields

$$r^{perih} \geq 1.61048 = r^{perih}_{min} \qquad\qquad |\Delta H| \leq 0.629509\mu$$

A.3 Estimates on terms involving Delaunay

This subsection collects estimates involving perturbation terms and Delaunay variables. Estimates throughout this section use $\mu = 10^{-3}$ and the above estimates on perturbation terms in polar. Additionally it is assumed that $J_0 = 1.8$ and $G \in [1.67, 1.81]$. For these parameters, one can show that eccentricity $e \in [0.52, 1.04]$. In the above subsection it is established that for these parameters, $r \geq 1.6$.

Remark: Some estimates are carried out in Delaunay and others in algebraically deformed Delaunay (ADDV). If an estimate is done using Delaunay, it is not hard to convert it to ADDV by simply attaching subscript ν's to all Delaunay

variables. From the definition of ADDV and since $\nu = 2.8\mu$ is small, then it is not hard to show that $G_\nu \in [1.67-\nu, 1.81-\nu]$ and $e_\nu \in [0.5, 1.03]$. Furthermore if $e \leq 1$, then $e_\nu \leq 0.998 < 1$.

Lemma A.3.1. *If* $J_0 = 1.8$, $\mu = 10^{-3}$, *and* $G \in [1.67, 1.81]$, *then* $|\frac{\partial \Delta H}{\partial L_\nu}| \leq 0.105512$. *Furthermore* $|\frac{\partial \Delta H}{\partial L_\nu}| \leq \frac{433\mu}{r^3}$ *for* $r > 1.6$.

Proof:

$$\frac{\partial \Delta H}{\partial L_\nu} = (\frac{\partial \Delta H}{\partial r})(\frac{\partial r}{\partial L_\nu}) + (\frac{\partial \Delta H}{\partial \varphi})(\frac{\partial \varphi}{\partial L_\nu})$$

Use the quantities in the above subsection to produce upper bounds on the derivatives of the perturbation terms. Use of a computer algebra system[1] yields

$$\frac{\partial r}{\partial L_\nu} = \frac{G_\nu^2 r + 2e_\nu^2 r^2 - G_\nu^4}{L_\nu e_\nu^2 r} \qquad \frac{\partial \varphi}{\partial L_\nu} = -\frac{G_\nu(G_\nu^2 + r)\sin(u_\nu)}{r^2 e_\nu}$$

For $\mu = 0.001$, $J_0 = 1.8$, and $G \in [1.67, 1.81]$, then $G\nu = G - 2.8\mu \leq 1.81$ and $e_\nu \in [0.5, 1.03]$. Furthermore, $L_\nu \geq 1.6$ everywhere on the energy surface. Hence

$$|\frac{\partial r}{\partial L_\nu}| = |\frac{G_\nu^2 r + 2e_\nu^2 r^2 - G_\nu^4}{L_\nu e_\nu^2 r}| \leq \frac{1.81^2 r + 2 \cdot 1.03^2 r^2 + 1.81^4}{1.6 \cdot 0.5^2 r}$$
$$|\frac{\partial \varphi}{\partial L_\nu}| = |-\frac{G_\nu(G_\nu^2 + r)\sin(u_\nu)}{r^2 e_\nu}| \leq \frac{1.81(1.81^2 + r)}{r^2 0.5}.$$

Note the upper bounds are at most $O(r)$. Hence

$$|\frac{\partial \Delta H}{\partial L_\nu}| \leq (|\frac{\partial \Delta H}{\partial r}|)^+ |(\frac{\partial r}{\partial L_\nu})| + (|\frac{\partial \Delta H}{\partial \varphi}|)^+ |(\frac{\partial \varphi}{\partial L_\nu})| = O(\frac{\mu}{r^3})$$

Using a computer algebra system, it is not hard to show the upper bound is in fact strictly decreasing in r and the upper bound of $r > 1.6$ yields that $|\frac{\partial \Delta H}{\partial L_\nu}| \leq$

[1] Actually the computer algebra system is used to generate these quantities in Delaunay variables. Since $\mathcal{D}_\nu = \mathcal{D} \circ (P_\varphi \mapsto P_\varphi - \nu)$, then as algebraic expressions they are the same as in Delaunay. However the variables themselves have different values.

0.105512. Additionally the CAS can explicitly show the upper bound is less than $\frac{433\mu}{r^3}$ for $r \geq 1.6$ $\square$

Lemma A.3.2. *Fix* $\mu = 10^{-3}$ *and* $J_0 = 1.8$. *Then* $|\frac{\partial \Delta H}{\partial G}| \leq 0.025$ *and hence* $\dot{g} = -1 + \frac{\partial \Delta H}{\partial G} < 0$.

Proof: Let us begin by computing.

$$\frac{\partial \Delta H}{\partial G} = \frac{\partial \Delta H}{\partial r}\frac{\partial r}{\partial G} + \frac{\partial \Delta H}{\partial \varphi}\frac{\partial \varphi}{\partial G}.$$

Its possible to bound $|\frac{\partial \Delta H}{\partial r}|$ and $|\frac{\partial \Delta H}{\partial \varphi}|$ with $(|\frac{\partial \Delta H}{\partial r}|)^+$ and $(|\frac{\partial \Delta H}{\partial \varphi}|)^+$ respectively. Using that $r \geq r_{min}^{perih} = 1.61048$, one finds $|\frac{\partial \Delta H}{\partial r}| \leq 1.81101\mu$ and $|\frac{\partial \Delta H}{\partial \varphi}| \leq 6.65233\mu$.

One can compute (via a CAS)

$$\frac{\partial r}{\partial G} = \frac{G(G^2 - r)}{re^2} \qquad \frac{\partial \varphi}{\partial G} = \frac{L(G + r)\sin(u)}{r^2 e}$$

$\frac{\partial r}{\partial G}$ has critical points at $u = 0, \pi$ (recall $r = L^2(1 - e\cos(u))$. Evaluation at the critical points gives the bound $|\frac{\partial r}{\partial G}| \leq \frac{G}{e}$. Using $e \in [0.5, 1.1]$ and $G \in [1.6, 1.82]$ gives us $|\frac{\partial r}{\partial G}| \in [1.45455, 3.64]$.

The story for $\frac{\partial \varphi}{\partial G}$ is a bit more complicated. One can compute the critical points in u and find two critical points u_1 and u_2 (these are found with a computer algebra system). u_2 is a complex root for $e < 1$ and for $e > 1$, $\frac{\partial \varphi}{\partial G}|_{u=u_2}$ is complex. Hence u_2 can be disregarded. It turn out that $\frac{\partial \varphi}{\partial G}|_{u=u_1} = \frac{f(e)}{G}$ where $f(e)$ is a function of e only. For $e \in [0.5, 1.1]$, then $f(e) \in [2.03336, 4.11667]$. Using $G \in [1.6, 1.82]$ yields $|\frac{\partial \varphi}{\partial G}| \in [1.11723, 2.57292]$.

Hence $|\frac{\partial \Delta H}{\partial G}| \leq 1.81101\mu \cdot 3.64 + 6.65233\mu \cdot 2.57292 = 0.023708 < 0.025$ $\square$

Corollary A.3.3. *If* $J_0 = 1.8$, $\mu = 10^{-3}$, *and* $G \in [1.67, 1.81]$ *then* $|\frac{\partial \Delta H}{\partial G_\nu}| \leq 0.025$.

Proof: In the above Lemma, we showed $|\frac{\partial \Delta H}{\partial G}| \leq 0.025$. This bound still holds since $\frac{\partial \Delta H}{\partial G_\nu} = \frac{\partial \Delta H}{\partial G}\frac{\partial G}{\partial G_\nu} = \frac{\partial \Delta H}{\partial G}$ and $\frac{\partial G_\nu}{\partial G} = 1$ since $G_\nu = G - \nu$. □

Lemma A.3.4. *If* $J_0 = 1.8$, $\mu = 10^{-3}$, *and* $G \in [1.66, 1.81]$, *then* $(\frac{\partial L_\nu}{\partial G_\nu}) \geq 2.85283$.

For the 2BP(SC), $L = (2J_0 - 2G)^{-\frac{1}{2}}$, so $(\frac{\partial L}{\partial G}) = 2(2J_0 - 2G)^{-\frac{3}{2}} \geq 6.74937$ for $J_0 = 1.8$ and $G \geq 1.66$.

Proof of Lemma A.3.4: Write the RCP3BP Hamiltonian in ADDV and use L_ν as implicit function of the other variables.

$$(J_0 + \nu) = \frac{1}{2\big(L_\nu(J_0, \ell_\nu, G_\nu, g_\nu)\big)^2} + G_\nu + \Delta H\bigg(L_\nu\big(J_0, \ell_\nu, G_\nu, g_\nu\big), \ell_\nu, G_\nu, g_\nu\bigg).$$

Take the derivative and solve for $\frac{\partial L_\nu}{\partial G_\nu}$ to get

$$\frac{\partial L_\nu}{\partial G_\nu} = \frac{1 - \frac{\partial \Delta H}{\partial G_\nu}}{L_\nu^{-3} + \frac{\partial \Delta H}{\partial L_\nu}} \tag{A.1}$$

From Lemmas A.3.1 and A.3.3 and the fact that $L_\nu \geq 1.6$, it follows that

$$(\frac{\partial L_\nu}{\partial G_\nu})^{-1} \leq \frac{L_\nu^{-3} + 0.0802431}{1 - 0.025} \leq 0.350529$$

Hence the claim follows. □

Lemma A.3.5. *For* $\mu = 0.001$, $r > 1.5$, $G \in [1.6, 1.81]$,

$$\left|\left(\frac{\partial^2 \Delta H}{\partial \ell \partial G}\right)\right| \leq \frac{21}{r^{7/2}(1-e)^{3/2}} + \frac{35|P_r|}{r^{5/2}(1-e)^{5/2}}$$

Proof: Starting with

$$\left(\frac{\partial \Delta H}{\partial \ell}\right) = \left(\frac{\partial \Delta H}{\partial r}\right)\left(\frac{\partial r}{\partial \ell}\right) + \left(\frac{\partial \Delta H}{\partial \varphi}\right)\left(\frac{\partial \varphi}{\partial \ell}\right)$$

compute

$$\left(\frac{\partial^2 \Delta H}{\partial \ell \partial G}\right) = \left(\frac{\partial \Delta H}{\partial r}\right)\left(\frac{\partial^2 r}{\partial \ell \partial G}\right) + \left(\frac{\partial r}{\partial \ell}\right)\left(\frac{\partial^2 \Delta H}{\partial r^2}\frac{\partial r}{\partial G} + \frac{\partial^2 \Delta H}{\partial r \partial \varphi}\frac{\partial \varphi}{\partial G}\right) + \left(\frac{\partial \Delta H}{\partial \varphi}\right)\left(\frac{\partial^2 \varphi}{\partial \ell \partial G}\right) + \left(\frac{\partial \varphi}{\partial \ell}\right)\left(\frac{\partial^2 \Delta H}{\partial r \partial \varphi}\frac{\partial r}{\partial G} + \frac{\partial^2 \Delta H}{\partial \varphi^2}\frac{\partial \varphi}{\partial G}\right).$$

Now each term shall be estimated. It is helpful to know the following conversions between polar and Delaunay. These formulas were found with the aid of a computer in some cases.

$$r = L^2\left(1 - e\cos(u)\right) \qquad P_r = \frac{Le\sin(u)}{r}$$

$$\frac{\partial r}{\partial G} = \frac{G(G^2 - r)}{re^2} \qquad \frac{\partial \varphi}{\partial G} = \frac{(G^2 + r)P_r}{re^2}$$

$$\frac{\partial r}{\partial \ell} = L^3 P_r \qquad \frac{\partial \varphi}{\partial \ell} = -\frac{GL^3}{r^2}$$

$$\frac{\partial^2 r}{\partial \ell \partial G} = \frac{(e^2 - 1)GL^5 P_r}{e^2 r^2} \qquad \frac{\partial^2 \varphi}{\partial \ell} = -\frac{L(2G^4L^2 + e^2L^2r^2 + G^2(4r^2 - 6L^2r))}{e^2 r^4}$$

For each term, only an upper bound in absolute value is sought. In general it is desirable to have as large a power of r in the denominator as possible, and as small a power of $(1 - e)$ in the denominator as possible.

$$\left|\left(\frac{\partial \Delta H}{\partial r}\right)\left(\frac{\partial^2 r}{\partial \ell \partial G}\right)\right| \leq \frac{15\mu}{r^4}\frac{(1 - e^2)GL^5 P_r}{e^2 r^2} \leq \frac{1.81L^5 P_r}{0.5^2 r^6} \leq \frac{14P_r}{(1 - e)^{5/2} r^{7/2}}$$

$$\left|\left(\frac{\partial r}{\partial \ell}\right)\left(\frac{\partial^2 \Delta H}{\partial r^2}\right)\left(\frac{\partial r}{\partial G}\right)\right| \leq L^3 P_r \leq \frac{108\mu}{r^5}\frac{Gr + G^3}{re^2} \leq \frac{108\mu L^3(1.81r + 1.81^3)P_r}{r^6 0.5^2} \leq \frac{2.5L^3 P_r}{r^5} \leq \frac{2.5P_r}{r^{7/2}(1 - e)^{3/2}}$$

$$\left|\left(\frac{\partial r}{\partial \ell}\right)\left(\frac{\partial^2 \Delta H}{\partial r \partial \varphi}\right)\left(\frac{\partial \varphi}{\partial G}\right)\right| \leq L^3 P_r \frac{319\mu}{r^4}\frac{(G^2 + r)P_r}{re^2} \leq \frac{319\mu L^3(1.81^2 + r)P_r}{0.5^2 r^5} \leq \frac{4.1L^3 P_r}{r^4} \leq \frac{4.1P_r}{r^{5/2}(1 - e)^{3/2}}$$

$$|\left(\frac{\partial\varphi}{\partial\ell}\right)\left(\frac{\partial^2\Delta H}{\partial r\partial\varphi}\right)\left(\frac{\partial r}{\partial G}\right)| \leq \frac{GL^3}{r^2}\frac{319\mu}{r^4}\frac{G(G^2+r)}{re^2} \leq \frac{1.81L^3 319\mu 1.81(1.81^2+r)}{0.5^2 r^7}$$
$$\leq \frac{14L^3}{r^6} \leq \frac{14}{r^{9/2}(1-e)^{3/2}}$$

$$|\left(\frac{\partial\varphi}{\partial\ell}\right)\left(\frac{\partial^2\Delta H}{\partial\varphi^2}\right)\left(\frac{\partial\varphi}{\partial G}\right)| \leq \frac{GL^3}{r^2} \leq \frac{719\mu}{r^5}\frac{(G^2+r)P_r}{re^2} \leq \frac{1.81L^3P_r(1.81^2+r)719\mu}{r^8 0.5^2}$$
$$\leq \frac{17L^3P_r}{r^7} \leq \frac{17P_r}{r^{11/2}(1-e)^{3/2}}$$

$$|\left(\frac{\partial\Delta H}{\partial\varphi}\right)\left(\frac{\partial^2\varphi}{\partial\ell\partial G}\right)| \leq \frac{39\mu}{r^3}\frac{L(2G^4L^2+e^2L^2r^2+G^2(4r^2+6L^2r))}{e^2r^4}$$
$$\leq \frac{39\mu L(2\cdot 1.81^4L^2+1.01^2L^2r^2+1.81^2(4r^2+6L^2r))}{0.5^2r^7}$$
$$\leq \frac{4L^3}{r^7}+\frac{4L^3}{r^6}+\frac{3L}{r^5}+\frac{L^3}{r^5}$$
$$\leq \frac{4}{r^{11/2}(1-e)^{3/2}}+\frac{4}{r^{9/2}(1-e)^{3/2}}+\frac{3}{r^{9/2}(1-e)^{1/2}}+\frac{1}{r^{7/2}(1-e)^{3/2}}$$

Adding all the terms with P_r's we find

$$\frac{14P_r}{(1-e)^{5/2}r^{7/2}}+\frac{2.5P_r}{r^{7/2}(1-e)^{3/2}}+\frac{17P_r}{r^{11/2}(1-e)^{3/2}}+\frac{4.1P_r}{r^{5/2}(1-e)^{3/2}}$$
$$\leq \frac{17+17r^2+5r^3+1.01(17+3r^2+5r^3)}{r^{11/2}(1-e)^{5/2}} \leq \frac{35P_r}{r^{5/2}(1-e)^{5/2}}$$

Adding all the terms without P_r's we find

$$\frac{4}{r^{11/2}(1-e)^{3/2}}+\frac{4}{r^{9/2}(1-e)^{3/2}}+\frac{3}{r^{9/2}(1-e)^{1/2}}+\frac{1}{r^{7/2}(1-e)^{3/2}}+\frac{14}{r^{9/2}(1-e)^{3/2}}$$
$$\leq \frac{4+27r+r^2}{r^{11/2}(1-e)^{3/2}} \leq \frac{21}{r^{7/2}(1-e)^{3/2}}$$

□

Appendix B

Estimates involving nearly integrable quantities

B.1 Estimates on change in Angular Momentum

In this appendix, Lemma 2.2.2 on the change in angular momentum is proved. Recall that

$$\dot{P}_\varphi = -\frac{\partial \Delta H}{\partial \varphi}$$

Hence

$$\Delta P_\varphi(t_0, t_1) = P_\varphi(t_1) - P_\varphi(t_0) = \int_{t_0}^{t_1} -\frac{\partial \Delta H}{\partial \varphi} dt$$

Now

$$\frac{d}{dt}\Big(\Delta H(r(t), \varphi(t))\Big) = \left(\frac{\partial \Delta H}{\partial r}(t)\right)\dot{r}(t) + \left(\frac{\partial \Delta H}{\partial \varphi}(t)\right)\dot{\varphi}(t)$$

and hence

$$\frac{\partial \Delta H}{\partial \varphi}(t) = \frac{1}{\dot{\varphi}(t)}\Big(\frac{\partial \Delta H}{\partial r}(t)\dot{r}(t) - \frac{d}{dt}(\Delta H(t))\Big)$$

Plugging in and using a change of variables gives

$$\begin{aligned}\Delta P_\varphi(t_0, t_1) &= \int_{t_0}^{t_1} -\frac{1}{\dot{\varphi}(t)}\Big(\frac{\partial \Delta H}{\partial r}(t)\dot{r}(t) - \frac{d}{dt}\Delta H(t)\Big)dt \\ &= \int_{t_0}^{t_1} \frac{1}{\dot{\varphi}(t)}(\frac{d}{dt}\Delta H(t))dt - \int_{r(t_0)}^{r(t_1)} \frac{1}{\dot{\varphi}(t(r))}\Big(\frac{\partial \Delta H}{\partial r}\Big)\Big(r, \varphi(t(r))\Big)dr\end{aligned}$$

Let $r_0 = r(t_0)$ and $r_1 = r(t_1)$. Suppose the comet is approaching the perihelion from the preceding aphelion, or from infinity. Then $r_1 \leq r_0$. As t increases, r decreases, and the estimate should account for more uncertainty in the value of P_φ given that

the perturbation term grows larger in magnitude closer to the Sun.

$$|\Delta P_\varphi(t_0,t_1)| \le \frac{1}{\min_{r\in[r_0,r_1]}|\dot\varphi(r)|}\left(|\int_{t_0}^{t_1}\frac{d}{dt}\Delta H(t)dt| + \int_{r_1}^{r_0}|\frac{\partial \Delta H}{\partial r}|dr\right)$$

Note that

$$\min_{r\in[r_0,r_1]}|\dot\varphi(r)| \ge \min_{r\in[r_0,r_1]}(1-\frac{P_\varphi}{r^2}) \ge 1-\frac{\max P_\varphi}{r_1^2}$$

Hence

$$\begin{aligned}|\Delta P_\varphi(t_0,t_1)| \le& \frac{1}{1-\frac{\max P_\varphi}{r_1^2}}(|\Delta H(t_1)-\Delta H(t_0)| + \int_{r_1}^{r_0}|\frac{\partial\Delta H}{\partial r}|dr)\\ &\le \frac{1}{1-\frac{\max P_\varphi}{r_1^2}}\Big((|\Delta H|)^+(r_0)+(|\Delta H|)^+(r_1)+\int_{r_1}^{r_0}(|\frac{\partial\Delta H}{\partial r}|)^+dr\Big)\end{aligned}$$

Claim: $\Big((|\Delta H|)^+(r_0)+(|\Delta H|)^+(r_1)+\int_{r_1}^{r_0}(|\frac{\partial\Delta H}{\partial r}|)^+dr\Big)$ is nondecreasing as a function of r_0 for $r_0 \ge r_1 \ge 1+\mu$.

Proof: Differentiate with respect to r_0 and note the derivative is identically zero. □

Since $(|\Delta H|)^+$ is decreasing as a function of r and $\lim_{r_0\to\infty}(|\Delta H|)^+(r_0)=0$, from this claim it follows that

$$|\Delta P_\varphi(t_0,t_1)| \le \rho(r(t_1)) = \rho(r_1) := \frac{1}{1-\frac{M}{r_1^2}}\Big((|\Delta H|)^+(r_1)+\int_{r_1}^{\infty}(|\frac{\partial\Delta H}{\partial r}|)^+dr\Big) \quad \text{(B.1)}$$

$$\frac{2\mu(1-\mu)r}{(r^2-M)(r-1+\mu)(r+\mu)}$$

provided that the radius is decreasing from t_0 to t_1. Using $M = (\max P_\varphi) = 1.81$ to evaluate $\rho(5)$ gives an upper bound on the change of P_φ over the whole outside region. Note that this argument can be made symmetric by considering change from the final conditions and reversing time. Hence, when approaching the perihelion from the preceding aphelion or from infinity, (1) angular momentum does

not change by more than $\rho(5) \approx 0.0215298\mu$ over the entire outside region, (2) angular momentum does not change by more than $\rho(r_{min}^{perih}) \approx 4.44885\mu$, and (3) angular momentum does not change by more than $2\rho(5) + 2\rho(r_{min}^{perih}) \approx 8.94077\mu$ during an R–Solar passage. Note that the construction allows for any type of R–Solar passage, elliptic, parabolic, or hyperbolic, provided that $P_\varphi \leq 1.81$ during the passage.

If one only cares about change in angular momentum after an R–Solar passage, then (3) is not an optimal bound. CAPD is used to perform rigorous integration over all 5–Solar passages with $P_\varphi \in [1.68753, 1.81]$. It finds $|\Delta P_\varphi| \leq 1.4\mu$ (see Theorem 2.2.4). Thus a more tight estimate on total change in angular momentum after an R–Solar passage is $1.4\mu + 2 \cdot 0.0215298\mu < 1.444\mu$.

This justifies the initial choice of $P_\varphi \leq 1.81$ in the analysis, since if the comets starts with $P_\varphi(0) = 1.8$ (i.e. $e = 1$) and approaches the Sun to make an R–Solar passage, then the most angular momentum could ever be is $P_\varphi = 1.80894077 < 1.81$. Comets with angular momentum slightly above $P_\varphi = J_0$, i.e. slightly above $e = 1$ after a 5-Solar passage escape the solar system.

Remark: $J_0 = 1.8$ and $\mu = 10^{-3}$ are implicitly used to generate the estimate on change in angular momentum since these constants are used in estimates on ρ, $(|\Delta H|)^+$, and $(|\frac{\partial \Delta H}{\partial r}|)^+$. The dependency on J_0 is not so strong; it was only used describe the domain of nearly parabolic motions, namely to give $(\max P_\varphi) \leq 1.81$. The software to estimate this quantity can be adapted to other μ and J_0.

B.2 An Analysis of the Variational Equations for the RCP3BP

This section analyzes the equations of first variation for the RCP3BP. Consider the following time dependent matrix $A(t)$ which depends on the flow of the RCP3BP at time t:

$$A(t) = \begin{pmatrix} 0 & 0 & 1 & 0 \\ \frac{-2P_\varphi}{r^3} & 0 & 0 & \frac{1}{r^2} \\ \frac{-3P_\varphi^2}{r^4} + \frac{2}{r^3} - \frac{\partial^2 \Delta H}{\partial r^2} & -\frac{\partial^2 \Delta H}{\partial r \partial \varphi} & 0 & \frac{2P_\varphi}{r^3} \\ -\frac{\partial^2 \Delta H}{\partial r \partial \varphi} & -\frac{\partial^2 \Delta H}{\partial \varphi^2} & 0 & 0 \end{pmatrix}$$

Let

$$X(t) = \begin{pmatrix} \frac{\partial r}{\partial r_0} & \frac{\partial r}{\partial \varphi_0} & \frac{\partial r}{\partial P_{r_0}} & \frac{\partial r}{\partial P_{\varphi_0}} \\ \frac{\partial \varphi}{\partial r_0} & \frac{\partial \varphi}{\partial \varphi_0} & \frac{\partial \varphi}{\partial P_{r_0}} & \frac{\partial \varphi}{\partial P_{\varphi_0}} \\ \frac{\partial P_r}{\partial r_0} & \frac{\partial P_r}{\partial \varphi_0} & \frac{\partial P_r}{\partial P_{r_0}} & \frac{\partial P_r}{\partial P_{\varphi_0}} \\ \frac{\partial P_\varphi}{\partial r_0} & \frac{\partial P_\varphi}{\partial \varphi_0} & \frac{\partial P_\varphi}{\partial P_{r_0}} & \frac{\partial P_\varphi}{\partial P_{\varphi_0}} \end{pmatrix}.$$

Then the equations of variation are given by a time-dependent linear ODE:

$$\dot{X} = A(t)X \tag{B.2}$$

The equations of variation tell how a vector $v = (v_1, v_2, v_3, v_4)$ is transported under the flow in the tangent space. Since all work is restricted on to the energy surface $\mathcal{S}(J_0)$, tangent vectors must be restricted to be tangent to the energy surface. Differentiating $H(r, \varphi, P_r, P_\varphi) = -J_0$, it is not hard to see that vectors must satisfy the constraint:

$$(\frac{\partial H}{\partial r})v_1 + (\frac{\partial H}{\partial \varphi})v_2 + (\frac{\partial H}{\partial P_r})v_3 + (\frac{\partial H}{\partial P_\varphi})v_4 = 0$$

Using this constraint on the initial conditions, a reduced linear system involving

only 3 of the 4 variables in each column of X can be solved. Additionally knowledge of solutions involving 3 of the column vectors may be used to obtain solutions to the fourth. It shall be made clear in context which variable is being implicitly defined. In all cases, call the equations of variation with the flow on $\mathcal{S}(J_0)$ and tangent vectors satisfying (B.2) the *reduced equations of variation.* It is not hard to show if an initial tangent vector satisfies (B.2), then it satisfies (B.2) for all time under the full flow. Hence when convenient, the full system shall be used with the understanding the the initial conditions are taken tangent to the energy surface.

Theorem B.2.1. *Consider RCP3BP*$(10^{-3}, 1.8)$ *and suppose the initial conditions for the flow of the are at the aphelion. If* $\left(\frac{\partial r}{\partial P_{\varphi_0}}, \frac{\partial \varphi}{\partial P_{\varphi_0}}, \frac{\partial P_\varphi}{\partial P_{\varphi_0}}\right)(0) = (0, 0, 1)$ *and the remaining initial condition satisfies (B.2) then*

1. $|\left(\frac{\partial P_\varphi}{\partial P_{\varphi_0}}\right)(t) - 1| \leq 0.000268671$ *for* $t \in [0, t_5]$ *where* t_5 *is the first positive time such that* $r(t_5) = 5$.

2. $\left(\frac{\partial P_\varphi}{\partial P_{\varphi_0}}\right)(t) \in [0.12, 1.79]$ *for* $t \in [0, T]$ *where* T *is the first positive time that the comet is at the perihelion.*

Note that for r large $A(t) \approx (0)$, the system is expected to behave roughly like $X(t) = X(0)$. Hence Theorem B.2.1 says that far enough from the sun, the variational equations don't vary too much. Indeed in the outside region, the variational equations behave very much like those of the 2BP(SC). See [Beu] for a presentation of closed form solutions to the equations of first variation for the 2BP.

The theorem is broken down into a series of lemmas. First a series of rough estimates is established in the outside region where the perturbation term is small.

These estimates may be done by hand. These rough estimates are then used to produce refined estimates of the behavior in the outside region. This shall yield the first claim of theorem. The second claim is proved with the assistance of a computer since the perturbation terms have a much stronger influence in the kick region and by hand estimates are insufficient to obtain good estimates.

Lemma B.2.2. *Consider RCP3BP*$(10^{-3}, 1.8)$ *and suppose the initial conditions for the flow are at the aphelion. If* $\left(\frac{\partial r}{\partial P_{\varphi_0}}, \frac{\partial \varphi}{\partial P_{\varphi_0}}, \frac{\partial P_\varphi}{\partial P_{\varphi_0}}\right)(0) = (0, 0, 1)$ *and the remaining initial condition satisfies (B.2), then*

$$\left| \left(\frac{\partial r}{\partial P_{\varphi_0}}, \frac{\partial \varphi}{\partial P_{\varphi_0}}, \frac{\partial P_\varphi}{\partial P_{\varphi_0}}\right)(t) - (0, 0, 1) \right| \leq 1.31926$$

for $t \in [0, t_5]$ *where* t_5 *is the first positive time such that* $r(t_5) = 5$*, and where the norm considered is the* $p = 1$ *norm.*

Proof of Lemma B.2.2: First the 2-degree-of-freedom Hamiltonian for the RCP3BP in polar is reduced to a 1.5-degree-of-freedom time periodic system. Then analysis of the corresponding reduced equations of variation is conducted.

Use the energy reduction procedure found for example in e.g [A], sect. 45 to define a time-rescaled Hamiltonian

$$H_{J_0} = -J_0 + P_r$$

where H given by (1.2) is the Hamiltonian for RCP3BP in rotating polar coordinates. Examining the equations of motion,

$$\frac{\partial H_{J_0}}{\partial P_r} = 1 \qquad \frac{\partial H_{J_0}}{\partial P_\varphi} = \frac{\frac{\partial H}{\partial P_\varphi}}{P_r}$$
$$\frac{\partial H_{J_0}}{\partial r} = \frac{\frac{\partial H}{\partial r}}{P_r} \qquad \frac{\partial H_{J_0}}{\partial \varphi} = \frac{\frac{\partial H}{\partial \varphi}}{P_r}$$

notice that flows of H on $\mathcal{S}(J_0) = \{H = -J_0\}$ and flows on H_{J_0} are the same up to rescaling of time, except at aphelion/perihelion points where $P_r = \dot{r}$ is zero. Furthermore $P_r = P_r(J_0, r, \varphi, P_\varphi)$ is explicitly given by (4.2) on $\mathcal{S}(J_0)$. The time rescaling for H_{J_0} is given by $r(t) \mapsto t$. Notice that this map is monotonic except at aphelions/perihelions and this is why the rescaling is not defined at those points.

Consider the equations of variations for the rescaled system. Let $v = \left(\frac{\partial r}{\partial P_{\varphi_0}}, \frac{\partial \varphi}{\partial P_{\varphi_0}}, \frac{\partial P_r}{\partial P_{\varphi_0}}, \frac{\partial P_\varphi}{\partial P_{\varphi_0}}\right)(0)$. Notice that P_r is given implicitly by (4.2), $v_3 = \frac{\partial P_r}{\partial P_{\varphi_0}}$ is given implicitly by (B.2), and r serves as the time variable. Hence it suffices to consider only the 2×2 system

$$\left(\frac{d}{dr}\right) \begin{pmatrix} \frac{\partial \varphi}{\partial P_{\varphi_0}} \\ \frac{\partial P_\varphi}{\partial P_{\varphi_0}} \end{pmatrix} = \frac{1}{P_r} \begin{pmatrix} 0 & \frac{1}{r^2} \\ -\frac{\partial^2 \Delta H}{\partial \varphi^2} & 0 \end{pmatrix} \begin{pmatrix} \frac{\partial \varphi}{\partial P_{\varphi_0}} \\ \frac{\partial P_\varphi}{\partial P_{\varphi_0}} \end{pmatrix} \tag{B.3}$$

Let $\tilde{A}(r)$ denote the reduced coefficient matrix above, and let $x = \left(\frac{\partial \varphi}{\partial P_{\varphi_0}}, \frac{\partial P_\varphi}{\partial P_{\varphi_0}}\right)$.

Suppose $r_1 \leq r_0$ and $P_r = P_r(J_0, r, \varphi, P_\varphi)$ is nonzero for $r \in (r_1, r_0)$. It follows from the standard theory of linear ODEs that for $r \in [r_1, r_0]$, the solutions to the reduced variational equations are of the form

$$x(r) = x(r_0) + \int_{r_0}^{r} \tilde{A}(s)x(s)ds.$$

Rewrite this as

$$x(r) - x(r_0) = \int_{r_0}^{r} \tilde{A}(s)x(r_0)ds + \int_{r_0}^{r} \tilde{A}(s)\big(x(s) - x(r_0)\big)ds.$$

Letting $|\cdot|$ denote the p-norm for $p = 1$,

$$|x(r) - x(r_0)| \leq \int_{r_1}^{r_0} |\tilde{A}(s)x(r_0)|ds + \int_{r}^{r_0} |\tilde{A}(s)||x(s) - x(r_0)|ds.$$

The first term on the right is independent of r (since the upper bound $\int_{r_1}^{r_0} |\tilde{A}(s)x(r_0)|ds \geq \int_{r}^{r_0} |\tilde{A}(s)x(r_0)|ds$ was used), hence Gronwall's Inequality can be applied to obtain

$$|x(r) - x(r_0)| \leq |x(r_0)| \cdot \int_{r_1}^{r_0} |\tilde{A}(s)|ds \cdot \exp\left(\int_{r_1}^{r_0} |\tilde{A}(s)|ds\right).$$

Hence to obtain a concrete estimation, it suffices to estimate $\int_{r_1}^{r_0} |\tilde{A}(s)|ds$. This is done in Lemma B.2.5 (proved below) which provides a function $a(r_1)$ to uniformly bound $\int_{r_1}^{r_0} |\tilde{A}(s)|ds$ over all $P_\varphi \in [1.7, 1.81]$. The estimates from the lemma yield

Claim: $\int_{r_1}^{r_0} |\tilde{A}(s)|ds \leq a(5) = 0.673031$

See Lemma B.2.5 for an explicit form of $a(r_1)$. The claim is believable since far from the Sun, the terms in the matrix $\tilde{A}$ goto zero at a rate of at most $O(\frac{1}{r^2})$ so integration with respect to r should produce a convergent quantity. The claim yields

$$|x(r) - x(r_0)| \leq 1.31926|x(r_0)|$$

□

The following lemma establishes claim (1) of Theorem B.2.1.

Lemma B.2.3. *Consider RCP3BP*$(10^{-3}, 1.8)$ *and suppose the initial conditions for the flow are at the aphelion. If* $\left(\frac{\partial r}{\partial P_{\varphi_0}}, \frac{\partial \varphi}{\partial P_{\varphi_0}}, \frac{\partial P_\varphi}{\partial P_{\varphi_0}}\right)(0) = (0, 0, 1)$ *and the remaining initial condition satisfies (B.2), then*

$$\left|\left(\frac{\partial P_\varphi}{\partial P_{\varphi_0}}\right)(t) - 1\right| \leq 0.268671\mu$$

for $t \in [0, t_5]$ *where* t_5 *is the first positive time such that* $r(t_5) = 5$.

It should be noted that in the 2BP(SC), $\left(\frac{\partial P_\varphi}{\partial P_{\varphi_0}}\right)(t) \equiv 1$ for all t. Hence the above lemma is in some sense a measure of non–integrability in the outside region in a similar vein to Lemma 2.2.2 which estimates the change in P_φ in the outside region to be at most 0.0215298μ. The order of magnitude larger change in the equations of variation is to be expected since these equations are more sensitive to instabilities than the original equations of motion.

Proof of Lemma B.2.3: Use the same reductions as in Lemma B.2.2. The equations of motion for $\left(\frac{\partial P_\varphi}{\partial P_{\varphi_0}}\right)(t)$ are

$$\left(\frac{d}{dr}\right)\left(\frac{\partial P_\varphi}{\partial P_{\varphi_0}}\right) = -P_r^{-1}\left(\frac{\partial^2 \Delta H}{\partial \varphi^2}\right)\left(\frac{\partial \varphi}{\partial P_{\varphi_0}}\right)$$

Lemma B.2.2 gives $|\left(\frac{\partial \varphi}{\partial P_{\varphi_0}}\right)| \leq 1.31926$. Using the bound $a_2(r_1)$ from Lemma B.2.5,

$$|\left(\frac{\partial P_\varphi}{\partial P_{\varphi_0}}\right) - 1| \leq \int_{r_1}^{r_0} |P_r^{-1}\left(\frac{\partial^2 \Delta H}{\partial \varphi^2}\right) 1.31926| dr \leq a_2(5) \cdot 1.31926 = 0.000268671$$

□

Having generated bounds in the outside region for equations of variation, computer assistance is used to obtain bounds in the kick region where the perturbation terms are larger and the above analysis is insufficient to produce useful bounds. The next lemma establishes claim (2) in the theorem.

Lemma B.2.4. *Consider RCP3BP*$(10^{-3}, 1.8)$ *and suppose the initial conditions for the flow are at the aphelion and furthermore suppose* $\left(\frac{\partial r}{\partial P_{\varphi_0}}, \frac{\partial \varphi}{\partial P_{\varphi_0}}, \frac{\partial P_\varphi}{\partial P_{\varphi_0}}\right)(0) = (0, 0, 1)$ *and the remaining initial condition satisfies (B.2). Then*

$$\left(\frac{\partial P_\varphi}{\partial P_{\varphi_0}}\right)(t) \in [0.12, 1.79]$$

where $t \in [t_5, T]$ where t_5 is the first positive time such that $r(t_5) = 5$ and T first positive time there is a perihelion.

Proof: Let $(v_1, v_2, v_4) = \left(\frac{\partial r}{\partial P_{\varphi_0}}, \frac{\partial \varphi}{\partial P_{\varphi_0}}, \frac{\partial P_\varphi}{\partial P_{\varphi_0}}\right)(t_5)$. Lemmas B.2.2 and B.2.3 say that $v_2 \in [-1.31927, 1.31927]$ and $v_4 \in 1 + [-0.000268671, 0.000268671]$; by assumption $v_1 = 0$. Use (B.2) to solve for the remaining initial condition v_3 as an interval. To do this, use $r = 5$, $\varphi \in [0, 2\pi]$, $P_\varphi \in P_\varphi(0) + [-\rho(5), \rho(5)]$ and P_r implicitly defined by (4.2). This produces a vector of intervals $v := (v_1, v_2, v_3, v_4)$ which contain the solution in the tangent space at the time $t = t_5$.

Use the CAPD rigorous numerical integrator to integrate the flow of the RCP3BP and its associated variational equations. CAPD can transport intervals of initial conditions. See appendix E.1. Use it to transport the interval vector v in the tangent space from $r = 5$ to the perihelion for all initial conditions in the base space. To do this use a 5^{th} order intervalized Taylor Method with step size $\Delta t = 0.1$ with initial conditions φ direction divided into box sizes of 0.1 and initial conditions in the P_φ direction divided into box sizes of 0.0001. CAPD flows the box of initial conditions until all points inside it has passed through the perihelion. It records $\left(\frac{\partial P_\varphi}{\partial P_{\varphi_0}}\right)(t) \in [0.12, 1.79]$. □

Remark: The bound produced is not nearly optimal. Non-rigorous numerics indicate that $\left(\frac{\partial P_\varphi}{\partial P_{\varphi_0}}\right)(t) \in [0.95, 1.05]$.

The technical estimates found in the above lemmas are now justified

Lemma B.2.5. *For $\mu = 10^{-3}$, $J_0 = 1.8$, $P_\varphi \in [1.7, 1.81]$, $r_1 \geq 5$, r_0 an aphelion radius (possibly infinite), and trajectory monotonically decreasing from r_0 to r_1, then*

there exists a function $a(r_1)$ *so that* $\int_{r_1}^{r_0} |\tilde{A}(s)|ds \leq a(r_1)$.

Proof of Lemma B.2.5: In section 2.2 the idea of extreme 2BPs was introduced. By considering the most angular momentum could change in the RCP3BP over the whole outside region $r > 5$ for a specific set of initial conditions, two body problems were constructed whose behaviors enclosed (in the sense of interval arithmetic) that of the RCP3BP which spawned it. See e.g, Lemma 2.2.2 which estimates change in angular momentum for a single trajectory.

The machinery of extreme 2BPs is used now. Unlike section 2.2, careful estimates are not needed for each trajectory; instead uniform upper bounds are needed on quantities for an entire class of trajectories on $\mathcal{S}(1.8)$ with $P_\varphi \in [1.7, 1.81]$. It suffices to compute uniform upper bounds on all 2BP trajectories with $P_\varphi \in [1.7 - \rho(5), 1.81 + \rho(5)]$.

Notice that every entry in the matrix $\tilde{A}$ is of the form $\frac{f(r,\varphi,P_\varphi)}{P_r}$ for some function f where r enters with a power of at most -2. In appendix D, a method of evaluating such integrals **in closed form** is established. The fact that there is a closed form means that a computer algebra system can obtain rigorous upper bounds on the integrals; no numerical integration is required. Define the following quantities:

$$a_1(r_1) = \max\left(\sup_{P_\varphi \in [1.7,1.8]} \lim_{x \to r^+} \frac{I_{-1}(r^-, r^+, r_1, x)}{\sqrt{2(1.8 - P_\varphi)}}, \sup_{P_\varphi \in [1.8,1.81]} \lim_{x \to \infty} I_{-1}^{hyp}(r^-, N, M, x, r_1) \right)$$

$$a_2(r_1) = 2\mu \max\left(\sup_{P_\varphi \in [1.7,1.8]} \lim_{x \to r^+} \frac{I_{-3}(r^-, r^+, r_1, x)}{\sqrt{2(1.8 - P_\varphi)}}, \sup_{P_\varphi \in [1.8,1.81]} \lim_{x \to \infty} I_{-3}^{hyp}(r^-, N, M, x, r_1) \right)$$

where r^+, r^-, N, M are given in section D; $r^\pm$ are formulas for the aphelion and perihelion of a 2BP. The bounds a_i are easily computable with a computer algebra system.

It follows from section A.1 for $r \geq 5$ that $|\frac{\partial^2 \Delta H}{\partial \varphi^2}| \leq \frac{2\mu}{r^4}$. Hence

$$\int_{r_1}^{r_0} |\frac{1}{r^2 P_r}| dr \leq a_1(r_1) \qquad \int_{r_1}^{r_0} |P_r^{-1} \frac{\partial^2 \Delta H}{\partial \varphi^2}| dr \leq a_2(r_1)$$

Since the $p = 1$ norm is used to bound the matrix A, then the corresponding norm induced on the matrix is taking maximum of the absolute value of the sum of columns. Hence the function $a(r_1) = \max\big(a_1(r_1), a_2(r_1)\big)$.

□

Appendix C

Miscellaneous Technical Proofs

This chapter is a collection of miscellaneous technical proofs which either involve heavy perturbation term estimates, heavy computer assistance, or in one way or another did not fit into the general exposition of the numbered chapters.

C.1 Polar Convexity

Lemma C.1.1. *Let $H = H_{Polar}$ be the Hamiltonian associated to RCP3BP given by formula (1.2). Then H and $\exp(H)$ are convex.*

Proof: Explicit computation reveals for $q = (r, \varphi)$, $p = (P_r, P_\varphi)$ that

$$Det(\partial_{pp} H) = \frac{1}{r^2} > 0$$
$$Tr(\partial_{pp} H) = 1 + \frac{1}{r^2} > 0$$

Hence $\partial_{pp} H$ is positive definite and the claim follows. □

C.2 Energy Reduction

This section outlines a method to produce a time periodic Hamiltonian with $(n-1)$ degrees of freedom from an autonomous Hamiltonian with n degrees of freedom with trajectories restricted to an energy surface. This method can be found in [A] sect. 45 (see also [BK]).

Suppose $H = H(I_1, ..., I_n, \theta_1, ..., \theta_n)$ is a Hamiltonian with solutions 2π-periodic in the $\theta_1, ..., \theta_n$ variables and suppose $\frac{\partial H}{\partial I_n} \neq 0$. Consider the Hamiltonian H' defined by

$$dH' = \sum_i^n \frac{\left(\frac{\partial H}{\partial I_i}\right)}{\left(\frac{\partial H}{\partial I_n}\right)} dI_i + \frac{\left(\frac{\partial H}{\partial \theta_i}\right)}{\left(\frac{\partial H}{\partial I_n}\right)} d\theta_i$$

Then trajectories of H and H' are identical up to rescaling of time by $\tilde{t} = \theta_n(t)$. Fix an energy surface $H = E$. This implicitly fixes one of the variables, say $I_n = I_n(I_1, ..., I_{n-1}, \theta_1, ...\theta_n)$. Consider the Hamiltonian

$$\tilde{H}(I_1, ..., I_{n-1}, \theta_1, ...\theta_n) =$$

$$H'\big(I_1, ..., I_{n-1}, \theta_1, ...\theta_n, I_n(I_1, ..., I_{n-1}, \theta_1, ...\theta_n)\big) - I_n(I_1, ..., I_{n-1}, \theta_1, ...\theta_n)$$

Then $\frac{\partial \tilde{H}}{\partial I_n} = 0$ and for $i < n$, $\frac{\partial \tilde{H}}{\partial I_i} = \frac{\left(\frac{\partial H}{\partial I_i}\right)}{\left(\frac{\partial H}{\partial I_n}\right)}$. Hence $\tilde{H}$ does not depend on I_n. Think of $\tilde{H}$ as a time-periodic Hamiltonian with time $\tilde{t} = \theta_n$.

C.3 Proof of Theorem 3.1.1

Using the bounds in appendices A.1 and B.1, Theorem 3.1.1 is proved.

Proof of Theorem 3.1.1:

Recall that constraining dynamics to the energy surface $\mathcal{S}(J_0)$ implicitly defines $P_r = P_r(J_0, r, \varphi, P_\varphi)$. The relation is given by (4.2). It is desirable to bound this expression independently of φ. Furthermore for $\mu > 0$, P_φ is no longer identically constant and it is desirable to bound this quantity independently of fluctuations in P_φ.

Suppose $\mathcal{P}_\mu^+$ is a forward separatrix for RCP3BP(μ, J_0). (The proof in the backward case is analogous.) Then $\mathcal{P}_\mu^+$ has a parameterization $(r, \varphi, P_r, P_\varphi)(t)$ for

$t > 0$. The goal is bound the P_r component. By definition of parabolic escape, $P_r(t) \to 0$ as $t \to \infty$. It follows from (4.2) that $P_\varphi(t) \to J_0$ as $t \to \infty$. It then follows from the definition of ρ in section B.1 that $P_\varphi(t) \leq J_0 + \rho(r(t))$ for $t \geq 0$.

An upper bound for P_r in formula (4.2) is

$$|P_r(J_0, r, \varphi, P_\varphi)| \leq \sqrt{-2J_0 + 2(J_0 + \rho(r)) - \frac{(J_0 + \rho(r))^2}{r^2} + \frac{2}{r} + 2(|\Delta H|)^+(r)}$$

This follows from extremizing ΔH using the bounds in section A.1, and the fact that as a function $P_r(J_0, r, \varphi, P_\varphi)$ is increasing in the variable P_φ in the outer Hill region, so it suffices to replace P_φ by $J_0 + \rho(r)$ to obtain an upper bound.

Claim: There exists $\nu > 0$ such that for $r > 1 + \mu$,

$$\sqrt{2\rho(r) - \frac{(J_0 + \rho(r))^2}{r^2} + \frac{2}{r} + 2(|\Delta H|)^+(r)} \leq \sqrt{\frac{2}{r} - \frac{(J_0 - \nu)^2}{r^2}}.$$

Proof of Claim: The expressions $\rho(r)$ and $(|\Delta H|)^+(r)$ are $O(\frac{\mu}{r^3})$ (see appendix A and bound (B.1)). Since $\rho(r) \geq 0$, then replacing $-\frac{(J_0+\rho(r))^2}{r^2}$ by $-\frac{(J_0-c)^2}{r^2}$ for some $c > 0$ has the effect of increasing the terms under the radical by a factor of $O(\frac{1}{r^2})$ which dominates the $O(\frac{\mu}{r^3})$ terms $2\rho(r) + 2(|\Delta H|)^+$. Hence there exists some smallest positive c, which is denoted ν for which the claimed the bound holds. $\square$

Lemma 1.1.1 says the radius of perihelion is bounded from below by $r = \frac{J_0^2}{2} - 8\mu$. Due to monotonicity,

$$\nu = J_0 - \sqrt{\big(J_0 + \rho(r)\big)^2 - 2r^2\big((|\Delta H|)^+(r) + \rho(r)\big)}\Big|_{r=\frac{J_0^2}{2}-8\mu}.$$

Note that right hand side of the inequality in the claim also arises by solving the equation $H_\nu(r, P_r, J_0) = 0$ for P_r, where H_ν is defined in (3.3). This quantity,

also given in (3.4), parameterizes the homoclinic loop for H_ν. Hence the separatrices for RCP3BP(μ, J_0) are contained inside of this loop.

To be explicit, use the parameters $\mu = 0.001$ and $J_0 = 1.8$. If P_r is radial velocity of a separatrix parameterized by $(r, \varphi, P_\varphi)(t)$ on $\mathcal{S}^{out}(1.8)$, one can prove

$$\begin{aligned} |P_r(1.8, r, \varphi, P_\varphi)(t)| &\leq \sqrt{-2 \cdot 1.8 + 2 \cdot P_\varphi - \frac{P_\varphi^2}{r^2} + \frac{2}{r} - 2\Delta H(r, \varphi)} \\ &\leq \sqrt{\frac{2}{r} - \frac{(1.8 - 2.8\mu)^2}{r^2}} \end{aligned}$$

Hence the RCP3BP$(10^{-3}, 1.8)$ separatrices are enclosed inside the homoclinic loop for H_ν with $\nu \leq 2.8\mu$. □

C.4 Analysis of some twisting terms

Claim: $|\left(\frac{\partial \ell_\nu}{\partial G_\nu(0)}\right)\left(\frac{\partial G_\nu}{\partial L_\nu}\right)| \leq C < \infty$ for all points with initial conditions in $\mathcal{W} \cap \Sigma$.

First see section 4.2.3 to put this claim into context.

Proof of Claim: First notice that

$$\frac{\partial \ell_\nu(t)}{\partial G_\nu(0)} = \int_0^t \frac{\partial \dot{\ell}_\nu}{\partial G_\nu(0)} ds = \int_0^t \frac{\partial \dot{\ell}_\nu}{\partial G_\nu} \frac{\partial G_\nu}{\partial G_\nu(0)} ds$$

Since finite bounds on $\frac{\partial G_\nu}{\partial G_\nu(0)} = \frac{\partial G}{\partial G_0} \in [0.12, 1.79]$ are known over a full period by Theorem B.2.1, then it suffices to come up with bounds on $\int_0^t \frac{\partial \dot{\ell}_\nu}{\partial G_\nu} ds$.

From the equations of motion,

$$\dot{\ell_\nu} = L_\nu^{-3} + \partial_{\ell_\nu} \Delta H(L_\nu, \ell_\nu, G_\nu, g_\nu)$$

Notice on $\mathcal{S}(J_0)$ that $L_\nu = L_\nu(J_0, G_\nu, \ell_\nu, g_\nu) = \frac{1}{\sqrt{2(J_0+\nu-G_\nu+\Delta H)}}$, so

$$\dot{\ell_\nu} = (2(J_0+\nu-G_\nu+\Delta H))^{3/2} + \partial_{\ell_\nu}\Delta H$$
$$\frac{\partial \dot{\ell}_\nu}{\partial G_\nu} = -3(2(J_0+\nu-G_\nu+\Delta H))^{1/2} + \partial_{\ell_\nu G_\nu}\Delta H$$

It follows that

$$\frac{\partial \ell_\nu}{\partial G_\nu}(t) = \int_0^t \big(-3(2(J_0+\nu-G_\nu+\Delta H))^{1/2} + \partial_{\ell_\nu G_\nu}\Delta H\big)ds$$

Each term in the integral shall be analyzed separately.

C.4.1 Analysis of the 2BP Part

The goal of this subsection is to obtain bounds on $\left(\frac{\partial G_\nu}{\partial L_\nu}\right)\int_0^t -3(2(J_0+\nu-G_\nu+\Delta H))^{1/2}dt$ for $t \in [0,T]$ where T is the time to perihelion and where initial conditions are started at the aphelion. This is the dominant term in the numerator of (4.5). For the 2BP, $\left(\frac{\partial G}{\partial L}\right)\int_0^T -3(2(J_0-G))^{1/2}dt = -6\pi L^{-1}$. For the RCP3BP analysis, bounds on ΔH as well as the bounds on the change of $G = P_\varphi$ over the flow need to be included.

Notice that

$$P_r = P_r(J_0, r, \varphi, G) = \frac{1}{r}\sqrt{2(J_0 - G + \Delta H)(r-r_-)(r_+-r)}$$

where $r_\pm = r_\pm(J_0, r, \varphi, G)$ are the aphelion and perihelion respectively. Then

$$\int_0^T (2(J_0+\nu-G_\nu+\Delta H))^{1/2}dt = \int_0^T \frac{rP_r dt}{\sqrt{(r-r_-)(r_+-r)}} = \int_{r_-}^{r_+} \frac{rdr}{\sqrt{(r-r_-)(r_+-r)}}$$

where $P_r = P_r(J_0+\nu, r, \varphi, G_\nu)$ and $r_\pm = r_\pm(J_0+\nu, r, \varphi, G_\nu)$. Notice this is of the form I_1 as in appendix D. Computing the integral $I_1(r_-, r_+, r_-, r_+)$ yields

$$\int_0^T (2(J_0+\nu-G_\nu+\Delta H))^{1/2}dt = \frac{\pi}{2}(r_+ + r_-)$$

Note that for the RCP3BP, $r_\pm$ are difficult to compute exactly since the time to reach the aphelion/perihelion is a dynamical quantity that depends on the flow. However in light of the implicit formulas (2.5) for $r_\pm$,

$$(r_- + r_+)(J_0, r, \varphi, P_\varphi) = \frac{\sqrt{1 - 2P_\varphi^2(J_0 - P_\varphi + \Delta H)}}{2J_0 - 2P_\varphi + 2\Delta H}$$

These quantities are easy to bound by bounding $G_\nu = G - \nu$ over the half-period. The quantity ν is known from Theorem 3.1.1 and formula (B.1) for the function $\rho(r)$ tells us how to bound G over the half-period; namely $|G_\nu(t) - G_\nu(0)| \leq \rho(r(t))$ for time $t \in [0, T]$. Then $(r_- + r_+)$ is bounded by

$$\frac{\sqrt{1 - 2(G_\nu(0) - \rho(1.6))^2(J_0 + \nu - (G_\nu(0) - \rho(1.6)) + (|\Delta H|)^+(1.6))}}{2J_0 + \nu - 2G_\nu(0) + 2\rho(1.6) + 2(|\Delta H|)^+(1.6)} \leq \big(r_- + r_+\big) \leq$$
$$\frac{\sqrt{1 - 2(G_\nu(0) + \rho(1.6))^2(J_0 + \nu - (G_\nu(0) + \rho(1.6)) - (|\Delta H|)^+(1.6))}}{2J_0 + \nu - 2G_\nu(0) - 2\rho(1.6) - 2(|\Delta H|)^+(1.6)}$$

It is not hard to show that the numerators of the upper and lower bounds are bounded. In fact for $J_0 = 1.8$, $\mu = 0.001$, $\nu = 2.8\mu$, $P_\varphi \in [1.66, 1.81]$, and $r \geq 1.6$, the numerator is contained in the interval $[0.239131, 1.04326]$.

Notice from formula (A.1) that

$$\frac{\partial G_\nu}{\partial L_\nu} = \frac{L_\nu^{-3} + \frac{\partial \Delta H}{\partial L_\nu}}{1 - \frac{\partial \Delta H}{\partial G_\nu}}$$

From Lemma A.3.3 shows that $1 - \frac{\partial \Delta H}{\partial G_\nu} \in [1 - 0.025, 1 + 0.025]$. Hence it suffices to obtain finite bounds for $L_\nu^{-3} + \frac{\partial \Delta H}{\partial L_\nu}$.

Notice that on $\mathcal{S}(1.8)$,

$$(2(1.8 + \nu - G_\nu(0) - \rho(1.6) - (|\Delta H|)^+(1.6)))^{3/2} \leq L_\nu^{-3} = (2(1.8 + \nu - G_\nu + \Delta H))^{3/2}$$
$$\leq (2(1.8 + \nu - G_\nu(0) + \rho(1.6) + (|\Delta H|)^+(1.6)))^{3/2}$$

From Lemma A.3.1,

$$|\frac{\partial \Delta H}{\partial L_\nu}| \leq \frac{433\mu}{r^3} \leq \frac{433\mu}{L_\nu^6(1-e_\nu)^3}$$

Now on $\mathcal{S}(J_0)$,

$$e_\nu = \sqrt{1-(G_\nu)^2(J_0+\nu-G_\nu)}$$

Hence for $J_0 = 1.8, \mu = 0.001, \nu = 2.8\mu, G \leq 1.8 + 2\mu$ then $e_\nu = 0.997391 < 1$. (For values of $G > 1.8 + 2\mu$ comets do not have aphelions. This is because if angular momentum decreased maximally, it would still remain above 1.8 after a full revolution when starting above $1.8 + 2\mu$. This is equivalent to saying $e(t) \geq 1$ for all time. See Lemma 2.2.2.) Hence it is possible to get a uniform upper bound on $(1-e_\nu)^{-3}$ for inside parabolic motions. Then

$$\begin{aligned}\frac{433\mu}{(1-e_\nu)^3}(2(J_0 - G_\nu(0) - \rho(1.6) - (|\Delta H|)^+(1.6)))^3 &\leq |\frac{\partial \Delta H}{\partial L_\nu}| \\ &\leq \frac{433\mu}{(1-e_\nu)^3}(2(J_0 - G_\nu(0) + \rho(1.6) + (|\Delta H|)^+(1.6)))^3\end{aligned}$$

It follows that for $J_0 = 1.8, \mu = 0.001, G \in [1.7, 1.81], r \geq 1.6$,

$$\begin{aligned}|\int_0^T (2(J_0+\nu-G_\nu+\Delta H))^{1/2} dt \cdot \frac{\partial G_\nu}{\partial L_\nu}| & \\ &\leq C_1 \frac{(2(J_0+\nu-G_\nu(0)+\rho(1.6)+(|\Delta H|)^+(1.6)))^{3/2}}{2J_0+2\nu-2G_\nu(0)-2\rho(1.6)-2(|\Delta H|)^+(1.6)} \\ &\leq C_2(2(J_0+\nu-G_\nu(0)+\rho(1.6)+(|\Delta H|)^+(1.6)))^{1/2} \\ &< \infty\end{aligned}$$

where $C_1, C_2 < \infty$ are constants. Note the upper bound looks like a $O(L_\nu^{-1})$ which

has found in the 2BP(SC) computation. This uses that

$$|\frac{1.8+\nu-G_\nu(0)+\rho(1.6)+(|\Delta H|)^+(1.6)}{1.8+\nu-G_\nu(0)-\rho(1.6)-(|\Delta H|)^+(1.6)}|<\infty$$

since for inside parabolic motions, $J_0+\nu-G_\nu(0)-\rho(1.6)-(|\Delta H|)^+(1.6)>0.5\mu$.

C.4.2 Analysis of the perturbation term

In this subsection the term $\left(\frac{\partial G_\nu}{\partial L_\nu}\right)\int_0^t\left(\partial_{\ell_\nu G_\nu}\Delta H\right)ds$ is analyzed. For the 2BP, this term is zero, and in general is $O(\frac{\mu}{L_\nu^3})$ small, so it should not contribute much to upper bound.

It follows[1] from Lemma A.3.5, that for $\mu=0.001$, $r>1.5$, $G\in[1.7,1.81]$,

$$|\left(\frac{\partial^2\Delta H}{\partial\ell\partial G}\right)|\leq\frac{21}{r^{7/2}(1-e_\nu)^{3/2}}+\frac{35|P_r|}{r^{5/2}(1-e_\nu)^{5/2}}$$

Now

$$\begin{aligned}\int_0^T|\left(\frac{\partial^2\Delta H}{\partial\ell\partial G}\right)|dt&\leq\int_0^T\frac{21}{r^{7/2}(1-e_\nu)^{3/2}}+\frac{35|P_r|}{r^{5/2}(1-e_\nu)^{5/2}}dt\\&\leq\int_{r_-}^{r_+}\frac{21}{P_r r^3(1-e_\nu)^{3/2}}+\frac{35}{r^2(1-e_\nu)^{5/2}}dr\end{aligned}$$

The second term in the integral is easy to evaluate in closed form and is clearly bounded.

Now

$$\int_{r_-}^{r_+}\frac{1}{P_r r^3}dr=\int_{r_-}^{r_+}\frac{1}{r^2\sqrt{2(J_0-P_\varphi+\Delta H)(r-r_-)(r_+-r)}}dr$$

[1]Lemma A.3.5 is stated in terms of Delaunay, however exactly the same bounds hold for ADDV. Simply put a ν on all the Delauany terms in the estimates.

This is of form I_{-2} from appendix D. It not hard to show that for $r_{\pm} \geq 1.6$ that

$$I_{-2}(r_-, r_+, r_-, r_+) = \frac{\pi(r_- + r_+)}{2(r_- \cdot r_+)^{3/2}} \leq 1.3$$

It follows that for inside parabolic motions,

$$\int_0^T |\left(\frac{\partial^2 \Delta H}{\partial \ell \partial G}\right)| \leq \frac{21 \cdot 0.77}{(1-e_\nu)^{3/2}\sqrt{2\big(J_0 + \nu - G_\nu - \rho(1.6) - (|\Delta H|)^+(1.6)\big)}} + \frac{35 \cdot 1.6}{(1-e_\nu)^{5/2}}$$

Now when multiplied by the upper bound for $\frac{\partial G_\nu}{\partial L_\nu}$, the result is of at most $C(2\big(J_0 + \nu - G_\nu - \rho(1.6) - (|\Delta H|)^+(1.6)\big))^{5/2}$ (for some C) which is bounded.

This completes the proof of the claim since both the dominant and perturbation term are bounded from above. Hence,

$$|\frac{\partial \ell_\nu}{\partial G}\frac{\partial G_\nu}{\partial L_\nu}| < C < \infty$$

□

Appendix D

Table of Integrals

D.1 Integrals for Elliptic 2BPs

Let us investigate some properties of the following commonly occurring integrals. At various times one encounters integrals of the form

$$\int_{t_0}^{t_1} r^k(t)dt = \int_{r_0}^{r_1} \frac{r^k}{\dot{r}}dr$$

Away from $e = 1$, this can be rewritten

$$F(J_0, r_0, r_1, P_\varphi, k) = \int_{r_0}^{r_1} \frac{r^{k+1}dr}{\sqrt{2(J_0 - P_\varphi + \Delta H)(r_+ - r)(r - r_-)}}$$

Suppose it is possible to bound $(J_0 - P_\varphi + \Delta H)$ as well as $r_\pm$ independently of time (see e.g. chapters A and B), where $r_\pm$ are the aphelion and perihelion radii as given in formula (2.5). Then to evaluate the integral (D.1) it suffices to know how to evaluate

$$I(a, b, c, d, k) := \int_c^d \frac{r^k dr}{\sqrt{(b - r)(r - a)}}$$

where in all cases, $a, b, c, d \geq 0$ and $a \leq c \leq r \leq d \leq b$. Specific forms are known for some k. For convenience functions are defined as $I_k(a, b, x)$ and

$I_k(a, b, c, d) := I_k(a, b, d) - I_k(a, b, c)$.

$$I_{-3}(a,b,x) :=$$

$$\left(\frac{\sqrt{ab}(b-x)(x-a)(2ab+3x(a+b))+(3a^2+2ab+3b^2)x^2\sqrt{(b-x)(x-a)}\arctan(\frac{\sqrt{b(x-a)}}{\sqrt{a(b-x)}})}{4(ab)^{\frac{5}{2}}x^2\sqrt{(b-x)(x-a)}}\right)$$

$$I_{-2}(a,b,x) := \left(\frac{\sqrt{ab}(b-x)(x-a)+(a+b)x\sqrt{(b-x)(x-a)}\arctan(\frac{\sqrt{b(x-a)}}{\sqrt{a(b-x)}})}{(ab)^{\frac{3}{2}}x\sqrt{(b-x)(x-a)}}\right)$$

$$I_{-1}(a,b,x) := \left(\frac{\arctan(\frac{x(a+b)-2ab}{2\sqrt{ab(b-x)(x-a)}})}{\sqrt{ab}}\right)$$

$$I_0(a,b,x) := \left(\arcsin(\frac{2x-b-a}{b-a})\right)$$

$$I_1(a,b,x) := \left(\frac{a+b}{2}\arcsin(\frac{2x-a-b}{b-a})-\frac{b-a}{2}\sqrt{1-\left(\frac{2x-a-b}{b-a}\right)^2}\right)$$

D.2 Integrals for Hyperbolic 2BPs

Using elongated Solar passages to model behavior of the comet is only effective provided the comet is sufficiently elliptic, i.e. eccentricity is sufficiently far from one. In the case $e \approx 1$, R–Solar passages are used as defined in section 2.1. However to perform the action comparison, rigorous justification of behavior in the outside region is still needed. The method of using extreme 2BPs as in section 2.2 can be applied, however when computing extreme 2BPs it is possible that one or more have hyperbolic behavior. In this case formulas (2.5) are no longer valid. The hyperbolic analog is

$$\int_{r_0}^{r_1}\frac{r^k dr}{\dot{r}} = \int_{r_0}^{r_1}\frac{r^{k+1}dr}{\sqrt{\left((1+\sqrt{1-2P_\varphi^2(J_0-P_\varphi-\Delta H)}-2(J_0-P_\varphi-\Delta H)r\right)\left(r-r_-\right)}}$$

This formula comes about by carefully rearranging formula 2.5 to remove the aphelion term. For convenience, let $N := 1 + \sqrt{1 - 2P_\varphi^2(J_0 - P_\varphi)}$ and $M = 2(P_\varphi - J_0)$.

Examination of the interval estimates in section 2.2 indicates that if the appropriate formulas for time, action, and difference in angle are given, then the estimates in section 2.2 still hold. Since the comet does not make an elongated Solar passage where it moves from $r = 5$ to an aphelion to back to $r = 5$, then the multiplier of 2 is not needed in the formulas for t_{out} and T_{out} as well as in similar formulas. Everywhere there is a 2ρ, it may be replaced with a ρ. Everywhere is an integral bound $2B_{out}(i)$, or $2D$, replace it with a $B_{out}(i)$, or D respectively. These places are indicated in text of section 2.2.

80–Solar passages are used to perform very high eccentricity action comparisons. Use $R_+^\pm = 80$ where ever it appears in section 2.2. If an extreme 2BP is elliptic, then it suffices to use $B_{out}(i)$'s as defined in section 2.2. Otherwise the bs and Bs must be modified to account for hyperbolic 2BP's.

It suffices to know how to integrate

$$\int_{r_0}^{r_1} \frac{r^k}{\dot{r}} dr = \int_{r_0}^{r_1} \frac{r^{k+1}}{\sqrt{\big(b + er\big)\big(r - a\big)}} dr \tag{D.1}$$

The following are the analogs of the integrals from above for hyperbolic motions. For convenience functions are defined as $I_k(a, b, e, x)$ and

$I_k(a, b, e, c, d) := I_k(a, b, e, d) - I_k(a, b, e, c)$.

$$I_{-3}^{hyp}(a, b, e, x) := \Big(\frac{\sqrt{ab}(b + ex)(x - a)(2ab - 3x(ae - b)) - (3b^2 - ae(2b - 3ae))x^2\sqrt{(b + ex)(x - a)}\arctan(\sqrt{\frac{b(x-a)}{a(b+ex)}})}{4(ab)^{\frac{5}{2}}x^2\sqrt{(b + ex)(x - a)}} \Big)$$

$$I^{hyp}_{-2}(a,b,e,x) := \left(\frac{\sqrt{ab}(b+ex)(x-a) - (ae-b)x\sqrt{(b+ex)(x-a)}\arctan(\frac{\sqrt{b(x-a)}}{\sqrt{a(b+ex)}})}{(ab)^{\frac{3}{2}}x\sqrt{(b+ex)(x-a)}} \right)$$

$$I^{hyp}_{-1}(a,b,e,x) := \left(\frac{2\arctan\left(\frac{\sqrt{b(x-a)}}{\sqrt{a(ex+b)}}\right)}{\sqrt{ab}} \right)$$

$$I^{hyp}_{0}(a,b,e,x) := \left(\frac{2\log\left(e\sqrt{x-a}+\sqrt{e(b+ex)}\right)}{\sqrt{e}}) \right)$$

$$I^{hyp}_{1}(a,b,e,x) := \left(\frac{\sqrt{(ex+b)(x-a)}}{e} + \frac{ae-b}{e^{\frac{3}{2}}}\log\left(e\sqrt{x-a}+\sqrt{e(b+ex)}\right) \right)$$

New b_{out}s and B_{out}s (for 80-Solar passages) are defined by

$$b^{\pm}_{out}(k) = I^{hyp}(r^{\pm}_{-}, x_{\pm}, y_{\pm}, 80, k) - I^{hyp}(r^{\pm}_{-}, x_{\pm}, y_{\pm}, 5, k)$$

$$B^{\pm}_{out}(k) = I^{hyp}(R^{\pm}_{-}, X_{\pm}, Y_{\pm}, 80, k) - I^{hyp}(r^{\pm}_{-}, x_{\pm}, y_{\pm}, 5, k)$$

$$x_{\pm} = 1 + \sqrt{1 + 2(P_{\varphi} \pm \rho(5) \pm w)^2(P_{\varphi} \pm \rho(5) \pm w - J_0)}$$

$$X_{\pm} = 1 + \sqrt{1 + 2(P_{\varphi} \pm \rho(5) \pm w \pm M)^2(P_{\varphi} \pm \rho(5) \pm w \pm M - J_0)}$$

$$y_{\pm} = = 2(P_{\varphi} \pm \rho(5) \pm w - J_0)$$

$$Y_{\pm} = = 2(P_{\varphi} \pm \rho(5) \pm w \pm M - J_0)$$

where w, M, $r^{\pm}_{-}$, and $R^{\pm}_{-}$ are defined as in section 2.2. Such bounds are easily computable on a computer.

Appendix E

Computer Assistance

"Let anyone integrate them who can." - Clairaut

E.1 Rigorous Numerics

A computer is needed to provide mathematically verified bounds on flows of ODE's to complete some of the estimates encountered in Theorem 2.2.4 and Theorem B.2.1, and algorithms in Chapter 5 related to localization intervals. Consider the initial value problem (IVP)

$$\begin{cases} \dot{x} & = f(x) \\ x(0) & = x_0 \end{cases} \tag{E.1}$$

Assume that solutions exist, are unique, and are defined for all time, and that f is sufficiently smooth (either C^∞ or real analytic). Suppose a fixed step size h in time is specified. If $x(t)$ is a solution to the IVP, then from Taylor's Theorem

$$x(t+h) = x(t) + hx'(t) + O(h^2) \approx x(t) + hf(x(t))$$

Euler's Method forgets the remainder and makes a linear approximation at each time step to give

$$\begin{cases} t_i &= t_{i-1} + h \\ x_i &= x_{i-1} + hf(x_{i-1}) \end{cases}$$

Each step of the Euler Method (which is an example of a first order Taylor method) makes an error of $O(h^2)$. Errors made truncating Taylor series methods are known as the *local truncation errors*, which for h small are usually not too bad. However the small errors made by disregarding the $O(h^2)$ term causes the method to track a slightly different solution after each time step. After many steps these small errors can accumulate and destroy the method's usefulness by tracking to a solution which has different behavior from the one desired. This is known as *global truncation error*. Even higher order Taylor methods as well as Runge-Kutta methods are still susceptible to this. The goal is to find and utilize methods which avoid these difficulties.

E.1.1 Interval Arithmetic

When working on a computer, there is another source of error which must be accounted for - floating point error - which arises because a computer is incapable of representing most real numbers.

Machine representable numbers are a subset of real numbers which a computer can perform computations with. Define *machine-*ϵ as the smallest positive number such that $1 \neq (1 + \epsilon)$ on our machine. It gives a kind of spacing between

machine representable numbers. This is dependent on the computer's architecture and software, however most computers adopt IEEE standards which specify such representable numbers, and use machine $\epsilon \approx 10^{-16}$. Assume that a standard such as [IEEE] has been adopted for all work in this document.

One method to get around the difficulties of machine representability is by using so called *interval arithmetic*. If $x \in \mathbb{R}$ we say $[a, b]$ is an *interval representation* for x with machine representable numbers a and b if $x \in [a, b]$. Intervals shall be denoted in calligraphic capital letters, e.g. $\mathcal{I}$. If $\mathcal{I} = [a, b]$, then define $max(\mathcal{I}) = b$ and $min(\mathcal{I}) = a$.

Suppose $f : \mathbb{R}^n \times \mathbb{R}^m \to \mathbb{R}$ is a smooth function and $\mathcal{I} \times \mathcal{J}$ is a product of intervals, The interval $\mathcal{K}$ *encloses* f on the domain $\mathcal{I} \times \mathcal{J}$ if $f(\mathcal{I}, \mathcal{J}) \subset \mathcal{K}$. Computing good enclosures is a principle difficulty in interval arithmetic. [KM] and [MZ] contain methods to make enclosures both rigorous and efficient(for a different approach see [MB1].) Typically complex functions f are broken into a composition of simple arithmetic rules. Rules for interval arithmetic roughly follow intuition. For example if $x \in [a, b]$ and $y \in [c, d]$, then $x + y \in [a + c, b + d]$. On a computer additional work must be done since it is not necessarily true that $a + c$ and $b + d$ are machine representable. To be safe, a computer may say that $x + y \in [a + c - \epsilon, b + d + \epsilon]$.

By saying "bound $f : \mathbb{R}^d \to \mathbb{R}$ over the domain D using interval arithmetic" what is really meant is following algorithm.

1. Cover D with n intervals (or products of intervals) $\mathcal{I}_i^d$ so that $D \subset \bigcup_i^n \mathcal{I}_i^d$.

2. Find enclosures $\mathcal{K}_i$ such that $f(\mathcal{I}_i^d) \subset \mathcal{K}_i$.

3. Compute $m = \min(\mathcal{K}_i)$ and $M = \max(\mathcal{K}_i)$

This algorithm generates numbers so that $f(x) \in [m, M]$ for all $x \in D$. The bounds depend on D, d, n, and the regularity of f. Generally speaking, decreasing $diam(\mathcal{I}_i^d)$ improves the bounds.

Several of the computations found in this document are done on a computer algebra system (CAS). For the purposes of this thesis, a *computer algebra system* is a program which rigorously manipulates algebraic and numerical expressions. A CAS can be programmed to use *exact arithmetic*, which is arithmetic using symbolic expressions to produce exact output without rounding. For example $\frac{1}{2} + \frac{1}{3} = \frac{5}{6}$ on a CAS. It is possible to perform *exact interval arithmetic* where intervals contain symbolic expressions and the bounds are manipulated using exact arithmetic. For the purposes of this thesis, a CAS is required to have the following capabilities. It must:

1. Manipulate algebraic expressions using exact arithmetic
2. Take symbolic derivatives (where possible)
3. Take symbolic integrals (where possible)
4. Manipulate formal power series (where possible)
5. Perform interval arithmetic accounting for rounding error

The estimates used in this document require many lower and upper bounds. Adopt the notation $(\cdot)^{\pm}$ to denote functions or numbers which are upper and lower bounds on the function $(\cdot)$. For a function $f(x, y)$ defined on the domain $\mathcal{I} \times \mathcal{J}$, let

"$f(x,y) \leq (f(x))^+$" mean that $(f(x))^+$ is a function of $x \in \mathcal{I}$ such that the bound holds for all $y \in \mathcal{J}$ in the domain of f. As such a function is not necessarily well defined, explicit constructions are given whenever this notation is used.

Returning to the problem of rigorous numerics for ODE's, the problem can now be reformulated in terms of interval arithmetic. Now consider the *Interval Value Problem (IvVP)* .

$$\begin{cases} \dot{x} & = f(x) \\ x(0) & \in \mathcal{I} = [x_0 - w, x_0 + w] \end{cases} \tag{E.2}$$

where now $\mathcal{I}$ is some interval of initial conditions (a w-window around x_0), x is now a product of intervals in $\mathbb{R}^d$, and all operations are performed via interval arithmetic. From a dynamical systems perspective, the IvVP transports a cube of initial conditions under the flow of the ODE. The advantage of an IvVP solver is that by covering the space of initial conditions with intervals, the solver tells us rigorously how the entire space moves under flow. This is because the flow of the IVP given in (E.1) is rigorously contained inside the flow of the IvVP given by (E.2).

E.1.2 CAPD

One might wonder how to construct a rigorous IvVP solver or even if they exist. Both questions are answered in [Z] and [WZ]. The main idea is as follows.

Recall the difficulty with non-rigorous methods is that they follow slightly different solutions at each step. Gronwall's inequality says that differing solutions move apart at most exponentially based on the magnitude of a Lipschitz constant,

which is roughly $||Df(x)||$. For example, the $O(h^2)$ local truncation error in Euler's Method is from the remainder term in Taylor's theorem which can be written in the form $x''(\xi)\frac{h^2}{2} = Df(\xi)f(\xi)\frac{h^2}{2}$ for some ξ. A naive way to produce a rigorous integrator is to bound the truncation error at each step. Poor bounds on the remainder require the integrator to use larger and larger interval bounds after each step, and these bounds can potentially grow exponentially, rendering the output useless. This is commonly known as the *wrapping effect*. It arises not only from Euler's Method, but from higher order methods as well.

In order to get tight estimates on the errors made after each step, accurate of estimates of $||Df(x)||$ are needed. In [Z], [WZ] and [MZ], efficient methods are outlined to do this. They introduce efficient representations of interval sets that allow for better bounds and introduce an alternative to Gronwall's inequality which appropriately deals with exponential decay. It is also noted that when solving equations of variation, the same main idea can be applied to $D^2f(x)$ and higher derivatives so that one can get efficient bounds for higher order equations of variation.

The theory developed in [Z] and [WZ] has been implemented in a package called CAPD. It is the primary tool for rigorous integration of the equations of motion used in this thesis.

E.1.3 Taylor Models

In this subsection, an alternative procedure to solve Interval Value Problem is described.

Definition E.1.1. *Suppose f is C^{n+1} in an open domain $D \subset \mathbb{R}^n$. The n^{th} order Taylor Model about $x_0 \in D$ is a pair (P, I) where P is n^{th} order Taylor Polynomial of f about x_0, and I is some interval such that for all $x \in D$ the function $f(x) \in P(x - x_0) + I$.*

Since f is C^{n+1}, then Taylor's theorem says that the size of I necessary to ensure the enclosure in the definition shrinks as n grows. Hence the definition is nothing more than a clever statement that says that smooth functions behave like their Taylor Polynomial approximations (up to some small error) inside a sufficiently small neighborhood.

Rules for "Taylor Model Arithmetic"have been generated in [BM1] and are similar to those of interval arithmetic. For example, suppose $T_1 = (P_1, I_1)$ and $T_2 = (P_2, I_2)$ are n^{th} order Taylor Models about $x_0 \in D$. Then

$$T_1 + T_2 = (P_1 + P_2, I_1 + I_2)$$

$$T_1 \cdot T_2 = (P_1 \cdot P_2 - P_h, B(P_h) + B(P_1) \cdot I_2 + B(P_2) \cdot I_1 + I_1 \cdot I_2$$

where P_h is the polynomial made up of all terms of order $(n + 1)$ or larger in $P_1 \cdot P_2$, and $B(P)$ is a bound on the polynomial P in the domain D. One can obtain a bound on any polynomial using the interval arithmetic. Other arithmetic operations, truncation, and the notion of an anti-derivative can also be defined and are done so in [MB1].

Note an immediate advantage of working with Taylor models is the reduced wrapping effect. For example if $x \in [-1, 1]$, then interval arithmetic would say $x - x = [-2, 2]$. A Taylor model on the other hand would use $[-1, 1]$ as the domain

and model x as a Taylor model $(x, [-\epsilon, \epsilon])$. Then $x - x$ would be modeled by $(x - x, [-2\epsilon, 2\epsilon]) = (0, [-2\epsilon, 2\epsilon])$. Then the bound on the model $B(0, [-2\epsilon, 2\epsilon]) = [-2\epsilon, 2\epsilon]$ which is much tighter than the enclosure obtained with interval arithmetic. Taylor models obtain better enclosures for functions over domains at the cost of additional storage and overhead in their manipulation.

Another advantage of working with Taylor Models is that bounds for most common functions are known and can be computed automatically with a computer. Bounds for polynomials, trigonometric, exponential, and logarithmic functions, as well as operations like $\frac{1}{x}$ and $\sqrt{x}$ (all referred to as 'intrinsic functions') have been computed in [MB1]. All of these quantities are known explicitly and for a domain of size h, they have remainders that scale like $O(h^{n+1})$ when using an n^{th} order Taylor model. Most complicated expressions (i.e. the ones most people care about) are made from composing these simple known quantities together and hence have nice Taylor Models with remainder intervals that scale like $O(h^{n+1})$. This is known as

Theorem E.1.2 (The Fundamental Theorem of Taylor Model Arithmetic)**.** *Suppose that the function f is described by an n^{th} order Taylor Model (P_f, I_f) on its domain D. Let g be a function which is composed of finitely many elementary operations and intrinsic functions, and suppose g is defined on the range of f. Let (P, I) be the Taylor Model which arises by plugging in (P_f, I_f) into g and evaluating using Taylor Model arithmetic. Then (P, I) is a Taylor Model for $g \circ f$. Furthermore, if the remainder interval I_f scales like $O(h^{n+1})$, then so does the remainder interval I. [MB1]*

The theory developed in [MB1] has been implemented in a package called **COSY**.

Taylor Models have an important operation which can be defined in a natural way: the operation of anti-differentiation. If (P, I) is a Taylor Model, then define the anti-differentiation operator

$$\partial^{-1}(P, I) = \left(\int P_{n-1}(x)dx, (B(P - P_{n-1}) + I) \cdot [a, b] \right)$$

where P_{n-1} is the $(n-1)$-th degree truncation of P, and $x \in [a, b]$. Notice this operation is easy to compute since integration of a polynomial is just manipulation of its coefficients. The bounds in the remainder term are easily computed with interval arithmetic. This is the key to implementing a rigorous ODE solver.

Consider the initial value problem (E.1) where $f(x) \in C^r(\mathbb{R}^n)$ for $r \geq 1$ sufficiently large. Recall that solutions to IVPs of this form can be written as an integral equation

$$x(t) = x(0) + \int_0^t f(x(s))ds \text{ for } t \leq h.$$

Define the Picard operator

$$A_f(x)(t) = x(0) + \int_0^t f(x(s))ds$$

A_f is a map from $C^0([0, h])$ onto itself and fixed points of A_f correspond to solutions of the IVP. The functional A_f is continuous because f is assumed to be continuous. The following theorem gives the existence of such fixed points.

Theorem E.1.3 (Schauder's Theorem)**.** *Let A be a continuous operator on the Banach Space X. Let $M \subset X$ be compact and convex, and let $A(M) \subset M$. Then A has a fixed point in M.*

In [BM2] it was shown that Schauder's Theorem can be applied to a subset of $X = C^0([0,h])$ which contains all Taylor Models. While this allows for the creation a rigorous integrator, it is still possible that the bounds obtained are poor. If the interval part is too large, then it is possible for solutions to grow apart exponentially for each step of the integrator. This is commonly known as the *wrapping effect*.

A technique called *Shrink Wrapping* outlined in [MB4] is used to further reduce the wrapping effect. It works by attempting to absorb a large remainder bound into the polynomial part of a Taylor Model. In doing so, the error can then be manipulated (and hopefully canceled) along with polynomial parts. This is outlined below. The curious reader is referred to [MB4] for the proofs of shrink wrapping theorems. (These proofs simply rely on taking norms and measuring distances to images of boxes.)

Suppose (P, I) is a d-dimensional Taylor Model of order n about the point x_0 in the domain $B = [-1,1]^d$. (It is always possible to rescale variables so that this holds.) Let C be the constant terms of the Taylor Model and M be the linear terms. Apply the operator $L(\cdot) = M^{-1}(\cdot - C)$ to $P + I$ to get $L(P+I) = Id + S + \hat{I}$ (where Id is the identity). Define the following constants.

$$\hat{I} \subset [-h,h]^d, \qquad s \leq |S_i(x)| \quad \forall x \in B, 1 \leq i \leq d, \qquad v \leq |\frac{\partial S_i(x)}{\partial x_i}| \; \forall x \in B, 1 \leq i,j \leq d$$

Define the *shrink wrap factor* q as

$$q = 1 + \frac{h}{(1-(d-1)v)(1-s)}$$

Theorem E.1.4 (Shrink Wrapping)**.** *Let $Q = Id + S$ be the Taylor Model described above, and suppose $R = [-h,h]^d + \bigcup_{x \in B} Q(x)$ is the range of the Taylor Model*

over the domain B. Let q be the shrink wrap factor defined above. Then $R \subset \bigcup_{x \in B}(qQ)(x)$. Hence multiplying the polynomial part by q makes it possible to set the interval remainder bound to zero. [MB4]

Shrink wrapping is incredibly useful since it makes it possible to absorb the interval remainders generated after each integration step into the polynomial part where it can more easily manipulated. An application of shrink wrapping to the integrator based on Schauder theorem allows for *very long time integration*. The author has implemented this theory in a package called **COSY-JERI**, written in **COSYscript**. It is the primary tool for verifying the crossings solutions and localization intervals from chapter 5.

E.1.3.1 Some Missing Lemmas

This section shall fill in some technical gaps which are used in the construction of **COSY-JERI**, but which are not explicitly stated in Berz's papers on integration with Taylor models. Specifically, in these papers never actually gave a detailed description of how to implement Schauder's Theorem to produce a rigorous integrator.

The key to applying Schauder's Theorem is to find a Taylor Model (P, I) so that $A(P+I) \subset P+I$ on a compact domain $D \subset \mathbb{R}^n$. Then the fixed point, i.e. the solution of the ODE, is contained in the Taylor Model. Notice that if I is small, then this method says the flow is closely modeled by the polynomial part. Finding such a Taylor Model is relatively easy computationally. Start with the zero polynomial, and repeatedly iterate it through $A = A_f$, each time disregarding terms of order

$(n+1)$ or higher. The following claim was started, but not proved in [BM2].

Lemma E.1.5. *Suppose $f \in C^{n+2}$. Let $p_0(x) = 0$ and for $i > 0$ consider the sequence $p_i(x) = (A_f(p_{i-1}(x)))_n$ where $()_n$ means truncate terms of the polynomial of degree $(n+1)$ or higher. Then for $i \geq (n+1)$ steps, $p_{i+1}(x) = p_i(x)$, i.e. the sequence of polynomials stabilizes.*

Proof: It shall be shown that after k applications of $A = A_f$ to the zero polynomial, all terms of degree $(k-1)$ are fixed. Since the Taylor Model is of degree n, then more than $(n+1)$ applications of $A = A_f$ forces the sequence to stabilize. It suffices to show:

Claim: Let $P = A^k(0)$. Then $A(P + O(t^k)) = P + O(t^k)$.

The proof of the claim is by induction on k.

Basis: $k = 1$. $P = A(0) = x_0$.

$$A(x_0 + O(t)) = x_0 + \int_0^t f(x_0 + O(\tau))d\tau = x_0 + O(t)$$

The equality on right follows from the fact that all terms in the integral pick up at least a factor of t after the integration.

Assume the result holds true for k. Now it shall be shown that it holds for $(k+1)$. Let $Q = A(P) = A^{k+1}(0)$. By the inductive hypothesis,

$$Q = R + S + O(t^{k+1})$$

where R is the degree $k-1$ polynomial such that $P = R + O(t^k)$ (hence R is fixed

under iterates of A), and S is the polynomial composed of the degree k terms in Q.

$$\begin{aligned}
A(Q) =& A(R+S+O(t^{k+1})) = x_0 + \int_0^t f(R+S+O(\tau^{k+1}))d\tau \\
&= x_0 + \int_0^t f(R+S) + f'(R+S)\cdot O(\tau^{k+1}) + \frac{f''(R+S)}{2}O(\tau^{k+1})^2 + ...d\tau \\
&= A(R+O(t^k)) + \int_0^t O(\tau^{k+1})(\text{H.O.T})d\tau \\
&= R + O(t^k) + O(t^{k+2}) \\
&= R + (k^{th} \text{ order terms}) + O(t^{k+1})
\end{aligned}$$

This follows from the Taylor Series expansion of f in terms of its argument x, and the inductive hypothesis. The claim will be complete if the (k^{th} order terms)=S. Notice that since $deg(S) = k$,

$$\begin{aligned}
\int_0^t f(R+S)d\tau &= \int_0^t f(R) + f'(R)S + \frac{f''(R)}{2}S^2 + ...d\tau \\
&= \int_0^t f(R)d\tau + \int_0^t R\cdot(\text{H.O.T.})d\tau \\
&= \int_0^t f(R)d\tau + O(t^{k+1})
\end{aligned}$$

hence all the terms in S get integrated and land in the $O(t^{k+1})$. Now

$$\begin{aligned}
A(P) &= A(R+(P-R)) \\
&= x_0 + \int_0^t f(R+(P-R))d\tau \\
&= x_0 + \int_0^t f(R) + f'(R)(P-R) + ...d\tau \\
&= A(R) + \int_0^t (P-R)(\text{H.O.T.})d\tau \\
&= A(R) + O(t^{k+1})
\end{aligned}$$

since $deg(P - R) = k$. Hence $A(Q) = A(R) + O(t^{k+1})$ and

$$\begin{aligned} A(R) &= A(P) + O(t^{k+1}) \\ &= A(A^k(0)) + O(t^{k+1}) \\ &= Q + O(t^{k+1}) \end{aligned}$$

so

$$A(Q) = Q + O(t^{k+1}) = R + S + O(t^{k+1})$$

which implies that (k^{th} order terms)=S. □

Using this algorithm, it is possible to generate a polynomial P invariant under A_f. It remains to give a bound on the remainder formula for rigorous integration using Taylor Models in order to complete the application of Schauder's Theorem as in [BM2]. Specifically, an interval I is required so that $A(P + I) \subset P + I$ on a compact neighborhood $D \subset \mathbb{R}$.

Lemma E.1.6. *Suppose f is real analytic in an ϵ-neighborhood of the range of P where $\epsilon \geq 2$ and P is the polynomial invariant under A_f. Then there exists a number h and an interval I such that for $0 \leq t \leq h$*

$$A(P + I) - P \subset I$$

Proof: Compute

$$A(P + I) = x_0 + \int_0^t f(P + I)d\tau$$

By the Fundamental Theorem of Taylor Model Arithmetic [MB1], $f(P + I)$ is a Taylor Model. Consider the decomposition:

$$f(P + I) = Q + R + \hat{I}$$

where Q is all terms of degree $(n-1)$ or less, R is all degree n terms, and $\hat{I}$ is the remainder. Since $A(P) = (P)_n$ and since $deg(R) = n$, then R integrates to an $(n+1)$ order term after an application of A_f, and hence

$$P = x_0 + \int_0^t Q d\tau.$$

Thus the other terms contribute exclusively to the remainder, i.e.

$$A(P+I) - P \subset \int_0^t (R + \hat{I}) d\tau$$

Let us better understand this relation since $\hat{I}$ depends upon I. Notice

$$\begin{aligned} A(P+I) &= x_0 + \int_0^t f(P+I) d\tau \\ &= x_0 + \int_0^t f(P) + f'(P)I + \frac{f''(P)}{2} I^2 + ... d\tau \\ &= x_0 + \int_0^t Q + R + f'(P)I + \frac{f''(P)}{2} I^2 + ... d\tau \\ &= P + \int_0^t R + f'(P)I + \frac{f''(P)}{2} I^2 + ... d\tau \end{aligned}$$

Since the class of functions considered is real analytic in a large domain, then the '...' converges. Now suppose the interval $I \subset [-d, d]$ where $d < 1$. Then

$$\begin{aligned} A(P+I) - P &\subset \int_0^t R + f'(P)I + \frac{f''(P)}{2} I^2 + ... d\tau \\ &\subset \int_0^t R + I \cdot (f'(P) + \frac{f''(P)}{2} + ...) d\tau \end{aligned}$$

Notice that the Taylor expansion of $f(P+1)$ about the point P gives

$$f(P+1) = f(P) + f'(P) + \frac{f''(P)}{2} + ...$$

where the sum converges due to the regularity class of the functions considered.

Hence

$$A(P+I)-P \subset \int_0^t R + I\cdot(f(P+1)-f(P))d\tau$$
$$\subset B(\int_0^t Rd\tau) + IB(\int_0^t (f(P+1)-f(P))d\tau)$$

where the operator B means 'bound' over $0 \le t \le h$ and over the domain D. In the event that $R = 0$, i.e. $f(P)$ has no n^{th} order terms, make an upper bound by replacing $R = 0$ with $R = t^n$.[1] If the above expression is contained inside of the interval I, it is possible to formally 'solve' for I to get

$$\frac{B(\int_0^t Rd\tau)}{1-B(\int_0^t (f(P+1)-f(P))d\tau)} \subset I. \tag{E.3}$$

In order to justify the assumption that $I \subset [-d,d]$ where $d < 1$ and remove the 'formally', the quantity h is specified. Suppose $t \in [-h,h]$. Clearly for $h = 0$, then left hand side of (E.3) evaluates to zero, which is to say that to model the initial condition requires no error. Notice the left hand side of (E.3) is continuous as a function of h, except at the point where the denominator is zero, i.e. the point where the bounds become $(-\infty,\infty)$. Hence by the intermediate value theorem, there is some h so that $d < 1$. □

Notice that the remainder interval I scales with h. This makes sense since it is easier to model the flow for a short period of time, than for a longer period. What is hidden is exactly how well it scales. The term R which is the n^{th} degree pieces of $f(P+I)$ behaves like $O(h^{n+1})$ so decreasing h (the time the ODE is modeled for), or increasing n results in a dramatic increase in accuracy.

[1] If instead $R = 0$ is left as is, then it would boil down to requiring t to be so that $B(\int_0^t (f(P+1)-f(P))d\tau) \subset [-\alpha,\alpha]$ for some $0 < \alpha < 1$.

The above lemma carries through without difficulty in the multidimensional case provided the remainder interval is the same in each dimension. This can probably be avoided with some more lengthy expressions for the remainder interval error, however this is pursue not pursued.

Note that (E.3) can be modified to allow for Taylor Models which are polynomials in both time t and initial conditions x_0. Suppose the initial conditions x_0 are contained inside of the Taylor model (G, J), i.e. $x_0 \in G + J$ where G is a degree n polynomial. It is possible to create a polynomial P invariant under $\tilde{A}(x)(t) = G + \int_0^t f(x(\tau))d\tau$. But then

$$A(P)(t) = G + J + \int_0^t f(x(\tau))d\tau = \tilde{A}(P)(t) + J =_n P + J.$$

The additional J is added to (E.3) to yield the bound

$$\frac{B(\int_0^h Rd\tau) + J}{1 - B(\int_0^h (f(P+1) - f(P))d\tau)} \subset I.$$

With the appropriate shrink wrapping (see e.g. [MB4]), $B(J) \approx 0$ and this extra term does not greatly ruin the degree n scaling for the remainder term.

E.1.3.2 Example

Consider the linear ODE

$$\begin{cases} \dot{x} & = \lambda x \\ x(0) & = 1 \end{cases}$$

Consider a degree $n = 3$ Taylor Model and model the ODE up to time $t = h$. Iteration of the operator A gives the polynomial

$$P(t) = x_0 \cdot (1 + \lambda t + \frac{(\lambda t)^2}{2} + \frac{(\lambda t)^3}{6})$$

And the remainder interval is now

$$\frac{B(\int_0^h \frac{\lambda(\lambda\tau)^3}{6} d\tau)}{1 - B(\int_0^h (\lambda \cdot (P+1) - \lambda(P)) d\tau)}$$

Which gives

$$d = \frac{(\lambda h)^4}{24(1 - \lambda h)}$$

Note that $|\lambda h| < 1$, otherwise the bound is useless. This constrains the choice of h. Additionally $|\lambda h|$ needs to be so small that $d < 1$. (For this particular value of n, a choice of $h = min(0.99, \frac{0.72}{|\lambda|})$ works.) For $\lambda h < 1$, expand d as a power series to get

$$\frac{(\lambda h)^4}{24(1 - \lambda h)} = \frac{1}{24}(\lambda h)^4(1 + \lambda h + (\lambda h)^2 + (\lambda h)^3 ...)$$

Compare this to the power series of the actual solution at time $t = h$:

$$Exp(\lambda h) = (1 + \lambda h + \frac{(\lambda h)^2}{2} + \frac{(\lambda h)^3}{6} + \frac{(\lambda h)^4}{24} + \frac{(\lambda h)^5}{120} + ...)$$

Notice that $P(h) + I$ has larger coefficients for terms of order 4 and higher. Hence the enclosure is valid.

E.2 Hardware and Software

The purpose of this section is to provide a technical guide to the programs and estimates used in the thesis. To verify claims in these papers a mixture of

programs written in **C++**, **Fortran 77**, and **Mathematica** are used. Specifically the **CAPD** library is used in C++ to implement rigorous numerical integration, the **COSY** library (implemented in **Fortran 77**) is used to rigorously manipulate Taylor models, and **Mathematica** is used for symbolic manipulation and interval arithmetic.

To verify the claims of the thesis, the following rigorous numerical tools are used:

- Interval arithmetic
- Taylor models
- Rigorous numerical integration to solve IvVPs
- Symbolic manipulation.

There are also tools developed to do nonrigorous numerical integration which is many orders of magnitude faster. Nonrigorous methods are not used in the actual proofs of the papers, however they are very helpful for quickly understanding the behavior of the systems considered.

This section is primarily intended to answer more technical questions pertaining to computer implementation and execution of the algorithms outlined in thesis which are not appropriate for journal paper in mathematics. The contents are not essential for understanding of the mathematical results, however they are necessary to verify the results in question. This section is not meant to be self contained and it is assumed the reader is familiar with some of the literature in the bibliography.

This section is organized in the following manner.

- Section E.2.5 contains a discussion of programs and where computer assistance is used.
- Section E.2.16 contains discussion of rigorous numerical integration as implemented by the **CAPD** library.
- Section E.2.20 contains discussion of rigorous numerical integration as implemented by **COSY-JERI**.
- Section E.2.15 contains information on installation and execution of the programs.

For reference, a list of programs as well as brief description of each one is included below.

E.2.1 Mathematica Notebooks

- **actcomp.nb** - Performs the action comparison method, using nonrigorous numerical integration. It uses elongated solar passages.
- **actcomp_hyp.nb** - Does the action comparison method using nonrigorous numerical integration. It uses 80-solar passages.
- **actcomp_res.nb** - Summary of numerical output from **actcomp.cpp** with visualizations of the data.
- **crossings.nb** - Trajectories which cross localization intervals.

- **delsimps.nb** - Derivatives of polar quantities with respect to Delaunay variables.
- **GK1Claims.nb** - This contains miscellaneous claims originally found [GK1].
- **GK2Claims.nb** - This contains miscellaneous claims originally found in [GK2].
- **localization_test.nb** - Finds the localization intervals using nonrigorous integration and a mesh of initial conditions.
- **RCP3BP_Estimates.nb** - This notebook contains many tools to convert between Delaunay and Polar variables as well as tools to find various orbital elements. It computes the derivatives for perturbation terms in both polar and Delaunay using it as well as some bounds. This notebook contains numerical integrators to generate numerical solutions to the RCP3BP in polar and Delaunay coordinates, as well as numerical solutions to the equations of variation. This notebook is used ubiquitously to generate claims found throughout this thesis.
- **RCP3BP_estimates_old.nb** - This notebook supports the modified action-angle variables found in section E.2.14.1.
- **simplifications_for_COSY.nb** - Simplified forms for the perturbation term in the alternative action-angle coordinate system found in section E.2.14.1.
- **twistcheck.nb** - Finds the twist region as described in 3.2.

- **usefulintegrals.nb** - Symbolic computation of integrals which frequently appear.

E.2.2 CAPD

- **actcomp.cpp** - Performs rigorous action comparison in the kick region. This file also records information the time to cross the kick region and change in angular momentum in kick the region.

- **C0integrator*.cpp** - Examples of a C^0–integrators. This are not used anywhere in proofs.

- **outactcomp.cpp** - Performs rigorous action comparison using elongated Solar passages. It requires the summary log files generated by **actcomp.cpp**.

- **outactcomp_hyp.cpp** - Performs rigorous action comparison using 100 - Solar passages. Requires the summary log files generated by **actcomp.cpp**.

- **reader.cpp** - Reads through the **Summary_Layer*.txt** log files and extracts an individual element of data from each.

- **readtime.cpp** - Reads through the **Layer*.txt** log files and extracts an individual element of data from each.

- **varbound.cpp** - Computes rigorous bounds on the equations of variation in the kick region.

E.2.3 COSY

- **COSY_JERI.fox** - A rigorous global optimizer and ODE solver using Taylor model arithmetic. Specific information about the RCP3BP is built into this package to compute rigorous numerical trajectories for RCP3BP in polar and modified Delaunay variables.

- **findpolarcross.fox** - A program to verify crossings of localization intervals.

- **gridstore.fox** - Performs the massive grid calculation needed to compute localization intervals. It produces the file **mydata_4.dat**.

- **gridread.fox** - Reads data and produces localization intervals. It requires the file **mydata_4.dat**.

- **RCP3BP_Derviatives.fox** - A library which contains derivatives of the RCP3BP in the action-angle variables described in section E.2.14.1.

- **RigInt.fox** - An example of rigorous integration using **COSY-JERI**. This is not used in any proofs.

- **RigOpt.fox** - An example of rigorous global optimization using **COSY-JERI**. This is not used in any proofs.

E.2.4 Relevant Data Files

- **Crossing_test*.DAT** - Log files pertaining to trajectories which cross the localization intervals. These are generated by **findpolarcross.fox**.

- **ExitTimes.txt** - Log file which contains the maximum time to cross the kick region for each layer. This is generated by **readtime.cpp** using data from **Layers*.txt**.

- **Layer*.txt** - Output of **actcomp.cpp** which contains data about each solution rigorously integrated.[2] Due to size, these are distributed by request only.

- **localization_intervals.txt** - This contains a summary of the localization intervals.

- **Max*.txt** and **Min*.txt** - Output of **reader.cpp** which contained extremized quantities by layer generated from the data in **Summary_Layer*.txt**.

- **mydata_4.dat** - Output of **gridstore.fox** which contains results of integration in action-angle variables over. This is stored in a zip file **mydata_4.zip**.

- **outact.txt** - Output of **outactcomp.cpp** which lists where the action comparison holds using elongated Solar passages.

- **outacthyp.txt** - Output of **outactcomp_hyp.cpp** which lists where the action comparison holds using 100–Solar passages.

- **outact_fail.txt** - Alternative output of **outactcomp.cpp** which outputs layers were the action comparison failed.

[2]In the implementation currently used, these files only contain data on how long it takes a trajectory to cross the kick region.

- **Summary_Layer*.txt** - Output of **actcomp.cpp** which contains a summary of data needed for the action comparison. These are stored in a zip file **summary.zip**.

E.2.5 Usage of the Programs

Computer assistance is used for the following.

1. Bounds on perturbation terms (Appendix A)
2. Bounds on total change in angular momentum (Appendix B)
3. Determining the twist region Tw^{Del} (Chapter 3)
4. Performing the action comparison (Chapter 2)
5. Expansion of the domain of definition (Chapter 3)
6. Analysis of the equations of variation (Appendix B)
7. Computing the localization intervals (Chapter 5)
8. Computing the crossings (Chapter 5)
9. Determining the number of iterations needed to cross the kick region. (Chapter 5)

E.2.6 Bounds on perturbation terms

In chapter A, bounds on the perturbation terms are developed.

Mathematica's symbolic manipulation capabilities are used to sum up such infinite series. This is done in the notebook **RCP3BP_Estimates.nb** in the section 'Assembles perturbation term dH approximation'.

The bounds on the perturbation terms are used to compute bounds on perihelion radii. These calculations are contained inside of the notebook **GK1claims.nb** in the section 'Minimum Perihelion.' Interval arithmetic is used to verify the claims that $\frac{\partial r^{perih}}{\partial P_\varphi} < 0$. The other estimates use numerical solvers to obtain the concrete numbers. Since all expressions evaluated were either algebraic, or a combination of algebraic and trigonometric, then **Mathematica**'s internal routines are capable of accurately evaluating the expressions in question up to arbitrary accuracy.

The only additional facts used were the bounds on the derivatives of Legendre polynomials. Suppose P_n is the n^{th} Legendre Polynomial. Then for $x \in [-1, 1]$

$$|P_n'(x)| \leq \frac{n(n+1)}{2}$$
$$|P_n''(x)| \leq \frac{(n-1)(n+1)(n+2)}{8}$$

These are used to generate the bounds on derivatives of ΔH involving φ.

Specific bounds on the derivatives of the perturbation terms for $\mu = 0.001$ and $r > 1.5$ were found in Appendix A. To find these bounds, **Mathematica** can find upper bounds on the terms from section A.1. This is done in the notebook **GK2claims.nb**.

E.2.6.1 Bounds on Terms Involving Perturbation Terms

A computer algebra system is used to compute derivatives in Delaunay. The routines for taking derivatives are found in **RCP3BP_Estimates.nb**. The simplifications are found in the notebook **delsimps.nb**. Some of the specific numerical quantities are found in **GK2claims.nb**.

In Lemma A.3.2, **Mathematica** is used compute the derivatives of r, ϕ with respect to the Delaunay variable G. The notebook **delsimps.nb** contains the symbolic manipulations to produce the identities used. The notebook **GK1claims.nb** contains the numerical quantities in question in the section 'Quantities in Lemma 10.1'.

E.2.7 Bounds on change in Angular Momentum

Proof of Lemma 2.2.2 on the change in angular momentum requires a function $\rho(r)$ measuring change in angular momentum over the orbit from aphelion to perihelion. In the construction, **Mathematica** is used to verify the claim that $\Big((|\Delta H|)^+(r_0) + (|\Delta H|)^+(r_1) + \int_{r_1}^{r_0}(|\frac{\partial \Delta H}{\partial r}|)^+ dr\Big)$ is nondecreasing as a function of r_0 for $r_0 \geq r_1 \geq 1+\mu$ by differentiating the expression with respect to r_0 and noting the derivative is identically zero. This is found in the notebook **GK1claims.nb** under the section 'Angmom claim'.

Additionally **Mathematica** is used to evaluate the integral in the the function ρ symbolically and simplify the expression. It produces

$$\rho(r) = \frac{2\mu(1-\mu)r}{(r^2-M)\big(\mu^2 + r(r-1) + \mu(2r-1)\big)}$$

where $M = maxP_\varphi$ is the upper bound on angular momentum. In Appendix B.1 this number was shown to be at most $M = 1.81$. However it is possible to improve this bound as well as the bound on the minimum perihelion. Notice that the value M needed for the proof is Theorem 1.1.2 is really the smallest angular momentum P_φ^* so that a trajectory of comet which so that a comet which passes through the perihelion with angular momentum P_φ^* escapes. Escape occurs if $P_\varphi(t) > J_0$ for all positive time. Hence the system may be written:

$$\begin{aligned} M - 2\rho(r^{perih}) =& J_0 \\ -J_0 =& H_{2BP}(r^{perih}, 0, 0, M) - (|\Delta H|)^+ \leq H(r^{perih}, \varphi, 0, M) \end{aligned}$$

This is a system of two equations in two variables, and **Mathematica** may solve to find the optimal $(r^{perih}, M) = (1.61513, 1.80403)$. This is done in the notebook **GK1claims.nb**. These numbers provide additional verification that our bounds of $M = 1.81$ and $r^{perih} \geq 1.61048$ are valid.

The third claim of Lemma 2.2.2 requires additional computer assistance. Recall that the proof of Theorem 2.2.4 rigorously integrate all 5-solar passages in our class of interest and record the final conditions. This is used to determine the total change in P_φ after a 5-solar passage. $\rho(5)$ is then used to estimate behavior in the outside region.

E.2.8 Determining the Twist Region

In section 3.2, a computer is used to find the size of the twist region. Proof of this lemma boiled down to computer verification of two facts:

1. The sign of

$$TT = \frac{\left(\frac{\partial H}{\partial G}\right)\left(\frac{\partial^2 H}{\partial L^2} + \frac{\partial^2 H}{\partial L \partial G}\frac{\partial G}{\partial L}\right) - \left(\frac{\partial H}{\partial L}\right)\left(\frac{\partial^2 H}{\partial L \partial G} + \frac{\partial^2 H}{\partial G^2}\frac{\partial G}{\partial L}\right)}{(\frac{\partial H}{\partial G})^2}$$

   is positive everywhere in a region, where

$$\frac{\partial G}{\partial L} = \frac{L^{-3} + \left(\frac{\partial \Delta H}{\partial L}\right)}{1 - \left(\frac{\partial \Delta H}{\partial G}\right)}$$

2. The sign of $\frac{\partial L(t)}{\partial L}$ is positive over one revolution of the comet about the sun.

To address item one, **Mathematica**'s symbolic manipulation abilities are used to explicitly compute the twist term TT. Note that the denominator of this term is always nonnegative and hence does not effect the sign, so only the numerator needs to be computed to determine sign change. The **Mathematica** notebook **twistcheck.nb** demonstrates sign change[3]. The variable 'ReducedTwistTermD' is the numerator of the twist term TT.

Numerical optimization is used over all angular variables, as well as the perturbation term[4] to find the minimal value of 'ReducedTwistTermD' for a fixed L value on the energy surface $\mathcal{S}(1.8)$. The nonrigorous numerical optimizations indicate that the twist term changes signs somewhere near $L = 1.61$, i.e. $e \approx 0.06$ and $L = 15.94$, i.e. $e \approx 0.994$.

Rigorous verification of these facts is much harder and is done with interval arithmetic. Descriptions of interval arithmetic are found in the references cited below. While interval arithmetic works well at bounding small domains, it can be

[3]This notebook requires the notebook **RCP3BP_Estimates.nb** to run.

[4]It follows from section E.2.6 that the perturbation term is known to be bounded by 0.64μ inside the domain of definition. The program uses $\Delta H \in [-0.7\mu, 0.7\mu]$.

very slow for larger ones. Due the complexity of the twisting term, evaluations are expensive. To get good bounds, small boxes must be used. To prove the nonrigorous numerical result rigorously would take a very long time with current computing power. The best that can be done at present is to instruct **Mathematica** to use machine precision when carrying out the numerical optimization.

Mathematica can also symbolically expand the twisting term in terms of $\frac{1}{L}$ and it can be shown it is at most $O(\frac{1}{L^4})$. Theory tells us it behaves like $\frac{-3}{L^4} + O(\mu)$, so twist is expected to be violated for high L values, which is seen in the notebook.

In the notebook **twistcheck**, values of the twist term in ADDV are also computed.

Item two follows from the fact that $\frac{\partial P_\varphi}{\partial P_{\varphi_0}} > 1$ over one revolution. This fact is proved in the section on analysis of the equation of variation.

E.2.9 Performing the Action Comparison

A quick nonrigorous method of performing the action comparison is automated in a **Mathematica** notebook, and a more in depth rigorous approach is the focus of several programs.

E.2.9.1 Nonrigorous Action Comparison

The **Mathematica** notebook **actcomp.nb** contains code optimized for $J_0 = 1.8$. At the start, set the value of 'PphiIC', the initial angular momentum, and execute all the cells. The notebook generates a large number of test solutions using

nonrigorous Runge-Kutta integration, computes action in the kick region, finds the extrema in action with respect to angle, finds the extreme angles, then uses extreme 2BP's to carry out the outside action comparison. The formulas are implemented exactly as described, modulo slightly different (and in some cases more descriptive) variable names. At the end of the notebook is the total comparison. If the interval contains numbers less than or equal to zero, the comparison has failed. Otherwise it works. Information on eccentricity and maximum radius are also computed at the end.

Here are some of the options in the program are some special choices.

- 'GridSize=512' says to use $2 \cdot 512 + 1$ test solutions.
- 'innercompdiff' is the action difference in the inner region, found numerically over the class of test solutions.
- 'maxpphidiff' is the maximum change in angular momentum over the class of 5-Solar passages considered and is estimated from the test solutions.
- 'pphiwindow=0.000025' is actually to account for extra thickness in the P_φ direction which occurs when conducting rigorous numerics. For nonrigorous numerics, it can be set to zero, however leaving it as 0.000025 can be useful to double check the enclosures produced during the rigorous action comparison.
- 'arcl=2' uses elongated solar passages. 'arcl=1' uses standard R-solar passages. This is the extra factor of 2 discussed in section 2.2.

The notebook **actcomp_hyp.nb** performs the action comparison using 80-Solar passages. It is of a similar structure to **actcomp.nb**, however it has several additional modules and functions to handle hyperbolic 2BPs.

The heuristic calculation using parabolic motion used the function 'ptime[$r, J0$]' which inputs radius and J_0 and outputs the time the parabolic 2BP is at in its orbit, where $t = 0$ corresponds to the perihelion. 'ptime', implemented in **RCP3BP_Estimates.nb** is the generates the second formula in (2.1.4). Additionally, **Mathematica**'s symbolic manipulation abilities can be used to invert this function and solve for $r(t)$. This produces the first formula for parabolic motion in (2.1.4). See **GK1Claims.nb**.

E.2.9.2 Rigorous Action Comparison

Performing the rigorous action comparison is a substantial computational task as rigorous numerical integration of all trajectories in the kick region must be performed, and the outside region must employ interval arithmetic to be rigorous. This is detailed in section 2.2. To perform both tasks, the **CAPD** package in **C++** is used. It employees the Lohner algorithm to rigorously integrate ODEs and also has built in libraries for interval arithmetic. See E.1 for a brief description, and the references [Z], [WZ], and [MZ] for more through details on the **CAPD** package. Examples of **CAPD** integrators are given in section E.2.16 of this document.

To perform the rigorous action comparison, the program **actcomp.cpp**. is used. The mathematical setup is recorded in the proof of Theorem 2.2.4, and the technical details (step sizes, dimensionality of various arrays, included packages)

are documented in the code, in some cases line by line. (See section E.2.16 of this document for a worked example). The program requires as input a start and stop range between 0 and 28001. Each value i corresponds to computing the action comparison for $P_\varphi \in [1.67 - i \cdot 0.000025, 1.67 + i \cdot 0.000025]$.[5] Call the data associated to each i a *layer.*

The program saves, for each value i, two log files, **Summary_Layer$i$.txt** and **Layer$i$.txt**. The summary log files contain only the information for the action comparison. The standard (Layer) log file contains information on each integrated trajectory. In order to avoid storing massive logs of data, **actcomp.cpp** has lines commented out, which when activated, saves all this data. However the default is to just log the action comparison data and the crossing times for trajectories.

Running **actcomp.cpp** is quite computationally intensive and can take months of time on a single processor. Since each layer i is independent, it is possible (and encouraged) to run different layers on different machines. At the end, simply place all the log files in one directory. The programs **reader.cpp** and **readtime.cpp** allow one to parse through the log files generated. The notebook **actcomp_res.nb** contains visual output of the data.

Once log files are generated, **outactcomp.cpp** and **outactcomp_hyp.cpp** uses them to complete the action comparison. **outactcomp.cpp** carries out the

[5]This is slightly different than has described in section 2.2. The reason for the difference is that previously the program had to take negative arguments, whereas now it does not. Furthermore this program uses smaller boxes which allows us to produce tighter results. Notably it gives $e^*(1.8, 0.001) \approx 0.57$ which is less than the 0.66 cited in Theorem 1.1.2.

comparison using elongated solar passages. It only accepts inputs (Layers) less than 25500. **ouactcomp_hyp.cpp** carries out the comparison using 100-solar passages[6]

The formulas in section 2.2 are implemented exactly as described, however using slightly different (and in some cases more descriptive) variable names. The program outputs eccentricities were there are no invariant curves. Logs for this are called **outact.txt** and **outact_hyp.txt**. It is possible to modify code (see comments in code) to output places where the comparison failed. This output is included in the file **outact_fail.txt** in the 'Logs and Data' subdirectory.

The data generated by the rigorous action comparison is used in Theorem 2.2.4. At present, the programs actually improve modestly on some of these numbers. The data is also used in the third claim of Lemma 2.2.2 on total change in angular momentum along an R-solar passage. The data on the time to cross the kick the region as found in Lemma 5.1.1 is also generated. The visualizations as in **actcomp_res.nb** are the origin of the graphs accompanying all of these respective claims.

In the outside region action comparison several closed form integrals are used. These are found in the notebook **usefulintegrals.nb**.

[6]This is slightly different than in section 2.2 which requires 80-solar passages. mathematically $R = 80$ works fine, but due to rounding used in interval arithmetic estimates, it is better for the program to use $R = 100$-solar passages.

E.2.10 Expansion of the domain

Theorem 3.1.1 establishes that $\nu = 2.8\mu$. The method outlined in the proof using upper bounds on ΔH and using ρ is carried out in **GK2claims.nb**.

E.2.11 Analysis of the Equations of Variation

To handle the bounds on equations of variation in the outside region, **Mathematica** is used to evaluate the terms $a_i(r_0)$ as outlined in section B.2. This functions are found in the notebook **GK2claims.nb**. These functions used integrals from the notebook **usefulintegrals.nb** which contains closed form integrals for the 2BP.

To handle the bounds on equations of variation in the outside region, **CAPD** is used to rigorously integrate the equations of variation over all 5–solar passages which initial conditions on the tangent space described as in the paper. The program is called **varbound.cpp** and it runs in about 5 hours. Cince it uses intervals in P_φ of size 0.0001, it is not very accurate and more refined analysis is possible at the cost of increased computation.

E.2.12 Computing Localization Intervals

A quick nonrigorous method of finding the localization intervals is automated in a **Mathematica** notebook, and a more in depth rigorous approach is the focus of several programs.

E.2.12.1 Nonrigorous Computation

The **Mathematica** notebook **localization_test.nb** computes localization intervals in Delaunay coordinates. Simply evaluate all the cells to get nonrigorous approximations for the localization intervals. (Note one must first evaluate the notebook **RCP3BP_Estimates.nb**.)

The notebook works by creating a grid of solutions with initial conditions all on the energy surface $H = -1.8$ and $g = 0$. For each solution, it computes δL and $\delta \ell$ as specified in chapter 5 and stores this additional data. It is possible to obtain visual representations of these data sets and the notebook does so. The notebook also records the location of the kick and outside regions by computing $|Lu|$. Confidence intervals are computed using the algorithm in section 5.1.3 with initial condition $\Delta L = 0.1$ with 3 iterations. Localization intervals are then computed by using quantities computed during generation of the confidence intervals. The numerical experiments contained in this notebook also give some of the heuristic estimates found in section 5.1.1.

A sample grid is input and evaluated to produce roughly the quantities found in the paper. These are only approximations due to the fact that the mesh is not very fine, and also due to the fact that in the rigorous case, additional care must be handled to deal with boxes of initial conditions.

E.2.12.2 Rigorous Computation

Rigorous computation of the localization intervals is broken up into two programs. Step 1 of algorithm in section 5.2 is the rigorous integration of a grid of boxes of initial conditions. The remaining steps can be carried out in a separate program once the first step is complete.

To carry out the massive grid integration, **gridstore.fox**, a **COSY-JERI** program, is used to rigorously integrate the equations of motion for the RCP3BP. The Modified action-angle variables in subsection E.2.14.1 are used. The domain of definition is divided into a large number of small boxes and each is integrated over one return time. Differences between initial and final conditions are saved in data files. Because the bounds need to be very tight, degree 4 or 5 Taylor Models are used as well as small boxes of initial conditions. This slows down computation time considerably. As such, difference parts of the domain were run on different CPUs and the resulting data files were all pooled together. The computation would take a long time on a single computer (approx 19.5 million seconds, or 225 days), however due to utilization of multiple processors, it actually only took about 2 weeks.

After **gridstore.fox** is finished, all the data files are merged together. The data files occupy several hundred megabytes of space and are available upon special request. Another **COSY-JERI** program, **gridread.fox**, reads the data files and checks that all elements of the domain in question are present. It then stores several more log files containing differences in action and angle variables which are organized by initial conditions. This program has routines to compute confidence

intervals. Because it uses small boxes of initial conditions, some boxes are counted as being both in the kick and outside regions. Calculations are carried out using interval arithmetic. The ordering condition is used to produce bounds on the localization intervals as specified below in the appendix. The program outputs n and the confidence interval associated to it.

E.2.13 Crossing Intervals

A quick nonrigorous method of computing crossing trajectories is automated in a **Mathematica** notebook, and a more in depth rigorous approach is the focus of several programs.

E.2.13.1 Nonrigorous Computation

All the tools to generate nonrigorous crossings are contained in the **RCP3BP_Estimates.nb** notebook. Once the localization intervals are known, simply use the nonrigorous numerical integration to cross them. All the solutions listed in section 5.3 are generated and plotted in the notebook **crossings.nb**. As mentioned in section 5.3, it is easier to compute crossings in polar coordinates since the equations are simpler to express, and therefore integration can be carried out more quickly and accurately.

Actually finding crossings is difficult and involves a lot of trial and error. Given a localization interval $[G^-, G^+]$, the computer can be programmed to generate several thousand solutions with initial conditions $P_\varphi = G^- - \epsilon$, where ϵ is some small

number. Typically it takes hours (or days) to generate test solutions. Each solution is checked to determine if it crosses the localization interval. Most do not. In some cases, all test solutions do not cross and more must be generated. Once a handful of crossings is found, the initial conditions are carefully perturbed by hand in an effort to produce a larger difference in the $P_\varphi = G$ direction, or a quicker crossing time. This is more less ad hoc and is also very time consuming. It is also completely irrelevant to the proofs, since only the existence of crossings is required, and once trajectories crossing the localization intervals are produced, the proof is complete.

E.2.13.2 Rigorous Computation

Once a potential crossing solution is located by nonrigorous methods above, it must be verified rigorously. The integrator **COSY-JERI** is used to do this. **COSY-JERI** is described more throughly in section E.2.20. The primary difficulty in verifying crossings is that verification requires both high precision (on order of 10^{-3} accuracy) and long integration times (on order of thousands of time units). The faster the crossing time, and the larger the jump, the easier the verification. This is why solutions were carefully chosen by hand.

The program **findpolarcross.fox** contains all the code necessary to verify a polar crossing. The program needs slight modification for each crossing, namely that the initial conditions, integration time, and order of the Taylor Model must be input by hand. Values for each crossing are stored in the log files. The program uses Taylor Models and Shrink Wrapping as described section E.1.3 to carry out

long term rigorous integration.

The program produces the log files **Crossing_test*.DAT** which contains a record of the solution at certain times, and also records the range in the $G = P_\varphi$ direction. The program outputs to the screen the current values of the solution after a time step, as well as the bounds in the G direction.

An important technical note is that since solutions are bounded as intervals, $G(t) \in [a(t), b(t)]$, then the crossing of the localization interval $[G^-, G^+]$ is only verified provided there is a time t_* when $b(t_*) < G^-$ and a time t^* when $a(t^*) > G^+$. This condition ensures that the trajectory actually crosses the localization interval, independent of any errors introduced from computer arithmetic. In some cases, candidate solutions crossed the localization in the nonrigorous **Mathematica** notebook, however they failed this containment condition and hence could not be used.

The process of checking a crossing is very memory and processor intensive. Typically high order Taylor models (order > 10) must be used which requires approximately a 1 gigabyte of memory and a fast processor. Verification times could take up to a week of continuous processor usage. It is likely this time could be improved with better choice of crossing solution or more careful optimization of the parameters in the integrator. However this was not attempted. It is very likely the time it would take to carefully optimize the code would exceed the time necessary to perform the integration.

Remark: At present **CAPD** can be used to integrate accurately up to around 500 time units. With some more careful coding on the author's part, **CAPD** should

be able to verify the crossing solutions' behavior.

E.2.14 Crossing the Kick Region

In Lemma 5.1.1, it is stated that it takes at most 3 iterates of $\mathcal{F}$ to cross the kick region for a certain set of parameters. To prove this rigorously, estimates on total change in angular momentum, estimates of the perturbation terms, as well as an upper bound on the time to make a 5-Solar passage are needed for the parameters listed. The program **actcomp.cpp**, as described above also records an upper bound on the time to make a 5-Solar Passage. Once the data files are generated, it is a simple matter to scan through them to obtain the desired upper bound.

E.2.14.1 Alternative Action-Angle Variables for RCP3BP

When the source code for parts of this thesis was written, the author was unaware of how prevalent Delaunay variables were in the literature. The software (**COSY-JERI**) was not been rewritten using Delaunay[7]. Instead alternative action variables were used to formulate several of the results. These variables are denoted

[7]It would require significant time recoding, rechecking, and rerunning the software. It is easier to just change the mathematical statements than do this.

$(J, J_r, \theta, \theta_r, \xi)$ are are associated to Delaunay variables in the following way.

$$J = L \qquad Jr = L - G$$

$$\theta = \ell - \theta_r \qquad \xi = u$$

$$\begin{aligned} u - e\sin(u) =& \ell = \theta + \theta_r \\ e =& \sqrt{1 - \frac{G^2}{L^2}} = \sqrt{1 - \frac{(J - Jr)^2}{J^2}} \\ \theta_r =& -g - 2\arctan(\sqrt{\frac{1+e}{1-e}}\tan(\frac{u}{2})) + \arccos(\frac{\cos(u) - e}{1 - e\cos(u)})sign(\sin(u)) \end{aligned}$$

The calculations for the localization intervals were computed using this modified coordinate system. This is not serious as $J = L$. Mathematically, the statements of certain theorems change, but the proofs remain the same, up to change of coordinates. These changes are stated now for completeness.

In the modified coordinate system,

$$H_{Modified} = -\frac{1}{2J^2} - (J - J_r) + \Delta H(J, J_r, \theta, \theta_r)$$

The perturbation term can be computed explicitly through the use of a computer algebra system, noting the following identities

$$\begin{aligned} r =& J^2(1 - ecos(\xi) \\ \cos(\varphi) =& \frac{\cos(\xi) - e}{1 - e\cos(\xi)} - \theta_r \\ e =& \sqrt{1 - \frac{(J - Jr)^2}{J^2}} \\ \xi - e\sin(\xi) =& \theta + \theta_r \end{aligned}$$

In this coordinate system, fixing an energy surface $H = -E$, where E is Jacobi constant, implicitly defines the variable $J_r \approx J - E + \frac{1}{2J^2}$. Take a Poincaré section

$\{\theta_r = 0 \mod 2\pi\}$. The Poincaré map is now

$$\mathcal{F} = \begin{pmatrix} \mathcal{F}_\theta \\ \mathcal{F}_J \end{pmatrix} : \begin{pmatrix} \theta_0 \\ J_0 \end{pmatrix} \mapsto \begin{pmatrix} \theta(t^*, \theta_0, J_0) \\ J(t^*, \theta_0, J_0) \end{pmatrix}$$

Proof of twisting remains the same, and the twist term is of the same form expect with J's instead of L's and θ's instead of ℓ's. There is still twisting for $e \leq 0.9$, the region where the integration in the algorithm of section 5.2 is performed. It still takes 3 iterates to cross the kick region. All extremized quantities remain the same with with J's instead of L's and θ's instead of ℓ's. The kick region and the procedure to define and refine confidence intervals remains the same.

The variable θ moves differently than ℓ and the corresponding ordering condition is

$$\theta_n - \theta_0 < 2\pi(1-n)$$

and the localization theorem is stated as

Theorem E.2.1 (Localization Intervals)**.** *Fix mass ratio μ, Jacobi constant J_0, and rotation symbol $\omega \in [\frac{1}{n+1}+, \frac{1}{n}-]$. Suppose $A_n < \omega^{-\frac{1}{3}}$ and ΔJ are nonnegative real numbers such that the $(A_n, \Delta J)$ containment assumption is satisfied for all solutions with initial conditions $J_0 = A_n$. Suppose $J_n > \omega^{-\frac{1}{3}}$ and $\Delta J'$ are nonnegative real numbers such that the $(B_n, \Delta J')$ containment assumption is satisfied for all solutions with initial conditions $L_0 = B_n$. Further suppose that*

$$N\delta\theta^{kick,min}_{(J_0,\Delta J^i)} + (n-N)\delta\theta^{out,min}_{(J_0,\Delta J^i)} \geq 2\pi(1-n)$$

and

$$N\delta\theta^{kick,max}_{(J_0',\Delta J'^i)} + ((N-1)-3)\delta\theta^{out,max}_{(J_0',\Delta J'^i)} \leq -2\pi n$$

holds, where N is the number of iterates needed to cross the Delaunay kick region. Then $[A_n, B_n]$ is an ω-localization interval. Moreover $A_n, B_n < \infty$.

Proof of the theorem is the same, except for using the modified ordering condition, and J's instead of L's and θ's instead of ℓ's.

E.2.15 Obtaining and Installing the Software

In this subsection, some details are given on how to obtain and install the software packages necessary to verify the claims in this thesis.

E.2.15.1 Required Packages

Three software packages are required to run the necessary programs: **CAPD**, **Mathematica**, and **COSY**. These packages are not distributed by the author. Below is information on obtaining them.

1. **CAPD** is a GPL open source software library and can be obtained from the "Computer Assisted Proofs in Dynamical Systems Group" free of charge. See

   `http://CAPD.ii.uj.edu.pl/`

   for details on obtaining and installing **CAPD**. It is recommended to use the latest available build. To compile **CAPD**, a **Linux**-type environment running the X graphics server is required.

2. **Mathematica** is a closed source software package, distributed for a fee by Wolfram Research. See

http://www.wolfram.com/

for details on obtaining and installing **Mathematica**. Version 5 was used when creating the software used in this document.

3. **COSY** is an open source software library distributed for free with a restricted license by Martin Berz at Michigan State. See

   www.COSYinfinity.org

   for details on obtaining and installing **COSY**. The build distributed in 2008 was the version used.

While developing and running this software, the author used **Ubuntu** 8.10, **Ubuntu** 9.04, or **Fedora Core** 7. All computers used had at least 256MB of RAM, a 4GB HDD, and a 1Ghz processor.

Installing the Programs:

E.2.15.2 CAPD

1. Obtain and Install **CAPD** on your system

2. Create a subdirectory called private in the **CAPD** directory structure. Goto the private subdirectory.

3. Inside of our zip file, there is a directory called **CAPD** with various programs in it. Copy the directory of the program of your choice to the folder 'private' that you just created.

4. Goto the subdirectory of 'private' that you just created. It contains a makefile.

5. Run the make command twice.

6. The program executable is in ~/**CAPD**/bin and has the same name as the .cpp file.

Tips for the Linux Installation

- Compilation may fail if you do not have the X-development library. Usually this manifests in a '... Xlib.h not found ...' in the compilation output.

- It is recommended to use wx if you want to modify any of the programs to incorporate graphics. When you compile the library or programs, use 'make target=wx'. To use this setting you must have Qt4 installed. This is usually included with KDE desktops, but not necessarily for Gnome.

E.2.15.3 Mathematica

The **Mathematica** notebook **RCP3BP_Estimates.nb** contains a library of functions that all other notebooks require. Evaluate all the cells in this notebook before running any other notebook.

E.2.15.4 COSY

1. Obtain and install **COSY** on your system. (See **COSY** documentation for help with this.)

2. Inside of the zip file, there is a directory called **COSY** with various programs in it. Copy these files into the directory you in which you just installed **COSY**.

3. Run **COSY** and then execute **RCP3BP_Derivatives.fox** to compile the RCP3BP_derivatives library.

4. Run **COSY** and then execute **COSY_JERI.fox** to compile the JERI add-on for rigorous integration and global optimization.

5. Run **COSY** and then execute any of the other programs you placed in the **COSY** directory.

Tips for the Windows Installation

- Before installing **COSY**, set Windows swap file page to 2GB (or more).

- The **RCP3BP_Derivatives** and **COSY_JERI** libraries, when compiled, take up a lot of space. It is recommended to have at least 250MB of free space before running any of the **COSY** programs.

E.2.16 A Quick Guide to Rigorous Integration in CAPD

In this section, the anatomy of a rigorous integrator in **CAPD** is examined. The **CAPD** package was designed by the 'Computer Assisted Proofs in Dynamical Systems' group in Krakow Poland. Our goal in this section is not is discuss the theoretical issues involved in the integration, but rather to work through an explicit example. It is highly recommended to read the following papers which contain the

details of the algorithms used in the **CAPD** as well as ideas on efficient implementation. There are several other worked examples found on the **CAPD** website.

Let us step through the process of compiling, running, and modifying a C^0 rigorous integrator. The initial example program is called 'C0integrator' and several modifications shall be made to it. All the **CAPD** programs used in the proofs of this thesis use this same underlaying construction, so it is important to understand these more basic examples first. Programs which integrate variational equations use a similar structure, however require more complicated objects. It is recommended to read the source code itself as well as the **CAPD** documentation.

Let us consider is the 2 dimensional ODE with parameter μ.

$$\dot{x} = -\mu y$$

$$\dot{y} = \mu x$$

$$\mu = 2$$

Our first example is a C^0 integrator using a 20^{th} order Taylor method. The system is integrated from $t = 0$ to $t = 100$. The integrator is given a box of initial conditions $x \in [-0.001, 0.001]$, $y \in [0.999, 1.001]$.

E.2.17 Compiling and Running the Example

The program **C0integrator.cpp** is used as an example.

1. Goto .../**CAPD**/private/examples .

2. Edit the makefile. 'gedit makefile'.

3. Change line PROGS to 'PROGS = C0integrator'.

4. At the command prompt. Type 'make' then hit enter.

5. At the command prompt. Type 'make' then hit enter again.

6. Edit C0integrator.cpp. This is the source code for the example.

7. Run .../**CAPD**/bin/C0integrator . This executes the example.

E.2.18 A Walk Through of the Example

Run the program, then read through the source code of the program. The code is commented. Below are several highlights which should give the interested reader the ability to modify the code for other ODEs. Here are the highlights.

E.2.18.1 Dimension

To set the dimensionality of the ODE use

```
const int DIMENSION=2;
```

The 2 is because a planar ODE is considered. Note you must be able to write your ODE as an autonomous system of first order equations. If the system is nonautonomous, there is another setup to use, however it is beyond the scope of this introduction.

E.2.18.2 Length of Integration

To set the length of integration time use

```
int length=static\_cast<int>( (100./T.getStep().rightBound()));
```

The 100 sets the length of integration to 100 time units. Notice that the example ODE is volume preserving, so the effects which cause the size of the box to grow are overestimates generated to account for roundoff error. Even after 100 time units, the box size has not grown too much.

E.2.18.3 Stepsize and order

To set the order and step size, use

```
double step=0.125;
int order = 20;
```

Smaller step size allow better enclosure over entire steps, but slows down the integration process. Higher order gets better enclosures, but takes longer. In general, its better to use high order and take large steps.

E.2.18.4 ODE input

CAPD accepts a variety of ODEs with vector fields built using the operations addition, subtraction, multiplication, division, and exponentiation, as well sin, cos, log, exp, and '$\sqrt{.}$'. One way to define an ODE is to input the vector field as text. For example

```
Map f="par:mu;var:x,y;fun:-mu*y,mu*x;";
```

The 'Map' object stores the vector field for the ODE. Note it takes parameters, as well as variables. Parameters and variables can be upper or lower case and be multiple letters. You *need* to define constants as parameters since as real numbers, they may not be machine representable. Setting them as parameters makes the result rigorous since it instructs **CAPD** to use interval arithmetic to treat constants as very small intervals of width machine-ϵ. The command to set parameters looks like

```
f.setParameter("mu",interval(2));
```

E.2.18.5 The dynamical set

The ODE solutions are stored as a 'dynamical set' which can be moved in time by an integration (which is specified by an 'integrator'), and is enclosed at a point in time, or over an interval in time. The representation of the set is important since efficient storage and manipulation can dramatically improve the bounds obtained from rigorous integration. A particularly efficient representation is the doubleton representation. It is described in [MZ] along with several others. The command to initialize the doubleton representation is

```
Rect2Set rect2(v,r);
```

This uses the 'Rect2' doubleton representation outlined in [MZ], which generally has the best overall performance of the possible representations **CAPD** supports for C^0 integration. Essentially it represents an interval as a midpoint, a range, and some error.

E.2.19 Enclosure Between Timesteps

Suppose bounds are desired on solutions to the ODE for all time in between one step of integration. This is issue is addressed in [Z] and the set W_1 in [Z] is the desired enclosure. Finding this set is implemented in **CAPD** as the command:

```
IntervalVector enc = {\bf CAPD}::dynsys::enclosure(T.getField(),w,T.getStep());
```

The enclosure command takes as arguments the vector field, the value of the vector at the start of the time step, and the size of the time step. It outputs an interval vector containing the enclosure for the timestep. The full setup is found in the example file **C0integratorENC.cpp**.

E.2.20 A Quick Guide to Rigorous Integration with COSY-JERI

COSY-JERI (or **COSY**- Joe's Electronic Rigorous Integrator) is a library which uses the Taylor Model manipulation abilities of **COSY** to implement the ideas for rigorous numerical integration found in Berz's papers. These papers don't seem to include all of the mathematical details (several of the papers are in physics or computer science journals). Some of these details are included in subsection E.1.3.1 and are essential to implementing a rigorous integrator. A quick review of Taylor Models is found in E.1.3.

This section outlines some of the libraries found in **COSY-JERI** and work through an example of a rigorous integrator. **COSY-JERI** consists of 2 library files, **RCP3BP_Derivatives.fox**, and **COSY_JERI.fox**. Both the libraries and the programs require **COSY** (see appendix E.2.15 for information on obtaining **COSY**).

COSY has its own language, **COSYscript**, which **COSY-JERI** is written in and it is helpful to have the **COSY** Programming Manual as a reference. The manual is distributed with **COSY** itself.

E.2.21 The RCP3BP_Derivatives Library

This library contains first and second order partial derivatives of the perturbation term in action angle coordinates as well as several related partial derivatives. A list of all the functions and details on arguments are found in documentation at the top of the library file. It is mathematically important to note that this code does not use Delaunay action-angle variables; it uses the action-angle variables found in section E.2.14.1.

The functions in this library were originally computed using **Mathematica**'s symbolic manipulation routines. The **Mathematica** notebook **simplifications_for_COSY.nb** contains the simplified expressions[8].

Some by hand simplifications are needed to further reduce the autogenerated formulas **Mathematica** produces. For example expressions which contain a $\sqrt{x}^4$ which causes **COSY** problems, and when it is known that $x > 0$, the expression is simplified to an x^2. A more serious example involved simplifying expressions with inverse trigonometric functions in them. This occasionally arose in functions involving φ in action-angle variables and in some cases involving inverse trig functions, multiples of π or $\frac{\pi}{2}$ are added to be consistent with sign conventions. These instances are documented in the source code.

[8]To check them, you first need to evaluate the notebook **RCP3BP_estimates_old.nb**.

COSY has a limit of 80 characters per line and in some cases complex expressions run over this limit. The library contains functions for several commonly occurring expressions, for example the function 'CTermX'. These are also documented in the notebook simplifications_for_**COSY**.nb.

Construction and testing of this library was rather time consuming and after completion, the authors became aware of both Delaunay variables and **CAPD**. It is likely that in the future results which currently depend on **COSY-JERI** shall be redone to use **CAPD**. The **CAPD** licensing agreement is also more friendly to research than that of **COSY**.[9]

E.2.22 The COSY-JERI Library

The **COSY-JERI** Library file, **COSY_JERI.fox**, contains functions and procedures to perform rigorous global optimization and rigorous ODE solving. It is meant to emulate the functions of **COSY-GO** and **COSY-VI** found in the papers of Berz, but is NOT closed-sourced.[10] Ideas for the algorithms come from papers and talks by Martin Berz and Kyoto Makino, as well as talks and code demos presented at CAP08 the conference for Computer Assisted Proofs in Dynamical Systems held in Barcelona in June 2008. This library is essentially a reverse-engineering of these closed source products.

The **COSY-JERI** library contains functions to perform shrink-wrapping and

[9]While **COSY-JERI** is distributed for free, it depends on **COSY**, which has a restrictive license.

[10]Berz does not distribute these files in any form.

blunting, 3D global optimization, basic linear algebra, and rigorous integration using a Schauder ODE Solver (see section E.1.3.1). At the top of this library, technical documentation is provided, and each function also contains commenting regarding technical details.

An important technical comment is that to use the **COSY-JERI** rigorous integrator, you must declare your ODE in the function 'ODEFUNCTION' contained in this file. This is due to limitations in **COSYscript** which require programs to be compiled sequentially. Thirteen ODEs are input in 'ODEFUNCTION' as examples, including the 2BP(SC) and the RCP3BP. See source code comments.

E.2.23 RigInt

Let us now examine an example of a rigorous integrator using Taylor Models with blunted shrink wrapping. (Shrink Wrapping is briefly discussed in section E.1.3 and in depth in [BM2].) The program in question is called **RigInt.fox**. The theoretical underpinnings of rigorous integration are contained in the papers [BM2] and [MB1]-[MB4] and briefly discussed in section E.1.3. Right now, let us point out some of the highlights for code implementing these ideas.

Consider the Van Der Pol equations

$$\dot{x} = y + x - \frac{x^3}{3}$$

$$\dot{y} = -x$$

for time $t = 0$ to $t = 100\pi$ in steps of $\Delta t = \frac{2\pi}{50}$ with initial conditions $x_0 \in [-2.001, 1.999]$ and $y_0 \in [-0.001, 0.001]$.

E.2.23.1 Dimensionality and Step Size

The code to set the ODE dimensionality and size of integration is

```
ODEDIM := 2;
timestep:=2*Pi/50;
timestop:=100*PI;
```

E.2.23.2 Initial Conditions

In order to set the initial conditions to $x_0 \in [-2.001, 1.999]$ and $y_0 \in [-0.001, 0.001]$ use

```
IC(1) := -2+TM(1)/1000;
IC(2) := 0+TM(2)/1000;
```

E.2.23.3 Vector Field

In the line

```
BoundFlow 4 ODEDIM Daorder IC timestep flowTM param;
```

the number 4 indicates to use the 4^{th} ODE as declared in ODEFUNCTION in the **COSY-JERI** library.

Other instances of the 'BoundFlow' involve the shrink wrapping and blunting routines. See code comments for details. If shrink wrapping fails, then the Taylor Models are linearized and the higher order terms moved to interval remainder. This typically allows shrink wrapping in the next step. However this dramatically inflates

the bounds on the ODE flow. See [MB4] for details.

E.2.23.4 Order

Use of 5^{th} order Taylor Models is implemented using

```
DAorder := 5; { DA Order}
```

Higher order Taylor models typically produce tighter bounds and allow integration to proceed for a longer time period. However, computationally, they require much more power and storage. (Consider the number of coefficients for a polynomial in 4 variables of degree 13 vs. one of degree 3.)

E.2.24 RigOpt and Rigorous Domain Bounding

Finding a verified minimum or maximum of a function using Taylor Models is relatively straightforward. Given a Taylor Model modeling a function, simply bound the polynomial term by using interval arithmetic where the interval is the domain of the Taylor Model, then add this bound to the remainder term to bound the function in question. In [BM1], a more precise is description is given.

If a global minimum or maximum of a function f is desired on a large domain D, simply divide up D into small subdomains, make a Taylor model on each subdomain, bound the Taylor model on each subdomain as above, and then take the maximum of all maxima generated by computing bounds on the patches. Decreasing the size of the subdomains generally increases the accuracy of the bounds. The end result of the optimization is a box (or boxes) which is known to contain the

maximum (maxima) (or minima), and an interval which contains the range of the function over the domain, all of which are completely rigorous.

To optimize over a large grid of small patches is very inefficient. A better way is to take the nature of Taylor models into account and note that the error term is proportional to the size of the domain to the n^{th} power for an n^{th} order Taylor model. A good way to globally optimize is to divide up a domain into a small number of subdomains, record which boxes contain potential maxima (or minima), then subdivide those. Even when subdividing into a small number, due to the nature of Taylor models, the improvement in bound can be quite significant. Iterating this procedure several times zooms in on the boxes containing the extrema. Berz uses a variant of this method in his own (privately held) library, **COSY-GO** (see [BM1]) but an open-source version is available in **COSY-JERI**.

E.2.24.1 Example

These ideas are implemented in the example program **RigOpt.fox** which is designed to optimize the function

$$f(x, y, x) = 1 - x^2 - y^2 - z^2$$

over the domain $[-1, 1]^3$. The function is input near the top of the program at the line

```
tmp:=LDB(1-SQR(X)-SQR(Y)-SQR(Z));
```

The command 'LDB' instructs **COSY** to use the domain bounder on its argument. The variables 'X', 'Y', and 'Z' are Taylor Models over some small domain. See

[BM1].

The domain $D = [-1, 1]^3$ is input in the line

```
FindMaximum3D IN((-1)\&1) IN((-1)\&1) IN((-1)\&1) temparray1 itermax mmx mxx;
```

Full documentation for this function is provided in **RigOpt.fox**. The rest of the source code is also commented and uses the recursive divide and conquer strategy discussed above. The code outputs a box containing the maxima. It can be used to find minima for a function f by finding maxima of $\frac{1}{f}$, or of $-f$.

RigOpt.fox uses optimization in 3 dimensions. While it is theoretically possible to do more, this is not currently implemented due to limitations of the **COSYscript** language. Another language based limitation is that functions to be optimized must be declared *before* the optimizer routine. In complex programs this results in the optimizer routine being copied and pasted several times due to the sequential line by line compilation and execution of **COSYscript**.

E.2.24.2 Poincaré Return Maps

Rigorous optimization is necessary to find Poincaré return maps. Suppose $\Phi(t)$ is a flow and Φ_0 is a value on the surface of a Poincaré section. To find the return time t, maximize $\frac{1}{(\Phi(t)-\Phi_0)^2}$. On the Poincaré section this value is $+\infty$ so it is easy for an optimizer to detect.

To concrete, for the RCP3BP in modified coordinates (see section E.2.14.1), the return time t is when $\theta_r(t) = 2\pi k$. The rigorous integrator can provide a Taylor Model of the flow in variables for time and initial conditions near the near point $2\pi k$. This Taylor Model can be feed into a rigorous global optimizer to find the

return time in question. The routine uses a 1–dimensional version of the 3D global optimizer used in **RigOpt.fox**. The function

```
PROCEDURE FindReturnTime FlowModel Tbounds kr Subdivstart itermax ReturnTime
```

is found in **COSY_JERI.fox** and has comments and details on the arguments specified in the source code. It may be modified for other return times provided good initial guesses are known.

Appendix F

A review of the 2BP

This chapter reviews basic facts about the 2BP(SC). Motions of the 2BP(SC) in rotating polar coordinates (r, φ) arise as solutions to Hamilton's equations with Hamiltonian

$$H_{Polar}(r, \varphi, P_r, P_\varphi) = \frac{P_r^2}{2} + \frac{P_\varphi^2}{2r^2} - P_\varphi - \frac{1}{r}$$

where P_r and P_φ are the conjugate momenta to r and φ respectively. Note that this is the RCP3BP Hamiltonian with $\mu = 0$. This is an integrable 2-degree of freedom system. Integrals of the system are

$$H_{Polar} = -J_0 \qquad\qquad P_\varphi = P_\varphi(0).$$

since it is not hard to see that $\dot{P}_\varphi \equiv 0$. Motions of the system are conic sections which are characterized by eccentricity on the energy surface $\mathcal{S}(J_0)$ (i.e. $H_{Polar} = -J_0$). When $e < 1$, these motions are ellipses. There are too special points on the ellipse of motion when the comet is closest and furthest from the Sun. Denote these points the perihelion and aphelion respectively. The radii of these points are given respectively by

$$r_\pm := \frac{P_\varphi^2}{1 \mp e}$$

where eccentricity e is given by

$$e = \sqrt{1 - 2P_\varphi^2(J_0 - P_\varphi)}$$

Kepler's Third Laws says the period of revolution is given by

$$T = \frac{\pi}{\sqrt{2}(J_0 - P_\varphi)^{3/2}} = 2\pi \left(\frac{P_\varphi^2}{1 - e^2} \right)^{3/2}$$

From these formulas, it is not hard to see there are degeneracies when $e = 1$. Nevertheless, there are still statements that can be made about parabolic and hyperbolic motions. See for example Lemma 2.1.4. Also see [AKN].

Analysis of the equations of first variation in Polar coordinates can be somewhat tricky. The solutions are in fact integrable. See [Beu] for a description. The only quantity readily accessible is $\frac{\partial P_\varphi}{\partial P_\varphi(0)} = 1$.

Computation of action is via the Lagrangian

$$L(r, \dot{r}, \varphi, \dot{\varphi}) = \frac{1}{2}(\dot{r}^2 + r^2(1 + \dot{\varphi})^2) + \frac{1}{r}$$

It is not hard to see this is a mechanical system of the form kinetic+potential.

When transforming the system into the so called Delaunay variables (see 3), the system has the Hamiltonian

$$H_{Del} = -\frac{1}{2L^2} - G$$

with action variables $0 \leq G \leq L$ and angles $\ell, g \in \mathbb{T}$. The system is still integrable with integrals

$$H_{Del} = -J_0 \qquad\qquad G = G(0).$$

and it is not hard to see that $\dot{L} = \dot{G} = 0$. The variable L^2 is the semimajor axis of the ellipse of motion, i.e. $L^2 = \frac{1}{2}(r_- + r_+)$ and from Kepler's Third Law, $T = 2\pi L^3$.

It is not hard to show that

$$\begin{aligned} r &= L^2\big(1 - e\cos(u)\big) \\ e &= \sqrt{1 - \frac{G^2}{L^2}} \\ u - e\sin(u) &= L^{-3}t = \ell \\ \sin(\varphi - \varphi_0) &= \frac{\sin(u)\sqrt{1-e^2}}{1 - e\cos(u)} \\ \cos(\varphi - \varphi_0) &= \frac{\cos(u) - e}{1 - e\cos(u)} \\ P_r &= \frac{Le\sin(u)}{r} \\ P_\varphi &= G \\ g &= -t \end{aligned}$$

where φ_0 is the perihelion angle, i.e. the angle the comet makes with respect to the positive x-axis then it is at the perihelion. Examining these equations it is also not hard to see that Delaunay variables have degeneracies at $e = 1$. Also see [AKN] for more relations.

It is easy to examine the equations of first variation in Delaunay. Every quantity is identically zero except for $\frac{\partial L}{\partial L_0} = \frac{\partial G}{\partial G_0} = \frac{\partial \ell}{\partial \ell_0} = \frac{\partial g}{\partial g_0} = 1$ and $\frac{\partial \ell}{\partial L_0} = -\frac{3}{L^4}$. The last term is the so called twist term. See section 3.2.

Using the section $P = g = 0 \mod 2\pi$, then dynamics can be reduced to that of an exact area preserving twist map given by

$$\mathcal{F}(\ell, L) = (\ell + 2\pi L^{-3}, L)$$

Note the property of twist follows for the map since $\frac{\partial \ell}{\partial L_0} = -\frac{6\pi}{L^4}$.

Computation of action is via the Lagrangian

$$L(\ell, \dot{\ell}) = \frac{3}{2}\dot{\ell}^{2/3}$$

It is not hard to parlay this into a generating function for the map (see section 6.1)

$$h(\ell_0, \ell_1) = \frac{3(\ell_1 - \ell_0)^{3/2}}{2\sqrt{2\pi}} = 3\pi L^{-2}$$

Note that this says the cheapest motions in terms of action is for L to remain constant along trajectories. Indeed in the integrable case this is exactly what is observed from solving the Hamiltonian equations of motion.

Bibliography

[A] Arnold, Vladimir I. *Mathematical methods of classical mechanics*. Translated from the 1974 Russian original by K. Vogtmann and A. Weinstein. Corrected reprint of the second (1989) edition. Graduate Texts in Mathematics, 60. Springer-Verlag, New York, 199?. xvi+516 pp. ISBN: 0-387-96890-3

[AKN] Arnol'd, Vladimir I.; Kozlov, Valery V.; Neishtadt, Anatoly. *I. Mathematical aspects of classical and celestial mechanics*. Dynamical systems. III. Translated from the Russian original by E. Khukhro. Third edition. Encyclopaedia of Mathematical Sciences, 3. Springer-Verlag, Berlin, 2006. xiv+518 pp. ISBN: 978-3-540-28246-4; 3-540-28246-7

[Al] V.M. Alekseyev, *Sur l'allure finale du mouvement dans le probleme des trois corps*, (Congres Internat. Mathematiciens (Nice), 1970; 2, (Paris, Gauthier-Villars), 1971, 893907

[Ban] Bangert, Victor. *Mather sets for twist maps and geodesics on tori*. Dynamics reported, Vol. 1, 1–56, Dynam. Report. Ser. Dynam. Systems Appl., 1, Wiley, Chichester, 1988.

[Be] Bernard, P. *The Dynamics of Pseudographs in Convex Hamiltonian Systems, J. Amer. Math. Soc. 21 (2008), no. 3, 615–669.*

[Be2] Bernard, Patrick. *Symplectic aspects of Mather theory.* Duke Math. J. 136 (2007), no. 3, 401–420.

[Beu] Beutler, Gerhard. *Methods of celestial mechanics.* Vol. I. Physical, mathematical, and numerical principles. In cooperation with Leos Mervart and Andreas Verdun. With 1 CD-ROM (Windows). Astronomy and Astrophysics Library. Springer-Verlag, Berlin, 2005. xvi+464 pp.

[BK] Bourgain, Jean, Kaloshin, Vadim. *On diffusion in high-dimensional Hamiltonian systems*. J. Funct. Anal. 229 (2005), no. 1, 1–61.

[BM1] Berz, M., Makino K. *Verified Global Optimization with Taylor Model-based Range Bounders*. Transactions on Computers. Issue 11, Vol 4, November 2005.

[BM2] Berz, Martin; Makino, Kyoko. *Verified integration of ODEs and flows using differential algebraic methods on high-order Taylor models.* Reliab. Comput. 4 (1998), no. 4, 361–369.

[CC] Celletti, Alessandra; Chierchia, Luigi. *KAM stability and celestial mechanics.* Mem. Amer. Math. Soc. 187 (2007), no. 878, viii+134

[GK1] Galante, Joseph Robert; Kaloshin, Vadim. *Destruction of Invariant Curves in the Restricted Circular Planar Three Body Problem Using Comparison of Action.* Preprint. To appear in the Duke Journal of Mathematics. Currently Avaliable at http://www-users.math.umd.edu/~joepi/downloads.html

[GK2] Galante, Joseph Robert; Kaloshin, Vadim. *The Method of Spreading Cumulative Twist and its Application to the Restricted Circular Planar Three Body Problem.* Preprint. Available at http://www-users.math.umd.edu/~joepi/downloads.html

[GK3] Galante, Joseph Robert; Kaloshin, Vadim. *Destruction of Invariant Curves in the Restricted Circular Planar Three Body Problem Using Ordering Condition.* Preprint. Avaliable at http://www-users.math.umd.edu/~joepi/downloads.html

[G1] Galante, Joseph Robert; Kaloshin, Vadim. *Estimating the Speed of Diffusion in the Restricted Circular Planar Three Body Problem.* Manuscript. Avaliable at http://www-users.math.umd.edu/~joepi/downloads.html

[GPS] Goldstein, Poole, Safko. *Classical Mechanics.* Addison Wesley; 3 edition (June 25, 2001), ISBN-13: 978-020165702

[G] Gole, Christopher. *Symplectic twist maps. Global variational techniques.* Advanced Series in Nonlinear Dynamics, 18. World Scientific Publishing Co., Inc., River Edge, NJ, 2001. xviii+305 pp. ISBN: 981-02-0589-9

[IEEE] IEEE-ANSI. *Standard for Binary Floating-Point Arithmetic.* 1985.

[KN] Kaloshin, Vadim; Nguyen, Tim. *Auxillary Lemmas.* Manuscript. Unpublished.

[KN2] Kaloshin, Vadim; Nguyen, Tim. *Remote Periodic and Quasiperiodic Motions in the Planar Circular Restricted 3-Body Problem of KAM and Aubry-Mather Type.* 2005. Manuscript. Avaliable online.

[KNP] Kaloshin, Vadim; Nguyen, Tim; Dmitri Pavlov. *Nonlocal Instability of the Restricted Planar Circular 3 Body Problem.* Manuscript Unpublished.

[KM] Kulisch, Ulrich W.; Miranker, Willard L. *Computer arithmetic in theory and practice.* Computer Science and Applied Mathematics. Academic Press, Inc. [Harcourt Brace Jovanovich, Publishers], New York-London, 1981. xv+249 pp. ISBN: 0-12-428650-X

[LS] Llibre, Jaume; Simo, Carlos. *Oscillatory solutions in the planar restricted three-body problem.* Math. Ann. 248 (1980), no. 2, 153–184.

[Ma2] Mather, John N. *Variational construction of orbits of twist diffeomorphisms.* J. Amer. Math. Soc. 4 (1991), no. 2, 207–263.

[MB1] Makino, Kyoko; Berz, Martin. *Taylor models and other validated functional inclusion methods.* Int. J. Pure Appl. Math. 4 (2003), no. 4, 379–456

[MB2] Makino, Kyoko; Berz, Martin. *Suppression of the wrapping effect by Taylor model-based verified integrators: the single step.* Int. J. Pure Appl. Math. 36 (2007), no. 2, 175–197.

[MB3] Makino, Kyoko; Berz, Martin. *Suppression of the wrapping effect by Taylor model-based verified integrators: long-term stabilization by preconditioning.* Int. J. Differ. Equ. Appl. 10 (2005), no. 4, 353–384 (2006).

[MB4] Makino, Kyoko; Berz, Martin. *Suppression of the Wrapping Effect by Taylor Model-Based Verified Integrators: Long-Term Stabilization by Shrink Wrapping.* Preprint. To appear in Int. J. Differ. Equ. Appl. Avaliable online at www.cosyinfinity.org

[MF] Mather, John N.; Forni, Giovanni *Action minimizing orbits in Hamiltonian systems.* Transition to chaos in classical and quantum mechanics (Montecatini Terme, 1991), 92–186, Lecture Notes in Math., 1589, Springer, Berlin, 1994.

[MS] McDuff, Dusa; Salamon, Dietmar; *Introduction to symplectic topology.* Second edition. Oxford Mathematical Monographs. The Clarendon Press, Oxford University Press, New York, 1998. x+486 pp. ISBN: 0-19-850451-9

[McG] McGehee, Richard. *A stable manifold theorem for degenerate fixed points with applications to celestial mechanics.* J. Differential Equations 14 (1973), 70–88.

[Mo1] Moser, Jurgen. *Recent Development in the Theory of Hamiltonian Systems.* SIAM Review. Vol 28, No 4. (Dec 1986) pg 459-485

[Mo3] Moser, Jurgen. *Stable and random motions in dynamical systems.* With special emphasis on celestial mechanics. Reprint of the 1973 original. With a foreword by Philip J. Holmes. Princeton Landmarks in Mathematics. Princeton University Press, Princeton, NJ, 2001. xii+198 pp. ISBN: 0-691-08910-8

[Moe] Moeckel, Rick. *A variational proof of the existence of transit orbits in the restricted three-body problem.* Dyn. Syst. 20 (2005), no. 1, 4558.

[MZ] Mrozek, Marian; Zgliczynski, Piotr. *Set arithmetic and the enclosing problem in dynamics*. Dedicated to the memory of Bogdan Ziemian. Ann. Polon. Math. 74 (2000), 237–259.

[NASA] http://www.nasa.gov/worldbook/jupiter_worldbook.html AND http://www.nasa.gov/worldbook/sun_worldbook.html

[R] Rainville, Earl D. *Elementary differential equations*. 2nd ed. The Macmillan Company, New York, 1958. xii+449 pp.

[RMB] Revol, N.; Makino, K.; Berz, M. *Taylor models and floating-point arithmetic: proof that arithmetic operations are validated in COSY.* J. Log. Algebr. Program. 64 (2005), no. 1, 135–154.

[S] Siburg, Karl Friedrich. *The principle of least action in geometry and dynamics*. Lecture Notes in Mathematics, 1844. Springer-Verlag, Berlin, 2004. xii+128 pp. ISBN: 3-540-21944-7

[Si] Sitnikov, K. A. *The Existence of Oscillatory Motions in the Three-Body Problem*. Dokl. Akad. Nauk SSSR 133 (2), 303306 (1960) [Sov. Phys., Dokl. 5, 647650 (1960)].

[SM] Siegel, Carl Ludwig; Moser, Jurgen K. *Lectures on celestial mechanics*. Translation by Charles I. Kalme. Die Grundlehren der mathematischen Wissenschaften, Band 187. Springer-Verlag, New York-Heidelberg, 1971. xii+290 pp.

[SS] Stiefel, E. L.; Scheifele, G. *Linear and regular celestial mechanics. Perturbed two-body motion, numerical methods, canonical theory*. Die Grundlehren der mathematischen Wissenschaften, Band 174. Springer-Verlag, New York-Heidelberg, 1971. ix+301 pp.

[WZ] Wilczak, Daniel; Zgliczynski, Piotr *The C^r Lohner-algorithm*. Preprint.

[Xia1] Xia, Zhihong *Arnold Diffusion and Instabilities in Hamiltonian Dynamics*. Preprint.

[Xia2] Xia, Zhihong *Melnikov method and transversal homoclinic points in the restricted three-body problem*. J. Differential Equations 96 (1992), no. 1, 170–184.

[Z] Zgliczynski, Piotr. *C^1 Lohner algorithm*. Found. Comput. Math. 2 (2002), no. 4, 429–465